The computational power of many-body systems

by

Zak Webb

A thesis
presented to the University of Waterloo
in fulfillment of the
thesis requirement for the degree of
Doctor of Philosophy
in
Physics and Astronomy (Quantum Information)

Waterloo, Ontario, Canada, 2016

Author's Declaration

I hereby declare that I am the sole author of this thesis. This is a true copy of the thesis, including any required final revisions, as accepted by my examiners.

I understand that my thesis may be made electronically available to the public.

Abstract

Many-body systems are well known throughout physics to be hard problems to exactly solve, but much of this is folklore resulting from the lack of an analytic solution to these systems. This thesis attempts to classify the complexity inherent in many of these systems, and give quantitative results for why the problems are hard. In particular, we analyze the many-particle system corresponding to a multi-particle quantum walk, showing that the time evolution of such systems on a polynomial sized graph is universal for quantum computation, and thus determining how a particular state evolves is as hard as an arbitrary quantum computation. We then analyze the ground energy properties of related systems, showing that for bosons, bounding the ground energy of the same Hamiltonian with a fixed number of particles is **QMA**-complete. Similar techniques also show that the single-particle case has related computational power. Finally, a nice relation between spin systems and hard-core bosons can be used to show that bounding the smallest eigenvalue of the XY-model is **QMA**-complete.

Acknowledgements

I would like to thank my advisor, Andrew Childs, for his great help and support during my graduate studies at the University of Waterloo. His research guidance and support during hard times was very helpful, and this thesis would not be written without his support.

I would also like to thank David Gosset, who acted as a sounding board, and guided much of my research. He was a fountain of useful ideas, with an ability to conceive of complex solutions to difficult problems. His work ethic made many of the results in this thesis possible.

I'd like to thank Norbert Lütkenhaus, who helped get me back on my feet during troubled times, as well as Chris Pugh, who got me started and kept me going. To all of my friends at the Institute for Quantum Computing, from the optics groups of my early years to the eclectic bunch now eating cookies at 4, thank you.

Dedication

This is dedicated to the ones I love, my family and friends.

Table of Contents

List of Figures

Chapter 1

Introduction

The first thing I would like to mention is that this thesis is not complete. I ran out of time and was unable to complete the thesis. I had to submit something to the graduate office, and this is it. I do apologize, and I expect to have major revisions required. At this point, I do not believe that any one chapter is actually completed, and in fact many of the state results have not been completely written up. Basically, I recognize that this thesis is defensible as is, and am planning major revisions.

When examining the physics literature, the three-body problem is extremely well known, as is its usual impossibility to solve. In these cases, people generally mean that there does not exist a closed form solution in general, but can we quantify exactly how hard the problem is?

In particular, if one is working with some particular many body system, how hard is it to compute various attributes about the system. I'd really like to know the answer.

While such questions have not generally been asked in physics, classifying the computation power of a problem in terms of the necessary resources in order to solve it is a foundational idea in computer science. The entire field of computational complexity arose in the attempt to classify these problems. This thesis will attempt to use tools founded in this field and apply them to the various physical systems.

1.1 Quantum walk

Over the years, randomness proved itself as a useful tool, allowing access to physical systems that are too large to accurately simulate. By assuming the dynamics of such systems can be modelled as independent events, Markov chains provide insight to the structure of the dynamics. These ideas can then be cast into the framework of random walk, where the generating Markov matrix describes the weighted, directed graph on which the walk takes place.

Using the principle of "put quantum in front," one can then analyze what happens when the random dynamics are replaced by unitary dynamics. This actually poses a little difficulty, as there is no obvious way to make a random walk have unitary dynamics. In particular, there are many ways that the particle can arrive at one particular vertex in the underlying graph, and thus after arriving at the vertex there is no way to reverse the dynamics.

There are (at least) two ways to get around this. One continues with the discrete-time structure of a random walk, and keeps track of a "direction" in addition to the position of the particle. Each step of the walk is then a movement in the chosen direction followed by a unitary update to the direction register. These Szegedy walks are extremely common in the literature, and go by the name of "discrete-time quantum walk."

Another way to get around the reversibility problem is to generalize the continuous-time model of random walks. In particular, assuming that the underlying graph is symmetric, we look at the unitary generated by taking the adjacency matrix of the graph as a Hamiltonian. This is a one-parameter family of unitaries, and thus easily reversible. The "continuous-time quantum walk" model is the one we'll be focussing on in this thesis.

1.2 Many-body systems

Everything in nature has many particles, and the reason that physicists are so interested in smaller dynamics is the relatively understandable fact that many-body systems are extremely complicated. The entire branch of statistical physics was created in an attempt to make a coherent understanding of these large systems, since writing down the dynamics of every particle is impossible in general.

Along these lines, many models of simple interactions between particles exist in the literature. As an example, on can consider a lattice of occupation sites, where bosons can sit at any point in the lattice. Without interactions between the particles, the dynamics are easily understood as decoupled plane waves. However, by including even a simple energy penalty when multiple particles occupy the same location (i.e. particles don't like to bunch), we no longer have a closed form solution and are required to look at things such as the Bethe ansatz.

1.3 Computational complexity

While this is a physics thesis, much of my work is focused on understanding the computational power of these physical systems, and as such an understanding of the classification framework is in order. I should explain some of the motivation behind this area of research, giving a bit of background for the physicist.

These classifications are generally described by languages, or subsets of all possible 0-1 strings. In particular, given some string x, the requisite power in order to determine whether the string belongs to a language or not describes the complexity of the language.

1.4 Layout of thesis

With all of this background in mind, we'd like to give a basic understanding of what this thesis is going to entail. The underlying theme of this thesis is to understand the computational power of quantum walk, when restricted to various questions. As such, we will look both at the single and multi-particle cases. Note that most of this thesis is based on the papers [15], [**?**], [16], and [**?**]. While I am an author on all four papers, Andrew Childs and David Gosset

are co-authors on all four papers, while Daniel Nagaj and Mouktik Raha are co-authors on [**?**].

However, in Chapter 2, we will at first define various terms related to computational complexity that will be of use to us, as well as some lemmas that might be of independent interest.

In Chapter **??** we will describe single-particle scattering on graphs. In particular, we will give some simple motivations and understanding of what is going on in a simple case. This chapter will also describe some basic algorithmic uses for the single particle case. This paper will include some review of previous papers [**TO DO:** *Cite quantum walk papers*] that I have not written, as well as a broad overview of techniques used in [15] and [**?**].

At this point, we will transition into understanding the computational power of time evolving according to single- and multi-particle quantum walks. In particular, Chapter **??** will include a novel proof that quantum walk of a single particle on an exponentially sized graph for polynomial time is universal quantum computing, using techniques slightly different than that of [**?**][**TO DO:** *Find correct citation*] . While this proof has not been submitted as a paper in any journal, it makes use of many of the techniques of [15]. In Chapter **??**, we extend this result to show that a multi-particle quantum walk with almost any finite-range interaction is universal for quantum computing, the main result of [15].

With the computational power of time evolved quantum walk, we will want to understand the ground energy problem of the quantum walk. In particular, Chapter **??** shows that determining whether the ground energy of a sparse, row-computable graph is above or below some threshold is **QMA**-complete, which is work is found in an appendix of the [16] paper. As this corresponds exactly to the ground energy problem of a single particle quantum walk on an exponentially large, but specifiable, graph, this shows that the ground energy problem for single-particle quantum walk is **QMA**-complete. Chapter **??** then expands on this result, and shows that the ground energy problem for multi-particle quantum walk with bosons on simple graphs is **QMA**complete. While this result follows the proof techniques of [15] and [**?**], the extension to arbitrary finite-range interactions for bosons is novel.

With the quantum walk interactions out of the way, Chapter 8 makes use of these results on the multi-particle ground energy problem to study the ground energy problem of various spin systems.

Finally, Chapter **??** concludes with some discussion of these results, along with some avenues for future research.

Chapter 2

Mathematical Preliminaries

Several topics in this thesis require a background that not all researcher will have experience in. Especially as this thesis is multi-disciplinary, I would like to include at least some basic introduction to various physical and computer science topics. Additionally, several lemmas used in this manuscript might be of independent interest, as their applicability is not restricted to the various models studied in this thesis.

2.1 Mathematical notation

Perhaps the most simple point that I would like to raise before the thesis begins in ernest is the notation that I will use throughout the paper. Much of the paper uses notation not necessarily standard in every area of physics or computer science, and I want to make sure that no confusion occurs. I will assume that various notations that are common do not need to be described, such at $\mathcal{H}$ describing a Hilbert space, or that $\mathbb{I}$ describes a the identity operator on a particular Hilbert space.

The first such notation will be for the shorthand definition of sets of particular size. Namely,

$$[k] := \{0, 1, \cdots, k-1\}. \tag{2.1}$$

This is a set of size k, with the elements ordered and labeled by the integers from 0 to $k-1$. We will often think of these as elements from $\mathbb{Z}_k$, with addition and multiplication defined over the integers modulo k.

Often this paper will want to investigate systems with many particles, and we will want an operator to only act nontrivially on one particle. In particular, if we have a Hilbert space $\mathcal{H}_{\text{total}} = \mathcal{H}_{\text{single}}^{\otimes N}$ that consists of N copies of some single Hilbert space, and if we have an operator M that acts on $\mathcal{H}_{\text{single}}$, we can define an operator $M^{(w)}$ that acts nontrivially only on the w-th copy of $\mathcal{H}_{\text{single}}$, namely

$$M^{(w)} = \mathbb{I}^{\otimes w-1} \otimes M \otimes \mathbb{I}^{N-w}. \tag{2.2}$$

In this manner, only the w-th copy of $\mathcal{H}_{\text{single}}$ is effected.

As we will also be working with graphs, we will want to note that the letter G usually denotes a particular graph. Further, $A(G)$ describes the adjacency matrix of the graph G.

$V(G)$ then describes the vertex set of G, and $E(G)$ describes the edge set of G. Note that this thesis will always deal with undirected graphs, with at most a single edge between vertices. As such, the adjacency matrix $A(G)$ will be a symmetric 0-1 matrix. We will at times want to work with a simple graph, in which self-loops do not occur, but unless otherwise specified a graph G might contain self-loops.

Much of the work in this thesis, especially when describing the ground energy of particular Hamiltonian, deals only with positive semi-definite operators. As such, if A is a positive semi-definite matrix, then $\gamma(A)$ is the smallest non-zero eigenvalue. Note that if A has a 0-eigenvalue, then this corresponds to the energy gap between the ground state and the first excited state, but if A does not have a 0-eigenvalue then this is simply the smallest eigenvalue of A.

Finally, let us assume that A acts on a Hilbert space $\mathcal{H}$, and that $\mathcal{S}$ is a subspace of $\mathcal{H}$. We will then write the restriction of A to the subspace $\mathcal{S}$ as $A\big|_{\mathcal{S}}$.

Big O notation.

2.2 Quantum information

As this thesis is about quantum information, I will assume a familiarity with the basics

2.3 Indistinguishable particles

A foundational aspect of this thesis is understanding how defining the small scale interactions between multiple particles effects the large scale behavior of the system. As we want to define the large scale systems in terms of these small systems, the Hamiltonians that we will be interested in will have symmetries when we permute the different particles.

More concretely, when we restrict our Hamiltonians to the case with n particles, each particle will have the same (finite) Hilbert space to work with, and the Hamiltonian will be symmetric under a relabelling of the particles. Explicitly, we will have that each particle will have a Hilbert space $\mathcal{H}_{\text{ind}} = \mathbb{C}^d$ for some dimension d, so that the total Hilbert space of n particles is $\mathcal{H}_{\text{tot}} = \mathcal{H}_{\text{ind}}^{\otimes n} = \mathbb{C}^{dn}$, and the Hamiltonian is an operator on $\mathcal{H}_{\text{tot}}$ that commutes with the operators that swap the individual particle Hilbert spaces.

[**TO DO:** *Make this more coherent*]

The reason that we do this is the simple fact that particles are almost always indistinguishable. As such, any initial state for these multiparticle Hamiltonians will have the same symmetry as the underlying particles.

2.4 Complexity Theory

While this thesis is for the physics department, many of the results require some basic quantum complexity theory. In particular, the computer science idea for classification of computational problems in terms of the requisite resources gives a particularly nice interpretation of why certain physical systems don't equilibrate, and give a simple explanation on why certain systems do not have a known closed form solution.

This is a simple introduction, with a focus designed to make the rest of this thesis comprehensible to those without a background in complexity theory. For a more formal introduction to Complexity Theory, I would recommend [29], with a more in depth review found in [3]. For a focus on complexity as found in quantum information, I would recommend [31].

2.4.1 Languages and promise problems

The main foundation of computational complexity is in the classification of languages based on the requisited resources to determine whether some string is in a language. Unfortunately, this requires the definition of many of these terms.

In particular, what exactly is a string? Any person who has taken a basic programming class knows that a string is simply a word, but the mathematical definition is slightly more complicated. In particular, we first need to define an alphabet, and then define a string over a particular alphabet.

Definition 1 (Alphabet)**.** An alphabet is a finite collection of symbols.

Usually, an arbitrary alphabet is denoted by Γ, while the binary alphabet is denoted by $\Sigma = \{0, 1\}$. The chosen alphabet has no impact on a particular complexity result, as any finite alphabet can be represented via the binary alphabet with overhead that is logarithmic in the size of the original alphabet (essentially, just use a binary encoding of the new alphabet).

With this definition of an alphabet, a string is simply a finite sequence of elements from the alphabet. In particular, we define Γ^n to be all length n sequences of elements from Γ, and then define

$$\Gamma^* = \bigcup_{n=0}^{\infty} \Gamma^n. \tag{2.3}$$

With this, Γ^* is the set of all strings over Γ.

Computational complexity then deals with understanding subsets of these strings. In particular, let Π_{yes} be a subset of Γ^*. The language problem related to Π_{yes} is to determine whether a given string $x \in \Gamma^*$ is contained within Π_{yes} or not. This can be trivial, such as for the case of $\Pi_{\text{yes}} = \Gamma^*$, or it can be impossible, such as in the case of the famous Halting Problem.

Related to these language problems are promise problems, in which there are two subsets of Γ^*, namely Π_{yes} and Π_{no}, such that $\Pi_{\text{yes}} \cap \Pi_{\text{no}} = \emptyset$. We are then *promised* that the $x \in \Gamma^*$ that we need to sort is contained either $\Pi_{\text{yes}} \cup \Pi_{\text{no}}$. This generally opens up some more interesting problems, as without this restriction certain complexity classes do not make sense.

[**TO DO:** *revise and revisit*]

2.4.2 Turing machines

Up to this point, we have only discussed classifications of strings, and stated that we will want to understand the various resources required to sort a given string into one of two

different sets, but we have not explained how these resources are defined. There are various ways to do this, depending on the various computational model one is interested in, but to give the most intuition we will need to define a Turing Machine. These machines are a mathematical construction that allow for the explicit definition of algorithms.

At their most basic level, a Turing machine is simply a finite program along with a (countably) infinite tape that allows the machine to store information. The input to the algorithm is initially written on the tape, and the machine starts in some initial configuration. The machine can only access it's internal memory along with a single character at a time from the infinite tape, and the program progresses by changing the internal state of the machine, changing one character on the tape, and moving along the tape. While extremely limited, these machines have so far captured our ideas of computation.

Formally, a Turing-machine is M is described by a tuple (Γ, Q, δ), where Γ is a finite set of symbol's that can be written on the infinite tape, Q is a set of possible internal states that M can store as internal memory, and δ is a function $Q \times \Gamma \to Q \times \Gamma \times \{L, S, R\}$ describing the required action of the machine M. Included in Q are two special "halting" states generally labeled `accept` and `reject`, such that the machine stops operating if it ever enters these two states, and the machine either accepts or rejects the current string. Note that we always assume that the alphabet contains a special character $\llcorner$that is not used for the input but denotes empty space along the infinite tape after the input string.

During an actual computation, a Turing Machine always starts with its internal state in a specified position, with the string used for input on the initial segment of the infinite tape and the special character $\llcorner$on every character after the input. Additionally, the pointer of the machine is located at the beginning of the tape, so that the machine is able to start reading the input (if needed). At each time step the machine then applies the transition function, updating its internal state, the character located at the current position of the tape, along with the current position of the tape until the machine reaches one of its halting states.

Note that there are several variations on these Turing Machines, such as those that have multiple infinite tapes instead of just one, and one that can move to an arbitrary position along the tape. These variations do not change the overall computational power of the model, just make it slightly more efficient. This definition is perhaps the most simple, and will suffice for now.

[**TO DO:** *get a picture of a TM here*]

One slight modification that will be useful for us is machines that compute a particular function. In particular, for a given function $f : \Gamma^* \to \Gamma^*$, we say that a Turing Machine M computes the function f if for all inputs x, the machine eventually halts and after it halts the tape will have $f(x)$ on the output tape (and nothing else).

2.4.2.1 Resources

With an explicit definition of Turing Machines, we also want to have some way to quantify the amount of resources used by a computation. Since each machine is expected to work on strings of arbitrary length, we somehow need to quantify the resources in terms of the input to a given string. So far, the important quantity in these resource problems has been the length of an input string x. Basically, the number of characters has been the interesting aspect to measure, since any machine will at least need to read the string.

With this n as the yardstick for any of our measurements, we then need to measure the length of the actual computation. In general, there are two ways to measure this length: the number of transitions that the computation used before it halted (as a measure of time), or else the number of elements of the tape that the machine visited during its computation (as a measure of space). It is important to realize that the exact value of these resources depend on the definitions used for the machine, such as the alphabet size or the number of internal states. As such, we will generally not be interested in the exact value for a given input, but will be more interested in the asymptotic scaling of the resources.

These requisite resources will generally be something of the form $\mathcal{O}(f(n))$ for some easily computable function f such as a polynomial or an exponential in n. These various scalings will give us a nice method of classifying the difficulty of computational problems. In general, we will say that a specific Turing Machine M runs in time $f(n)$ if for all inputs it halts in time $t(x)$ and $t(x) \in \mathcal{O}(f(n))$.

2.4.2.2 Uniform circuit families

While Turing Machines are sufficient for classical computation, when we want to describe some quantum complexity classes it will be useful to instead discuss quantum circuits. However, an important aspect of Turing Machines is that they are defined independently of the size of the input, while circuits need to have unique definitions for all different input sizes.

One might be tempted to simply define a computation via circuits by whether or not there exists a circuit of a given length, but this ends up giving an unreasonable amount of power to the computational model. In particular, the algorithm can hide computation in the definition of the circuit, as opposed to the actual running of the circuit itself.

To get around this, we will need to compute the circuit for the computation given the length. Namely, we will have a Turing Machine take as input the string length in unary, and the machine will output a description of the circuit. I won't go into the details here, but the

Definition 2 (Uniform family of circuits)**.** A collection $\{C_x : x \in S \subseteq \Sigma^*\}$ of circuits is a (polynomial-time) *uniform family of circuits* if there exists a deterministic Turing Machine M such that

- M runs in polynomial time.
- For all $x \in S$, M outputs a description of C_x.

Note that this definition makes no reference to the type of circuit, although we will generally assume that the circuit comes from some specific gate set.

[**TO DO:** *completely update this*]

2.4.3 Useful complexity classes

Once we have an understanding of what defines a relation, and how these are related, we can attempt to classify those languages that require different resources in order to solve.

2.4.3.1 Classical complexity classes

Perhaps the most well known question in computational complexity is the **P**vs **NP**problem. However, what exactly are these classes. At a most basic level, one can think of **P**as those classification problems that have an efficient classical solution, while **NP**are those that can be checked in an efficient manner.

Definition 3 (P). A promise problem $\mathcal{A} = (\mathcal{A}_{\text{yes}}, \mathcal{A}_{\text{no}})$ is in the class **P**if there exists a polynomial-time Turing Machine M such that $M(x)$ accepts x if and only if $x \in \mathcal{A}_{\text{yes}}$.

Note that the Turing Machine M is required to halt on all inputs, and thus this is exactly what we mean by a polynomial-computation. Some simple examples of languages in ¶are [**TO DO:** *find* **P***languages*]

Definition 4 (NP). A promise problem $\mathcal{A} = (\mathcal{A}_{\text{yes}}, \mathcal{A}_{\text{no}})$ is in the class **NP**if there exists a polynomial q and a polynomial-time Turing Machine M such that

- if $x \in \mathcal{A}_{\text{yes}}$, then there exists a string $y \in \Sigma^{q(|x|)}$ such that $M(x, y)$ accepts.
- if $x \in \mathcal{A}_{\text{no}}$, then for all strings $y \in \Sigma^{(q(|x|)}$, $M(x, y)$ rejects.

Essentially, a language is in **NP**if a given string can be proven to be in the language. This includes useful problems such as whether a given graph has a 3-coloring, whether an integer p has at least k prime factors, and all problems in ¶.

2.4.3.2 Bounded-Error Quantum Polynomial Time

With these classical problems now defined, we will want to understand what happens when we include quantum mechanics. There is a way to define a quantum Turing machine, in an analog to the classical case, but the current state of the art has instead gone toward using quantum circuits instead.

Intuitively, the idea behind Bounded-Error Quantum Polynomial Time (**BQP**) consists of those problems that can be solved by a quantum computer efficiently. However, we need to somehow encode the circuit

Definition 5 (BQP). A promise problem $\mathcal{A} = (\mathcal{A}_{\text{yes}}, \mathcal{A}_{\text{no}})$ if there exist a uniform family of quantum circuits $Q = \{Q_n : n \in \mathbb{N}\}$ such that

- If $x \in \mathcal{A}_{\text{yes}}$, then $Q_{|x|}(|\, x\rangle) \geq \frac{2}{3}$.
- If $x \in \mathcal{A}_{\text{no}}$, then $Q_{|x|}(|\, x\rangle) \leq \frac{1}{3}$.

Note that these t

2.4.3.3 Quantum Merlin-Arthur

In addition to having an understanding of when a quantum computer can solve a particular problem, we will also want an understanding of those problems that most likely cannot be

Definition 6 (QMA). A promise problem $\mathcal{A} = (\mathcal{A}_{\text{yes}}, \mathcal{A}_{\text{no}})$ if there exists a uniform family of quantum circuits $Q = \{Q_n : n \in \mathbb{N}\}$ such that

- If $x \in \mathcal{A}_{\text{yes}}$, then there exists a state $|\psi\rangle \in \mathbb{C}^{p(|x|)}$ such that $Q_{|x|}(|x\rangle, |\psi\rangle) \geq \frac{2}{3}$.
- If $x \in \mathcal{A}_{\text{no}}$, then for all states $|\psi\rangle \in \mathbb{C}^{p(|x|)}$, $Q_{|x|}(|x\rangle, |\psi\rangle) \leq \frac{1}{3}$.

Intuitively, this is like the class **NP**in that the circuit only accepts if there exists a proof that the input is in the language. This proof might be extremely difficult to construct, but it still exists.

2.4.3.4 Reductions and Complete Problems

While we are interested in these complexity classes, it is often difficult to work with the exact definitions used. As an example, in the definition of **NP**, to show something for all of the class we would somehow need to encode the entire computation of the Turing machine in our proof. One way to get around this is via reductions.

Essentially a reduction is a polynomial-time computable function from one computational problem to another. Because this reduction is easy to compute, if we can solve the second problem, then we can also solve the first problem. More concretely, let $\mathcal{A} = (\mathcal{A}_{\text{yes}}, \mathcal{A}_{\text{no}}$ and $\mathcal{B} = (\mathcal{B}_{\text{yes}}, \mathcal{B}_{\text{no}})$ be two promise problems. We say that there

2.5 Hamiltonian simulation

[**TO DO:** *Give a high level overview of the simulation algorithm?*]

With the definitions of the various complexity classes, and in particular defining complete problems for these classes, we will find that we often need to reduce one problem to another, in order to show that a given problem is contained within a complexity class. Of particular interest to us will be the simulation of Hamiltonian dynamics, as all of the problems in this thesis are defined in terms of Hamiltonians.

In particular, we will need to show how to simulate the evolution of a sparse, row-computable Hamiltonian on a given state $|\phi\rangle$. The state $|\phi\rangle$ might be a en efficiently computable state, or it might be a provided to us in a **QMA**-style procedure, but we are really only interested in understanding the dynamics.

The problem of simulating Hamiltonian dynamics has been featured rather heavily in the literature, as it was the original motivation that Feynman gave for quantum computers [20, 21]. In particular, Lloyd showed how to simulate sums of local operators [23], and this idea was generalized by Aharanov and Ta-Shma to (efficiently computable) sparse Hamiltonians [1]. Since then, various schemes have improved the requirements on time [4, 32, 5], as well as the dependence on the precision [6, 7] and various other avenues of research [10, 25], have managed to greatly improve our ability to simulate quantum dynamics.

While Hamiltonians that are a sum of local operations are relatively easy to understand, d-sparse Hamiltonians are relatively more complex. The reason that much of the literature has focused on local Hamiltonians is that they are easy to specify, as we need only write down each of the local Hamiltonians. In particular, they are succinct representations for Hamiltonians on an exponential-sized Hilbert space, such that each non-zero term of

the Hamiltonian corresponding to a specific basis vector can be determined efficiently. Additionally, these local-Hamiltonians are further restricted to only have non-zero transition amplitudes for states that satisfy some locality conditions, but for the purposes of simulation the succinctness property is what we care about.

Namely, the fact that a local Hamiltonian is succinctly representable is all that is used in the algorithms for simulating Hamiltonian dynamics. As such, if we can generalize these properties, we can generalize the Hamiltonians that we can simulate. A row-computable, d-spare matrix is such a generalization, in which each row of a given Hamiltonian has at most d non-zero entries, and there exists some efficiently computable function $f_i(x)$ that outputs the value (and position) of the ith nonzero entry of the xth row. Note that k-local Hamiltonians are d-sparse (for some d depending on the local dimension and connectivity), and easily row-computable; this is the natural generalization.

The basic idea behind most simulation algorithms is to color each non-zero matrix element of the Hamiltonian H so that the matrix corresponding to each color satisfies some technical property, show how to simulate each color individually for a short period of time, and then show how to combine the individual simulations into a simulation of the entire Hamiltonian. The current state of the art [8] uses several techniques, including quantum walk algorithms, simulations of linear combinations of unitaries, and Bessel functions, but their main result is the following

Theorem 1 (Theorem 1 of [8])**.** *A d-sparse Hamiltonian H acting on n qubits can be simulated for time t within error ϵ with*

$$\mathcal{O}\Big(\tau \frac{\log(\tau/\epsilon)}{\log\log(\tau/\epsilon)}\Big) \tag{2.4}$$

queries and

$$\mathcal{O}\Big(\tau \big[n + \log^{5/2}(\tau/\epsilon)\big] \frac{\log(\tau/\epsilon)}{\log\log(\tau/\epsilon)}\Big) \tag{2.5}$$

additional 2-qubit gates, where $\tau := d\|H\|_{\max} t$.

Note that the theorem was proved in the black box model, where the function f was provided via black box. Assume that f is superlinear in both n and $\log^{5/2}(\tau/\epsilon)$, the time-complexity for simulating such a Hamiltonian is simply the product of the complexity of f with (2.4). Note that if f is efficient to compute, this is an efficient simulation of the Hamiltonian dynamics.

2.6 Various Mathematical Lemmas

In addition to these various complexity results, it will also be useful to have a list of certain mathematical lemmas that will be used several times in the thesis. These lemmas might also be of independent interest.

2.6.1 Truncation Lemma

Perhaps the first such lemma we called the truncation lemma. The idea behind this lemma is to approximate the evolution of a state under some particular Hamiltonian with another, where the differences between the two Hamiltonians only occur far from the support of the given state. One would expect that since the state must evolve "far" in order to reach the differs between the two Hamiltonians, the evolution between the two will be close. This lemma makes this intuition precise.

Lemma 1 (Truncation Lemma)**.** *Let H be a Hamiltonian acting on a Hilbertspace $\mathcal{H}$ and let $|\Phi\rangle \in \mathcal{H}$ be a normalized state. Let $\mathcal{K}$ be a subspace of $\mathcal{H}$, let P be the projector onto $\mathcal{K}$, and let $\tilde{H} = PHP$ be the Hamiltonian within this subspace. Suppose that, for some $T > 0$, $W \in \{H, \tilde{H}\}$, $N_0 \in \natural$, and $\delta > 0$, we have, for all $0 \leq t \leq T$,*

$$e^{-iWt}|\Phi\rangle = |\gamma(t)\rangle + |\epsilon(t)\rangle \text{ with } \||\epsilon(t)\rangle\| \leq \delta$$

and

$$(1-P)H^r|\gamma(t)\rangle = 0 \text{ for all } r \in \{0, 1, \ldots, N_0 - 1\}.$$

Then, for all $0 \leq t \leq T$,

$$\left\| \left(e^{-iHt} - e^{-i\tilde{H}t} \right) |\Phi\rangle \right\| \leq \left(\frac{4e\|H\|t}{N_0} + 2 \right) \left(\delta + 2^{-N_0}(1+\delta) \right).$$

This lemma actually combines two different methods. The first assumes that the

Proposition 1. *Let H be a Hamiltonian acting on a Hilbert space $\mathcal{H}$, and let $|\Phi\rangle \in \mathcal{H}$ be a normalized state. Let $\mathcal{K}$ be a subspace of $\mathcal{H}$ such that there exists an $N_0 \in \natural$ so that for all $|\alpha\rangle \in \mathcal{K}^\perp$ and for all $n \in \{0, 1, 2, \ldots, N_0 - 1\}$, $\langle\alpha|H^n|\Phi\rangle = 0$. Let P be the projector onto $\mathcal{K}$ and let $\tilde{H} = PHP$ be the Hamiltonian within this subspace. Then*

$$\|e^{-it\tilde{H}}|\Phi\rangle - e^{-itH}|\Phi\rangle\| \leq 2\left(\frac{e\|H\|t}{N_0} \right)^{N_0}.$$

Proof. Define $|\Phi(t)\rangle$ and $|\tilde{\Phi}(t)\rangle$ as

$$|\Phi(t)\rangle = e^{-itH}|\Phi\rangle = \sum_{k=0}^{\infty} \frac{(-it)^k}{k!} H^k|\Phi\rangle \qquad |\tilde{\Phi}(t)\rangle = e^{-it\tilde{H}}|\Phi\rangle = \sum_{k=0}^{\infty} \frac{(-it)^k}{k!} \tilde{H}^k|\Phi\rangle.$$

Note that by assumption, $\tilde{H}^k|\Phi\rangle = H^k|\Phi\rangle$ for all $k < N_0$, and thus the first N_0 terms in

the two above sums are equal. Looking at the difference between these two states, we have

$$\begin{aligned}
\| |\Phi(t)\rangle - |\tilde{\Phi}(t)\rangle \| &= \left\| \sum_{k=0}^{\infty} \frac{(-it)^k}{k!} \left(H^k - \tilde{H}^k \right) |\Phi\rangle \right\| \\
&= \left\| \sum_{k=0}^{N_0-1} \frac{(-it)^k}{k!} \left(H^k - \tilde{H}^k \right) |\Phi\rangle - \sum_{k=N_0}^{\infty} \frac{(-it)^k}{k!} \left(H^k - \tilde{H}^k \right) |\Phi\rangle \right\| \\
&\leq \sum_{k=N_0}^{\infty} \frac{t^k}{k!} \left(\|H\|^k + \|\tilde{H}\|^k \right) \\
&\leq 2 \sum_{k=N_0}^{\infty} \frac{t^k}{k!} \|H\|^k
\end{aligned}$$

where the last step uses the fact that $\|\tilde{H}\| \leq \|P\|\|H\|\|P\| = \|H\|$. Thus for any $c \geq 1$, we have

$$\begin{aligned}
\| |\Phi(t)\rangle - |\tilde{\Phi}(t)\rangle \| &\leq \frac{2}{c^{N_0}} \sum_{k=N_0}^{\infty} \frac{(ct)^k}{k!} \|H\|^k \\
&\leq \frac{2}{c^{N_0}} \exp(ct\|H\|).
\end{aligned}$$

We obtain the best bound by choosing $c = N_0/\|Ht\|$, which gives

$$\| |\Phi(t)\rangle - |\tilde{\Phi}(t)\rangle \| \leq 2 \left(\frac{e\|H\|t}{N_0} \right)^{N_0}$$

as claimed. (If $c < 1$ then the bound is trivial.) □

Proposition 2. *Let $U_1, \ldots, U_n$ and $V_1, \ldots, V_n$ be unitary operators. Then for any $|\psi\rangle$,*

$$\left\| \left(\prod_{i=n}^{1} U_i - \prod_{i=n}^{1} V_i \right) |\psi\rangle \right\| \leq \sum_{j=1}^{n} \left\| (U_j - V_j) \prod_{i=j-1}^{1} U_i |\psi\rangle \right\|. \tag{2.6}$$

Proof. The proof is by induction on n. The case $n = 1$ is obvious. For the induction step, we have

$$\left\| \left(\prod_{i=n}^{1} U_i - \prod_{i=n}^{1} V_i \right) |\psi\rangle \right\| = \left\| \left(\prod_{i=n}^{1} U_i - V_n \prod_{i=n-1}^{1} U_i + V_n \prod_{i=n-1}^{1} U_i - \prod_{i=n}^{1} V_i \right) |\psi\rangle \right\| \tag{2.7}$$

$$\leq \left\| (U_n - V_n) \prod_{i=n-1}^{1} U_i |\psi\rangle \right\| + \left\| \left(\prod_{i=n-1}^{1} U_i - \prod_{i=n-1}^{1} V_i \right) |\psi\rangle \right\| \tag{2.8}$$

$$\leq \sum_{j=1}^{n} \left\| (U_j - V_j) \prod_{i=j-1}^{1} U_i |\psi\rangle \right\| \tag{2.9}$$

where the last step uses the induction hypothesis. □

Proof of Lemma **??**. For $M \in \natural$ write

$$\begin{aligned}
\|(e^{-iHt} - e^{-i\tilde{H}t})|\,\Phi\rangle\| &= \left\| \left(\left(e^{-iH\frac{t}{M}}\right)^M - \left(e^{-i\tilde{H}\frac{t}{M}}\right)^M \right) |\,\Phi\rangle \right\| \\
&\leq \sum_{j=1}^{M} \left\| \left(e^{-iH\frac{t}{M}} - e^{-i\tilde{H}\frac{t}{M}}\right) e^{-iW(j-1)\frac{t}{M}} |\,\Phi\rangle \right\| \\
&\leq \sum_{j=1}^{M} \left\| \left(e^{-iH\frac{t}{M}} - e^{-i\tilde{H}\frac{t}{M}}\right) \left(|\,\gamma(\tfrac{(j-1)t}{M})\rangle + |\,\epsilon(\tfrac{(j-1)t}{M})\rangle \right) \right\| \\
&\leq 2M\delta + \sum_{j=1}^{M} \left\| \left(e^{-iH\frac{t}{M}} - e^{-i\tilde{H}\frac{t}{M}}\right) \frac{|\,\gamma(\frac{(j-1)t}{M})\rangle}{\left\||\,\gamma(\frac{(j-1)t}{M})\rangle\right\|} \right\| \left\||\,\gamma(\tfrac{(j-1)t}{M})\rangle\right\| \\
&\leq 2M\delta + 2M \left(\frac{e\|H\|t}{MN_0}\right)^{N_0} (1+\delta)
\end{aligned}$$

where in the second line we have used Proposition **??** and in the last step we have used Proposition **??** and the fact that $\||\gamma(t)\rangle\| \leq 1 + \delta$. Now, for some $\eta > 1$, choose

$$M = \left\lceil \frac{\eta e \|H\| t}{N_0} \right\rceil$$

for $0 < t \leq T$ to get

$$\begin{aligned}
\|(e^{-iHt} - e^{-i\tilde{H}t})|\,\Phi\rangle\| &\leq 2M \left(\delta + \eta^{-N_0}(1+\delta)\right) \\
&\leq 2 \left(\frac{\eta e \|H\| t}{N_0} + 1 \right) \left(\delta + \eta^{-N_0}(1+\delta)\right).
\end{aligned}$$

The choice $\eta = 2$ gives the stated conclusion. □

Note that it would be slightly better to take a smaller value of η. However, this does not significantly improve the final result; the above bound is simpler and sufficient for our purposes.

2.6.2 Nullspace Projection Lemma

When we discuss the ground spaces and ground energies of various Hamiltonians, we will often want to know what happens to the ground spaces and ground energies when two such Hamiltonians are added together (such as adding penalties enforcing particular initial states). As such, the Nullspace Projection Lemma exactly discusses how such systems add together. As far as I am aware this lemma was initially used (implicitly) by Mizel et. al. [**TO DO:** *find correct reference*] We then used this in our proof of the **QMA**-completeness for the Bose-Hubbard model. We then found an additional place that used a similar lemma, with slightly better bounds. While the improvement is minor, here is a proof of the improved bound (and note that the improvement was left as a proof for the reader in the newer result).

Lemma 2 (Nullspace Projection Lemma)**.** *Let H_A and H_B be positive semi-definite matrices. Suppose that the nullspace, S, of H_A is nonempty, and that*

$$\gamma\big(H_B|_S\big) \geq c > 0 \qquad \textit{and} \qquad \gamma(H_A) \geq d > 0. \tag{2.10}$$

Then,

$$\gamma(H_A + H_B) \geq \frac{cd}{d + \|H_B\|}. \tag{2.11}$$

Proof. Let $|\psi\rangle$ be a normalized state satisfying

$$\langle\psi|H_A + H_B|\psi\rangle = \gamma(H_A + H_B). \tag{2.12}$$

Let Π_S be the projector onto the nullspace of H_A. First suppose that $\Pi_S|\psi\rangle = 0$, in which case

$$\langle\psi|H_A + H_B|\psi\rangle \geq \langle\psi|H_A|\psi\rangle \geq \gamma(H_A) \tag{2.13}$$

and the result follows. On the other hand, if $\Pi_S|\psi\rangle \neq 0$ then we can write

$$|\psi\rangle = \alpha|a\rangle + \beta|a^\perp\rangle \tag{2.14}$$

with $|\alpha|^2 + |\beta|^2 = 1$, $\alpha \neq 0$, and two normalized states $|a\rangle$ and $|a^\perp\rangle$ such that $|a\rangle \in S$ and $|a^\perp\rangle \in S^\perp$. (If $\beta = 0$ then we may choose $|a^\perp\rangle$ to be an arbitrary state in $S^\perp$ but in the following we fix one specific choice for concreteness.) Note that any state $|\phi\rangle$ in the nullspace of $H_A + H_B$ satisfies $H_A|\phi\rangle = 0$ and hence $\langle\phi|a^\perp\rangle = 0$. Since $\langle\phi|\psi\rangle = 0$ and $\alpha \neq 0$ we also see that $\langle\phi|a\rangle = 0$. Hence any state

$$|f(q, r)\rangle = q|a\rangle + r|a^\perp\rangle \tag{2.15}$$

is orthogonal to the nullspace of $H_A + H_B$, and

$$\gamma(H_A + H_B) = \min_{|q|^2+|r|^2=1} \langle f(q, r)|H_A + H_B|f(q, r)\rangle. \tag{2.16}$$

Within the subspace Q spanned by $|\,a\,\rangle$ and $|\,a^\perp\,\rangle$, note that

$$H_A|_Q = \begin{pmatrix} w & v^* \\ v & z \end{pmatrix} \qquad H_B|_Q = \begin{pmatrix} 0 & 0 \\ 0 & y \end{pmatrix} \tag{2.17}$$

where $w = \langle a|H_B|a\rangle$, $v = \langle a^\perp|H_B|a\rangle$, $y = \langle a^\perp|H_A|a^\perp\rangle$, and $z = \langle a^\perp|H_B|a^\perp\rangle$, and that we are interested in the smaller eigenvalue of

$$M = H_A|_Q + H_B|_Q = \begin{pmatrix} w & v^* \\ v & y + z \end{pmatrix}. \tag{2.18}$$

Letting ϵ_+ and ϵ_- be the two eigenvalues of M with $\epsilon_+ \geq \epsilon_-$, note that

$$\epsilon_+ = \|M\| \leq \|H_A|_Q\| + \|H_B|_Q\| \leq y + \|H_B|_Q\| \leq y + \|H_B\|, \tag{2.19}$$

where we have used the Cauchy interlacing theorem to note that $\|H_B|_Q\| \leq \|H_B\|$. Additionally, we have that

$$\epsilon_+\epsilon_- = \det(M) = w(y+z) - |v|^2 \geq wy \tag{2.20}$$

where we used the fact that $H_B|_Q$ is positive-semidefinite. Putting this together, we have that

$$\gamma(H_A + H_B) = \min_{|q|^2+|r|^2=1} \langle f(q,r)|H_A + H_B|f(q,r)\rangle = \epsilon_- \geq \frac{wy}{y + \|H_B\|}. \tag{2.21}$$

As the right hand side increased monotonically with both w and y, and as $w \geq \gamma(H_B|_S) \geq c$ and $y \geq \gamma(H_A) \geq d$, we have

$$\gamma(H_A + H_B) \geq \frac{cd}{d + \|H_B\|} \tag{2.22}$$

as required. □

Chapter 3

Scattering on graphs

[**TO DO:** *write a better introduction, including more citations*]

Scattering is one of the more basic ideas of physics, with a surprisingly large usefulness. The old joke about physicists throwing two frogs at each other [**TO DO:** *cite*] in order to understand their internal components has a grain of truth; particle accelerators [**TO DO:** *cite*] , gravitational lensing [**TO DO:** *cite*] , and x-ray crystallography [**TO DO:** *cite*] are just some examples out of many in which scattering plays a key role in physicists probing of the universe.

Along these lines, we would wonder at the usefulness of scattering in quantum information. High energy physics uses scattering to probe atoms and molecules [**TO DO:** *cite multiple*] , but we would want to discretize the system for use in quantum information [**TO DO:** *should I include some bit about discretized quantum field theories? Probably not*] . In this manner, we would replace the continuum by a discrete set of positions, and understand the evolution in such a model.

With this discretization, we are analyzing a system propagating on an infinite graph, and thus we can also think of this as the limit of a continuous time quantum walk to infinite graphs. We know that quantum walks are useful algorithmic devices [**TO DO:** *cite QW algorithms*] , and one might wonder whether these infinite systems can allow for intuitive algorithms. It turns out that this answer is yes, and the original motivation for graph scattering was an algorithm using graph scattering to solve a problem on boolean formulas faster than any randomized classical computation [19]. This algorithm was easily understood using the intuition from scattering, and thus graph scattering became a useful tool for understanding quantum walk algorithms.

This chapter should serve as a broad introduction to graph scattering. In particular, the notations of scattering matrices, bound states, and wavepackets have all been used in previous works. This chapter attempts to standardize notations, while also explaining how everything works. While there is some original work in this chapter, we also utilize and state several of the results from [19, 10, 17, 13] in which the author did not contribute.

3.1 Free particles in the continuum

Let us first take a look at one of the most simple quantum systems seen in any quantum mechanics text (e.g., [22] or [27]): a free particle in one dimension. Without any potential or interactions, we have that the time independent Schrödinger equation reads

$$\frac{\partial^2}{\partial x^2}\psi(x) = -\frac{2m}{\hbar^2}E\psi(x) = -k^2\psi(x), \tag{3.1}$$

which requires the (unnormalizable) solutions,

$$\psi(x) = A\exp(-ikx) + B\exp(ikx) \tag{3.2}$$

for real k and for arbitrary constant A and B. These *momentum states* correspond to particles travelling with momentum k along the real line, and form a basis for the entire Hilbert space.

While these momentum states are useful for understanding the propagation of particles in the quantum setting, if we want to understand more complicated behavior we need to change the potential energy of the system. In particular, we will now include some finite-range potential V that is non-zero only for $|x| < d$ for some constant d, so that outside this range the eigenstates remain unchanged. The only difference is that we will deal with a superposition of states for each energy instead of the pure momentum states, forcing some relation between the A and B of equation (3.2). Namely, the eigenstates of this system become

$$\psi(x) = \begin{cases} \exp(-ikx) + R(k)\exp(ikx) & x \leq -d \\ T(k)\exp(-ikx) & x \geq d \\ \phi(x,k) & |x| \leq d \end{cases} \tag{3.3}$$

for some functions $R(k)$, $T(k)$, and $\phi(x,k)$ that depends on the interaction V. As intuition, these states can be seen as a particle with momentum k coming in from the left, hitting the potential, and then scattering (which motivates the T and R labels).

In addition to these scattering states, it is also possible for bound states to exist. These are normalizable states that have most (or all) of their amplitude near the non-zero potential, so that they do not affect scattering states that originate far from the interaction. They simply exist as additional states in the Hilbert space.

[**TO DO:** *possibly include a δ-function potential scattering problem in the thesis*]

3.1.1 Free particles on an infinite path

With the simple free-particle example in mind, let us now examine the discretized system. Namely, instead of allowing arbitrary real positions, let us restrict attention to some regular 1-D lattice, such as the natural numbers. Further, much as there is a natural linear ordering on the positions in the continuum, and in order for a particle to move between a and b it must travel over all positions between a and b, in the discretized system we only allow particles to move between adjacent integers. Explicitly, the position basis for this discretized Hilbert space will be labeled by $n \in \mathbb{N}$, with transport only allowed between integers that differ by one.

If we then want to understand how this discretized system works, it will be useful to discretize the entire Schrödinger equation. Along those lines, remember that the second derivative of a function f at x can be written as

$$\frac{d^2}{dx^2}f(x) = \lim_{h\to 0}\frac{f(x+h) - 2f(x) - f(x-h)}{h^2}. \tag{3.4}$$

Since we were originally working in the continuum, we could let h go to zero without any problems. In our discretize world, however, there exists some smallest difference in x, namely 1. As such, we have that in our discretized space, the operator corresponding to the second position derivative can be written as

$$\Delta^2 = \sum_{x=-\infty}^{\infty} |\,x\rangle\big(\langle\,x-1\,| - 2\langle\,x\,| + \langle\,x+1\,|\big) = \sum_{x=-\infty}^{\infty}\big(|\,x\rangle\langle\,x-1\,| + |\,x\rangle\langle\,x+1\,|\big) - 2\mathbb{I}. \tag{3.5}$$

If we then rescale the energy levels, we have that the identity term in the right hand side of (3.5) can be removed, so that Δ^2 on this discretized one-dimensional system is proportional to the adjacency matrix of an infinite path.

With this representation of the second derivative operator, we can see that when discretized, the time-independent Schrödinger equation for a free particle becomes

$$\Delta^2|\,\psi\rangle = \Big(\sum_{x=-\infty}^{\infty}\big(|\,x+1\rangle\langle\,x\,| + |\,x-1\rangle\langle\,x\,|\big) - 2\mathbb{I}\Big)|\,\psi\rangle = E'_\psi|\,\psi\rangle. \tag{3.6}$$

If we rescale the energy term, and then break the vector equation into its components, we find that

$$\langle\,x+1\,|\,\psi\rangle + \langle\,x-1\,|\,\psi\rangle = E_\psi\langle\,x\,|\,\psi\rangle \tag{3.7}$$

for all $x \in \mathbb{Z}$. Taking motivation from the continuous case, we then make the ansatz that $\langle\,x\,|\,\psi\rangle = e^{ikx}$ for some k, and find

$$\langle\,x+1\,|\,\psi\rangle + \langle\,x-1\,|\,\psi\rangle = e^{ik}e^{ikx} + e^{-ik}e^{ikx} = E_\psi e^{ikx} = E_\psi\langle\,x\,|\,\psi\rangle \qquad \Rightarrow \tag{3.8}$$

$$E_\psi = e^{ik} + e^{-ik} = 2\cos(k). \tag{3.9}$$

If we then use the fact that E_ψ must be real, and that the amplitudes should not diverge to infinity as $x \to \pm\infty$, we find that the only possible values of k are between $[-\pi, \pi)$. Hence, in analogy with the continuous case, the eigenbasis of the Hamiltonian corresponds to momentum states, but where the possible momenta only range over $[-\pi, \pi)$. We represent this momentum state with momenta k as $|\,\tilde{k}\,\rangle$.

Additionally, we can discuss the "speed" of these eigenstates, which is given by the derivative of the energy with respect to momentum. We con then see that

$$s = \left|\frac{dE_k}{dk}\right| = 2\sin(|k|), \tag{3.10}$$

which is to be compared with $s \propto |k|$ for in the continuum case. While the discretization does change the relationship between momentum, energy, and speed, if we restrict ourselves

to small k (so that the discretization is not noticeable), we recover the linear relationship. In this way, as the distance between vertices grows smaller, we recover the continuum case.

One slight problem with this discussion is that these momentum states are not normalizable, and thus technically are not states in the Hilbert space. This problem is identical to that of the continuum, and thus we shall not worry about these states of the extended Hilbert space. However, one problem that is unique to our discretized system is that there are an uncountable number of momentum states, while the position basis contains only a countable number of basis states. It turns out that the resolution to this conundrum is that the two bases have different orthogonality conditions: the position basis elements are Kronecker delta orthogonal, while the momentum basis elements are Dirac δ-function orthogonal. Namely,

$$\langle \tilde{k} \,|\, \tilde{p} \rangle = \sum_{x=-\infty}^{\infty} e^{-ikx} e^{ikp} = \sum_{x=-\infty}^{\infty} e^{i(p-k)x} = 2\pi\delta(p-k), \tag{3.11}$$

so that we can decompose the identity on this space as

$$\mathbb{I} = \sum_{x=-\infty}^{\infty} |\, x \rangle\langle\, x \,| = \frac{1}{2\pi} \int_{-\pi}^{\pi} dk |\, \tilde{k} \rangle\langle\, \tilde{k} \,|. \tag{3.12}$$

3.2 Graph scattering

Essentially, at this point we have recovered many of the results of the continuous free particle, but with a discretized position space. The main idea behind the discretization was the change in the second derivative operator, and noting that it became proportional to the adjacency matrix of a simple graph. This seems very similar to the case of continuous time quantum walks, in which the Hamiltonian is explicitly taken to be the adjacency matrix of a (finite sized) graph.

As such, let us assume that the Hamiltonian of the entire system is proportional to the adjacency matrix for these graph scattering problems. If we now want to add some finite potential to the system, in an attempt to discretize the scattering formalism, we could add a potential function, with explicit potential energies at various vertices of the infinite path. However, if we wish to examine scattering only on unweighted graphs, we need to be a little more clever.

To solve this problem, we will connect graphs in such a way that far from our connections the graphs will look identical to that of an infinite path, but near our changes the graph can differ drastically from an infinite path. In particular, we will use an arbitrary (finite) graph as a base, and connect semi-infinite (infinite in one direction) paths to this base graph.

With this construction, the eigenvalue equation must still be satisfied along the semi-infinite paths, and thus the form of the eigenstates along the paths must still be of the form e^{ikx} for some k and x. However, we can no longer assume that k is real, as the fact that the attached semi-infinite paths are only infinite in one direction allow for an exponentially decaying amplitudes along the paths. Additionally, we can have nontrivial correlations between the amplitudes among the different paths, similar to the correlated reflection and transmission coefficients in the continuous case.

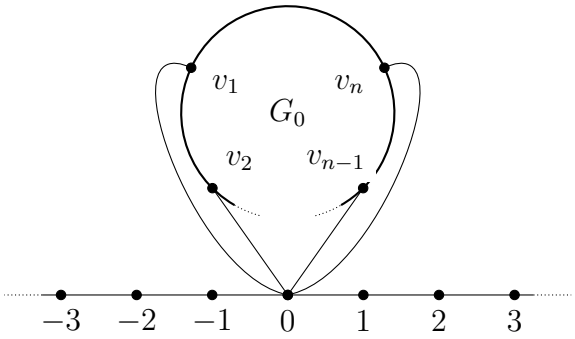

Figure 3.1: A simple example for graph scattering. A graph $\widetilde{G}$ is attached to an infinite path.

Note that the topic of graph scattering is widely used in the literature. Most of this section is not original work, and should be taken as background material. In particular, these results are taken from [19, 10, 17, 13]

[**TO DO:** *Find more accurate citations*]

3.2.1 Infinite path and a Graph

In the most simple example, let us attached a graph $\widetilde{G}$ to an infinite path. In particular, we assume that $\widetilde{G}$ is attached to a single vertex of the infinite path, and that the graph is attached by adding an edge from each vertex in $S \subset V(\widetilde{G})$ to one specific vertex of the infinite path, which we label 0, as seen in Figure 3.1. Calling this new graph G, the adjacency matrix of G, and thus the Hamiltonian for this scattering problem, can be seen to be

$$A(G) = A(\widetilde{G}) + \sum_{v \in S \subset V(\widetilde{G})} |v\rangle\langle 0| + |0\rangle\langle v| + \sum_{x=-\infty}^{\infty} |x\rangle\langle x+1| + |x+1\rangle\langle x|. \tag{3.13}$$

If we then want to inspect the eigenvectors of this Hamiltonian, we find that the eigenvalue equation on the infinite path is identical to that of an infinite path without the graph attached. Hence, we can see that any eigenstate of the Hamiltonian must take the form $Ae^{ikx} + Be^{-ikx}$ for some k along the infinite paths.

With this assumption, we can see that there are three distinct cases for the form of the eigenstates. In particular, the eigenstate could have no amplitude along the infinite paths, being confined to the finite graph $\widehat{G}$. It could also be a normalizable state not confined to the finite graph $\widehat{G}$, in that the amplitude along the infinite paths decays exponentially. Finally, the eigenstate could be an unnormalizable state, in which case we will call it a scattering state.

In the first case, where the state is confined to the graph $\widetilde{G}$, we have the major restriction that the state $|\psi\rangle$ satisfies

$$\langle x|\psi\rangle = 0 \tag{3.14}$$

for all $x \in \mathbb{N}$. Additionally, if $|\phi\rangle$ is the restriction of $|\phi\rangle$ to the finite graph $\widetilde{G}$, we have that

$$A(\widetilde{G})|\phi\rangle = E|\phi\rangle \tag{3.15}$$

so that $|\phi\rangle$ is an eigenstate of the graph $\widetilde{G}$, that also satisfies

$$\sum_{v \in S} \langle v|\phi\rangle = 0. \tag{3.16}$$

These restrictions together show that these completely bound states have an extremely restricted form as eigenstates of $A(\widetilde{G})$, but the infinite path does not really affect them. In particular, their energies are not restricted by anything other than the graph itself, but we are guaranteed to have at most $|V(\widetilde{G})|$ of these confined bound states.

In the second case, we could have that the eigenstate is normalizable, but is not confined to the graph $\widetilde{G}$. In this case, we have that the amplitudes along the infinite paths must go to zero, but they must still be a sum of exponentials. As such, we have that $|\psi\rangle$ must be of the form

$$\langle x|\psi\rangle = Az^x \tag{3.17}$$

for some $z \in (-1, 1) \setminus \{0\}$ for all $x \in \mathbb{N}$, so that the energy must be $z + z^{-1}$ (the case for $z = 0$ forces $A = 0$, and we are in the first case). Additionally, we can see that if $|\phi\rangle$ is the restriction of $|\psi\rangle$ to those vertices inside the graph $A(\widetilde{G})$, they must satisfy

$$A(\widetilde{G}) + A\sum_{v \in S} |v\rangle\langle v|\phi\rangle = 2\cos(k)|\phi\rangle, \tag{3.18}$$

a modified version of the eigenvalue equation for the graph $A(\widetilde{G})$.

Let us finally assume that the state is a scattering state. Note that the eigenvalue of the state must be in the range $[-2, 2]$, and that the form of the eigenstate along the paths must be scalar multiples of e^{ikx} and e^{-ikx}, for some $k \in [-\pi, \pi]$. Explicitly, the state must be of the form

$$\langle x|\psi\rangle = \begin{cases} Ae^{ikx} + Be^{ikx} & x \leq 0 \\ Ce^{ikx} + De^{ikx} & x \geq 0 \end{cases} \tag{3.19}$$

where we note that the amplitude can change at $x = 0$, since we have attached the graph $\widetilde{G}$. However, we do have that $A + B = C + D$, since the amplitude at 0 is single valued, and that the eigenvalue of this state is given by $2\cos(k)$. Note that we have not yet determined the form of the eigenstate inside the graph $\widetilde{G}$, but if we define $|\phi\rangle$ to be the restriction of $|\psi\rangle$ to the finite graph $\widetilde{G}$, then $|\phi\rangle$ must satisfy the equation

$$A(G)|\phi\rangle + (A + B)\sum_{v \in S} |v\rangle\langle v|\phi\rangle = 2\cos(k)|\phi\rangle, \tag{3.20}$$

where the additional term arises from the fact that the vertices in S are connected to the vertex 0. Finally, we have that

$$2\cos(k)\langle 0|\psi\rangle = Ae^{-ik} + Be^{ik} + Ce^{ik} + De^{-ik} + \sum_{v \in S}\langle v|\phi\rangle, \tag{3.21}$$

since the eigenvalue equation must be satisfied at 0.

In the first two cases, we have that the state is highly localized to the area surrounding the graph $\widetilde{G}$, and thus they do not have a large effect on wavefunctions that originate far from the graph. However, the aptly named scattering states can be used to determine the time evolution of these wave functions. In particular, if we look at the case where $A = 1$ and $D = 0$, we can see that

$$\langle x \,|\, \psi \rangle = \begin{cases} e^{-ikx} + Be^{ikx} & x \leq 0 \\ Ce^{-ikx} & x \geq 0 \end{cases} \tag{3.22}$$

so that $1 + B = C$. Note that this is reminiscent of a scattering state, with reflection amplitude B and transmission amplitude C. We can then take as intuition that these scattering states represent a wavepacket with momentum exactly k traveling towards the graph G, and then scattering with these amplitudes. We will use this intuition for our definitions of scattering on more general graphs.

3.2.2 General graphs

Let us now turn our attention to scattering on more general graphs. In particular, let $\widehat{G}$ be any finite graph, with $N + m$ vertices and an adjacency matrix given by the block matrix

$$A(\widehat{G}) = \begin{pmatrix} A & B^\dagger \\ B & D \end{pmatrix}, \tag{3.23}$$

where A is an $N \times N$ matrix, B is an $m \times N$ matrix, and D is an $m \times m$ matrix. When examining graph scattering, we will be interested in the graph G given by the graph-join of $\widehat{G}$ and N semi-infinite paths, with an additional edge between each of the first N vertices of $\widehat{G}$ and the first vertex of one semi-infinite path. A schematic example can be seen in Figure 3.2.

We shall label call the first N vertices of the graph *terminal vertices*, as they connect the semi-infinite paths to the finite graph $\widehat{G}$, and we shall label them as $(1, i)$, where $i \in [N]$. Analogously, we will refer to the vertices on the N semi-infinite paths as (x, i) for $x \in \mathbb{N}^+$ and $i \in [N]$, with the i label referring to the particular semi-infinite path on which the vertex is labeled, while the label x denotes the location along the path. We also refer to the remaining m vertices of $\widehat{G}$ as the *internal vertices* of $\widehat{G}$, and label them as $w \in [m]$. With this labeling of the vertices of G, the adjacency matrix of G is then given by

$$A(G) = A(\widehat{G}) + \sum_{j=1}^{N} \sum_{x=1}^{\infty} \big(|\, x, j \,\rangle\langle\, x+1, j \,| + |\, x+1, j \,\rangle\langle\, x, j \,| \big). \tag{3.24}$$

At this point, we want to examine the possible eigenstates of the matrix $A(G)$. It turns out that there are 3 different kinds of eigenstates, corresponding to the different qualitative properties of the eigenstate along the semi-infinite paths, exactly as in the case studied in Section 3.2.1.

While we will mostly be interested in the third such type, corresponding to scattering off of the graph, the other two kinds remain important for a decomposition of the identity. In

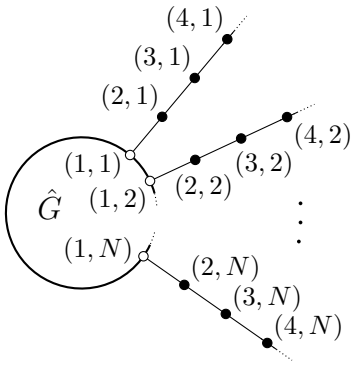

Figure 3.2: An infinite graph G obtained from a finite graph $\widehat{G}$ by attaching n semi-infinite paths. The open circles are *terminals*, vertices of $\widehat{G}$ to which semi-infinite paths are attached. The internal vertices of $\widehat{G}$ are not shown.

particular, we will be guaranteed that these three kinds of eigenstates will form an orthogonal basis for the Hilbert space, and thus we will be able to use this decomposition to guarantee particular behavior of time evolved states.

3.2.2.1 Confined bound states

The easiest states to analyze are the confined bound states, which are eigenstates in which the only nonzero amplitudes are on vertices inside the finite graph $\widehat{G}$. If any vertex on the semi-infinite paths has nonzero amplitude for some eigenstate of the Hamiltonian, then the form of the Hamiltonian forces all vertices on that path to have nonzero amplitude, and thus these confined bound states are exactly those states that have finite support in the basis of vertex states.

To find these confined bound states, we restrict our Hilbert space to the space spanned by the internal vertices of $\widehat{G}$. The states of interest then correspond to the eigenstates of D (the induced adjacency matrix of $A(G)$ when restricted to the internal vertices of $\widehat{G}$) with the additional restriction that the state lies in the nullspace of $B^\dagger$, so that we can extend this state to the full Hilbert space by simply assuming all other amplitudes are zero.

As we originally assumed that there are only m internal vertices of $\widehat{G}$, there are at most m such confined bound states. Additionally, note that there are no restrictions on the eigenvalues of these states, other than those that are inherited from any restrictions placed on it by D (such as the energy being bounded by the maximum degree of $\widehat{D}$).

3.2.2.2 Unconfined bound states

The next possible type of eigenstates are those that are not confined to the finite graph $\widehat{G}$ but are still normalizable. Since these states still have amplitude along the semi-infinite paths, we know that they must be of the form Ae^{ikx}, for some A and k. However, when k is not real (corresponding to a decaying amplitude along the paths), we have that

$$2\cos(k) = 2\cos(k_r + ik_i) = 2\cos(k_r)\cosh(k_i) - i\sin(k_r)\sinh(k_i). \tag{3.25}$$

Hence, if we assume that the state is normalizable, then $k_i \neq 0$, and as the adjacency matrix is Hermitian, we must have that the eigenvalue is real, forcing $k_r = \pi n$ for some $n \in \mathbb{N}$. Note that this then implies that $e^{ik} = z$, for some $z \in (-1, 1) \setminus \{0\}$ (where 0 corresponds to the confined bound states).

As the eigenvalue equation for these states are guaranteed to be satisfied along the paths, we need to construct the form of the eigenstates inside the graph $\widehat{G}$. We can then see that the eigenvalue equation for these vertices is given by

$$\left[\begin{pmatrix} A & B^\dagger \\ B & D \end{pmatrix} + \begin{pmatrix} z & \\ & 0 \end{pmatrix} \right] \begin{pmatrix} \vec{\alpha} \\ \vec{\beta} \end{pmatrix} = \left(z + \frac{1}{z} \right) \begin{pmatrix} \vec{\alpha} \\ \vec{\beta} \end{pmatrix} \tag{3.26}$$

where $\vec{\alpha} \in \mathbb{C}^N$ and $\vec{\beta} \in \mathbb{C}^m$. Note that the amplitudes for a vertex (x, i) is given by $\vec{\alpha}_i z^{x-1}$. Note that we are implicitly assuming that $\vec{\alpha} \neq \vec{0}$, for in that case we are working with a confined bound state.

While there is no immediate reason to guess that the total number of bound states is finite, it has been shown that this number is indeed finite (see [13] for a more thorough explanation, using Levinson's theorem for graphs).

[**TO DO:** *I know that they are finite from the Levinson's theorem, but is there any other reason to guarantee that they are finite?*]

3.2.2.3 Scattering states

We finally reach the point of scattering states, or those unnormalizable eigenstates of the Hamiltonian. We first assume that these states are orthogonal to all bound states, and in particular that we are orthogonal to all confined bound states, as this allows us to uniquely construct the scattering states (without this assumption, if there existed a confined bound state at the appropriate energy, then we could simply add any multiple of the confined bound state to get a different scattering state).

Taking some intuition from the classical case, we will construct a set of states that correspond to sending a particle in towards the graph $\widehat{G}$ along one of the semi-infinite paths and understanding how it scatters off of the graph. Namely, for each $i \in [N]$ we will assume that there exists a state with amplitude along the i-th path of the form $e^{ikx} + S_{i,i}(k)e^{-ikx}$ for $k \in (-\pi, 0)$, and that the rest of the paths have amplitudes given by $S_{i,q}(k)e^{ikx}$. More concretely, we assume that the form of the states is given on the infinite paths by

$$\langle x, q \,|\, \mathrm{sc}_j(k) \rangle = \delta_{j,q} e^{-ikx} + S_{qj} e^{ikx}. \tag{3.27}$$

We then need to see whether such an eigenstate exists. In this case, note that S_{qj} corresponds to the transmitted amplitude along the q-th path if the particle was incident along the j-th path. In the continuous case, S forms a unitary matrix, which essentially means that any incoming particle must also leave, and be distinguishable from a particle incident from a different direction. This intuition will also hold in the discrete case, but we will show this later.

[**TO DO:** *this seems a little clunkly; try to go over and rewrite*]

If we continue to make the assumption that these states exist, we can also write the amplitudes of the m interval vertices as a column vector, as $\vec{\psi}_i(k)$, in which $\vec{\psi}_i(k)$ is the

projection of $|\mathrm{sc}_j(k)\rangle$ onto the internal vertices of $\widehat{G}$. We can then collect these vectors into an $m \times N$ matrix, namely

$$\Psi(k) := \begin{pmatrix} \vec{\psi}_1(k) & \vec{\psi}_2(k) & \cdots & \vec{\psi}_N(k) \end{pmatrix} \tag{3.28}$$

Noting that the amplitudes for $|\mathrm{sc}_j(k)\rangle$ on the terminal vertices is given by $e^{-ik}\delta_{j,q} + S_{qj}(k)e^{ik}$, we can then collect all of the eigenvalue equations for the vertices in $\widehat{G}$ (both internal and termal) as

$$\begin{pmatrix} A & B^\dagger \\ B & D \end{pmatrix} \begin{pmatrix} e^{-ik}\mathbb{I} + S(k)e^{ik} \\ \Psi(k) \end{pmatrix} + \begin{pmatrix} e^{-2ik}\mathbb{I} + e^{2ik}S(k) \\ 0 \end{pmatrix} = 2\cos(k) \begin{pmatrix} e^{-ik}\mathbb{I} + S(k)e^{ik} \\ \Psi(k) \end{pmatrix}, \tag{3.29}$$

where we have constructed the scattering matrix $S(k)$ using the scattering amplitudes $S_{qj}(k)$.

By examining the lower half of this matrix equation, we can see that

$$\Psi(z) = \frac{1}{2\cos(k)\mathbb{I} - D}\big(e^{-ik}B + e^{ik}BS(z)\big), \tag{3.30}$$

which gives the amplitudes of the internal vertices in terms of the scattering matrix. Note that we have assumed that the matrix D does not have an eigenvalue equal to $2\cos(k)$, but this assumption will not be critical, as the eventual matrix $|\Psi\rangle(z)$ will be defined by analytic continuation.

Let us now examine the upper half of the matrix equation, to find

$$A\big(e^{-ik}\mathbb{I} + e^{ik}S(k)\big) + B^\dagger\Psi(k) + \big(e^{-2ik}\mathbb{I} + e^{2ik}S(z)\big) = 2\cos(k)\big(e^{-ik}\mathbb{I} + e^{ik}S(k)\big) \tag{3.31}$$

$$-\left(\mathbb{I} - e^{ik}\Big(A + B^\dagger\frac{1}{2\cos(k) - D}B\Big)\right)S(k) = \mathbb{I} - e^{-ik}\Big(A + B^\dagger\frac{1}{2\cos(k) - D}B\Big). \tag{3.32}$$

Hence, if we define

$$Q(k) = \mathbb{I} - e^{ik}\Big(A + B^\dagger\frac{1}{2\cos(k) - D}B\Big), \tag{3.33}$$

we find that

$$S(k) = -Q(k)^{-1}Q(-k), \tag{3.34}$$

if we assume that the matrix $Q(k)$ can be inverted. Note that for all $k \in (-\pi, 0)$, this might only be impossible for k in which D has a $2\cos(k)$ eigenvalue, in which case we have already run into a problem with the definition of $\Psi(k)$.

Putting this all together, we then have that the states $|\mathrm{sc}_j(k)\rangle$ exist for all $k \in (-\pi, 0)$ for which D does not have a $2\cos(k)$ eigenvalue. We will see in Section 3.2.2.5 that this restriction is an artifact of our construction of $S(k)$, and thus the scattering states will be well defined for all $k \in (-\pi, 0)$.

3.2.2.4 Half-bound states

As a limiting case for both the scattering states and the unconfined bound states, we have those states with $k = 0$ or $k = \pi$ (or equivalently with $z = \pm 1$). In either case, the two momenta correspond to particles that don't move, but the states themselves are not normalizable. They won't play much of a role in this paper, but I did want to mention them.

3.2.2.5 Scattering states for all k

While the above construction is a useful definition of the scattering states for most $k \in (-\pi, 0)$, unfortunately there are specific values of k (namely those for which D has eigenvalue $2\cos(k)$) in which the above analysis doesn't hold, due to the singularity of particular matrices. If we want to show that these scattering states exist for all $k \in (-\pi, 0)$, we need to somehow show that these singularities are just a problem of the analysis and are not intrinsic barriers to existence. Note that this construction closely follows that of [13].

Along these lines, let us extend our analysis to complex z, instead of only focusing on amplitudes of the form e^{ik}. We will define the matrix

$$\gamma(z) := \begin{pmatrix} zA - \mathbb{I} & zB^\dagger \\ zB & zD - (1+z^2)\mathbb{I} \end{pmatrix}. \tag{3.35}$$

This matrix is closely related to the eigenvalue equation for vertices of the graph $\widehat{G}$, but with e^{ik} replaced with z.

With this definition, it will be useful to note the following matrix equalities. In particular, assuming that z is a complex number such that the following matrices are not singular, we have:

$$\begin{pmatrix} \mathbb{I} & zB^\dagger \\ 0 & zD - (1+z^2)\mathbb{I} \end{pmatrix} \begin{pmatrix} -Q(z) & 0 \\ \frac{z}{zD-(1+z^2)\mathbb{I}} B & \mathbb{I} \end{pmatrix} = \begin{pmatrix} -Q(z) + zB^\dagger \frac{1}{D-(z+z^{-1})} B & zB^\dagger \\ zB & zD - (1+z^2)\mathbb{I} \end{pmatrix} \tag{3.36}$$

$$= \gamma(z) \tag{3.37}$$

Additionally, if we note that the inverse of a block diagonal matrix can be written as

$$\begin{pmatrix} X & Y \\ Z & W \end{pmatrix}^{-1} = \begin{pmatrix} \big(X - YW^{-1}Z\big)^{-1} & -X^{-1}Y\big(W - ZX^{-1}Y\big)^{-1} \\ -W^{-1}Z\big(X - YW^{-1}Z\big)^{-1} & \big(W - ZX^{-1}Y\big)^{-1} \end{pmatrix}, \tag{3.38}$$

we can then invert this equation for $\gamma(z)$ as

$$\gamma(z)^{-1} = \begin{pmatrix} -Q(z) & 0 \\ \frac{z}{zD-(1+z^2)\mathbb{I}} B & \mathbb{I} \end{pmatrix}^{-1} \begin{pmatrix} \mathbb{I} & zB^\dagger \\ 0 & zD - (1+z^2)\mathbb{I} \end{pmatrix}^{-1} \tag{3.39}$$

$$= \begin{pmatrix} -Q(z)^{-1} & 0 \\ \frac{z}{zD-(1+z^2)\mathbb{I}} BQ(z)^{-1} & \mathbb{I} \end{pmatrix} \begin{pmatrix} \mathbb{I} & -B^\dagger \frac{z}{zD-(1+z^2)\mathbb{I}} \\ 0 & \frac{1}{zD-(1+z^2)\mathbb{I}} \end{pmatrix}. \tag{3.40}$$

Combining these two matrix equations, we can then find that

$$\begin{aligned}
\gamma(z)^{-1}\gamma(z^{-1}) &= \begin{pmatrix} -Q(z)^{-1} & 0 \\ \frac{z}{zD-(1+z^2)\mathbb{I}}BQ(z)^{-1} & \mathbb{I} \end{pmatrix} \begin{pmatrix} \mathbb{I} & -B^\dagger \frac{z}{zD-(1+z^2)\mathbb{I}} \\ 0 & \frac{1}{zD-(1+z^2)\mathbb{I}} \end{pmatrix} \\
&\qquad \times \begin{pmatrix} \mathbb{I} & z^{-1}B^\dagger \\ 0 & z^{-1}D-(1+z^{-2})\mathbb{I} \end{pmatrix} \begin{pmatrix} -Q\big(z^{-1}\big) & 0 \\ \frac{z^{-1}}{z^{-1}D-(1+z^{-2})\mathbb{I}}B & \mathbb{I} \end{pmatrix} \qquad (3.41) \\
&= \begin{pmatrix} -Q(z)^{-1} & 0 \\ \frac{z}{zD-(1+z^2)\mathbb{I}}BQ(z)^{-1} & \mathbb{I} \end{pmatrix} \begin{pmatrix} \mathbb{I} & 0 \\ 0 & z^{-2}\mathbb{I} \end{pmatrix} \begin{pmatrix} -Q\big(z^{-1}\big) & 0 \\ \frac{z^{-1}}{z^{-1}D-(1+z^{-2})\mathbb{I}}B & \mathbb{I} \end{pmatrix} \qquad (3.42) \\
&= \begin{pmatrix} -Q(z)^{-1} & 0 \\ \frac{z}{zD-(1+z^2)\mathbb{I}}BQ(z)^{-1} & z^{-2}\mathbb{I} \end{pmatrix} \begin{pmatrix} -Q\big(z^{-1}\big) & 0 \\ \frac{z^{-1}}{z^{-1}D-(1+z^{-2})\mathbb{I}}B & \mathbb{I} \end{pmatrix} \qquad (3.43) \\
&= \begin{pmatrix} Q(z)^{-1}Q(z^{-1}) & 0 \\ \frac{1}{D-(z+z^{-1})\mathbb{I}}B\big(z^{-2}\mathbb{I}-Q(z)^{-1}Q(z^{-1})\big) & z^{-2}\mathbb{I} \end{pmatrix} \qquad (3.44) \\
&= -\begin{pmatrix} S(z) & 0 \\ z^{-1}\Psi(s) & -z^{-2}\mathbb{I} \end{pmatrix}, \qquad (3.45)
\end{aligned}$$

where we have extended the definition of S and Ψ to all complex z instead of just e^{ik}

With these matrix equations, we have a representation of the scattering matrix and the interior amplitudes in terms of the matrix γ. If we then note that

$$\gamma(z)^{-1} = \frac{1}{\det\gamma(z)}\operatorname{adj}\gamma(z) \qquad (3.46)$$

where $\operatorname{adj}\gamma(z)$ is the adjugate matrix of $\gamma(z)$, then by (3.45) we can then see that the entries of $\gamma(z)$, and thus the entries of $S(z)$ and $\Psi(z)$, are rational functions of z.

With this fact, to show that the problems defining the states $|\mathrm{sc}_j(k)\rangle$ are a result of our analysis rather than intrinsic difficulties, we need only show that there are no poles in the matrix elements for $S(z)$ or $\Psi(z)$ for z on the unit circle. We actually have that for all such z, there is an upper bound on the norm of the scattering amplitudes, which might depend on the graph $\widehat{G}$.

Lemma 3. *Given $\widehat{G}$, there exists a constant $\lambda \in \mathbb{R}$ such that $|\langle v|sc_j(k)\rangle| < \lambda$ for all $k \in [-\pi,\pi)$, $j \in \{1,\dots,N\}$, and $v \in \widehat{G}$.*

Proof. Note that

$$\gamma\left(\frac{1}{z}\right) = \frac{1}{z^2}\gamma(z) + \left(\frac{1}{z^2}-1\right)\widehat{P} \qquad (3.47)$$

where

$$\widehat{P} = \begin{pmatrix} 1 & 0 \\ 0 & 0 \end{pmatrix} \qquad (3.48)$$

projects onto the N vertices of $\widehat{G}$ attached to semi-infinite paths. Hence

$$-\gamma(z)^{-1}\gamma\left(\frac{1}{z}\right) = -\frac{1}{z^2} + \left(1-\frac{1}{z^2}\right)\gamma(z)^{-1}\widehat{P}. \qquad (3.49)$$

Let $\{|\psi_c\rangle \colon c \in \{1,\dots,n_c\}\}$ be eigenstates of $\widehat{H}$ satisfying $\widehat{P}|\psi_c\rangle = 0$, and let this set be an orthonormal basis for the span of all such states. Then

$$\left(1-\frac{1}{z^2}\right)\gamma(z)^{-1}\widehat{P} = \left(1-\frac{1}{z^2}\right)\left(1-\sum_{j=1}^{n_c}|\psi_c\rangle\langle\psi_c|\right)\gamma(z)^{-1}\left(1-\sum_{j=1}^{n_c}|\psi_c\rangle\langle\psi_c|\right)\widehat{P} \quad (3.50)$$

since each $|\psi_c\rangle$ is an eigenvector of $\gamma(z)$ and $\widehat{P}|\psi_c\rangle = 0$. Reference [13] shows (in Part 2 of the proof of Theorem 1) that

$$\det\left(\frac{1}{1-z^2}\right)M(z) \neq 0 \text{ for } |z| = 1, \quad (3.51)$$

where $M(z)$ is the $(N+m-n_c)\times(N+m-n_c)$ matrix of $\gamma(z)$ in the subspace of states orthogonal to the span of $\{|\psi_c\rangle \colon c \in \{1,\dots,n_c\}\}$. Therefore

$$\begin{aligned}\frac{1}{z}\langle v|\mathrm{sc}_j(k)\rangle &= -\langle v|\gamma(z)^{-1}\gamma\left(\frac{1}{z}\right)|j\rangle \\ &= \langle v|\left(1-\frac{1}{z^2}\right)\left(1-\sum_{j=1}^{n_c}|\psi_c\rangle\langle\psi_c|\right)\gamma(z)^{-1}\left(1-\sum_{j=1}^{n_c}|\psi_c\rangle\langle\psi_c|\right)|j\rangle\end{aligned}$$

has no poles on the unit circle, and the result follows.

□

As such, we have that the scattering states are well defined for all $k \in (-\pi, 0)$.

3.2.3 Scattering matrix properties

While the use of the γ matrix gives an explicit construction of the form of the eigenstates on the internal vertices, the alternate definition in terms o the Q matrix can be used to easily show several properties of the scattering matrix. In particular, remember that

$$S(k) = -Q(z)^{-1}Q(z^{-1}), \quad (3.52)$$

where $z = e^{ik}$, and the matrices $Q(z)$ are given by

$$Q(z) = \mathbb{I} - z\Big(A + B^\dagger\frac{1}{\frac{1}{z}+z-D}B\Big). \quad (3.53)$$

Note that $Q(z)$ and $Q(z^{-1})$ commute for all $z \in \mathbb{C}$, as they can both be written as $\mathbb{I}+zH(z+z^{-1})$.

Using this expression for the scattering matrix, it is easy to see that $S(k)$ is a unitary matrix, as

$$S(k)^\dagger = -Q(z^{-1})^\dagger(Q(z)^{-1})^\dagger \quad (3.54)$$

and that

$$Q(z)^\dagger = \mathbb{I}^\dagger - z^\dagger\Big(A^\dagger + B^\dagger\Big(\frac{1}{\frac{1}{z}+z-D}\Big)^\dagger(B^\dagger)^\dagger\Big) = \mathbb{I} - z^\dagger\Big(A + B^\dagger\frac{1}{\frac{1}{z^\dagger}+z^\dagger-D}B\Big) = Q(z^\dagger) \quad (3.55)$$

and thus

$$S(k)^\dagger = -Q(z^{-1})^\dagger (Q(z)^{-1})^\dagger = -Q(z)Q(z^{-1})^{-1} = Q(z^{-1})^{-1}Q(z) = S(k)^{-1} \tag{3.56}$$

where we used the fact that $z = e^{ik}$ so that $z^\dagger = z^{-1}$, and the fact that $Q(z)$ and $Q(z^{-1})$ commute.

Additionally, we can make use of the fact that S is derived from an unweighted graph to show that the scattering matrices are symmetric. In particular, note that $Q(z)$ is symmetric for all z, since D is symmetric, symmetric matrices are closed under inversion, A is symmetric and B is a 0-1 matrix. As such, we have that

$$S(k)^T = -\big(Q(z)^{-1}Q(z^{-1})\big)^T = -Q(z^{-1})^T (Q(z)^{-1})^T \tag{3.57}$$

$$= -Q(z^{-1})Q(z)^{-1} = -Q(z)^{-1}Q(z^{-1}) = S(k) \tag{3.58}$$

where we used the fact that $Q(z)$ and $Q(z^{-1})$ commute.

Putting this together, we have that $S(k)$ is a symmetric, unitary matrix for all k.

3.2.4 Orthonormality of the scattering states

We now have some basic ideas behind the scattering behavior. In particular, we have that the scattering states exist for all k, and that the scattering matrices are symmetric and unitary. However, one of the most important behaviors we need is that the scattering states are orthonormal, and that they form a basis for the Hilbert space corresponding to the graph.

We will first show that two scattering states are orthonormal.

Lemma 4. *Let $k, p \in (-\pi, 0)$, and let $i, j \in [N]$. We then have that*

$$\langle\, sc_i(p) \,|\, sc_j(k) \,\rangle = \frac{1}{2\pi}\delta_{i,j}\delta(p-k), \tag{3.59}$$

where the two sides are equal as functionals against integration.

Proof. Let

$$\Pi_1 = \sum_{x=1}^{\infty}\sum_{q=1}^{N} |x,q\rangle\langle x,q| \qquad \Pi_2 = \mathbb{I} - \sum_{x=2}^{\infty}\sum_{q=1}^{N} |x,q\rangle\langle x,q| \qquad \Pi_3 = \sum_{q=1}^{N} |1,q\rangle\langle 1,q|. \tag{3.60}$$

First write

$$\begin{aligned}
\langle \mathrm{sc}_i(p)|\Pi_1|\mathrm{sc}_j(k)\rangle &= \sum_{x=1}^{\infty}\sum_{q=1}^{N}(\delta_{iq}e^{ipx} + S^*_{qi}(p)e^{-ipx})(\delta_{jq}e^{-ikx} + S_{qj}(k)e^{ikx}) \\
&= \frac{1}{2}\left(\delta_{ij} + \sum_{q=1}^{N} S^*_{qi}(p)S_{qj}(k)\right)\left(\sum_{x=1}^{\infty} e^{i(p-k)x} + \sum_{x=1}^{\infty} e^{-i(p-k)x}\right) \\
&\quad + \frac{1}{2}\left(\delta_{ij} - \sum_{q=1}^{N} S^*_{qi}(p)S_{qj}(k)\right)\left(\sum_{x=1}^{\infty} e^{i(p-k)x} - \sum_{x=1}^{\infty} e^{-i(p-k)x}\right) \\
&\quad + \frac{1}{2}(S^*_{ji}(p) + S_{ij}(k))\left(\sum_{x=1}^{\infty} e^{-i(p+k)x} + \sum_{x=1}^{\infty} e^{i(p+k)x}\right) \\
&\quad + \frac{1}{2}(S^*_{ji}(p) - S_{ij}(k))\left(\sum_{x=1}^{\infty} e^{-i(p+k)x} - \sum_{x=1}^{\infty} e^{i(p+k)x}\right).
\end{aligned}$$

We use the following identities for $p, k \in (-\pi, 0)$:

$$\begin{aligned}
\sum_{x=1}^{\infty} e^{i(p-k)x} + \sum_{x=1}^{\infty} e^{-i(p-k)x} &= 2\pi\delta(p-k) - 1 \\
\sum_{x=1}^{\infty} e^{i(p+k)x} + \sum_{x=1}^{\infty} e^{-i(p+k)x} &= -1 \\
\sum_{x=1}^{\infty} e^{i(p-k)x} - \sum_{x=1}^{\infty} e^{-i(p-k)x} &= i\cot\left(\frac{p-k}{2}\right) \\
\sum_{x=1}^{\infty} e^{i(p+k)x} - \sum_{x=1}^{\infty} e^{-i(p+k)x} &= i\cot\left(\frac{p+k}{2}\right).
\end{aligned}$$

These identities hold when both sides are integrated against a smooth function of p and k. Substituting, we get

$$\begin{aligned}
\langle \mathrm{sc}_i(p)|\Pi_1|\mathrm{sc}_j(k)\rangle &= 2\pi\delta_{ij}\delta(p-k) + \delta_{ij}\left(\frac{i}{2}\cot\left(\frac{p-k}{2}\right) - \frac{1}{2}\right) \\
&\quad + \sum_{q=1}^{N} S^*_{qi}(p)S_{qj}(k)\left(-\frac{i}{2}\cot\left(\frac{p-k}{2}\right) - \frac{1}{2}\right) \\
&\quad + S^*_{ji}(p)\left(-\frac{1}{2} - \frac{i}{2}\cot\left(\frac{p+k}{2}\right)\right) \\
&\quad + S_{ij}(k)\left(-\frac{1}{2} + \frac{i}{2}\cot\left(\frac{p+k}{2}\right)\right)
\end{aligned} \tag{3.61}$$

where we used unitarity of the S-matrix to simplify the first term. Now turning to Π_2 we have

$$\langle \mathrm{sc}_i(p)|H\Pi_2|\mathrm{sc}_j(k)\rangle = 2\cos(p)\langle \mathrm{sc}_i(p)|\Pi_2|\mathrm{sc}_j(k)\rangle \tag{3.62}$$

and

$$\langle \mathrm{sc}_i(p)|H\Pi_2|\mathrm{sc}_j(k)\rangle = \langle \mathrm{sc}_i(p)|\Bigg(2\cos(k)\Pi_2|\mathrm{sc}_j(k)\rangle + \sum_{q=1}^{N}(e^{-ik}\delta_{qj} + S_{qj}(k)e^{ik})|2,q\rangle - \sum_{q=1}^{N}(e^{-2ik}\delta_{qj} + S_{qj}(k)e^{2ik})|1,q\rangle\Bigg).$$

Using these two equations we get

$$\begin{aligned}(2\cos(p) - 2\cos(k))\langle \mathrm{sc}_i(p)|\Pi_2|\mathrm{sc}_j(k)\rangle &= \delta_{ij}(e^{2ip-ik} - e^{-2ik+ip}) + S^*_{ji}(p)(e^{-2ip-ik} - e^{-2ik-ip}) \\ &\quad + S_{ij}(k)(e^{2ip+ik} - e^{2ik+ip}) \\ &\quad + \sum_{q=1}^{N} S^*_{qi}(p)S_{qj}(k)(e^{-2ip+ik} - e^{2ik-ip}).\end{aligned}$$

Noting that

$$\langle \mathrm{sc}_i(p)|\Pi_3|\mathrm{sc}_j(k)\rangle = \sum_{q=1}^{N}(\delta_{iq}e^{ip} + S^*_{qi}(p)e^{-ip})(\delta_{jq}e^{-ik} + S_{qj}(k)e^{ik}), \tag{3.63}$$

we have

$$\begin{aligned}\langle \mathrm{sc}_i(p)|\Pi_2 - \Pi_3|\mathrm{sc}_j(k)\rangle &= \delta_{ij}\left(\frac{e^{2ip-ik} - e^{-2ik+ip}}{2\cos(p) - 2\cos(k)} - e^{ip-ik}\right) \\ &\quad + S^*_{ji}(p)\left(\frac{e^{-2ip-ik} - e^{-2ik-ip}}{2\cos(p) - 2\cos(k)} - e^{-ip-ik}\right) \\ &\quad + S_{ij}(k)\left(\frac{e^{2ip+ik} - e^{2ik+ip}}{2\cos(p) - 2\cos(k)} - e^{ip+ik}\right) \\ &\quad + \sum_{q=1}^{N} S^*_{qi}(p)S_{qj}(k)\left(\frac{e^{-2ip+ik} - e^{2ik-ip}}{2\cos(p) - 2\cos(k)} - e^{-ip+ik}\right) \\ &= \delta_{ij}\left(\frac{1}{2} - \frac{i}{2}\cot\left(\frac{p-k}{2}\right)\right) + S^*_{ji}(p)\left(\frac{1}{2} + \frac{i}{2}\cot\left(\frac{p+k}{2}\right)\right) \\ &\quad + S_{ij}(k)\left(\frac{1}{2} - \frac{i}{2}\cot\left(\frac{p+k}{2}\right)\right) \\ &\quad + \sum_{q=1}^{N} S^*_{qi}(p)S_{qj}(k)\left(\frac{1}{2} + \frac{i}{2}\cot\left(\frac{p-k}{2}\right)\right).\end{aligned} \tag{3.64}$$

Adding equation (3.61) to equation (3.64) gives equation (3.59). □

With the fact that the scattering states are orthogonal, it will also be useful to see that they form an orthonormal basis for the Hilbert space. In particular, Childs and Gosset showed in [13] that this holds. Assuming that the confined bound states were spanned by the orthonormal states $\{|\psi_c\rangle : c \in [n_c]\}$ and that the orthogonal bound states are spanned by the orthonormal basis $\{|\phi_b\rangle : b \in [n_b]\}$, they showed the following theorem:

Theorem 2 (Theorem 1 of [13]). *Let v and w be any two vertices of the graph G. Then*

$$\langle v | \left[\int_{-\pi}^{0} \frac{dk}{2\pi} |sc_j(k)\rangle\langle sc_j(k)| + \sum_{b=1}^{n_b} |\phi_b\rangle\langle\phi_b| + \sum_{c=1}^{n_c} |\psi_c\rangle\langle\psi_c| \right] |w\rangle = \delta_{v,w}. \tag{3.65}$$

[**TO DO:** *Should I include a proof of this theorem? It's not mine, but I will use.*]

Most of our results will be in regards to the scattering states, but having this decomposition of the identity will allow us to show better bounds. In particular, we will be able to guarantee that certain states have almost no support on states other than scattering states.

3.3 Applications of graph scattering

While graph scattering is a relatively new area of study, it has found several applications. As the behavior of a scattered particle is heavily dependent on both the momentum and the graph used for scattering, we can use the scattering behavior as a probe of properties about the graph, as well as a kind of probe for the momentum of the incoming particle. In particular, if we know the momentum of a wavepacket, we can determine the scattering amplitudes to gain information about the graph, such as whether it has eigenstates at particular momentum. If we know a graphs scattering behavior, we can then use the scattering to check whether a wavepacket has a desired momentum, and then do something to the particular wavepacket.

3.3.1 NAND Trees

The original motivating idea for understanding graph scattering was an oracular separation between quantum and classical computation, for a problem involving NAND trees. In particular, Edward Fahri, Jeffrey Goldstone, and Sam Gutmann gave a scattering algorithm [19] for this problem that was provably faster than any classical algorithm.

A NAND tree is a function on N variables, where N is a power of two, such that the value of the leaves are given by the input to the function, while each parent node's value is given by the NAND of its children's values. The NAND tree problem is then to evaluate the root.

Now for any oracular problem, we are given black-box access to the input, and want to minimize the total number of queries to the input. In particular, the actual runtime of an algorithm generally is not measured, and instead we simply count the number of bits of the input the algorithm accesses. While this might not always give a realistic gauge for the time a particular problem takes to solve, it does allow for information theoretic bounds on the number of queries. In particular, oracular problems often allow us to guarantee that any algorithm will require a certain number of queries in order to solve the problem.

If we perform an analysis on the NAND tree problem, any deterministic algorithm will require N queries in order to evaluate the root, as in the worst case we will need to examine every bit of the input. However, if we instead work with probabilistic computation, there is a randomized algorithm [26] that can solve this problem in $\mathcal{O}(N^\alpha)$ time, where $\alpha =$

$\log_2(1+\sqrt{33})-2 \approx 0.753$. Additionally, any randomized algorithm will require this many queries [28]. Fahri, Goldstone, and Gutmann were able to construct a quantum algorithm that solves the NAND tree using only $\mathcal{O}(\sqrt{N})$ queries, which is provably better than in the classical case.

The reason that we are interested in this is that the original algorithm uses graph scattering explicitly. In particular, a binary tree is attached to an infinite path at the root, and then additional vertices are attached to the leaves depending on whether the binary value is 0 or 1. It turns out that at energy 0 (i.e., momentum $-\pi/2$), such a tree has perfect transmission from one path to the other if the tree evaluates to 1, and perfect reflection if the tree evaluates to 0. Hence, if a wave packet with momentum centered around $-\pi/2$ is scattered off of such a graph, by determining the location of the particle after it has scattered we evaluate the tree.

In this case, the requisite size of the wavepacket turns out to be $\mathcal{O}(\sqrt{N})$, and thus this amount of time is required in order for the scattering to occur. The total evolution time is closely related to the number of queries that the algorithm uses during the computation, and thus this is a quantum algorithm that has a provable advantage over classical computing.

3.3.2 Momentum dependent actions

While the NAND tree algorithm gives a good example of how graph scattering can work as an algorithmic tool, in that the scattering evaluates a binary function, the scattering behavior was relatively simple: a particle transmits or reflects. However, we can use similar ideas in order to have nontrivial scattering behavior, by creating graphs that have different behaviors at different momenta, or that perfectly transmits to some subset of the attached paths (i.e., a generalization of perfect transmission to multiple semi-infinite paths).

[**TO DO:** *Should I include schematic pictures of these gadgets? I'm not sure if that would improve readability*]

3.3.2.1 R/T gadgets

The easiest thing we could hope for is the same behavior as in the NAND tree algorithm, with two attached paths and at some fixed momenta the wavepacket either completely transmits, or it completely reflects. However, we will utilize a single graph with several different momenta.

In particular, these reflection/transmission (R/T) gadgets will have two sets of momenta. One set will have perfect transmission, while the other will have perfect reflection. While these gadgets have relatively simple scattering behavior, they can be used to filter particular momenta, or as building blocks in more complicated gadgets. Additionally, the simple behavior will allow us to show that certain scattering behaviors are not possible.

3.3.2.2 Momentum Switches

We can generalize the idea of R/T gadgets to multiple semi-infinite paths, so that the gadget has a kind of routing behavior. In particular, we can attempt to construct graphs with three attached semi-infinite paths, in which when a wavepacket is incident along one particular

path, it either perfectly transmits to the second path, or it perfectly transmits to the third path, depending on the incident momenta. In this way, we construct something like a momentum dependent railroad switch, sending different wavepackets to different locations.

These momentum switches are extremely useful, as they will allow us to construct much more interesting momentum dependent behavior. By using two of these gadgets in series (with the paths 2 and 3 connected to each other), we can then place a single obstacle along only one of the paths. Since only those momenta that travel along that particular path are incident on the additional obstacle, we can use this to do something like applying a momentum dependent phase.

3.3.3 Encoded unitary

While the above two gadgets can be thought to have one input but two output paths, we can generalize this idea to having multiple input paths. In particular, if we have two input and two output paths, we can encode a logical qubit in a dual-rail encoding (i.e., one path corresponds to a state $|0\rangle$, while the other corresponds to a state $|1\rangle$). If we can ensure that wavepackets incident along the input paths always transmit to the output paths, we can think of this as applying a unitary gate to the encoded qubit.

In particular, by constructing a gadget whose S-matrix at a particular momentum is block diagonal, with two zero blocks along the diagonal, we have that a wavepacket at that momenta always transmits from the input to the output vertices. Additionally, as the S-matrix is itself unitary, we have that the 2×2 block matrix that corresponds to the transmitted amplitudes is also unitary, and thus we have applied a unitary operation to the encoded qubit.

3.4 Constructing graphs with particular scattering behavior

While we have shown that the scattering behavior of some given graph is easy to compute, finding graphs with a given behavior is much more difficult. We don't even know whether such an operation is decidable, and thus finding an algorithm to construct a graph with a given S-matrix seems unlikely. However, there are specific behaviors at particular momenta in which constructions are known, and exhaustive searches of small sized graphs have yielded graphs with nice scattering properties.

In particular, Andrew Childs found several gadgets in his paper proving the universality of quantum walks [10]. After this result, Blumer, Underwood and Feder [9] performed an exhaustive search over all graphs with at most 9 vertices, finding those graphs that implement an encoded unitary at several momenta of interest. Childs, Gosset, and Webb then constructed several gadgets in [15]. This section is mainly based on [14], a paper by Chlids, Gosset, Nagaj, Raha, and Webb, as it gives explicit constructions for gadgets with particular behavior.

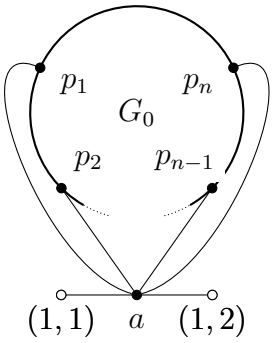

Figure 3.3: A type 1 R/T gadget. Vertices of G_0 that are not part of the periphery $P = \{p_1, \ldots, p_n\}$ are not shown.

3.4.1 R/T gadgets

Perhaps the most simple behavior, and the one that will for which we will have the easiest time finding a solution, are two-terminal gadgets that either perfectly reflect at some particular momenta, or perfectly transmit. These R/T gadgets can be thought of as a proof-of-principle for constructing gadgets, but they also have uses of their own.

This problem is still rather complicated when we work with arbirtary graphs with two terminal vertices, things become much simpler if we work with a graph attached to an infinite path via a single vertex. In this case, we can determine exactly when the gadget will lead to perfect reflection, and when it will lead to perfect transmission.

Along these lines, we will investigate the scattering behavior of graphs where $\widehat{G}$ is of the form found in Figure 3.3. While we still have that $\widehat{G}$ is of the form described in Section 3.2.2, the graph G with the semi-infinite paths is that of a infinite path, with the graph G_0 attached to the vertex a. As such, the graph that will be of more interest is the graph G_0 consisting of those vertices other than those along the infinite path. We will label those vertices $p_i \in V(G_0)$ connected to the vertex a as *periphery* vertices, and we will label the set of periphery vertices as P. In the special case that $|P| = 1$, or that a single vertex of G_0 is connected to a, we will call the gadget a type 2 R/T gadget (see Figure 3.4 for an example of a type 2 R/T gadget).

For a given R/T gadget $\widehat{G}$, those momenta for which perfect reflection occurs shall be collected in the *reflection set* which shall be denoted $\mathcal{R}$. Similarly, those momenta for which perfect transmission occurs shall be collected in the *transmission set* which shall be label $\mathcal{T}$. Note that these two sets have empty intersection, and that there isn't any nice relationship between them.

Let us now examine the scattering eigenstates for the graph $\widehat{G}$. For any scattering state $|\mathrm{sc}_1(k)\rangle$, by examining the eigenvalue equation at vertices $(1,1)$ and $(1,2)$ we see that the amplitude at vertex a satisfies

$$\langle a|\mathrm{sc}_1(k)\rangle = 1 + R(k) = T(k). \tag{3.66}$$

Thus perfect reflection at momentum k occurs if and only if $R(k) = -1$ and $\langle a|\mathrm{sc}_1(k)\rangle = 0$, while perfect transmission occurs if and only if $T(k) = 1$ and $\langle a|\mathrm{sc}_1(k)\rangle = 1$. Using this fact, we now derive conditions on the graph G_0 that determine when perfect transmission and reflection occur.

For any type 1 R/T gadget, we have necessary and sufficient conditions for momentum k to be in the reflection set: G_0 should have an eigenvector for which the sum of amplitudes on the periphery is nonzero.

Lemma 5. *Let $\widehat{G}$ be a type 1 R/T gadget. A momentum $k \in (-\pi, 0)$ is in the reflection set $\mathcal{R}$ if and only if G_0 has an eigenvector $|\chi_k\rangle$ with eigenvalue $2\cos(k)$ satisfying*

$$\sum_{i=1}^{n} \langle p_i | \chi_k \rangle \neq 0. \tag{3.67}$$

Proof. Let us first suppose that $\widehat{G}$ has perfect reflection at momentum k, i.e., $R(k) = -1$ and $\langle a | \mathrm{sc}_1(k) \rangle = 0$. As $\langle (1,1) | \mathrm{sc}_1(k) \rangle = e^{-ik} - e^{ik} \neq 0$ and $\langle (1,2) | \mathrm{sc}_1(k) \rangle = 0$, to satisfy the eigenvalue equation at vertex a, we have

$$\sum_{j=1}^{n} \langle p_j | \mathrm{sc}_1(k) \rangle = e^{ik} - e^{-ik} \neq 0. \tag{3.68}$$

Further, since G_0 only connects to vertex a and the amplitude at this vertex is zero, the restriction of $|\mathrm{sc}_1(k)\rangle$ to G_0 must be an eigenvector of G_0 with eigenvalue $2\cos(k)$. Hence the condition is necessary for perfect reflection.

Next suppose that G_0 has an eigenvector $|\chi_k\rangle$ with eigenvalue $2\cos(k)$ satisfying (3.67), with the sum equal to some nonzero constant c. Define a scattering state $|\psi_k\rangle$ on the Hilbert space of the full graph G with amplitudes

$$\langle v | \psi_k \rangle = \frac{e^{ik} - e^{-ik}}{c} \langle v | \chi_k \rangle \tag{3.69}$$

for all $v \in V(G_0)$, $\langle a | \psi_k \rangle = 0$, and

$$\langle (x,j) | \psi_k \rangle = \begin{cases} e^{-ikx} - e^{ikx} & j = 1 \\ 0 & j = 2 \end{cases} \tag{3.70}$$

for all $x \in \mathbb{Z}^+$.

We claim that $|\psi_k\rangle$ is an eigenvector of G with eigenvalue $2\cos(k)$. The state clearly satisfies the eigenvalue equation on the semi-infinite paths since it is a linear combination of states with momentum $\pm k$. At vertices of G_0, the state is proportional to an eigenvector of G_0, and since the state has no amplitude at a, the eigenvalue equation is also satisfied at these vertices. It remains to see that the eigenvalue equation is satisfied at a, but this follows immediately by a simple calculation.

Since $|\psi_k\rangle$ has the form of a scattering state with perfect reflection, we see that $R(k) = -1$ and $T(k) = 0$ as claimed. □

In a similar manner, the following lemma gives a sufficient condition for a momentum k to be in the transmission set (which is also necessary for type 2 gadgets). Let g_0 denote the induced subgraph on $V(G_0) \setminus P$ where $P = \{p_i : i \in [n]\}$ is the periphery.

Lemma 6. *Let $\widehat{G}$ be a type 1 R/T gadget and let $k \in (-\pi, 0)$. Suppose $|\xi_k\rangle$ is an eigenvector of g_0 with eigenvalue $2\cos k$ and with the additional property that, for all $i \in [n]$,*

$$\sum_{\substack{v \in V(g_0): \\ (v,p_i) \in E(G_0)}} \langle v | \xi_k \rangle = c \neq 0 \tag{3.71}$$

for some constant c that does not depend on i. Then k is in the transmission set $\mathcal{T}$. If $\hat{G}$ is a type 2 R/T gadget, then this condition is also necessary.

Proof. If g_0 has a suitable eigenvector $|\xi_k\rangle$ satisfying (3.71), define a scattering state $|\psi_k\rangle$ on the full graph G, with amplitudes $\langle a|\psi_k\rangle = 1$,

$$\langle v | \psi_k \rangle = \begin{cases} -\frac{1}{c}\langle v | \xi_k \rangle & v \in V(g_0) \\ 0 & v \in P \end{cases} \tag{3.72}$$

in the graph G_0, and

$$\langle (x,j) | \psi_k \rangle = \begin{cases} e^{-ikx} & j = 1 \\ e^{ikx} & j = 2 \end{cases} \tag{3.73}$$

for $x \in \mathbb{Z}^+$. As in the proof of Lemma 5, the state $|\psi_k\rangle$ is clearly satisfies the eigenvalue equation (with eigenvalue $2\cos(k)$) at vertices on the semi-infinite paths and vertices of g_0. The factor of $-\frac{1}{c}$ in (3.72) is chosen so that the eigenvalue condition is satisfied at vertices in P. It is easy to see that the eigenvalue condition is also satisfied at a.

Since $|\psi_k\rangle$ is a scattering eigenvector of G with eigenvalue $2\cos(k)$ and perfect transmission, we have $T(k) = 1$.

Now suppose $\widehat{G}$ is a type 2 R/T gadget, with $P = \{p\}$. Perfect transmission along with the eigenvalue equation at vertex a implies

$$\langle p | \mathrm{sc}_1(k) \rangle = 0, \tag{3.74}$$

so the restriction of $|\mathrm{sc}_1(k)\rangle$ to g_0 must be an eigenvector (since p is the only vertex connected to g_0). The eigenvalue equation at p gives

$$\langle a | \mathrm{sc}_1(k) \rangle + \sum_{w\colon (w,p) \in E(G_0)} \langle w | \mathrm{sc}_1(k) \rangle = 0 \quad \Longrightarrow \quad \sum_{w\colon (w,p) \in E(G_0)} \langle w | \mathrm{sc}_1(k) \rangle = -1. \tag{3.75}$$

Hence the restriction of $|\mathrm{sc}_1(k)\rangle$ to $V(g_0)$ is an eigenvector of the induced subgraph, with the additional property that the sum of the amplitudes at vertices connected to p is nonzero. □

With these two lemmas, if we can guarantee the form of the eigenstates for the graph G_0, we can guarantee certain momenta to be in either the reflection or the transmission set.

3.4.1.1 Explicit constructions

While the two lemmas do give a nice abstract explanation for the construction of R/T gadgets, it doesn't provide us with a concrete example. As such, let us look at two simple graphs and examine when they satisfy the conditions of the lemmas.

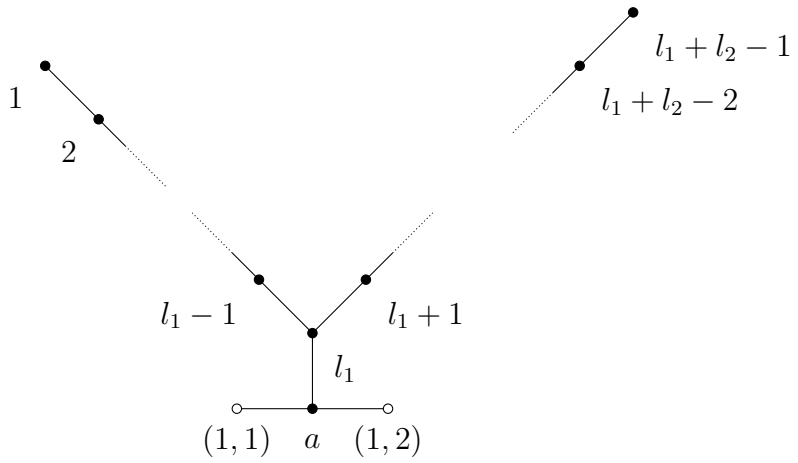

Figure 3.4: An R/T gadget built from a path of length $l_1 + l_2 - 2$.

As a first example, suppose G_0 is a finite path of length $l_1 + l_2 - 2$ connected to a at the l_1th vertex, as shown in Figure 3.4. As this is a type 2 R/T gadget, we can then determine the reflection and transmission sets as a function of l_1 and l_2.

Using Lemma 5, we see that perfect reflection occurs at momentum $k \in (-\pi, 0)$ if and only if the path has an eigenvector with eigenvalue $2\cos(k)$ with non-zero amplitude on vertex l_1. Recall that the path of length L (where the length of a path is its number of edges) has eigenvectors $|\psi_j\rangle$ for $j \in [L+1]$ given by

$$\langle x|\psi_j\rangle = \sin\left(\frac{\pi j x}{L+2}\right) \tag{3.76}$$

with eigenvalues $\lambda_j = 2\cos(\pi j/(L+2))$. Hence

$$\mathcal{R}_{\text{path}} = \left\{-\frac{\pi j}{l_1+l_2} : j \in [l_1+l_2-1] \text{ and } \frac{j l_1}{l_1+l_2} \notin \mathbb{Z}\right\}. \tag{3.77}$$

To characterize the momenta at which perfect transmission occurs, consider the induced subgraph obtained by removing the l_1th vertex from the path of length $l_1 + l_2 - 2$ (a path of length $l_1 - 2$ and a path of length $l_2 - 2$). We can choose bases for the eigenspaces of this induced subgraph so that each eigenvector has all of its support on one of the two paths, and has nonzero amplitude on only one of the vertices $l_1 - 1$ or $l_1 + 1$. Thus Lemma 6 implies that $\widehat{G}$ perfectly transmits for all momenta in the set

$$\mathcal{T}_{\text{path}} = \left\{-\frac{\pi j}{l_1} : j \in [l_1 - 1]\right\} \cup \left\{-\frac{\pi j}{l_2} : j \in [l_2 - 1]\right\}. \tag{3.78}$$

As an explicit example, if we set $l_1 = l_2 = 2$, we get $\mathcal{T}_{\text{path}} = \{-\frac{\pi}{2}\}$ and $\mathcal{R}_{\text{path}} = \{-\frac{\pi}{4}, -\frac{3\pi}{4}\}$.

Now let us suppose G_0 is a cycle of length r. Labeling the vertices by $x \in [r]$, where $x = r$ is the vertex attached to the path (as shown in Figure 3.5), the eigenvectors of the r-cycle are

$$\langle x|\phi_m\rangle = e^{2\pi i x m/r} \tag{3.79}$$

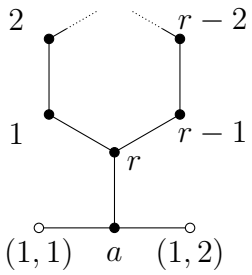

Figure 3.5: An R/T gadget built from an r-cycle.

with eigenvalue $2\cos(2\pi m/r)$, where $m \in [r]$. For each momentum $k = -2\pi m/r \in (-\pi, 0)$, there is an eigenvector with nonzero amplitude on the vertex r (i.e., $\langle r|\phi_m\rangle \neq 0$), so Lemma 5 implies that perfect reflection occurs at each momentum in the set

$$\mathcal{R}_{\text{cycle}} = \left\{ -\frac{\pi j}{r} : j \text{ is even and } j \in [r-1] \right\}. \tag{3.80}$$

To see which momenta perfectly transmit, we use Lemma 6. Consider the induced subgraph obtained by removing vertex r. This subgraph is a path of length $r-2$ and has eigenvalues $2\cos(\pi m/r)$ for $m \in [r-1]$ as discussed in the previous section. Using the expression (3.76) for the eigenvectors, we see that the sum of the amplitudes on the two ends is nonzero for odd values of m. Perfect transmission occurs for each of the corresponding momenta:

$$\mathcal{T}_{\text{cycle}} = \left\{ -\frac{\pi j}{r} : j \text{ is odd and } j \in [r-1] \right\}. \tag{3.81}$$

For example, the 4-cycle (i.e., square) has $\mathcal{T}_{\text{cycle}} = \{-\frac{\pi}{4}, -\frac{3\pi}{4}\}$ and $\mathcal{R}_{\text{cycle}} = \{-\frac{\pi}{2}\}$.

3.4.1.2 Reversing reflection and transmission sets

With these explicit examples of R/T gadgets, it will be useful to know how to interchange the reflection and transmission set. Namely, if we have one gadget that transmits all momenta in $\mathcal{T}$ and reflects all momenta in $\mathcal{R}$, it will be useful to also have a gadget that reflects all momenta in $\mathcal{T}$ and transmits all momenta in $\mathcal{R}$. Basically, we will be able to use these two gadgets together to construct gadgets with more interesting scattering behavior.

In particular, let $\widehat{G}$ be a type 2 R/T gadget, as seen in Figure 3.6a, and assume that it has a reflection set $\mathcal{R}$ and a transmission set $\mathcal{T}$. We will construct a type 1 R/T gadget $\widehat{G}^{\leftrightarrow}$ with reflection set $\mathcal{R}' \supset \mathcal{T}$ and transmission set $\mathcal{T}' \supset \mathcal{R}$. The graph $\widehat{G}^{\leftrightarrow}$ is depicted pictorially in Figure 3.6b.

Explicitly, the R/T gadget $\widehat{G}^{\leftrightarrow}$ is obtained by taking two copies of the subgraph g_0 from the type 2 R/T gadget in Figure 3.6a, connecting both to a single additional vertex u, and connecting one copy of g_0 to the infinite path at a. More concretely, for each vertex $w_j \in V(g_0)$, the graph $\widehat{G}^{\leftrightarrow}$ has two vertices $w_j^{(1)}$ and $w_j^{(2)}$, and the graph $\widehat{G}^{\leftrightarrow}$ inherits the edge set of g_0. Additionally, for each $w_j \in V(g_0)$ connected to the periphery vertex p, we have that $w_j^{(i)}$ is connected to u, and $w_j^{(1)}$ is connected to a.

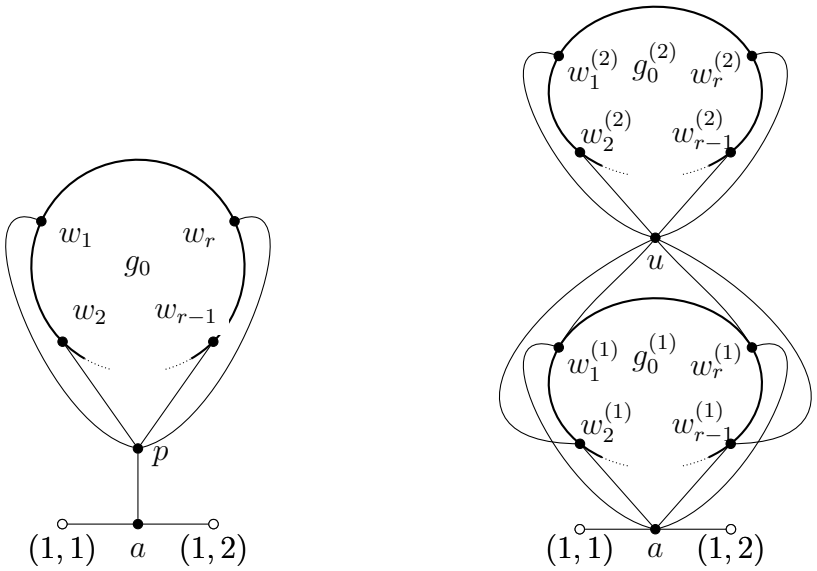

Figure 3.6: (a) A type 2 R/T gadget, (i.e., a type 1 gadget with $|P| = 1$). (b) The R/T gadget $\widehat{G}^{\leftrightarrow}$ reversing the reflection and transmission sets of (a).

With this definition, we now prove that the graph $\widehat{G}^{\leftrightarrow}$ reverses the reflection and transmission sets of $\widehat{G}$.

Lemma 7. *Let $\widehat{G}$ be a type 2 R/T gadget with transmission set $\mathcal{T}$ and reflection set $\mathcal{R}$. The type 1 R/T gadget $\widehat{G}^{\leftrightarrow}$ defined above has transmission set $\mathcal{T}' \supseteq \mathcal{R}$ and reflection set $\mathcal{R}' \supseteq \mathcal{T}$.*

Proof. First consider a momentum $k \in \mathcal{T}$. Using the condition derived in Lemma 6, we see that g_0 has an eigenvector $|\xi_k\rangle$ with eigenvalue $2\cos(k)$ where the sum of the amplitudes on vertices $w_1, \ldots, w_r$ is nonzero. Now consider the induced subgraph $G_0^{\leftrightarrow}$ of Figure 3.6b obtained by removing vertices $(1,1)$, $(1,2)$, and a. This subgraph has an eigenvector $|\chi_k^{\leftrightarrow}\rangle$ with eigenvalue $2\cos(k)$ given by

$$\langle v^{(i)}|\chi_k^{\leftrightarrow}\rangle = (-1)^i\langle v|\xi_k\rangle \quad \text{and} \quad \langle u|\chi_k^{\leftrightarrow}\rangle = 0 \tag{3.82}$$

for all vertices $v \in V(g_0)$ and for $i \in \{1,2\}$. The fact that $|\chi_k^{\leftrightarrow}\rangle$ is an eigenvector follows from the fact that $|\xi_k\rangle$ is an eigenvector of g_0. Additionally, we have that

$$\sum_{j=1}^{r}\langle w_j^{(1)}|\chi_k^{\leftrightarrow}\rangle = -\sum_{j=1}^{r}\langle w_j|\xi_k\rangle \neq 0. \tag{3.83}$$

Using Lemma 5, we see that perfect reflection occurs at momentum k, and thus $\mathcal{T} \subseteq \mathcal{R}'$.

Next suppose $k \in \mathcal{R}$. Lemma 5 states that G_0 has an eigenvector $|\chi_k\rangle$ with eigenvalue $2\cos(k)$ such that $\langle p|\chi_k\rangle \neq 0$. Now consider the induced subgraph $g_0^{\leftrightarrow}$ of Figure 3.6b obtained by removing vertices $(1,1)$, $(1,2)$, a, and $w_1^{(1)}, \ldots, w_r^{(1)}$. This graph has an eigenvector

$|\xi_k^{\leftrightarrow}\rangle$ with eigenvalue $2\cos(k)$ defined by

$$\langle v|\xi_k^{\leftrightarrow}\rangle = \begin{cases} \langle v|\chi_k\rangle & \text{for } v \in V(g_0^{(2)}) \\ \langle p|\chi_k\rangle & v = u \\ 0 & \text{otherwise.} \end{cases} \tag{3.84}$$

To see that this is an eigenvector, observe that $g_0^{\leftrightarrow}$ is a disconnected graph and $|\chi_k\rangle$ is an eigenvector of one of its components. Using this and Lemma 6 (since u is the only vertex adjacent to the periphery of $\hat{G}^{\leftrightarrow}$ with non-zero amplitude), we see that $k \in \mathcal{T}'$, so $\mathcal{R} \subseteq \mathcal{T}'$. □

3.4.2 Momentum switches

To construct a momentum switch between a given pair of momenta, it will be worthwhile to first construct two R/T gadgets between the momenta, with the two gadgets having swapped reflection and transmission sets. We can then construct something like a railroad switch, by placing the two gadgets immediately after a 3-claw. With this design, the incident wavepacket will only see one of the two outgoing paths, and the resulting S-matrix will be exactly what we want.

In particular, we can construct a momentum switch between the reflection and transmission sets $\mathcal{R}$ and $\mathcal{T}$ of a type 2 R/T gadget. We attach the gadget and its reversal (defined in Section 3.4.1.2) to the leaves of a claw, as shown in Figure 3.7. Specifically, given a type 2 R/T gadget $\widehat{G}$, the corresponding momentum switch $\widehat{G}^{\prec}$ consists of a copy of G_0, a copy of $G_0^{\leftrightarrow}$, and a claw, with the three leaves of the claw acting as the terminal vertices. Vertex p of G_0 is connected to leaf 2 of the claw, and vertices $w_1^{(1)}, \ldots, w_r^{(1)}$ of $G_0^{\leftrightarrow}$ are each connected to leaf 3 of the claw.

Intuitively, the momentum switch acts the same as a railroad switch. For momenta in the transmission set, the gadget perfectly transmits while its reversal perfectly reflects, so the claw is effectively a path connecting terminals 1 and 2. For momenta in the reflection set, the roles of transmission and reflection are reversed, so the claw is effectively a path connecting terminals 1 and 3.

We can now prove that this gadget acts as a momentum switch, by constructing the desired scattering eigenstates.

Lemma 8. *Let $\widehat{G}$ be a type 2 R/T gadget with reflection set $\mathcal{R}$ and transmission set $\mathcal{T}$. The gadget $\hat{G}^{\prec}$ described above is a momentum switch between the sets $\mathcal{R}$ and $\mathcal{T}$.*

Proof. We construct a scattering eigenstate for each momentum $k \in \mathcal{T}$ with perfect transmission from path 1 to path 2, and similarly construct a scattering eigenstate for each momentum $k' \in \mathcal{R}$ with perfect transmission from 1 to 3. These eigenstates show that $S_{2,1}(k) = 1$ and $S_{3,1}(k') = 1$. Since the S-matrix is symmetric and unitary, this gives the complete form of the S-matrix for all momenta in $\mathcal{R} \cup \mathcal{T}$. In particular, this shows that $\hat{G}^{\prec}$ is a momentum switch between $\mathcal{R}$ and $\mathcal{T}$.

We first construct the scattering states for momenta $k \in \mathcal{T}$. Lemma 6 shows that the graph g_0 has a $2\cos(k)$-eigenvector $|\xi_k\rangle$ satisfying equation (3.71) with some nonzero constant

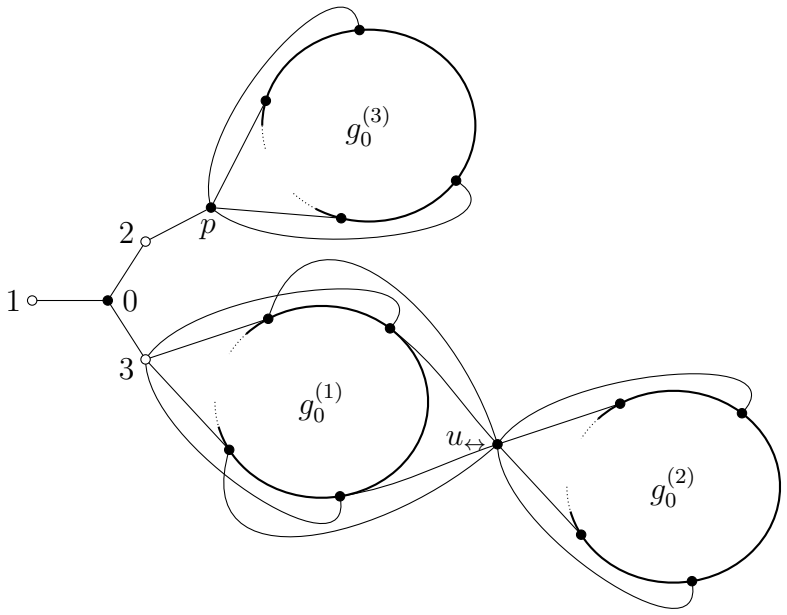

Figure 3.7: A momentum switch $\hat{G}^{\prec}$ built from a type 2 R/T gadget and its reversal.

c. We define a state $|\,\mu_k\,\rangle$ on $G^{\prec}$ and we show that it is a scattering eigenstate with perfect transmission between paths 1 and 2. The amplitudes of $|\,\mu_k\,\rangle$ on the semi-infinite paths and the claw are

$$\langle (x,1)|\mu_k\rangle = e^{-ikx} \qquad \langle 0|\mu_k\rangle = 1 \qquad \langle (x,2)|\mu_k\rangle = e^{ikx} \qquad \langle (x,3)|\mu_k\rangle = 0. \tag{3.85}$$

The rest of the graph consists of the three copies of the subgraph g_0 and the vertices p and $u_\leftrightarrow$. The corresponding amplitudes are

$$\langle\, v\,|\,\mu_k\,\rangle = \begin{cases} -\frac{1}{c}\langle\, v\,|\,\xi_k\,\rangle & v \in V(g_0^{(1)}) \\ \frac{1}{c}\langle\, v\,|\,\xi_k\,\rangle & v \in V(g_0^{(2)}) \\ -\frac{e^{ik}}{c}\langle\, v\,|\,\xi_k\,\rangle & v \in V(g_0^{(3)}) \\ 0 & v = p \text{ or } v = u_\leftrightarrow. \end{cases} \tag{3.86}$$

We claim that $|\,\mu_k\,\rangle$ is an eigenstate of the Hamiltonian with eigenvalue $2\cos(k)$. As in previous proofs, the state clearly satisfies the eigenvalue condition on the semi-infinite paths and at the vertices of G_0 and $G_0^{\leftrightarrow}$, and the factors of $\frac{1}{c}$ in the above equation are chosen so that the state also satisfies the eigenvalue condition at vertices p and $u_\leftrightarrow$. Since $|\,\mu_k\,\rangle$ is a scattering state with perfect transmission from path 1 to path 2, we see that $S_{2,1}(k) = 1$.

We now construct an eigenstate $|\,\nu_{k'}\,\rangle$ with perfect transmission from path 1 to path 3 for each momentum $k' \in \mathcal{R}$. This state has the form

$$\langle (x,1)|\nu_{k'}\rangle = e^{-ik'x} \qquad \langle 0|\nu_{k'}\rangle = 1 \qquad \langle (x,2)|\nu_{k'}\rangle = 0 \qquad \langle (x,3)|\nu_{k'}\rangle = e^{ik'x} \tag{3.87}$$

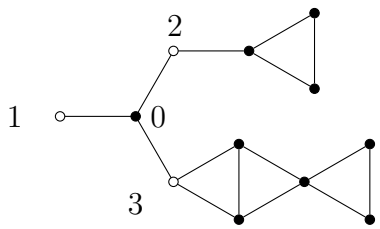

Figure 3.8: A momentum switch between $-\frac{\pi}{3}$ and $-\frac{2\pi}{3}$.

on the semi-infinite paths and the claw. Lemma 5 shows that G_0 has a $2\cos(k')$-eigenstate $|\chi_{k'}\rangle$ with $\langle p|\chi_{k'}\rangle \neq 0$, which determines the form of $|\nu_{k'}\rangle$ on the remaining vertices:

$$\langle v|\nu_{k'}\rangle = \begin{cases} -\frac{1}{\langle p|\chi_{k'}\rangle}\langle v|\chi_{k'}\rangle & v \in V(G_0) \\ -\frac{e^{ik'}}{\langle p|\chi_{k'}\rangle}\langle v|\chi_{k'}\rangle & v \in V(g_0^{(2)}) \\ -e^{ik'} & v = u^{\leftrightarrow} \\ 0 & \text{otherwise.} \end{cases} \tag{3.88}$$

As before, it is easy to check that this a momentum-k' scattering state with perfect transmission from path 1 to path 3, so $S_{3,1}(k') = 1$.

Thus the gadget from Figure 3.7 is a momentum switch between $\mathcal{R}$ and $\mathcal{T}$. □

3.4.2.1 Explicit example

Using this construction for momentum switches, we can obtain a momentum switch from any of the examples discussed in Section 3.4.1.1. Explicitly, using the R/T gadget built from the 3-cycle, we get a momentum switch between $-\frac{\pi}{3}$ and $-\frac{2\pi}{3}$, as shown in Figure 3.8. More generally, using an r-cycle, we obtain a switch between momenta of the form $-\frac{\pi j}{r}$ with odd or even values of j. As another example, using a path of length 4 connected at the center vertex, we obtain a switch between $-\frac{\pi}{4}$ and $-\frac{\pi}{2}$.

3.4.3 Encoded unitaries

While there is no known efficient method to find graphs that fixed scattering behavior, it is possible to search over all small graphs in order to find gadgets with some particular scattering behavior. This was the manner in which the gadgets for most known scattering results were found, such as in Childs' original universality proof for graph scattering [10] and Childs, Gosset, and Webb's universality result [15]. Additionally, Blumer, Underwood, and Feder have a paper [9] in which they searched over all graphs with up to 9 vertices for scattering behavior at particular momentum.

Essentially, the main idea behind this method is a brute force search. Since we can easily compute the scattering matrix for a particular graph at a particular momentum, if we want to find a graph that has some prescribed scattering behavior, we simply assume that such a graph exists and search for it over all graphs, starting with those having a small number of vertices. While this exhaustive search is not guaranteed to find such a graph, a surprising number of systems can be found with this structure. In particular, if we restrict ourselves

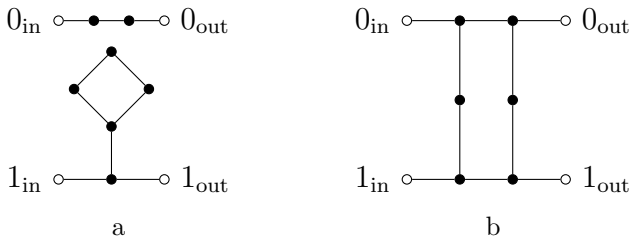

Figure 3.9: Encoded one-qubit gates at $k = -\frac{\pi}{4}$. (a) A phase gate. (b) Basis-changing gate.

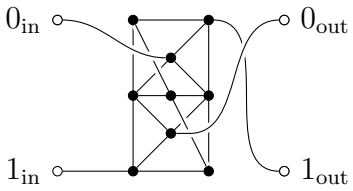

Figure 3.10: Graph implementing a Hadamard gate at $k = -\frac{\pi}{2}$.

to momenta that are simple multiples of π, such as $-\frac{\pi}{2}$ or $-\frac{\pi}{4}$, then most simple scattering behaviors can be found.

Of particular interest to us will be gadgets with four terminal vertices, such that the scattering matrix at some particular momenta takes the form

$$S(k) = \begin{pmatrix} 0 & U^T \\ U & 0 \end{pmatrix}. \tag{3.89}$$

Namely, if we use a dual-rail encoding for a qubit, and think of one pair of semi-infinite paths as the input rails and the other pair as the output rails, then after scattering this gadget will have applied the unitary U to the encoded qubit.

Later in the thesis, we will be interested in finding a universal gate set for both $-\frac{\pi}{4}$ and $-\frac{\pi}{2}$. As such, we can take as examples those graphs that will be of interest to us later.

In particular, we have that the graph in Figure 3.9a has a scattering matrix of the form of equation (3.89) at momentum $k = -\frac{\pi}{4}$, with

$$U = \begin{pmatrix} e^{-i\frac{\pi}{4}} & 0 \\ 0 & 1 \end{pmatrix}, \tag{3.90}$$

while the gadget in Figure 3.9b also has a scattering matrix of the form (3.89) at momentum $k = -\frac{\pi}{4}$, where

$$U = -\frac{i}{\sqrt{2}} \begin{pmatrix} 1 & -i \\ -i & 1 \end{pmatrix}. \tag{3.91}$$

Similarly, we have that at $k = -\frac{\pi}{2}$, the graph of Figure 3.10 has a scattering matrix of the form (3.89), with

$$U = -\frac{e^{i\frac{\pi}{4}}}{\sqrt{2}} \begin{pmatrix} 1 & 1 \\ 1 & -1 \end{pmatrix}. \tag{3.92}$$

With these examples, we then have a universal gate set for single-qubit unitaries at $-\frac{\pi}{4}$, which will be sufficient for our eventual purposes.

3.5 Various facts about scattering

While the previous constructions yield graphs with particular behavior which will be useful when attempting to construct scattering algorithms, we will also want to understand some simple relations between graphs and their respective scattering matrices. In particular, understanding what properties are necessary in order to have a given scattering matrix, and understanding the relation between various the scattering matrices of various momenta will be useful in constructing additional scattering graphs.

3.5.1 Degree-3 graphs are sufficient

One of the most simple assumptions that could be made is that certain scattering behaviors require high degree graphs. In particular, having many connections might allow for additional correlations between outputs on larger graphs.

If we restrict our attention to a finite number of rational momenta, however, this does not turn out to be the case. We can show that any graph can be replaced by a degree-three graph with a identical scattering behavior at some fixed momenta. In particular, we will show that a single vertex can be replaced by a finite path while still satisfying the eigenvalue equation at the fixed momenta, where the length of the path is dependent on the fixed momenta.

As degree two graphs are the graph joins of cycles and paths, degree three graphs are the smallest graphs to have nontrivial scattering behaviors. This lemma shows that, in a certain sense, they are also all that are required.

Lemma 9. *Let $\widehat{G}$ be a finite graph, and let M be a finite set of rational multiples of π. If $v \in V(G)$ is a degree d vertex, there exists a graph H that extends G with the vertex v being replaced by a degree-$(\lceil \frac{d}{2} \rceil + 1)$ subgraph such that the scattering matrices at the momenta $k \in M$ are preserved.*

Proof. The main idea behind this proof is to partition the vertices adjacent to v into two sets, and then replace v by a finite path, with the two sets connected to opposites ends of the finite path. By choosing the length of the path correctly, we can show that the amplitudes at either end of the path are the same as the amplitude on v at each momenta in M, and thus the eigenvalue equation remains satisfied without changing the scattering behavior.

In particular, let v be the degree d vertex in G, and let $S = \{w \in V(G) : w \sim v\}$ be the set of vertices adjacent to v. Additionally, let us arbitrarily partition S into two sets, S_1 and S_2, such that $\big||S_1| - |S_2|\big| \leq 1$.

As each $k \in M$ is a rational multiple of π, there exists some $m \in \mathbb{N}^+$ such that $\frac{mk}{2\pi} \in \mathbb{N}$ for all $k \in M$. Let us then examine the graph H where v is replaced by a path of length m, and where S_1 is attached to one end of the path while S_2 is attached to the other end. Explicitly:

$$V(H) = \big(V(G) \setminus \{v\}\big) \cup \{(v, j) : j \in [m+1]\} \tag{3.93}$$

$$E(H) = \big\{e \in E(G) : v \notin e\big\} \cup \big\{\{(v, j), (v, j+1)\} : j \in [m]\big\} \cup \big\{\{s, (v, 0)\} : s \in S_1\big\} \cup \big\{\{s, (v, m)\} : s \in S_2\big\}. \tag{3.94}$$

Now, for any $k \in M$, let $|\phi\rangle$ be an eigenstate of $A(G)$ with eigenvalue $2\cos(k)$. We will show that there exists an eigenstate $|\psi\rangle$ of $A(H)$ with energy $2\cos(k)$ such that for any $w \in V(G) \setminus \{v\}$, $\langle w|\phi\rangle = \langle w|\psi\rangle$.

Concretely, for any vertex other than v, let us define $|\psi\rangle$ in this manner, and note that by assumption, $|\psi\rangle$ satisfies the eigenvalue equation with energy $2\cos(k)$ for all vertices other than those in S or those replacing v. Additionally, let

$$\alpha = \sum_{w \in S_1} \langle w|\phi\rangle, \qquad \beta = \langle v|\phi\rangle, \qquad \text{and} \qquad \gamma = \sum_{w \in S_2} \langle w|\phi\rangle. \tag{3.95}$$

We will then defined the amplitude along the path replacing the vertex v as

$$\langle (v,j)|\psi\rangle = \beta\cos(kj) + \frac{\gamma - \beta\cos(k)}{\sin(k)}\sin(kj). \tag{3.96}$$

Note that $\langle (v,0)|\psi\rangle = \langle (v,m)|\psi\rangle = \beta = \langle v|\phi\rangle$, and thus the eigenvalue equation is satisfied at all vertices in S. As the eigenstates along a path with energy $2\cos(k)$ are scalar multiples of $\sin(kx)$ and $\cos(kj)$, we can also see that the eigenvalue equation is necessarily satisfied for all (v,j) with $j \neq 0$ and $j \neq m$.

If we then examine the eigenvalue equation at $(v,0)$, we can see that

$$\sum_{s \in S_1} \langle s|\psi\rangle + \langle (v,1)|\psi\rangle = \alpha + \beta\cos(k) + \frac{\gamma - \beta\cos(k)}{\sin(k)}\sin(k) \tag{3.97}$$

$$= \alpha + \gamma \tag{3.98}$$

$$= 2\cos(k)\beta = 2\cos(k)\langle (v,0)|\psi\rangle \tag{3.99}$$

where the third equality follows from the fact that $|\phi\rangle$ satisfies the eigenvalue equation at v with eigenvalue $2\cos(k)$, and thus we have that the eigenvalue equation for H is satisfied at $(v,0)$.

Let us finally examine the eigenvalue equation at (v,m), noting that

$$\sum_{s \in S_2} \langle s|\psi\rangle + \langle (v,m-1)|\psi\rangle = \gamma + \beta\cos(k(m-1)) + \frac{\gamma - \beta\cos(k)}{\sin(k)}\sin(k(m-1)) \tag{3.100}$$

$$= \gamma + \beta\cos(k) - \big(\gamma - \beta\cos(k)\big) \tag{3.101}$$

$$= 2\cos(k)\beta = 2\cos(k)\langle (v,0)|\psi\rangle \tag{3.102}$$

where the second equality follows from some trigonometric identities. We can then see that $|\psi\rangle$ satisfies the eigenvalue equation at (v,m) with energy $2\cos(k)$.

Putting this together, we have that $|\psi\rangle$ is an eigenvector of $A(H)$ with energy $2\cos(k)$ such that $|\psi\rangle$ and $|\phi\rangle$ are identical on those vertices contained in both G and H. As this result holds for any energy $2\cos(k)$ eigenvector of $A(G)$, and as the two graphs are identical along the semi-inifinite paths, we have that the scattering states for these two graphs are identical, and thus the scattering matrices are preserved under this degree reduction procedure. □

By repeated use of this lemma, we can then reduce any graph used as a scattering gadget down to a degree-3 graph without changing the scattering matrix at some fixed momentum.

3.5.2 Some behavior impossible

So far, all of our constructions have generally assumed that the scattering behavior that we want does exist. Hence, if we simply search over large enough graphs, we will eventually find a graph that implements our desired scattering behavior.

However, it turns out that in some cases this is not a valid assumption. In particular, there exist pairs of momenta for which no R/T gadget can be constructed. The main idea is that for specific momentum, there exists a basis for the scattering states in which all amplitudes are taken from a field extension of the rationals. If two momenta are related by a Galois conjugation over this field, then perfect reflection at one momenta implies perfect reflection at the second.

As an illuminating example, we will use those states with momenta $k = -\frac{\pi}{4}$ and $p = -\frac{3\pi}{4}$. For the two momenta, the corresponding energy is $2\sqrt{2}$ or $-2\sqrt{2}$, and in this case the Galois conjugation is simply replacing $\sqrt{2}$ by $-\sqrt{2}$.

3.5.2.1 Basis vectors with entries in $\mathbb{Q}(\sin(k), \cos(k))$

Recall the general setup shown in Figure 3.2: N semi-infinite paths are attached to a finite graph $\widehat{G}$, resulting in an infinite graph G. Additionally, we have that the adjacency matrix for $\widehat{G}$ can be written in block diagonal form

$$A(\widehat{G}) = \begin{pmatrix} A & B^\dagger \\ B & D \end{pmatrix}, \tag{3.103}$$

where A is an $N \times N$ matrix, B is an $m \times N$ matrix, and D is an $m \times m$ matrix. We have that the N semi-infinite paths are attached, in order, to the first N vertices of $\widehat{G}$.

Let us now consider an eigenvector $|\tau_k\rangle$ of the adjacency matrix of G with eigenvalue $2\cos(k)$ for $k \in (-\pi, 0)$. We have from Theorem 2 that this eigenspace is spanned by incoming scattering states with momentum k and confined bound states (which have zero amplitude on the semi-infinite paths) . We can thus write the amplitudes of $|\tau_k\rangle$ on the semi-infinite paths as

$$\langle (x, j) | \tau_k \rangle = \kappa_j \cos(k(x-1)) + \sigma_j \sin(k(x-1)) \tag{3.104}$$

for $x \in \mathbb{Z}^+$, $j \in [N]$, and $\kappa_j, \sigma_j \in \mathbb{C}$, and the amplitudes on the internal vertices as

$$\langle w | \tau_k \rangle = \iota_w \tag{3.105}$$

for $\iota_w \in \mathbb{C}$, where w indexes the internal vertices. Since the state $|\tau_k\rangle$ satisfies the eigenvalue equation on the semi-infinite paths, it remains to satisfy the conditions specified by the block matrix equation

$$\begin{pmatrix} A & B^\dagger \\ B & D \end{pmatrix} \begin{pmatrix} \kappa \\ \iota \end{pmatrix} + \cos(k) \begin{pmatrix} \kappa \\ 0 \end{pmatrix} + \sin(k) \begin{pmatrix} \sigma \\ 0 \end{pmatrix} = 2\cos(k) \begin{pmatrix} \kappa \\ \iota \end{pmatrix}.$$

Hence, the nullspace of the matrix

$$M = \begin{pmatrix} A - \cos(k)\mathbb{I} & \sin(k)\mathbb{I} & B^\dagger \\ 0 & 0 & 0 \\ B & 0 & D - 2\cos(k)\mathbb{I} \end{pmatrix} \tag{3.106}$$

is in one-to-one correspondence with the $2\cos(k)$-eigenspace of the infinite matrix (here the first block corresponds to κ, the second to σ, and the third to ι). Further, M only has entries in $\mathbb{Q}(\cos(k), \sin(k))$, so its nullspace has a basis with amplitudes in $\mathbb{Q}(\cos(k), \sin(k))$, as can be seen using Gaussian elimination.

We can then use this, along with the form of the eigenstates along the semi-infinite paths, to see that all of the amplitudes can be written as elements over the rationals extended by $\sin(nk)$ and $\cos(nk)$ for all $n \in \mathbb{N}^+$. While this is not particularly useful in general, if k is a rational multiple of π, this is a finite extension. Further, there exist special cases in which this field extension is a quadratic extension, such that all of the amplitudes can be taken from $\mathbb{Q}[\sqrt{d}]$ for some d.

As a slight caveat noted above, the spectrum of G may include confined bound states (Theorem 2) with eigenvalues at $2\cos(k)$. However, any such state is also in the nullspace of the matrix M, while also satisfying the rational constraints that both κ and σ are zero. As such, these states can always be written with amplitudes over the field $\mathbb{Q}[\sin(k), \cos(k)]$. Thus forcing the scattering eigenstates to be orthogonal to these confined bound states only involves constraints over the same field, and we still have that the scattering eigenstates can be written with all of their amplitudes over the field $\mathbb{Q}$ extended by $\sin(nk)$ and $\cos(nk)$.

As an explicit example, let us examine the case where $2\cos(k) = \pm\sqrt{2}$ corresponding to $k = -\frac{\pi}{4}$ or $k = -\frac{3\pi}{4}$. In these cases $\mathbb{Q}(\cos(k), \sin(k)) = \mathbb{Q}(\sqrt{2})$, and we may choose a basis for the nullspace of M with amplitudes from $\mathbb{Q}(\sqrt{2})$. Furthermore, $\cos(kx), \sin(kx) \in \mathbb{Q}(\sqrt{2})$ for all $x \in \mathbb{Z}^+$, so with such a choice of basis, each amplitude of $|\tau_k\rangle$ is also an element of $\mathbb{Q}(\sqrt{2})$.

We can then use the fact that $\mathbb{Q}[\sqrt{2}]$ can be thought of as a two-dimensional vectorspace over $\mathbb{Q}$ to see that any member of this extended rational basis can be written as

$$|\tau_k\rangle = |u_k\rangle + \sqrt{2}|w_k\rangle, \tag{3.107}$$

for rational vectors $|u_k\rangle$ and $|w_k\rangle$. Further, as $H^2|\tau_k\rangle = 2|\tau_k\rangle$, we can see that $H|u_k\rangle = \pm 2|w_k\rangle$ and $H|w_k\rangle = \pm|u_k\rangle$, so

$$|\tau_k\rangle = (H \pm \sqrt{2}\mathbb{I})|w_k\rangle, \tag{3.108}$$

where the $\pm$ depends on whether we are working with $k = -\frac{\pi}{4}$ or $-\frac{3\pi}{4}$.

While this expression does not easily generalize to most pairs of momenta, we do have a similar equation whenever the extended field is a quadratic extension, where 2 replaced with d.

3.5.2.2 Impossibility of R/T gadgets

With the above rational basis for scattering states, we will be able to transform an eigenstate at one energy into an eigenstate at another energy via a Galois conjugation. However, the existence of particular eigenstates will not immediately give us the results that we want.

Along these lines, we will use the following basic fact about two-terminal gadgets several times:

Fact 1. *If a two-terminal gadget has a momentum-k scattering state $|\phi\rangle$ with zero amplitude along path 2, then the gadget perfectly reflects at momentum k.*

Proof. Without loss of generality, we may assume that $|\phi\rangle$ is orthogonal to all confined bound states. If $|\phi\rangle$ has zero amplitude along path 2, then there exist some $\mu, \nu \in \mathbb{C}$ such that

$$\langle (x,2)\,|\phi\rangle = \mu\langle (x,2)\,|\mathrm{sc}_2(k)\rangle + \nu\langle (x,2)\,|\mathrm{sc}_1(k)\rangle = \mu e^{-ikx} + \mu R e^{ikx} + \nu T e^{ikx} = 0 \quad (3.109)$$

for all $x \in \mathbb{Z}^+$. Since this holds for all x, we have $\mu = \mu R + \nu T = 0$. Since μ and ν cannot both be zero, we have $T = 0$. □

For an R/T gadget, the scattering states (at some fixed momentum) that are orthogonal to the confined bound states span a two-dimensional space. As shown in Section 3.5.2.1, we can expand each scattering eigenstate over an extension to the field $\mathbb{Q}$. Let us restrict our attention to the case where this extension is quadratic, with discriminant d.

In particular, let us assume that the scattering state at k has energy $\sqrt{d}$ (with d non-square) and can be written in a basis with entries over $\mathbb{Q}(\sqrt{d})$, where each basis vector takes the form (3.108). This gives

$$|\mathrm{sc}_1(k)\rangle = (H + \sqrt{d}\mathbb{I})(\alpha|a\rangle + \beta|b\rangle)$$

where $\alpha, \beta \in \mathbb{C}$, $\alpha \neq 0$, and $|a\rangle$ and $|b\rangle$ are rational d-eigenvectors of H^2.

If $T(k) = 0$, then for all $x \geq 0$,

$$\langle x,2|\mathrm{sc}_1(k)\rangle = 0 = \langle x,2|(H + \sqrt{d}\mathbb{I})(\alpha|a\rangle + \beta|b\rangle). \quad (3.110)$$

Dividing through by α and rearranging, we get that for all $x \geq 0$,

$$\frac{\beta}{\alpha}(\langle x,2|H|b\rangle + \sqrt{d}\langle x,2|b\rangle) = -\langle x,2|H|a\rangle - \sqrt{d}\langle x,2|a\rangle.$$

If the left-hand side is not zero, then $\beta/\alpha \in \mathbb{Q}(\sqrt{d})$ since H, $|a\rangle$, and $|b\rangle$ are rational. If the left-hand side is zero, then $(H + \sqrt{d}\mathbb{I})|a\rangle$ is an eigenstate at energy $2\cos(k)$ with no amplitude along path 2, so $\beta = 0$ (using Fact 1), and again $\beta/\alpha \in \mathbb{Q}(\sqrt{d})$.

Now write $\beta/\alpha = r + s\sqrt{d}$ with $r, s \in \mathbb{Q}$, and consider the rational d-eigenvector of H^2

$$|c\rangle := |a\rangle + (r + sH)|b\rangle. \quad (3.111)$$

Note that

$$\alpha(H + \sqrt{d}\mathbb{I})|c\rangle = \alpha(H + \sqrt{d}\mathbb{I})|a\rangle + \alpha(rH + r\sqrt{d} + sH^2 + sH\sqrt{d})|b\rangle. \quad (3.112)$$

Since $|b\rangle$ is a d-eigenvector of H^2 and $\beta/\alpha = r + s\sqrt{d}$, this simplifies to

$$\alpha(H + \sqrt{d}\mathbb{I})|c\rangle = \alpha(H + \sqrt{d}\mathbb{I})|a\rangle + \beta(H + \sqrt{d}\mathbb{I})|b\rangle = |\mathrm{sc}_1(k)\rangle, \quad (3.113)$$

so $|\mathrm{sc}_1(k)\rangle$ can be written as $\alpha(H + \sqrt{d}\mathbb{I})$ times a rational d-eigenvector of H^2.

Since $\langle x,2|\mathrm{sc}_1(k)\rangle = 0$ for all $x \geq 1$ (and $\alpha \neq 0$), we have

$$\langle x,2|(H + \sqrt{d}\mathbb{I})|c\rangle = \langle x,2|H|c\rangle + \sqrt{d}\langle x,2|c\rangle = 0. \quad (3.114)$$

As H is a rational matrix and $|c\rangle$ is a rational vector, the rational and irrational components must both be zero, implying $\langle x, 2|c\rangle = \langle x, 2|H|c\rangle = 0$ for all $x \geq 1$. Furthermore, since $|\mathrm{sc}_1(k)\rangle$ is a scattering state with zero amplitude on path 2, it must have some nonzero amplitude on path 1 and thus there is some $x_0 \in \mathbb{Z}^+$ for which $\langle x_0, 1|c\rangle \neq 0$ or $\langle x_0, 1|H|c\rangle \neq 0$.

Now consider the state obtained by replacing $\sqrt{d}$ with $-\sqrt{d}$, or in other words after performing a Galois conjugation:

$$|\overline{\mathrm{sc}}_1(k)\rangle := \alpha(H - \sqrt{d}\mathbb{I})|c\rangle. \tag{3.115}$$

This is a $-\sqrt{d}$-eigenvector of H, which can be confirmed using the fact that $|c\rangle$ is a d-eigenvector of H^2. As $\langle x, 2|H|c\rangle = \langle x, 2|c\rangle = 0$ for all $x \geq 1$, $\langle x, 2|\overline{\mathrm{sc}}_1(k)\rangle = 0$ for all $x \geq 1$. Furthermore the amplitude at vertex $(x_0, 1)$ is nonzero, i.e., $\langle x_0, 1|\overline{\mathrm{sc}}_1(k)\rangle \neq 0$, and hence $|\overline{\mathrm{sc}}_1(k)\rangle$ has a component orthogonal to the space of confined bound states (which have zero amplitude on both semi-infinite paths). Hence, there exists a scattering state with eigenvalue $-\sqrt{d}$ with no amplitude on path 2. By Fact 1, the gadget perfectly reflects at momentum p, where $p = -\pi - k$ corresponds to this energy. It follows that no perfect R/T gadget (and hence no perfect momentum switch) exists between these momenta.

As particular cases, we can take $k = -\frac{\pi}{4}$, where $d = 2$. In this case, we have that there does not exist an R/T gadget splitting k and $-\frac{3\pi}{4}$. Similarly, it is possible to show that $k = -\frac{\pi}{6}$ can be written in a basis with entries over $\mathbb{Q}[\sqrt{3}]$, and thus there does not exist a R/T gadget between k and $-\frac{5\pi}{6}$.

3.5.2.3 Approximate R/T gadget

[**TO DO:** *I never particularly liked this bit, and I'll think I'll include it later if I have the time*]

3.5.3 Laplacians vs adjacency matrix

[**TO DO:** *If I have time, write this section. The basic idea is similar to proof removing self-loops from the graph for the BH model. In particular, in order to turn a degree 3 graph into a 3-regular graph, we use three copies of the original graph. For each degree-2 vertex u in the original graph, we add another vertex u_0 to the overall graph, and add edges from all three u_i for $i \in [3]$ to u_0. For each degree-1 vertex, we do this twice. Note that for each eigenstate of the original graph, there are two with nearly the same amplitudes. We can then use these for our scattering eigenstates*]

3.6 Wavepacket scattering

Up until this point, we have taken as intuition that the scattering states correspond to an incoming wavepacket at some momentum, and then scatterings with a corresponding S-matrix. However, this is somewhat weird, in that the scattering states are eigenstates of the Hamiltonian, and thus do not change over time, while scattering states explicitly move.

In this section, we will show that our intuitive naming is useful. In particular, we will show that preparing a wavepacket centered at some momenta will scatter as the S-matrix of the corresponding scattering state. Further, the shape of the wavepacket will remain approximately the same.

This section is devoted to proving the following lemma describing the scattering behavior of a Gaussian wavepacket.

Theorem 3. *Let $\widehat{G}$ be an $(N+m)$-vertex graph, let G be the graph obtained from $\widehat{G}$ by attaching N semi-infinite paths to the first N of its vertices, and let S be the corresponding S-matrix. Let $|\psi_j(0)\rangle$ be a cut-off Gaussian distribution with momentum k and standard deviation σ centered at μ, with the cut-off at a distance L from the center. Namely, let*

$$|\psi^j(0)\rangle = \gamma \sum_{x=\mu-L}^{\mu+L} e^{-ikx} e^{-(x-\mu)^2/2\sigma^2} |x,j\rangle, \tag{3.116}$$

where γ is the normalization of $|\psi^j(0)\rangle$. Then let us define the state

$$|\alpha^j(t)\rangle = \begin{cases} \gamma e^{-2it\cos k} \sum_{x=\mu(t)-L}^{\mu(t)+L} e^{-ikx} e^{-(x-\mu(t))^2/2\sigma^2} |x,j\rangle & t < \frac{\mu-L}{2|\sin k|} \\ \gamma e^{-2it\cos k} \sum_{x=\mu(t)-L}^{\mu(t)+L} \sum_{q=1}^{N} S_{qj}(k) e^{ikx} e^{-(x+\mu(t))^2/2\sigma^2} |x,q\rangle & t > \frac{\mu+L}{2|\sin k|}, \end{cases} \tag{3.117}$$

where

$$\mu(t) = \mu - \lceil 2t\sin(k) \rceil. \tag{3.118}$$

If $\sigma = c_1 \frac{L}{\sqrt{\log L}}$ for some constant c_1, we then have that for $0 < t < \frac{\mu-L}{2|\sin k|}$ and for $\frac{\mu+L}{2|\sin k|} < t < c_2 L$ (assuming the bounds make sense),

$$\| e^{-iH_g t} |\psi^j(0)\rangle - |\alpha^j(t)\rangle \| \leq \chi \sqrt{\frac{\log L}{L}}, \tag{3.119}$$

for some constant χ.

Note that this theorem requires that the standard deviation and the original distance from the graph be related. Further, this theorem doesn't give an approximation to the time-evolved state when the approximation has non-zero amplitude inside the graph $\widehat{G}$.

[**TO DO:** *I'm almost positive that I can get this bound down to $\frac{\log L}{L}$, essentially getting rid of the square root. If I have time I want to get back to this*]

3.6.1 Jacobi Θ-function

Before we delve into the proof of the wavepacket scattering, it will be useful to define a kind of discrete approximation to a Gaussian. In particular, let us define the function

$$h_L^\sigma(\phi) = \sum_{n=-L}^{L} e^{i\phi n} e^{-\frac{x^2}{2\sigma^2}}. \tag{3.120}$$

This is closely related to the amplitude of the original wavepacket in Theorem 3, and will be used extensively in our proof.

Additionally, this function is closely related to the Jacobi theta function, for which we refer the reader to Chapter 10 of [30] for a broad overview. This function, $\Theta(z,q)$ is defined for all complex z and all q with positive imaginary part as

$$\Theta(z,q) = \sum_{n=-\infty}^{\infty} e^{\pi i n^2 \tau} e^{2\pi i n z} \tag{3.121}$$

and is related to our h as

$$h_\infty^\sigma(\phi) = \sum_{n=-\infty}^{\infty} e^{i\phi n} e^{-\frac{n^2}{2\sigma^2}} = \Theta\left(\frac{\phi}{2\pi}, \frac{i}{2\pi\sigma^2}\right). \tag{3.122}$$

The Jacobi theta function has several symmetries, such as the fact that $\Theta(z,q) = \Theta(-z,q)$, and one that is similar to the Fourier transform. In particular, using our language and Theorem 1.6 from Chapter 10 of [30], we have

$$h_\infty^\sigma(\phi) = \Theta\left(\frac{\phi}{2\pi}, \frac{i}{2\pi\sigma^2}\right) = \sqrt{2\pi}\sigma e^{-\frac{\sigma^2\phi^2}{2}} \Theta\big(i\phi\sigma^2, 2\pi i\sigma^2\big) = \sqrt{2\pi}\sigma e^{-\frac{\sigma^2\phi^2}{2}} h_\infty^{1/(2\pi\sigma)}\big(2\pi i\phi\sigma^2\big). \tag{3.123}$$

This can be viewed as a discrete version of a Fourier transform, as the summand goes from a Gaussian distribution with standard deviation σ to one that has standard deviation σ^{-1}. Additionally, note that the argument to the h function is now complex.

Let us now give some bounds comparing the various h_L^σ. Note that this simple bound for the normal distribution came from [18]. Assuming that $L > 0$, and that ϕ is real, we have that

$$\begin{aligned}
\big|h_\infty^\sigma(\phi) - h_L^\sigma(\phi)\big| &= \Big| \sum_{n=L+1}^{\infty} 2\cos(n\phi) e^{-\frac{n^2}{2\sigma^2}} \Big| && (3.124)\\
&\leq 2 \sum_{n=L+1}^{\infty} e^{-\frac{n^2}{2\sigma^2}} && (3.125)\\
&\leq 2 \int_L^\infty e^{-\frac{x^2}{2\sigma^2}} dx && (3.126)\\
&= 2\sigma \int_{L/\sigma}^\infty e^{-\frac{u^2}{2}} du && (3.127)\\
&< 2\sigma \int_{L/\sigma}^\infty \frac{\sigma u}{L} e^{-\frac{u^2}{2}} du && (3.128)\\
&= \frac{2\sigma^2}{L} e^{-\frac{L^2}{2\sigma^2}}, && (3.129)
\end{aligned}$$

while if $L = 0$ we instead have

$$\left|h^\sigma_\infty(\phi) - 1\right| = \left|\sum_{n=1}^{\infty} 2\cos(n\phi)e^{-\frac{n^2}{2\sigma^2}}\right| \tag{3.130}$$

$$\leq 2e^{-\frac{1}{2\sigma^2}} + \sum_{n=2}^{\infty} e^{-\frac{n^2}{2\sigma^2}} \tag{3.131}$$

$$\leq 2e^{-\frac{1}{2\sigma^2}} + 2\int_1^{\infty} e^{-\frac{x^2}{2\sigma^2}}dx \tag{3.132}$$

$$< 2e^{-\frac{1}{2\sigma^2}} + 2\sigma^2 e^{-\frac{1}{2\sigma^2}} \tag{3.133}$$

$$= 2(1+\sigma^2)e^{-\frac{1}{2\sigma^2}}. \tag{3.134}$$

These two bounds will allow us to approximate many of the relevant numbers.

We will now try to bound the size of $h^\sigma_\infty(\phi)$, for small (but real) σ and imaginary ϕ (so as to use the discrete Fourier transform). In particular, if we assume that $1 > \sigma^2|\phi|$, we will have

$$h^\sigma_\infty(\phi) = \sum_{n=-\infty}^{\infty} e^{in\phi}e^{-\frac{n^2}{2\sigma^2}} \tag{3.135}$$

$$= 1 + \sum_{n=1}^{\infty} 2\cos(n\phi)e^{-\frac{n^2}{2\sigma^2}} \tag{3.136}$$

$$\leq 1 + 2\sum_{n=1}^{\infty} e^{-\frac{n^2}{2\sigma^2}+n|\phi|} \tag{3.137}$$

$$< 1 + 2e^{-\frac{1}{2\sigma^2}+|\phi|} + 2e^{\frac{\sigma^2|\phi|^2}{2}}\sum_{n=2}^{\infty}\exp\Big[-\frac{1}{2}\Big(\frac{n}{\sigma}-\sigma|\phi|\Big)^2\Big] \tag{3.138}$$

$$< 1 + 2e^{-\frac{1}{2\sigma^2}+|\phi|} + 2e^{\frac{\sigma^2|\phi|^2}{2}}\int_1^{\infty}\exp\Big[-\frac{1}{2}\Big(\frac{x}{\sigma}-\sigma|\phi|\Big)^2\Big]dx \tag{3.139}$$

$$= 1 + 2e^{-\frac{1}{2\sigma^2}+|\phi|} + 2\sigma e^{\frac{\sigma^2|\phi|^2}{2}}\int_{\frac{1}{\sigma}-\sigma|\phi|}^{\infty} e^{-\frac{u^2}{2}}du \tag{3.140}$$

$$< 1 + 2e^{-\frac{1}{2\sigma^2}+|\phi|} + \frac{2\sigma e^{\frac{\sigma^2|\phi|^2}{2}}}{\frac{1}{\sigma}-\sigma|\phi|}\int_{\frac{1}{\sigma}-\sigma|\phi|}^{\infty} ue^{-\frac{u^2}{2}}du \tag{3.141}$$

$$= 1 + 2e^{-\frac{1}{2\sigma^2}+|\phi|} + \frac{2\sigma}{\frac{1}{\sigma}-\sigma|\phi|}e^{-\frac{1}{2\sigma^2}+\phi} \tag{3.142}$$

$$= 1 + 2\left[1 + \frac{\sigma^2}{1-\sigma^2|\phi|}\right]e^{-\frac{1}{2\sigma^2}+\phi} \tag{3.143}$$

In most of the cases we will use, the value of the h function can be approximated by the equivalent value if we use a Guassian distribution over the continuum, plus some small error term that is exponential in either the standard deviation σ or its inverse. As such, we will generally take as intuition that these h functions are Gaussians, which will allow us to construct approximations that are easier to work with.

3.6.2 Propagated approximation bounds

We will want to show that $|\alpha^j(t)\rangle$ is always normalized for $t < \frac{\mu - L}{2|\sin k|}$ and for $t > \frac{\mu + L}{2|\sin k|}$. In the first case, we have that

$$\langle \alpha_j(t) | \alpha_j(t) \rangle = \gamma^2 \sum_{x=\mu(t)-L} \mu(t) + L e^{-\frac{(x-\mu(t))^2}{\sigma^2}} = \gamma^2 h_L^{\sigma/\sqrt{2}}(0) = 1, \tag{3.144}$$

where we used the fact that the approximated wavepacket had not yet hit the finite graph. In the second case, we instead have

$$\langle \alpha_j(t) | \alpha_j(t) \rangle = \gamma^2 \sum_{x=\mu(t)-L} \mu(t) + L \sum_{q=1}^{N} S^*_{qj(k)} S_{qj}(k) e^{-\frac{(x-\mu(t))^2}{\sigma^2}} \tag{3.145}$$

$$= \gamma^2 \sum_{x=\mu(t)-L} \mu(t) + L e^{-\frac{(x-\mu(t))^2}{\sigma^2}} = 1 \tag{3.146}$$

where we used the fact that S is a unitary matrix, and our previous results.

Additionally, it will be helpful to actually have bounds on γ^{-2}. In particular, we have that

$$\gamma^{-2} = h_L^{\sigma/\sqrt{2}}(0) < h_\infty^{\sigma/\sqrt{2}}(0) = \sqrt{\pi}\sigma h_\infty^{1/(\pi\sigma\sqrt{2})}(0) \leq \sqrt{\pi}\sigma \left[1 + 2\left(1 + \frac{1}{2\pi^2\sigma^2}\right) e^{-\pi^2\sigma^2}\right] \tag{3.147}$$

as an upper bound, while

$$\gamma^{-2} = h_L^{\sigma/\sqrt{2}}(0) = h_\infty^{\sigma/\sqrt{2}}(0) - \left(h_L^{\sigma/\sqrt{2}}(0) - h_\infty^{\sigma/\sqrt{2}}(0)\right) \geq \sqrt{\pi}\sigma - \frac{\sigma^2}{L} e^{-\frac{L^2}{\sigma^2}} \tag{3.148}$$

$$= \sqrt{\pi}\sigma \left(1 - \frac{\sigma}{L\sqrt{\pi}} e^{-\frac{L^2}{\sigma^2}}\right) \tag{3.149}$$

can be used as a lower bound. However, these bounds are not particular nice to use and thus we will use the slightly weaker bounds of

$$\gamma^{-2} \leq \sqrt{\pi}\sigma \left[1 + 3e^{-\pi^2\sigma^2}\right] \tag{3.150}$$

and

$$\gamma^{-2} \geq \sqrt{\pi}\sigma \left[1 - e^{-\frac{L^2}{\sigma^2}}\right], \tag{3.151}$$

where we assume that $L > \sigma > 1$.

3.6.3 Proof of Theorem 3

Proof. The main idea behind this proof will be to show that $|\psi_j(0)\rangle$ and $|\alpha_j(t)\rangle$ are both well approximated by a Gaussian distribution over momentum states near k, and then show that the time evolved Gaussian approximation of $|\psi_j(0)\rangle$ is well approximated by the Gaussian approximation for $|\alpha_j(t)\rangle$.

In particular, let us examine the inner product between a scattering state $|\mathrm{sc}_j(k+\phi)\rangle$ and $|\alpha_j(t)\rangle$. We can see that

$$\begin{aligned}
&\langle \mathrm{sc}_j(k+\phi)\,|\,\alpha_j(t)\rangle \\
&\quad = \begin{cases} \gamma e^{-2it\cos k}\sum_{x=\mu(t)-L}^{\mu(t)+L}\left(e^{i\phi x}+S^*_{jj}(k+\phi)e^{-i(2k+\phi)x}\right)e^{-\frac{(x-\mu(t))^2}{2\sigma^2}} & t<\frac{\mu-L}{2|\sin(k)|} \\ \gamma e^{-2it\cos k}\sum_{x=\mu(t)-L}^{\mu(t)+L}\sum_{q=1}^{N}\Big(\delta_{qj}e^{i(2k+\phi)x} & \\ \qquad +S^*_{qj}(k+\phi)S_{qj}(k)e^{-i\phi x}\Big)e^{-\frac{(x+\mu(t))^2}{2\sigma^2}} & t>\frac{\mu+L}{2|\sin(k)|} \end{cases}
\end{aligned} \tag{3.152}$$

While this looks like somewhat complicated expression, most of the amplitude results from the terms multiplied by $e^{\pm i\phi x}$. If we approximate $S^*_{qj}(k+\phi)$ by $S^*_{qj}(k)$, for either of the time ranges the above expression can be seen as $e^{-2it\cos k}e^{i\phi\mu(t)}h^\sigma_L(\phi)$ plus some small error terms. Additionally, for ϕ small compared to σ, $h^\sigma_\infty(\phi)\propto e^{-\frac{\sigma^2\phi^2}{2}}$, so let us define

$$|\,w_j(t)\rangle = \eta e^{-2it\cos k}\int_{-\delta}^{\delta}\frac{d\phi}{2\pi}e^{i\phi\mu(t)}e^{-\frac{\sigma^2\phi^2}{2}}|\,\mathrm{sc}_j(k+\phi)\rangle \tag{3.153}$$

where δ is a constant that we will define later, and where η is an approximate normalization factor defined as

$$\eta^{-2}=\int_{-\infty}^{\infty}\frac{d\phi}{2\pi}e^{-\sigma^2\phi^2}=\frac{1}{2\sqrt{\pi}\sigma} \tag{3.154}$$

The state $|\,w_j(t)\rangle$ will be our Gaussian approximation to the state $|\,\alpha_j(t)\rangle$.

Note that the states $|\,w_j(t)\rangle$ are not exactly normalized, but that

$$\langle\, w_j(t)\,|\,w_j(t)\rangle = \eta^2\int_{-\delta}^{\delta}\frac{d\phi}{2\pi}e^{-\sigma^2\phi^2}=\eta^2\int_{-\infty}^{\infty}\frac{d\phi}{2\pi}e^{-\sigma^2\phi^2}-2\eta^2\int_{\delta}^{\infty}\frac{d\phi}{2\pi}e^{-\sigma^2\phi^2} \tag{3.155}$$

$$= 1-\frac{2\sigma}{\sqrt{\pi}}\int_{\delta}^{\infty}d\phi e^{-\sigma^2\phi^2}. \tag{3.156}$$

Hence, we have that

$$\langle\, w_j(t)\,|\,w_j(t)\rangle \geq 1-\frac{1}{\delta\sigma\sqrt{\pi}}e^{-\sigma^2\delta^2} \tag{3.157}$$

and

$$\langle\, w_j(t)\,|\,w_j(t)\rangle \leq 1-\frac{2\sigma\delta}{\sqrt{\pi}(2\sigma^2\delta^2+1)}e^{-\sigma^2\delta^2} \tag{3.158}$$

We will also want to know the overlap of these approximations with the states that they

will approximate, namely $|\alpha_j(t)\rangle$. If $t < \frac{\mu - L}{2|\sin k|}$, then we have that

$$\langle w_j(t)\,|\,\alpha_j(t)\rangle = \eta e^{2it\cos k}\int_{-\delta}^{\delta}\frac{d\phi}{2\pi}\langle \mathrm{sc}_j(k+\phi)\,|\,\alpha_j(t)\rangle e^{-\frac{\sigma^2\phi^2}{2}}e^{-i\phi\mu(t)} \tag{3.159}$$

$$= \gamma\eta\int_{-\delta}^{\delta}\frac{d\phi}{2\pi}e^{-\frac{\sigma^2\phi^2}{2}}\big(h_L^\sigma(\phi) + S_{jj}^*(k+\phi)e^{-2i(\phi+k)\mu(t)}h_L^\sigma(2k+\phi)\big) \tag{3.160}$$

$$\begin{aligned}= \gamma\eta\int_{-\delta}^{\delta}\frac{d\phi}{2\pi}e^{-\frac{\sigma^2\phi^2}{2}}h_\infty^\sigma(\phi) + \gamma\eta\int_{-\delta}^{\delta}\frac{d\phi}{2\pi}e^{-\frac{\sigma^2\phi^2}{2}}\big(h_L^\sigma(\phi) - h_\infty^\sigma(\phi)\big)\\ + \gamma\eta\int_{-\delta}^{\delta}\frac{d\phi}{2\pi}S_{jj}^*(k+\phi)e^{-2i(\phi+k)\mu(t)}e^{-\frac{\sigma^2\phi^2}{2}}h_\infty^\sigma(2k+\phi)\\ + \gamma\eta\int_{-\delta}^{\delta}\frac{d\phi}{2\pi}S_{jj}^*(k+\phi)e^{-2i(\phi+k)\mu(t)}e^{-\frac{\sigma^2\phi^2}{2}}\big(h_L^\sigma(2k+\phi) - h_\infty^\sigma(2k+\phi)\big).\end{aligned} \tag{3.161}$$

If $t > \frac{\mu + L}{2|\sin k|}$, we instead have

$$\langle w_j(t)\,|\,\alpha_j(t)\rangle = \eta e^{2it\cos k}\int_{-\delta}^{\delta}\frac{d\phi}{2\pi}\langle \mathrm{sc}_j(k+\phi)\,|\,\alpha_j(t)\rangle e^{-\frac{\sigma^2\phi^2}{2}}e^{-i\phi\mu(t)} \tag{3.162}$$

$$\begin{aligned}= \gamma\eta\int_{-\delta}^{\delta}\frac{d\phi}{2\pi}e^{2i(k+\phi)\mu(t)}S_{jj}(k)e^{-\frac{\sigma^2\phi^2}{2}}h_L^\sigma(2k+\phi)\\ + \gamma\eta\sum_{q=1}^{N}\int_{-\delta}^{\delta}\frac{d\phi}{2\pi}S_{qj}^*(k+\phi)S_{qj}(k)e^{-\frac{\sigma^2\phi^2}{2}}h_L^\sigma(\phi)\end{aligned} \tag{3.163}$$

$$\begin{aligned}= \gamma\eta\int_{-\delta}^{\delta}\frac{d\phi}{2\pi}e^{-\frac{\sigma^2\phi^2}{2}}h_\infty^\sigma(\phi) + \gamma\eta\sum_{q=1}^{N}\int_{-\delta}^{\delta}\frac{d\phi}{2\pi}\big(S_{qj}^*(k+\phi) - S_{qj}^*(k)\big)S_{qj}(k)e^{-\frac{\sigma^2\phi^2}{2}}h_\infty^\sigma(\phi)\\ + \gamma\eta\sum_{q=1}^{N}\int_{-\delta}^{\delta}\frac{d\phi}{2\pi}S_{qj}^*(k+\phi)S_{qj}(k)e^{-\frac{\sigma^2\phi^2}{2}}\big(h_L^\sigma(\phi) - h_\infty^\sigma(\phi)\big)\\ + \gamma\eta\int_{-\delta}^{\delta}\frac{d\phi}{2\pi}e^{2i(k+\phi)\mu(t)}S_{jj}(k)e^{-\frac{\sigma^2\phi^2}{2}}h_\infty^\sigma(2k+\phi)\\ + \gamma\eta\int_{-\delta}^{\delta}\frac{d\phi}{2\pi}e^{2i(k+\phi)\mu(t)}S_{jj}(k)e^{-\frac{\sigma^2\phi^2}{2}}\big(h_L^\sigma(2k+\phi) - h_\infty^\sigma(2k+\phi)\big).\end{aligned} \tag{3.164}$$

In both cases, most of the norm comes from the first term, and the rest will be small error

terms. In particular, we see that

$$\int_{-\delta}^{\delta} \frac{d\phi}{2\pi} e^{-\frac{\sigma^2\phi^2}{2}} h_\infty^\sigma(\phi) = \frac{\sigma}{\sqrt{2\pi}} \int_{-\delta}^{\delta} d\phi e^{-\sigma^2\phi^2} h_\infty^{1/(2\pi\sigma)}(2\pi i\sigma^2\phi) \tag{3.165}$$

$$\leq \frac{2\sigma}{\sqrt{2\pi}} \int_0^{\delta} d\phi e^{-\sigma^2\phi^2} \Big[1 + 2\Big(1 + \frac{1}{2\pi\sigma^2}\frac{1}{2\pi-\phi}\Big) e^{-2\pi\sigma^2(\pi-\phi)}\Big] \tag{3.166}$$

$$\leq \frac{2\sigma}{\sqrt{2\pi}} \Big[1 + 2\Big(1 + \frac{1}{2\pi\sigma^2}\frac{1}{2\pi-\delta}\Big) e^{-2\pi\sigma^2(\pi-\delta)}\Big] \int_0^{\delta} d\phi e^{-\sigma^2\phi^2} \tag{3.167}$$

$$\leq \frac{1}{\sqrt{2}} \Big[1 + 3e^{-\pi^2\sigma^2}\Big] \tag{3.168}$$

where we assumed that $\delta < \frac{\pi}{2}$. If we also note that $h_L^\sigma(i\phi) \geq 1$ for all L and all real ϕ, we have

$$\int_{-\delta}^{\delta} \frac{d\phi}{2\pi} e^{-\frac{\sigma^2\phi^2}{2}} h_\infty^\sigma(\phi) = \frac{\sigma}{\sqrt{2\pi}} \int_{-\delta}^{\delta} d\phi e^{-\sigma^2\phi^2} h_\infty^{1/(2\pi\sigma)}(2\pi i\sigma^2\phi) \tag{3.169}$$

$$\geq \frac{\sigma}{\sqrt{2\pi}} \int_{-\delta}^{\delta} d\phi e^{-\sigma^2\phi^2} \tag{3.170}$$

$$= \sigma\sqrt{2\pi}\eta^{-2} \langle\, w_j(t) \,|\, w_j(t) \,\rangle \tag{3.171}$$

$$\geq \frac{1}{\sqrt{2}} \Big(1 - \frac{1}{\delta\sigma\sqrt{\pi}} e^{-\sigma^2\delta^2}\Big). \tag{3.172}$$

Now let us assume that $t < \frac{\mu - L}{2|\sin k|}$ and examine the first case. We can use the bound of (3.129) to see that

$$\Big| \int_{-\delta}^{\delta} \frac{d\phi}{2\pi} e^{-\frac{\sigma^2\phi^2}{2}} \big(h_L^\sigma(\phi) - h_\infty^\sigma(\phi)\big) \Big| \leq \int_{-\delta}^{\delta} \frac{d\phi}{2\pi} e^{-\frac{\sigma^2\phi^2}{2}} \big|h_L^\sigma(\phi) - h_\infty^\sigma(\phi)\big| \tag{3.173}$$

$$\leq \int_{-\delta}^{\delta} \frac{d\phi}{2\pi} \frac{2\sigma^2}{L} e^{-\frac{L^2}{2\sigma^2}} e^{-\frac{\sigma^2\phi^2}{2}} \tag{3.174}$$

$$\leq \frac{\sigma^2}{\pi L} e^{-\frac{L^2}{2\sigma^2}} \int_{-\infty}^{\infty} d\phi e^{-\frac{\sigma^2\phi^2}{2}} \tag{3.175}$$

$$= \sqrt{\frac{2}{\pi}} \frac{\sigma}{L} e^{-\frac{L^2}{2\sigma^2}}, \tag{3.176}$$

For the third term, we can continue to use the relations for the h functions and note that

$$\Big| \int_{-\delta}^{\delta} \frac{d\phi}{2\pi} S_{jj}^*(k+\phi) e^{-2i(\phi+k)\mu(t)} h_\infty^\sigma(2k+\phi) e^{-\frac{\sigma^2\phi^2}{2}} \Big|$$

$$\leq \int_{-\delta}^{\delta} \frac{d\phi}{2\pi} h_\infty^\sigma(2k+\phi) e^{-\frac{\sigma^2\phi^2}{2}} \tag{3.177}$$

$$= \int_{-\delta}^{\delta} \frac{d\phi}{\sqrt{2\pi}} \sigma e^{-\frac{\sigma^2}{2}\left((2k+\phi)^2+\phi^2\right)} h_\infty^{1/(2\pi\sigma)}(2\pi i(2k+\phi)\sigma^2) \tag{3.178}$$

$$\leq \frac{\sigma}{\sqrt{2\pi}} \int_{-\delta}^{\delta} d\phi e^{-\frac{\sigma^2}{2}\left((2k+\phi)^2+\phi^2\right)} \Big(1 + 2\Big[1 + \frac{1}{2\pi\sigma^2}\frac{1}{2\pi - |2k+\phi|}\Big] e^{-2\pi\sigma^2(\pi - |2k+\phi|)}\Big) \tag{3.179}$$

where we used equation (3.143) in the third step. If $2|k| + \delta < \pi$, then $h_\infty^{1/(2\pi\sigma)}(2k+\phi)$ can be bounded by 2 for $\sigma > (\pi - 2|k| - \delta)^{-1}$. We then have

$$\Big| \int_{-\delta}^{\delta} \frac{d\phi}{2\pi} S_{jj}^*(k+\phi) e^{-2i(\phi+k)\mu(t)} h_\infty^\sigma(2k+\phi) e^{-\frac{\sigma^2\phi^2}{2}} \Big| \leq \sqrt{\frac{2}{\pi}}\sigma \int_{-\delta}^{\delta} d\phi e^{-\frac{\sigma^2}{2}\left((2k+\phi)^2+\phi^2\right)} \tag{3.180}$$

$$= \sqrt{\frac{2}{\pi}}\sigma \int_{-\delta}^{\delta} d\phi e^{-\sigma^2 k^2 - \sigma^2(k+\phi)^2} \tag{3.181}$$

$$\leq \sqrt{\frac{2}{\pi}}\sigma e^{-\sigma^2 k^2} \int_{-\infty}^{\infty} d\phi e^{-\sigma^2\phi^2} \tag{3.182}$$

$$= \sqrt{2} e^{-\sigma^2 k^2}. \tag{3.183}$$

However, if we instead have that $2|k| + \delta > \pi$, then we can instead bound equation (3.179) as

$$\Big| \int_{-\delta}^{\delta} \frac{d\phi}{2\pi} S_{jj}^*(k+\phi) e^{-2i(\phi+k)\mu(t)} h_\infty^\sigma(2k+\phi) e^{-\frac{\sigma^2\phi^2}{2}} \Big|$$

$$\leq \sqrt{\frac{2}{\pi}}\sigma \int_{-\delta}^{\delta} d\phi e^{-\frac{\sigma^2}{2}\left((2k+\phi)^2+\phi^2\right)} \left(1 + 2\left[1 + \frac{1}{2\pi\sigma^2}\frac{1}{2\pi - |2k+\phi|}\right] e^{-2\pi\sigma^2(\pi - |2k+\phi|)}\right) \tag{3.184}$$

$$\leq 4\sqrt{\frac{2}{\pi}}\sigma \int_{-\delta}^{\delta} d\phi e^{-\frac{\sigma^2}{2}\left((2k+\phi)^2+\phi^2\right)} e^{2\pi\sigma^2(2|k|+\delta-\pi)} \tag{3.185}$$

$$= 4\sqrt{\frac{2}{\pi}}\sigma \int_{-\delta}^{\delta} d\phi e^{2\sigma^2\left(-k^2+2\pi|k|-\pi^2+\pi\delta-k\phi-\frac{\phi^2}{2}\right)} \tag{3.186}$$

$$= 4\sqrt{\frac{2}{\pi}}\sigma e^{2\sigma^2[-(\pi-|k|)^2+\pi\delta]} \int_{-\delta}^{\delta} d\phi e^{-\sigma^2(\phi^2+2k\phi)} \tag{3.187}$$

$$\leq 4\sqrt{\frac{2}{\pi}}\sigma e^{2\sigma^2[-(\pi-|k|)^2+(\pi+|k|)\delta]} \int_{-\delta}^{\delta} d\phi e^{-\sigma^2\phi^2} \tag{3.188}$$

$$\leq 4\sqrt{2} e^{-\sigma^2(\pi-|k|)^2} \tag{3.189}$$

where we assumed that $\delta < \frac{(\pi-|k|)^2}{\pi+|k|}$. In either case, we have that

$$\Big| \int_{-\delta}^{\delta} \frac{d\phi}{2\pi} S_{jj}^*(k+\phi) e^{-2i(\phi+k)\mu(t)} h_\infty^\sigma(2k+\phi) e^{-\frac{\sigma^2\phi^2}{2}} \Big| \leq 4\sqrt{2} e^{-\sigma^2\delta}. \tag{3.190}$$

Finally, we can again use the same argument as in equation (3.176) to see that in to bound the final term as

$$\Big| \int_{-\delta}^{\delta} \frac{d\phi}{2\pi} S_{jj}^*(k+\phi) e^{2i(\phi+k)\mu(t)} \left(h_L^\sigma(2k+\phi) - h_\infty^\sigma(2k+\phi)\right) e^{-\frac{\sigma^2\phi^2}{2}} \Big|$$

$$\leq \int_{-\delta}^{\delta} \frac{d\phi}{2\pi} \left|h_L^\sigma(2k+\phi) - h_\infty^\sigma(2k+\phi)\right| e^{-\frac{\sigma^2\phi^2}{2}} \tag{3.191}$$

$$\leq \sqrt{\frac{2}{\pi}}\frac{\sigma}{L} e^{-\frac{L^2}{2\sigma^2}} \tag{3.192}$$

where we used (3.176) in the last line. This is sufficient for us to bound the norm of $\langle w_j(t)\,|\,\alpha_j(t)\rangle$ for small t.

With all of these bounds, we then have that if $t < \frac{\mu - L}{2|\sin k|}$, since most of the amplitude of $\langle \alpha_j(t)\,|\,w_j(t)\rangle$ is on the term equal to $\langle w_j(t)\,|\,w_j(t)\rangle$,

$$\begin{aligned}
\| |\alpha_j(t)\rangle - |w_j(t)\rangle \|^2 &= \langle \alpha_j(t)\,|\,\alpha_j(t)\rangle + \langle w_j(t)\,|\,w_j(t)\rangle - 2\Re\big[\langle \alpha_j(t)\,|\,w_j(t)\rangle\big] && (3.193)\\
&\leq 1 + \langle w_j(t)\,|\,w_j(t)\rangle \\
&\quad - 2\gamma\eta\left[\frac{1}{\sqrt{2}}\langle w_j(t)\,|\,w_j(t)\rangle - \sqrt{\frac{2}{\pi}}\frac{\sigma}{L}e^{-\frac{L^2}{2\sigma^2}} - 4\sqrt{2}e^{-\sigma^2\delta} - \sqrt{\frac{2}{\pi}}\frac{\sigma}{L}e^{-\frac{L^2}{2\sigma^2}}\right] && (3.194)\\
&= 1 + \big(1 - \sqrt{2}\gamma\eta\big)\langle w_j(t)\,|\,w_j(t)\rangle + 4\sqrt{2}\gamma\eta\Big[\frac{\sigma}{\sqrt{\pi}L}e^{-\frac{L^2}{2\sigma^2}} + 2e^{-\sigma^2\delta}\Big] && (3.195)
\end{aligned}$$

We can then use our bounds on γ from equations (3.150) and (3.151), along with the bounds on $\langle w_j(t)\,|\,w_j(t)\rangle$ to see that

$$\begin{aligned}
&\| |\alpha_j(t)\rangle - |w_j(t)\rangle \|^2 \\
&\quad\leq 1 + \left[1 - \sqrt{2}\sqrt{2\sqrt{\pi}\sigma}\frac{1}{\sqrt{\sqrt{\pi}\sigma}}\left(1 + 3e^{-\pi^2\sigma^2}\right)^{-1/2}\right]\left(1 - \frac{1}{\delta\sigma\sqrt{\pi}}e^{-\sigma^2\delta^2}\right) \\
&\qquad + 4\sqrt{2}\sqrt{2\sqrt{\pi}\sigma}\frac{1}{\sqrt{\sqrt{\pi}\sigma}}\left[1 - e^{-\frac{L^2}{2\sigma^2}}\right]^{-1/2}\left[\frac{\sigma}{\sqrt{\pi}L}e^{-\frac{L^2}{2\sigma^2}} + 2e^{-\sigma^2\delta}\right] && (3.196)\\
&\quad\leq 1 + \left[1 - 2 + 3e^{-\pi^2\sigma^2}\right]\left(1 - \frac{1}{\delta\sigma\sqrt{\pi}}e^{-\sigma^2\delta^2}\right) + 8\left[1 + e^{-\frac{L^2}{\sigma^2}}\right]\left[\frac{\sigma}{\sqrt{\pi}L}e^{-\frac{L^2}{2\sigma^2}} + 2e^{-\sigma^2\delta}\right] && (3.197)\\
&\quad\leq 3e^{-\pi^2\sigma^2} + \frac{1}{\delta\sigma\sqrt{\pi}}e^{-\sigma^2\delta^2} + \frac{16\sigma}{\sqrt{\pi}L}e^{-\frac{L^2}{2\sigma^2}} + 32e^{-\sigma^2\delta} && (3.198)\\
&\quad\leq 36e^{-\sigma^2\delta} + \frac{16\sigma}{\sqrt{\pi}L}e^{-\frac{L^2}{2\sigma^2}} && (3.199)
\end{aligned}$$

where we assumed that $\sigma > (\delta\sqrt{\pi})^{-1}$.

If we now examine the cases for which $t > \frac{\mu + L}{2|\sin k|}$, we have some slightly different errors to bound, but most will utilize the same tricks. The one that needs different ideas, however, will utilize the fact that S is a matrix of bounded rational functions. In particular, the Lipschitz constant

$$\Gamma = \max_{q,j\in[N]}\max_{p\in[-\pi,\pi]}\left|\frac{d}{dk'}S_{qj}(k')\Big|_{k'=p}\right| \tag{3.200}$$

is well defined. Using this, we then have that

$$\begin{aligned}
&\Big|\int_{-\delta}^{\delta}\frac{d\phi}{2\pi}\big(S_{qj}^*(k+\phi)-S_{qj}^*(k)\big)S_{qj}(k)e^{-\frac{\sigma^2\phi^2}{2}}h_\infty^\sigma(\phi)\Big| \\
&\quad\le\int_{-\delta}^{\delta}\frac{d\phi}{2\pi}\big|S_{qj}^*(k+\phi)-S_{qj}^*(k)\big|e^{-\frac{\sigma^2\phi^2}{2}}h_\infty^\sigma(\phi) &(3.201)\\
&\quad\le\frac{\kappa}{\pi}\int_0^{\delta}d\phi\phi e^{-\frac{\sigma^2\phi^2}{2}}h_\infty^\sigma(\phi) &(3.202)\\
&\quad=\kappa\sigma\sqrt{\frac{2}{\pi}}\int_0^{\delta}d\phi\phi e^{-\sigma^2\phi^2}h_\infty^{1/(2\pi\sigma)}(2\pi i\sigma^2\phi) &(3.203)\\
&\quad\le\kappa\sigma\sqrt{\frac{2}{\pi}}\big(1+3e^{-\pi^2\sigma^2}\big)\int_0^{\delta}d\phi\phi e^{-\sigma^2\phi^2} &(3.204)\\
&\quad=\frac{\kappa}{\sigma\sqrt{2\pi}}\big(1+3e^{-\pi^2\sigma^2}\big)\big(1-e^{-\sigma^2\delta^2}\big) &(3.205)
\end{aligned}$$

where we used our previous bounds on $h_\infty^\sigma(\phi)$. We also have

$$\begin{aligned}
\Big|\int_{-\delta}^{\delta}\frac{d\phi}{2\pi}S_{qj}^*(k+\phi)S_{qj}(k)\big(h_L^\sigma(\phi)-h_\infty^\sigma(\phi)\big)e^{-\frac{\sigma^2\phi^2}{2}}\Big| &\le\int_{-\delta}^{\delta}\frac{d\phi}{2\pi}\big|h_L^\sigma(\phi)-h_\infty^\sigma(\phi)\big|e^{-\frac{\sigma^2\phi^2}{2}} &(3.206)\\
&\le\sqrt{\frac{2}{\pi}}\frac{\sigma}{L}e^{-\frac{L^2}{2\sigma^2}} &(3.207)
\end{aligned}$$

where we use equation (3.176) in the last line. Continuing to extend our previous results, we can utilize equation (3.190) to see that

$$\left|\int_{-\delta}^{\delta}\frac{d\phi}{2\pi}e^{2i(k+\phi)\mu(t)}S_{jj}(k)e^{-\frac{\sigma^2\phi^2}{2}}h_\infty^\sigma(2k+\phi)\right|\le\int_{-\delta}^{\delta}\frac{d\phi}{2\pi}e^{-\frac{\sigma^2\phi^2}{2}}h_\infty^\sigma(2k+\phi)\le 4\sqrt{2}e^{-\sigma^2\delta}. \tag{3.208}$$

Finally, we can again use equation (3.176) to show

$$\begin{aligned}
&\left|\int_{-\delta}^{\delta}\frac{d\phi}{2\pi}e^{2i(k+\phi)\mu(t)}S_{jj}(k)\big(h_L^\sigma(2k+\phi)-h_\infty^\sigma(2k+\phi)\big)e^{-\frac{\sigma^2\phi^2}{2}}\right| \\
&\quad\le\int_{-\delta}^{\delta}\frac{d\phi}{2\pi}\big|h_L^\sigma(2k+\phi)-h_\infty^\sigma(2k+\phi)\big|e^{-\frac{\sigma^2\phi^2}{2}} &(3.209)\\
&\quad\le\sqrt{\frac{2}{\pi}}\frac{\sigma}{L}e^{-\frac{L^2}{2\sigma^2}}. &(3.210)
\end{aligned}$$

We now have the ability to bound the error arising from approximating $|\alpha_j(t)\rangle$ for $t >$

$\frac{\mu+L}{2|\sin k|}$. In particular, we have

$$\begin{aligned}
\||\alpha_j(t)\rangle - |w_j(t)\rangle\|^2 &= \langle\alpha_j(t)|\alpha_j(t)\rangle + \langle w_j(t)|w_j(t)\rangle - 2\Re\big[\langle\alpha_j(t)|w_j(t)\rangle\big] && (3.211)\\
&\leq 1 + \langle w_j(t)|w_j(t)\rangle - 2\gamma\eta\Bigg[\frac{1}{\sqrt{2}}\langle w_j(t)|w_j(t)\rangle \\
&\quad - \sum_{q=1}^{N}\frac{\kappa}{\sigma\sqrt{2\pi}}\big(1+3e^{-\pi^2\sigma^2}\big)\big(1-e^{-\sigma^2\delta^2}\big) - \sum_{q=1}^{N}\sqrt{\frac{2}{\pi}}\frac{\sigma}{L}e^{-\frac{L^2}{2\sigma^2}} \\
&\quad - 4\sqrt{2}e^{-\sigma^2\delta} - \sqrt{\frac{2}{\pi}}\frac{\sigma}{L}e^{-\frac{L^2}{2\sigma^2}}\Bigg] && (3.212)\\
&\leq 1 + \big(1-\sqrt{2}\gamma\eta\big)\langle w_j(t)|w_j(t)\rangle + 2\gamma\eta\Bigg[\frac{N\kappa}{\sigma\sqrt{2\pi}}\big(1+3e^{-\pi^2\sigma^2}\big) \\
&\quad + \sqrt{\frac{2}{\pi}}\frac{(N+1)\sigma}{L}e^{-\frac{L^2}{2\sigma^2}} + 4\sqrt{2}e^{-\sigma^2\delta}\Bigg]. && (3.213)
\end{aligned}$$

If we use the same bounds as for $t < \frac{\mu-L}{2|\sin k|}$ we find

$$\begin{aligned}
&\||\alpha_j(t)\rangle - |w_j(t)\rangle\|^2 && (3.214)\\
&\quad\leq 1 + \big(1-2+3e^{-\pi^2\sigma^2}\big)\Big(1-\frac{1}{\delta\sigma\sqrt{\pi}}e^{-\sigma^2\delta^2}\Big) \\
&\qquad + 2\sqrt{2}\Big(1+e^{-\frac{L^2}{\sigma^2}}\Big)\left(\frac{N\kappa}{\sigma} + \sqrt{\frac{2}{\pi}}\frac{(N+1)\sigma}{L}e^{-\frac{L^2}{2\sigma^2}} + 4\sqrt{2}e^{-\sigma^2\delta}\right) && (3.215)\\
&\quad\leq 3e^{-\pi^2\sigma^2} + \frac{1}{\delta\sigma\sqrt{\pi}}e^{-\sigma^2\delta^2} + 4\sqrt{2}\left(\frac{N\kappa}{\sigma} + \sqrt{\frac{2}{\pi}}\frac{(N+1)\sigma}{L}e^{-\frac{L^2}{2\sigma^2}} + 4\sqrt{2}e^{-\sigma^2\delta}\right) && (3.216)\\
&\quad\leq 36e^{-\sigma^2\delta} + \frac{32N\kappa}{\sigma} + \frac{8(N+1)}{\sqrt{\pi}}\frac{\sigma}{L}e^{-\frac{L^2}{2\sigma^2}} && (3.217)
\end{aligned}$$

At this point, we can now bound the error that arises when approximating $|\alpha_j(t)\rangle$ by a Gaussian for any $t < \frac{\mu-L}{2|\sin(k)|}$ and for any $t > \frac{\mu+L}{2|\sin(k)|}$. However, we don't yet know how well $|\alpha_j(t)\rangle$ approximates $|\psi_j(t)\rangle$. Note, however, that $|\alpha_j(0)\rangle = |\psi_j(0)\rangle$, and thus we already have an approximation to the initial state. We can then look easily time-evolve this approximation, and compare it to the Gaussian approximation for $|\alpha_j(t)\rangle$.

Let us define

$$|v_j(0)\rangle = |w_j(0)\rangle = \eta\int_{-\delta}^{\delta}\frac{d\phi}{2\pi}e^{i\phi\mu}e^{-\frac{\sigma^2\phi^2}{2}}|\mathrm{sc}_j(k+\phi)\rangle \tag{3.218}$$

and then define

$$|v_j(t)\rangle = e^{-iHt}|v_j(0)\rangle = \eta\int_{-\delta}^{\delta}\frac{d\phi}{2\pi}e^{i\phi\mu-2it\cos(k+\phi)}e^{-\frac{\sigma^2\phi^2}{2}}|\mathrm{sc}_j(k+\phi)\rangle. \tag{3.219}$$

We then want to compare this time evolved state with our approximation to $|\alpha_j(t)\rangle$. We can see

$$\langle v_j(t)|w_j(t)\rangle = \eta^2 \int_{-\delta}^{\delta} \frac{d\phi}{2\pi} e^{2it\cos(k+\phi)-2it\cos(k)} e^{i\phi\mu - i\phi\mu - i\phi\lceil 2t\sin k\rceil} e^{-\sigma^2\phi^2} \tag{3.220}$$

$$= \eta^2 \int_{-\delta}^{\delta} \frac{d\phi}{2\pi} e^{-\sigma^2\phi^2} - \eta^2 \int_{-\delta}^{\delta} \frac{d\phi}{2\pi} \big(1 - e^{2it\cos(k+\phi)-2it\cos(k)+i\phi\lceil 2t\sin k\rceil}\big) e^{-\sigma^2\phi^2}. \tag{3.221}$$

The first term is simply the norm of both $|v_j(t)\rangle$ and $|w_j(t)\rangle$, while the third term can be bounded as

$$\left| \int_{-\delta}^{\delta} \frac{d\phi}{2\pi} \big(1 - e^{2it\cos(k+\phi)-2it\cos(k)+i\phi\lceil 2t\sin k\rceil}\big) e^{-\sigma^2\phi^2} \right| \tag{3.222}$$

$$\leq \int_{-\delta}^{\delta} \frac{d\phi}{2\pi} \big|1 - e^{2it\cos(k+\phi)-2it\cos(k)+i\phi\lceil 2t\sin k\rceil}\big| e^{-\sigma^2\phi^2} \tag{3.223}$$

$$\leq \int_{-\delta}^{\delta} \frac{d\phi}{2\pi} \big|2t\cos(k+\phi) - 2t\cos(k) + \phi\lceil 2t\sin k\rceil\big| e^{-\sigma^2\phi^2} \tag{3.224}$$

$$\leq \int_{-\delta}^{\delta} \frac{d\phi}{2\pi} \Big(2t\big|\cos(k)\cos(\phi) - \sin(k)\sin(\phi) - \cos(k) + \phi\sin(k)\big| + |\phi|\Big) e^{-\sigma^2\phi^2} \tag{3.225}$$

$$\leq \int_{-\delta}^{\delta} \frac{d\phi}{2\pi} \Big(t\big|\cos(k)\phi^2 + \sin(k)|\phi|^3\big| + |\phi|\Big) e^{-\sigma^2\phi^2} \tag{3.226}$$

$$\leq 2\int_{0}^{\delta} \frac{d\phi}{2\pi} \big(2t\phi^2 + \phi\big) e^{-\sigma^2\phi^2} \tag{3.227}$$

$$\leq \frac{1}{2\pi\sigma^2} + \frac{t}{2\sqrt{\pi}\sigma^3}. \tag{3.228}$$

Noting that the norm of $\langle v_j(t)|v_j(t)\rangle$ doesn't change with time, we have that

$$\||v_j(t)\rangle - |w_j(t)\rangle\|^2 = \langle v_j(t)|v_j(t)\rangle + \langle w_j(t)|w_j(t)\rangle - \langle v_j(t)|w_j(t)\rangle - \langle w_j(t)|v_j(t)\rangle \tag{3.229}$$

$$\leq 2\eta^2 \int_{\delta}^{\delta} \frac{d\phi}{2\pi} e^{-\sigma^2\phi^2} - 2\eta^2 \int_{\delta}^{\delta} \frac{d\phi}{2\pi} e^{-\sigma^2\phi^2} + \frac{2\eta^2}{2\pi\sigma^2} + \frac{2\eta^2 t}{2\sqrt{\pi}\sigma^3} \tag{3.230}$$

$$= 2\frac{\sqrt{\pi}}{\sigma} + \frac{2t}{\sigma^2}. \tag{3.231}$$

Finally, we can combine these three bounds, noting that $|\psi_j(0)\rangle = |\alpha_j(0)\rangle$, and that $\||w_j(t)\rangle - |\alpha_j(t)\rangle\|$ is larger for $t > \frac{\mu+L}{2|\sin k|}$ than for $t < \frac{\mu-L}{2|\sin k|}$. In particular, we have for all

$t \leq \frac{\mu - L}{2|\sin k|}$ and for all $t > \frac{\mu + L}{2|\sin k|}$ that

$$\begin{aligned}
&\| |\psi_j(t)\rangle - |\alpha_j(t)\rangle \| \\
&\quad \leq \| |\psi_j\rangle(t) - |v_j(t)\rangle \| + \| |v_j(t)\rangle - |w_j(t)\rangle \| + \| |w_j(t)\rangle - |\alpha_j(t)\rangle \| \qquad (3.232) \\
&\quad \leq \left[36e^{-\sigma^2\delta} + \frac{16\sigma}{\sqrt{\pi}L} e^{-\frac{L^2}{\sigma^2}} \right]^{1/2} + \left[\frac{2\sqrt{\pi}}{\sigma} + \frac{2t}{\sigma^2} \right]^{1/2} \\
&\qquad\quad + \left[36e^{-\sigma^2\delta} + \frac{32N\kappa}{\sigma} + \frac{8(N+1)}{\sqrt{\pi}} \frac{\sigma}{L} e^{-\frac{L^2}{2\sigma^2}} \right]^{1/2}. \qquad (3.233)
\end{aligned}$$

If we then assume that $\sigma = \frac{c_1 L}{\sqrt{\log L}}$ for some constant c_1, and that $t < c_2 L$ for some constant c_2, we have that for L large enough

$$\begin{aligned}
&\| |\psi_j(t)\rangle - |\alpha_j(t)\rangle \| \\
&\quad \leq \left(\frac{c_3}{\sqrt{\log L}} \frac{1}{L} \right)^{1/2} + \left(\frac{c_4 \sqrt{\log L}}{L} + \frac{c_2 \log L}{L} \right)^{1/2} + \left(\frac{c_5 \sqrt{\log L}}{L} + \frac{c_6}{L\sqrt{\log L}} \right)^{1/2} \qquad (3.234) \\
&\quad \leq \chi \sqrt{\frac{\log L}{L}} \qquad (3.235)
\end{aligned}$$

for some constant χ.

□

3.7 Conclusions and extensions

[**TO DO:** *I still don't like this conclusions section, but something is better than nothing*]

At this point, we have a general understanding of graph scattering off of a single graph. The idea of a wavepacket moving along an infinite path makes sense, as does its scattering behavior off of some given graph. We know how to calculate this scattering behavior for a given graph at a particular momenta, and we have bounds on the error arising from such a scattering event.

Additionally, we know how to construct graphs with simple scattering behaviors. While these behaviors depend on the eigenstates of arbitrary graphs, we have given examples that might be of use as building blocks for some scattering algorithm.

Finally, we have also shown that some scattering behavior cannot exist. While this means that certain schemes cannot be simplified, this is of theoretical interest. Further, it also allows us to stop searching for graphs with these behaviors.

While these form a nice foundation, more research can always be done in these fields. Ideally, giving an explicit algorithm that constructs a graph with a particular scattering behavior, or says that such a graph doesn't exist, would be of great interest. Even if such an algorithm took an exponential amount of time, this would be a theoretical achievement since we don't know whether this problem is currently decidable.

Less ambitiously, if we could give such an algorithm for a restricted set of graphs, such as that given for type 1 and type 2 R/T gadgets, but generalized to multiple input and outputs.

Along different lines, improving the bounds on our scattering behavior, or showing that they cannot be improved by more than a constant, would give better bounds on results later in the thesis. This scattering behavior is foundational to the idea of computation via scattering, and thus improved bounds result in smaller guaranteed errors.

Essentially, graph scattering seems to be a new subfield in the study of graphs, with several areas of research opening up.

Chapter 4

Universality of Quantum Walk

Quantum walk is an intuitive framework for developing quantum algorithms, inspired by the classical model of random walk. This framework has lead to examples of exponential speedups over classical computation [12], as well as optimal algorithms for element distinctness [2] and formula evaluation [19]. Additionally, the framework of Chapter 3 can be thought of as a special kind of continuos-time quantum walk.

With all of these algorithmic uses, we would then wonder at the computational power of this model. Using the ideas of graph scattering, Childs [10] was able to show that the model of continuous time quantum walk is universal for quantum computation (and later showed the same for discrete-time quantum walk [11]). This chapter will also show this result, but with a slightly different proof technique.

In particular, we will use results on the scattering behavior of finite-length wave-packets to implement single gates, and we will then show how to compose these scattering events for an entire computation. This chapter is really a primer for Chapter 5, as many of the proof-techniques and ideas of this chapter will be used for the multi-particle case as well.

Most of this chapter will be devoted to showing how to simulate a circuit of a given form via graph scattering.

[**TO DO:** *Move wavepacket propagation to this chapter?*]

4.1 Single qubit simulation

With our eventual goal of simulating an entire circuit via graph scattering, we will first need to understand how to perform single-qubit computations. We will use many of the results of Chapter 3, and show that specific scattering behavior can be used as a computational tool. This section will first encode the qubit, then show how to have a simulate a single gate, and finally show how to simulate multiple single-qubit gates. These results will then be generalized for multiple-qubits in Section 4.2, and will be used nearly verbatim in Chapter 5.

4.1.1 Single qubit encoding

In our search for simulations, we will first need to encode the logical state into some graph state. We can then take inspiration from the current literature, or else see motivation from

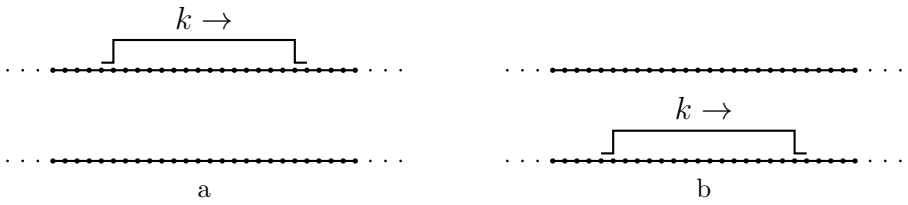

Figure 4.1: A qubit is encoded using single-particle wave packets at momentum k. (a) An encoded $|0\rangle$. (b) An encoded $|1\rangle$.

classical asynchronous systems, to encode our logical system via dual-rails. In particular, a single qubit will correspond to two infinite paths, with a single wave-packet at specified momentum k traveling along one of the two paths. If the particle is located on the first (top) path, then the encoded qubit is in the logical state $|0\rangle$, while if the particle is on the second (bottom) path then the encoded qubit is in the logical state $|1\rangle$. Schematically, this can be seen in Figure 4.1.

[**TO DO:** *change figure to Gaussian as opposed to square?*]

If we didn't mind using an infinite Hilbert space to encode our qubits, we could actually use the eigenstates of the two paths to correspond to the two logical states, but we will eventually want to assume that the encodings have a well-defined position in space to ensure that we need only measure a (relatively) small number of qubits in order to determine the location of the particle with high probability. To ensure this localization in space (and to use some of our error bounds on the time evolution), we will assume that the logical states are encoded using a truncated Gaussian wave-packet, with four attributes that specify the state: the momentum k, the standard deviation σ, the center of mass μ, and the cutoff range L (which will be closely related to σ). With these four values, and assuming that the vertices of the infinite path are labeled as (x, z) for $x \in \mathbb{Z}$ and $z \in \mathbb{F}_2$, we then have that the logical qubit in our system will be encoded into the states

$$|z\rangle_{\log} = \gamma \sum_{x=\mu-L}^{\mu+L} e^{ikx} e^{-\frac{(x-\mu)^2}{2\sigma^2}} |x, z\rangle. \tag{4.1}$$

It is important to realize that none of these four values depend on the value of the encoded qubit; this will allow us to interfere the wave-packets arising from different paths to the same computational basis path as there will be no extraneous information about the logical state.

This encoding is specifically chosen so that we can use Theorem 3, and guarantee various attributes about the time evolution of such systems.

4.1.2 One single-qubit unitary

With an actual encoding of a logical qubit, the next step will be to apply an encoded unitary to the logical state. However, our current encoding is on two (disconnected) paths, and as such if we want to apply any unitary that mixes amplitudes among the two basis states we somehow need to connect the two paths. (Unitaries diagonal in the computational basis will use the same formalism, but they have additional constraints that might make them easier to apply.)

Note that Chapter 3 was all about connecting (semi-) infinite paths, where the amplitudes move from one path to another. As hinted in the chapter, we can implement encoded unitaries in this manner, if we restrict ourselves to specific momenta and specific scattering gadgets. Namely, we will examine graphs $\widehat{G}$ with four terminal vertices such that at the momentum k encoding the qubits, the scattering matrices take the form

$$S(k) = \begin{pmatrix} 0 & U^T \\ U & 0 \end{pmatrix}, \tag{4.2}$$

where U is a specific 2×2 unitary matrix. This will then allow us to apply the unitary U to the encoded qubit.

More explicitly, we will have four semi-infinite paths, and we will label the four paths by 0_{in}, 1_{in}, 0_{out}, and 1_{out} (where this labeling is the same as in equation (4.2)). We assume that the wave-packet encoding a qubit travels toward the graph $\widehat{G}$ along the two paths 0_{in} and 1_{in}. Far from the graph the evolution of this wavepacket is nearly identical to that of an infinite path, and thus our encoded qubit is well defined. As the wavepacket scatters through the graph $\widehat{G}$, the state of the qubit is not well defined, but after scattering, most of the amplitude is on the 0_{out} and 1_{out} paths, and is in the form of an encoded qubit.

For specific μ, L, σ, and t, we the have from Theorem 3 that the outgoing wave-packet for the two computational basis states is well approximated by the wave-packet corresponding to the state $U|z\rangle$. If we remember that the form of the wave-packet doesn't depend on the value of the initial encoded qubit, we can see that the evolution of the two basis states interfere, and thus for any encoded state $|\phi\rangle$, the outgoing wavepacket is well approximated by the encoded $U|\phi\rangle$. This is exactly what we were looking for.

[**TO DO:** *make graph?*]

4.1.3 Evolution on a finite graph

Unfortunately, a single unitary will not be sufficient for our purposes; while we could probably find a four-terminal graph that computes whether a given circuit accepts or rejects it's input, most of the computation would go into the construction of the graph. As such, we will need to place multiple graphs as obstacles for the computation. This causes problems, though, in that our construction extensively utilizes the semi-infinite paths in our analysis; we somehow need to truncate the graph while maintaining our results on the evolution.

To do this, we will apply our truncation lemma (Lemma 1), as it was designed specifically for this reason. Assuming that two Hamiltonians are identical on some set of basis states, and assuming that the support of the initial state is far (in some specified sense) from the difference, then the evolution of the state is the same for the two Hamiltonians, up to a small error term. By using this lemma on the scattering graph with semi-infinite paths, we can then see that if the paths are long enough (as compared to the location of the initial state), then the evolution of an initial wave-packet is relatively unchanged by the removal of the far vertices. Basically, Lemma 1 will allow us to prove an analog of Theorem 3 for finite graphs.

More concretely, let $H = A(G)$ is the Hamiltonian for a single particle scattering off of a finite graph $\widehat{G}$ with N paths. Let $G(K)$ be the finite graph obtained from G by truncating each of the paths to have a total length K (so that the endpoints of the paths are labeled

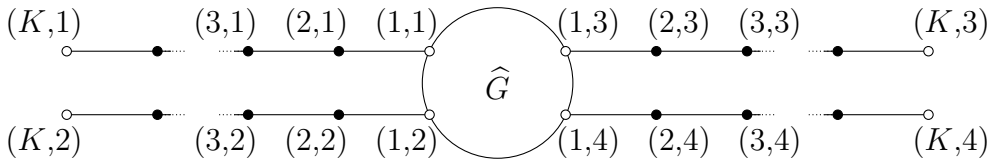

Figure 4.2: A graph $G(K)$ used to perform a single-qubit gate on an encoded qubit.

(K, j) for $j \in \{1, \ldots, N\}$), and choose $\widetilde{H} = A(G(K))$. Let the subspace $\mathcal{K}$ be spanned by basis states corresponding to vertices in $G(K)$. Choose a momentum $k \in (-\pi, 0)$, a position μ, and a cutoff length L, and let $|\Phi\rangle = |\psi^j(0)\rangle$ be the same initial state as in Theorem **??**. We will choose the evolution time T so that for $0 \leq t \leq T$, the time-evolved state remains far from the vertices labeled (K, j) (for each $j \in \{1, \ldots, N\}$), and thus far from the effect of truncating the paths. Note that this requires $K > \mu + L$. More precisely, we will choose $T = \mathcal{O}(L)$ and $K = \mathcal{O}(L)$ so that, for times $0 \leq t \leq T$, the state $|\alpha^j(t)\rangle$ from Theorem 3 has no amplitude on vertices within a distance $N_0 = \Omega(L)$ from the endpoints of the paths. For such times t we have

$$(1 - P)\, H^r |\alpha^j\,(t)\rangle = 0 \text{ for all } 0 \leq r < N_0, \tag{4.3}$$

where P is the projector onto $\mathcal{K}$. With these values, we can apply Lemma 1 where $W = H = A(G)$, $|\gamma(t)\rangle = |\alpha^j(t)\rangle$, and the bound $\delta = \mathcal{O}(\sqrt{\frac{\log L}{L}})$ from Theorem 3. The lemma then says that, for $0 \leq t \leq T$,

$$\left\| \left(e^{-iA(G)t} - e^{-iA(G(K))t}\right) |\psi^j(0)\rangle \right\| = \mathcal{O}\left(\sqrt{\frac{\log L}{L}}\right) \tag{4.4}$$

so, for $0 \leq t \leq T$, when combined with Theorem 3, we can see

$$\left\| e^{-iA(G(K))t} |\psi^j(0)\rangle - |\alpha^j(t)\rangle \right\| = \mathcal{O}\left(\sqrt{\frac{\log L}{L}}\right). \tag{4.5}$$

In other words, for small enough evolution times, the conclusion of Theorem 3 still holds if we replace the full Hamiltonian $A(G)$ with the truncated Hamiltonian $A(G(K))$.

Now that we have guaranteed bounds on the scattering behavior for finite graphs, we can give explicit bounds on the time-evolution of encoded qubits. In particular, let us assume that $\widehat{G}$ is a four-terminal gadget used to implement a given unitary U at momentum k, and let us assume that our initial states are encoded as Guassian wavepackets a distance μ from the graph, with a cutoff distance L. We will give explicit values of K, along with μ and L, so that the scattering event will cause the unitary U to be applied to the encoded qubits.

[**TO DO:** *is this the correct σ definition?*]

Explicitly, assuming that the four paths are labeled as in Figure **??**, where 0_{in}, 1_{in}, 0_{out} and 1_{out} are labeled as 1, 2, 3, and 4, respectively, we have that our input logical basis states are

$$|\,z\rangle_{\text{log,in}} = \gamma \sum_{x=\mu-L}^{\mu+L} e^{ikx} e^{-\frac{(x-\mu)^2}{2\sigma^2}} |\,x, z+1\rangle, \tag{4.6}$$

where we assume that $\sigma = \frac{L}{2\sqrt{\log L}}$, as in Theorem 3. Further, we can make us of the theorem, noting that $|z\rangle_{\log,\text{in}}$ are of the form $|\alpha^{z+1}(0)\rangle$, to define output logical states as well:

$$|z\rangle_{\log,\text{out}} = \gamma e^{-2iT\cos k} \sum_{x=\mu-L}^{\mu+L} e^{-ikx} e^{-\frac{(x-\mu)^2}{2\sigma^2}} |x, z+3\rangle, \tag{4.7}$$

where $T = \frac{\mu}{\sin|k|}$. Note that the momentum k for the output logical states implies that the particles are moving away from the graph $\widehat{G}$. In addition to these logical basis states, we can define

$$|\psi\rangle_{\log,\text{in}} = \alpha|0\rangle_{\log,\text{in}} + \beta|1\rangle_{\log,\text{in}} \tag{4.8}$$

and

$$|U\psi\rangle_{\log,\text{out}} = \big(\alpha U_{00} + \beta U_{01}\big)|0\rangle_{\log,\text{out}} + \big(\alpha U_{10} + \beta U_{11}\big)|1\rangle_{\log,\text{out}}. \tag{4.9}$$

With these definitions, we will want to show that the input states evolve to the corresponding output states:

[**TO DO:** *change this lemma to allow for K that aren't exactly $2\mu - 1$, but instead are some constant times μ. Basically, N_0 might be slightly smaller than $\mu/2$.*]

Lemma 10. *Let $k \in (-\pi, 0)$, and let $\widehat{G}$ be a four-terminal gate gadget, such that its scattering matrix at momentum k is of the form (4.2). Letting the logical states $|z\rangle_{log,in}$ and $|z\rangle_{log,out}$ be defined as in (4.6) and (4.7), where $\mu \geq 2L$ and $K = 2\mu - 1$ and $T = \frac{\mu}{\sin|k|}$, we have that there exists some constant ξ such that for all $0 \leq t \leq T$*

$$\Big\| e^{iA(G(K))t}|\phi(0)\rangle - |\phi(t)\rangle \Big\| \leq \xi\sqrt{\frac{\log L}{L}}, \tag{4.10}$$

where

$$|\phi(t)\rangle = \alpha|\alpha^1(t)\rangle + \beta|\alpha^2(t)\rangle, \tag{4.11}$$

and the $|\alpha^j(t)\rangle$ are as defined in Theorem 3. In particular, we have

$$\Big\| e^{iA(G(K))T}|\psi\rangle_{log,in} - |U\psi\rangle_{log,out} \Big\| \leq \xi\sqrt{\frac{\log L}{L}}. \tag{4.12}$$

Proof. Note that

$$\begin{aligned} &\Big\| e^{iA(G(K))t}|\phi(0)\rangle - |\phi(t)\rangle \Big\| \\ &\qquad \leq |\alpha| \Big\| e^{iA(G(K))t}|\alpha^1(0)\rangle - |\alpha^1(t)\rangle \Big\| + |\beta| \Big\| e^{iA(G(K))t}|\alpha^2(0)\rangle - |\alpha^2(t)\rangle \Big\|. \end{aligned} \tag{4.13}$$

We now have nearly have the form of the bound in Theorem 3, but where we use truncated paths.

We will use Lemma 1, with $H = A(G)$, $\tilde{H} = A(G(K))$, and $N_0 = \mu - 2 - L$, and where the error bound $\delta = \chi\sqrt{\frac{\log L}{L}}$ comes from Theorem 3. Assuming that L is taken large enough so that $\delta < 1$, the lemma then gives us that for all $0 \leq t \leq T$,

$$\left\| \left(e^{-iA(G)t} - e^{-iA(G(K))t}\right) |\alpha^j(0)\rangle \right\| \leq \left(\frac{4e\|A(G)\|t}{\mu - 2 - L} + 2\right)\left[\chi\sqrt{\frac{\log L}{L}} + 2^{-\mu+L+2}\left(1 - \chi\sqrt{\frac{\log L}{L}}\right)\right]. \tag{4.14}$$

If we then note that $\|A(G)\|$ is bounded by the maximum degree of the graph G (a constant), and that $\mu - L - 2 \geq 3\mu$, we then have

$$\left\| \left(e^{-iA(G)t} - e^{-iA(G(K))t}\right) |\alpha^j(0)\rangle \right\| \leq \left(\frac{12ed}{\mu}\frac{\mu}{\sin|k|} + 2\right)(\chi + 1)\sqrt{\frac{\log L}{L}} \leq \zeta\sqrt{\frac{\log L}{L}}, \tag{4.15}$$

where ζ is a constant (but does depend on k and the graph $\widehat{G}$).

We can then combine these results, as

$$\begin{aligned} &\left\| e^{iA(G(K))t} |\alpha^j(0)\rangle - |\alpha^j(t)\rangle \right\| \\ &\quad \leq \left\| \left(e^{iA(G(K))t} - e^{iA(G)t}\right) |\alpha^j(0)\rangle \right\| + \left\| e^{iA(G)t} |\alpha^j(0)\rangle - |\alpha^j(t)\rangle \right\| \leq \left(\chi + \zeta\right)\sqrt{\frac{\log L}{L}}. \end{aligned} \tag{4.16}$$

From this, we can then see that

$$\begin{aligned} &\left\| e^{iA(G(K))t} |\phi(0)\rangle - |\phi(t)\rangle \right\| \\ &\quad \leq |\alpha| \left\| e^{iA(G(K))t} |\alpha^1(0)\rangle - |\alpha^1(t)\rangle \right\| + |\beta| \left\| e^{iA(G(K))t} |\alpha^2(0)\rangle - |\alpha^2(t)\rangle \right\| && (4.17) \\ &\quad \leq \left(|\alpha| + |\beta|\right)\left(\chi + \zeta\right)\sqrt{\frac{\log L}{L}}, && (4.18) \end{aligned}$$

and by setting $\xi = \sqrt{2}(\chi + \zeta)$ we have the requisite bound (for large enough L).

If we then note that $\phi(0) = |\psi\rangle_{\log,\text{in}}$ and $\phi(T) = |U\psi\rangle_{\log,\text{out}}$, we also have the particular bound we were looking for. □

Essentially, Lemma 10 tells us that even when truncated to finite length paths, the scattering events on our graphs apply an encoded unitary to the logical states. This is represented pictorially in Figure 4.3.

4.1.4 Multi-gate computations

With our analysis of an encoded single-qubit's evolution for one scattering event on a finite graph, we should be able to analyze multiple scattering events, corresponding to a circuit of some finite length. In particular, if we want to apply multiple unitaries to a single qubit, we can place the corresponding scattering gadgets $\widehat{G}_i$ in series, and then connect the outputs of $\widehat{G}_i$ to the inputs of $\widehat{G}_{i+1}$ by a path of length $K - 2$. We can then use Lemma 1 to analyze

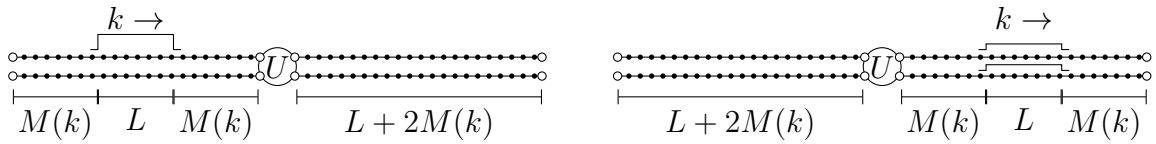

Figure 4.3: A single-qubit gate U acts on an encoded qubit. The wave packet starts on the paths on the left-hand side of the figure, a distance $M(k)$ from the ends of the paths. After time $t_{\rm I} = 3L/2$ the logical gate has been applied and the wave packet has traveled a distance $2M(k) + L$ (up to error terms that are bounded as $\emptyset(L^{-1/4})$).

each scattering event in series, using the output logical state of the ith scattering event for the input logical state of the $(i+1)$th scattering event.

[**TO DO:** *make a figure*]

Let us assume that a single-qubit circuit $\mathcal{C}$ is composed of g unitaries, where the ith unitary applied is given by U_i. Moreover, let us assume that at a momentum k, the graphs $\widehat{G}_i$ have scattering matrices of the form (4.2) corresponding to the unitary U_i (i.e., at momentum k, the graph $\widehat{G}_i$ implements an encoded U_i). We can then construct a graph $G_{\mathcal{C}}$ which we will use to compute the circuit $\mathcal{C}$ using wave-packets at momentum k.

[**TO DO:** *technically, there is an off by one error with my bounds. Using the*]

The graph $G_{\mathcal{C}}$ is constructed by combining the $G_i(K)$ into a single graph, where $G_i(K)$ is defined in Section **??**. We combine the $G_i(K)$ into a single graph by associating the output paths of $G_i(K)$ with the input paths of $G_{i+1}(K)$. Assuming that the vertices of $G_i(K)$ are labeled as (u, i), this essentially means that most of the vertices along the long paths have two labels, $(x, 3, i)$ and $(K - x + 1, 1, i + 1)$ or $(x, 4, i)$ and $(K - x + 1, 2, i + 1)$. Equivalently, the graph $G_{\mathcal{C}}$ can be constructed by removing the input paths (paths 1 and 2) for all the $G_i(K)$ (except for $G_1(K)$), shorten each of the terminal paths by 1 (except for $G_g(K)$), and then connect the end of the paths for $G_i(K)$ to the input terminals of $G_{i+1}(K)$.

[**TO DO:** *make a simple figure*]

With this construction of $G_{\mathcal{C}}$, note that if we look only at the vertices supported within the copy of $G_i(K)$, we actually have the graph $G_i(K)$. As such, we will be able to use Lemma 1 and Lemma 10 to determine the evolution while a Gaussian wave-packet is located near the graph $\widehat{G}_i$. If we assume that the initial wave-packet is located in the correct position near $\widehat{G}_i$, we can iteratively apply this idea, where the "input" logical state for the $(i+1)$th scattering event is simply the "output" from the ith scattering event. As such, the logical state after the gth scattering event will correspond to the logical state after the circuit $\mathcal{C}$ has been applied.

[**TO DO:** *check this math*]

Concretely, let us choose some cutoff length L, set $\sigma = \frac{L}{2\sqrt{\log L}}$, chose $\mu = 2L$ and $K = 2\mu$ and $T = \frac{\mu}{\sin|k|}$. With these choices, our initial logical state will be nearly identical to (4.6), but where the basis states also have a label corresponding to fact that there are multiple long paths:

$$|\,z\,\rangle_{\rm log,in} = \gamma \sum_{x=\mu-L}^{\mu+L} e^{ikx} e^{-\frac{(x-\mu)^2}{2\sigma^2}} |\,x, z+1, 1\,\rangle. \tag{4.19}$$

In a similar manner, the final state of the qubit will be defined as

$$|z\rangle_{\log,\text{out}} = \gamma e^{-2iTg\cos k} \sum_{x=\mu-L}^{\mu+L} e^{-ikx} e^{-\frac{(x-\mu)^2}{2\sigma^2}} |x, z+3, g\rangle, \tag{4.20}$$

Additionally, we will need to define logical states at several times throughout the computation, corresponding to the states after each applied unitary. As such, we will define the logical state after the jth scattering event (and before the $(j+1)$th scattering event) as

$$|z\rangle_{\log,j} = \gamma e^{-2iTj\cos k} \sum_{x=\mu-L}^{\mu+L} e^{ikx} e^{-\frac{(x-\mu)^2}{2\sigma^2}} |x, z+1, j+1\rangle \tag{4.21}$$

$$= \gamma e^{-2iTj\cos k} \sum_{x=\mu-L}^{\mu+L} e^{-ikx} e^{-\frac{(x-\mu)^2}{2\sigma^2}} |x, z+3, j\rangle. \tag{4.22}$$

[**TO DO:** *make the words work*]

$$\left\| e^{iA(G_{\mathcal{C}})gT} |\psi\rangle_{\log,\text{in}} - |U_{\mathcal{C}}\psi\rangle_{\log,\text{out}} \right\|$$
$$\leq \sum_{j=0}^{g-1} \left\| e^{iA(G_{\mathcal{C}})T} |U_j U_{j-1} \cdots U_1 \psi\rangle_{\log,j} - |U_{j+1} U_j \cdots U_1 \psi\rangle_{\log,j+1} \right\| \tag{4.23}$$

Note that each individual term is close to that in Lemma 10, but where the Hamiltonian is given by $A(G_{\mathcal{C}})$ as opposed to $A(G(K))$. However, we can use Lemma 1, with $H = A(G_{\mathcal{C}})$, $\tilde{H} = G(K-1)$, $N_0 = \frac{\mu}{4}$, and the error δ from Lemma 10, we have that for all logical states $|\phi\rangle$,

$$\left\| e^{iA(G_{\mathcal{C}})T} |\phi\rangle_{\log,j} - |U_{j+1}\phi\rangle_{\log,j+1} \right\|$$
$$\leq \left(\frac{16e\|A(G_{\mathcal{C}})\|T}{\mu} + 2 \right) \left[\xi \sqrt{\frac{\log L}{L}} + 2^{-\mu+L+2} \left(1 - \chi \sqrt{\frac{\log L}{L}} \right) \right] \tag{4.24}$$
$$\leq \kappa_j \sqrt{\frac{\log L}{L}}, \tag{4.25}$$

where κ is depends on k and the maximum degree of $G_{\mathcal{C}}$ (which we assume to be constant). We can then see that

$$\left\| e^{iA(G_{\mathcal{C}})gT} |\psi\rangle_{\log,\text{in}} - |U_{\mathcal{C}}\psi\rangle_{\log,\text{out}} \right\|$$
$$\leq \sum_{j=0}^{g-1} \left\| e^{iA(G_{\mathcal{C}})T} |U_j U_{j-1} \cdots U_1 \psi\rangle_{\log,j} - |U_{j+1} U_j \cdots U_1 \psi\rangle_{\log,j+1} \right\| \tag{4.26}$$
$$\leq g\kappa \sqrt{\frac{\log L}{L}}. \tag{4.27}$$

As such, if we take L larger than $g^2\kappa^2$ we find that the error can be made arbitrarily small, and thus we were able to simulate a single-qubit unitary via scattering. [**TO DO:** *figure out product log stuff*]

4.1.5 Explicit encodings

[**TO DO:** *Find universal gate set for several momenta ($\pi/2$, $\pi/4$, $\pi/3$, etc.)*]

4.2 Multi-qubit computations

Now that we have a decent understanding of how to encode a single qubit computation via scattering, we now need to understand multi-qubit computations. The intuitive construction will remain the same, but the requisite number of vertices will become rather large. In particular, our construction will require an exponential number of long paths. This exponential size is required, however, as the Hilbert space of a single-particle quantum walk is only as large as the number of vertices of the graph

Let us now give the encoding of n qubits in our scattering framework. As in Section 4.1.1, we will encode the state as a wave-packet traveling along an infinite path, where the value of the qubit is encoded in the path on which the particle is located. For a single qubit, this meant that we had two infinite paths, corresponding to logical 0 and 1. For n qubits, however, this means that we need 2^n infinite paths, one path corresponding to each basis state.

We will still have four important quantities that are independent of the state of the qubit, namely the momentum of the wave-packet k, the position of the center of the wave-packet μ (which does depend on t), the cutoff distance L, and the standard deviation of the Guassian σ. As such, if we label the 2^n infinite paths by the strings $\mathbf{z} \in \mathbb{F}_2^n$, and the vertices as $(x, \mathbf{s})$ for $x \in \mathbb{Z}$ and $\mathbf{z} \in \mathbb{F}_2^n$, we have that the logical states are encoded in the wave-packets

$$|\mathbf{z}\rangle_{\log} = \gamma \sum_{x=\mu-L}^{\mu+L} e^{ikx} e^{-\frac{(x-\mu)^2}{2\sigma^2}} |x, \mathbf{z}\rangle. \tag{4.28}$$

Note that we again use this construction so that we will be able to analyze the dynamics via Theorem 3.

4.2.1 Single gates

Now that we have an encoding of our qubits, we will need to somehow apply encoded unitary gates. We have already done most of the work in Section 4.1, and we just need to show how to use the single-qubit results in our larger encoding, and how to perform multi-qubit entangling gates.

Our implementation of single-qubit unitaries for multi-qubit computations is to use many copies of the single-qubit implementation. In particular, since a single qubit unitary U acting on qubit $w \in [n]$ can be written as

$$\mathbb{I}_{2^{w-1}} \otimes U \otimes \mathbb{I}_{2^{n-w}} = \sum_{x \in \mathbb{F}_2^{w-1}, y \in \mathbb{F}_2^{n-w}} |x\rangle\langle x| \otimes U \otimes |y\rangle\langle y|, \tag{4.29}$$

we can apply the unitary U on the encoded w qubit by ensuring that the scattering occurs for each computational basis state of the other qubits. This means that by placing 2^{n-1}

copies of the graph $\widehat{G}$ as obstacles in the paths, one for each computational basis state, the scattering behavior is exactly as expended.

[**TO DO:** *check whether errors add*]

[**TO DO:** *make multi qubit gate figure*]

For multi-qubit entangling unitaries, the solution is even more simple; we simply relabel the output paths. If we note that many multi-qubit gates such as a controlled-NOT gate or a Toffoli gate simply permutes the computational basis states, along with the fact that the particular path a particle travels along corresponds to its logical state, by relabeling the paths, or equivalently permuting the paths, we apply an encoded entangling gate. Schematically, this can be seen in Figure **??**. Note that this method of applying a multi-qubit gate is independent of the encoding momenta, and thus can be used for all such momenta.

Assuming that a given two-qubit unitary V occurs after some single-qubit unitary U, we construct a graph implementing VU by taking a copy of $G_U(K)$, and then permuting its output paths. Note that this means that for a given copy of $\widehat{G}_j$, the logical states corresponding to the input paths might be different from the logical states corresponding to the output paths.

[**TO DO:** *make Figure* **??** *entangling gate*] .

Explicitly, assuming that the 2^{n+1} paths are labeled as in Figure **??**, where the path for z_{in} for $z \in \mathbb{F}_2^n$ is labeled as $z+1$, while the z_{out} are labeled as $z+2^n+1$, we have that our input logical basis states are

$$|\, z\rangle_{\text{log,in}} = \gamma \sum_{x=\mu-L}^{\mu+L} e^{ikx} e^{-\frac{(x-\mu)^2}{2\sigma^2}} |\, x, z+1\rangle, \tag{4.30}$$

where we assume that $\sigma = \frac{L}{2\sqrt{\log L}}$, as in Theorem 3. Note that this is identical to the sinlge particle case (4.6), but with more input paths. We can then take inspiration from the single qubit case, and define the output logical states as well:

$$|\, z\rangle_{\text{log,out}} = \gamma e^{-2iT\cos k} \sum_{x=\mu-L}^{\mu+L} e^{-ikx} e^{-\frac{(x-\mu)^2}{2\sigma^2}} |\, x, z+2^n+1\rangle, \tag{4.31}$$

where $T = \frac{\mu}{\sin|k|}$. Note that the momentum k for the output logical states implies that the particles are moving away from the graph $\widehat{G}$. In addition to these logical basis states, we can define

$$|\, \psi\rangle_{\text{log,in}} = \sum_{z\in\mathbb{F}_2^n} \alpha_z |\, z\rangle_{\text{log,in}} \tag{4.32}$$

and

$$|\, U\psi\rangle_{\text{log,out}} = \sum_{y,z\in\mathbb{F}_2^N} U_{zy} |\, z\rangle_{\text{log,out}}, \tag{4.33}$$

where U is thought of as a unitary on n qubits. With these definitions, we will want to show that the input states evolve to the corresponding output states. This essentially follows from Lemma 10, but where we need to do some small work showing that the errors don't grow like the number of paths.

Corollary 1. *Let $k \in (-\pi, 0)$, let $\widehat{G}$ be a four-terminal gate gate, such that its scattering matrix at momentum k is of the form (4.2), and let V be a permutation of the underlying basis states. Letting the logical states $|z\rangle_{log,in}$ and $|z\rangle_{log,out}$ be as in (??) and (4.31), where $\mu \geq 2L$ and $\frac{3\mu}{2} \leq K \leq 2\mu$ and $T = \frac{\mu}{\sin|k|}$, we have that there exists some constant such that for all $0 \leq t \leq T$,*

$$\left\| e^{iA(G_V^n(K))t} |\phi(0)\rangle - |\phi(t)\rangle \right\| \leq \xi \sqrt{\frac{\log L}{L}}, \tag{4.34}$$

where

$$|\phi(t)\rangle = \sum_{z \in \mathbb{F}_2^n} \beta_z |\alpha^{z+1}(t)\rangle, \tag{4.35}$$

and the $|\alpha^j(t)\rangle$ are as defined in Theorem 3. In particular, we have

$$\left\| e^{iA(G_V^n(K))T} |\psi\rangle_{log,in} - |U\psi\rangle_{log,out} \right\| \leq \xi \sqrt{\frac{\log L}{L}}. \tag{4.36}$$

Proof. Note that $G_V^n(K)$ is a disconnected graph, with 2^{n-1} components. As such, we have that $e^{iA(G_V^n(K)t}$ decomposes into the product of 2^{n-1} commuting operators, all acting on disjoint Hilbert spaces. This then implies that the error in propagation is at most the error on any of the components.

In each component, however, we can use Lemma 10, to see that the first part of the corollary holds, with the appropriate error (and with a constant equal to that of Lemma 10). Hence, the total error is bounded by $xi\sqrt{\frac{\log L}{L}}$.

For the second part of the corollary, we can use Lemma 10 to see that the result holds on each component of $G_V^n(K)$, and thus holds in general. □

4.2.2 Multi-gate computations

At this point, we have most of the requirements for our universality result. We know from Section 4.2.1 how to apply a single encoded unitary on multiple qubits, and we know from Section 4.1.4 how to apply multiple single-qubit gates. We need only to combine these two results.

We will make use of the same block structure as in Section 4.1.4, where the graph corresponding to a single unitary is shown in Figure 4.4. Additionally, we will assume that the circuit we want to simulate only consists of a single-qubit gates followed by a two-qubit gate. This assumption isn't difficult to enforce, as these gates can simply consist of identity operations. The circuit that we want to simulate is then given by

$$U_{\mathcal{C}} = V_g U_g V_{g-1} U_{g-1} \cdots V_1 U_1, \tag{4.37}$$

where each V_j is a two-qubit gate, and each U_1 is a one-qubit gate.

As in Section 4.1.4, we will construct a graph for this circuit, $G_{\mathcal{C}}$, by examining the graphs $G_{U_j}^{V_j}$ for each $j \in [g]$, and then combining them by associating the output paths of

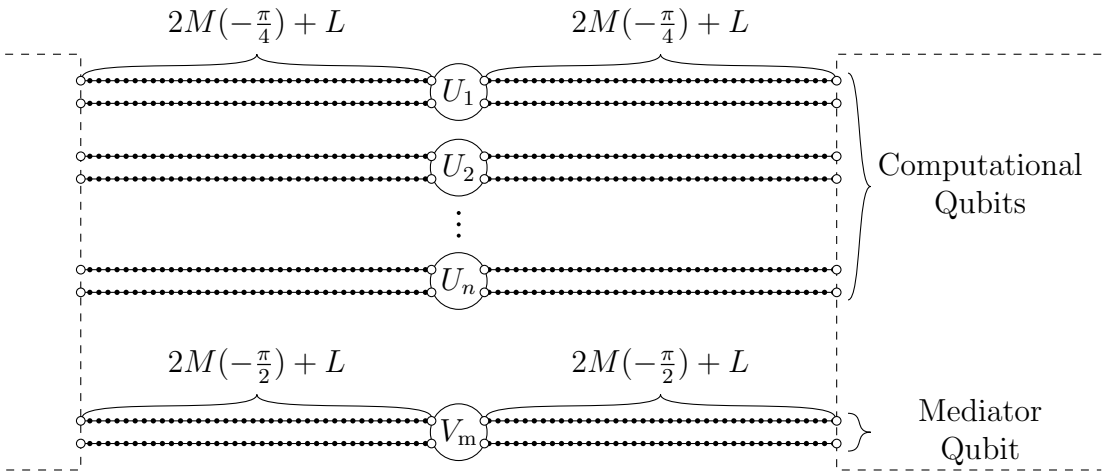

Figure 4.4: The intuitive idea for a single-particle block.

$G_{U_j}^{V_j}(K)$ with the input paths of $G_{U_{j+1}}^{V_{j+1}}(K)$. Explicitly, the vertices along the output paths of $G_{U_j}^{V_j}(K)$ labeled as $(x, 2^n + z, j)$ for $z \in [2^n]$ are the same vertices on the input paths of $G_{U_{j+1}}^{V_{j+1}}(K)$ labeled as $(K - x + 1, z, j + 1)$. This can bee seen pictorially in Figure 4.4 for one of these blocks.

[**TO DO:** *fix figure Figure 4.4*]

With this construction, we have exactly the same idea as in the Section 4.1.4 to analyze the time-evolution of a particular initial logial state, and the analysis proceeds accordingly. If we use Lemma 1 to only use the vertices close to a the wavepacket (and in particular the nearest copy of $G_{V_j}^{U_j}(K)$) we can use Corollary 1 to approximate the evolution.

Concretely, let us choose some cutoff length L, set $\sigma = \frac{L}{2\sqrt{\log L}}$, chose $\mu = 2L$ and $K = 2\mu$ and $T = \frac{\mu}{\sin|k|}$. With these choices, our initial logical state will be nearly identical to (4.6), but where the basis states also have a label corresponding to fact that there are multiple long paths:

$$|\,z\rangle_{\text{log,in}} = \gamma \sum_{x=\mu-L}^{\mu+L} e^{ikx} e^{-\frac{(x-\mu)^2}{2\sigma^2}} |\,x, z+1, 1\rangle. \tag{4.38}$$

In a similar manner, the final state of the qubit will be defined as

$$|\,z\rangle_{\text{log,out}} = \gamma e^{-2iTg\cos k} \sum_{x=\mu-L}^{\mu+L} e^{-ikx} e^{-\frac{(x-\mu)^2}{2\sigma^2}} |\,x, z+2^n+1, g\rangle, \tag{4.39}$$

Additionally, we will need to define logical states at several times throughout the computation, corresponding to the states after each applied unitary. As such, we will define the

logical state after the jth scattering event (and before the $(j+1)$th scattering event) as

$$|z\rangle_{\log,j} = \gamma e^{-2iTj\cos k} \sum_{x=\mu-L}^{\mu+L} e^{ikx} e^{-\frac{(x-\mu)^2}{2\sigma^2}} |x, z+1, j+1\rangle \tag{4.40}$$

$$= \gamma e^{-2iTj\cos k} \sum_{x=\mu-L}^{\mu+L} e^{-ikx} e^{-\frac{(x-\mu)^2}{2\sigma^2}} |x, z+2^n+1, j\rangle. \tag{4.41}$$

[**TO DO:** *make the words work*]

$$\left\| e^{iA(G_{\mathcal{C}})gT} |\psi\rangle_{\log,\text{in}} - |U_{\mathcal{C}}\psi\rangle_{\log,\text{out}} \right\|$$
$$\leq \sum_{j=0}^{g-1} \left\| e^{iA(G_{\mathcal{C}})T} |U_j U_{j-1} \cdots U_1 \psi\rangle_{\log,j} - |U_{j+1} U_j \cdots U_1 \psi\rangle_{\log,j+1} \right\| \tag{4.42}$$

Note that each individual term is close to that in Lemma 10, but where the Hamiltonian is given by $A(G_{\mathcal{C}})$ as opposed to $A(G(K))$. However, we can use Lemma 1, with $H = A(G_{\mathcal{C}})$, $\tilde{H} = G(K-1)$, $N_0 = \frac{\mu}{4}$, and the error δ from Lemma 10, we have that for all logical states $|\phi\rangle$,

$$\left\| e^{iA(G_{\mathcal{C}})T} |\phi\rangle_{\log,j} - |U_{j+1}\phi\rangle_{\log,j+1} \right\|$$
$$\leq \left(\frac{16e\|A(G_{\mathcal{C}})\|T}{\mu} + 2 \right) \left[\xi \sqrt{\frac{\log L}{L}} + 2^{-\mu+L+2} \left(1 - \chi \sqrt{\frac{\log L}{L}} \right) \right] \tag{4.43}$$
$$\leq \kappa_j \sqrt{\frac{\log L}{L}}, \tag{4.44}$$

where κ is depends on k and the maximum degree of $G_{\mathcal{C}}$ (which we assume to be constant). We can then see that

$$\left\| e^{iA(G_{\mathcal{C}})gT} |\psi\rangle_{\log,\text{in}} - |U_{\mathcal{C}}\psi\rangle_{\log,\text{out}} \right\|$$
$$\leq \sum_{j=0}^{g-1} \left\| e^{iA(G_{\mathcal{C}})T} |U_j U_{j-1} \cdots U_1 \psi\rangle_{\log,j} - |U_{j+1} U_j \cdots U_1 \psi\rangle_{\log,j+1} \right\| \tag{4.45}$$
$$\leq g\kappa \sqrt{\frac{\log L}{L}}. \tag{4.46}$$

As such, if we take L larger than $g^2\kappa^2$ we find that the error can be made arbitrarily small.

[**TO DO:** *figure out product log stuff*]

4.3 Universality via single-particle scattering

With our results so far, we technically haven't yet shown that our results are

Now that we know that the time-evolution of a particular state on a sparse (and efficiently computable) graph can be used to simulate an arbitrary quantum circuit, to show that such

computation is universal for quantum computation we need to show the simulation in the other direction. This is not particularly difficult, but is a necessary step.

In particular, let us discuss the problem of

Problem 1 (Quantum Walk Evolution)**.** Given a d-sparse, row-computable simple graph G on $\Theta(2^n)$ vertices, an efficiently preparable initial state $|\phi^G_{\text{init}}\rangle$, a subset of the vertices $\mathcal{V}_{\text{accept}}$ (for which membership is easily verified), and a time $T \in \text{poly}(n)$, determine whether

- $\langle \phi^G_{\text{init}} | e^{iA(G)T} \Pi_{\mathcal{V}} e^{-iA(G)T} | \phi^G_{\text{init}} \rangle \geq \frac{2}{3}$, or
- $\langle \phi^G_{\text{init}} | e^{iA(G)T} \Pi_{\mathcal{V}} e^{-iA(G)T} | \phi^G_{\text{init}} \rangle \leq \frac{1}{3}$,

where we are guaranteed that one case holds.

Note that the efficient preparation of $|\phi^G_{\text{init}}\rangle$, and the fact that membership $\mathcal{V}$ is easily verified, are used to insure that the bulk of the computational power arises from the time evolution on G, and that we are not hiding the computation in the preparation of the initial state or in our measurements.

4.3.1 Simulation of a quantum circuit

Let us first show that an arbitrary quantum circuit can be simulated by the time evolution of an efficiently specifiable state on a succinctly represented graph. This is the point at which we will use our graph scattering techniques.

In particular, choose some $k \in (-\pi, 0)$ for which we have a universal set of quantum scattering gates are known (such as those in Section 4.1.5, and let $\mathcal{C}_x$ be a circuit corresponding to the circuit verification problem instance x, such that $\mathcal{C}_x$ can be decomposed into a sequence of one- and two-qubit gates from the universal gate set $\mathcal{S}_k$ and controlled-not gates (as defined in Section 4.1.5). We assume that the circuit $\mathcal{C}_x$ acts on m qubits (where $m \in \text{poly}(n)$), and that the circuit satisfies:

- if $x \in$ Quantum Circuit Verification, then $\Pr(\mathcal{C}_x, 0^m) > 1 - 2^{-|x|}$,
- if $x \notin$ Quantum Circuit Verification, then $\Pr(\mathcal{C}_x, 0^m) < 2^{-|x|}$.

In other words, with high probability the circuit $\mathcal{C}_x$ computes whether the instance x is in Quantum Circuit Verification.

Note that we almost have from Section 4.2 that such a simulation is possible, we just need to ensure that the unitary $\mathcal{C}_x$ has the decomposition required, that the associated graph is d-sparse and row-computable, that the initial state is efficiently preparable, and that the subset of vertices corresponding to an accepting computation is easily verifiable.

For the first problem, note that we can easily change the circuit $\mathcal{C}_x$ into a circuit of the form described in Section 4.2 by doubling the number of unitaries in the circuit. In particular, if $\mathcal{C}_x = U_g U_{g-1} \cdots U_1$, the quantum walk will simulate the circuit $\mathcal{D}_x = V_g V_{g-1} \cdots V_1$, where

$$V_j = \begin{cases} U_j \mathbb{I}_2^{(1)} & U_j \text{ is a 2-qubit gate} \\ \mathbb{I}_4^{(1,2)} U_j & U_j \text{ is a 1-qubit gate.} \end{cases} \tag{4.47}$$

In this manner, $\mathcal{D}_x$ is an alternating sequence of 1- and 2-qubit gates. For a given L, we can thus use the construction of Section 4.2 for the graph $\mathcal{D}_x$.

To see that the Hamiltonian corresponding to $G_{\mathcal{D}_x}(K)$ is d-sparse and row-computable, note that the Hamiltonian simply corresponds to the adjacency matrix of the graph. As such, the sparsity is exactly equal to the maximum degree of the graph, which is bounded by some constant $d_{\max}$, which depends on the scattering gadgets for the momentum k.

To see that the graph is row-computable, note that our construction already gives us the ability to efficiently determine the neighbors of a vertex. In the labeling scheme given, vertices along each path are labeled according to the basis state it corresponds to, the number of scattering gadgets to it's left, and the position along the gadget, and are only connected to vertices the two vertices with positions that differ by 1. The vertices contained in a copy of $\widehat{G}_j$ for some graph scattering gadget j are labeled by the computational state of the qubits not affected by the corresponding unitary, along with the labeling of the graph $\widehat{G}_j$, and are only connected to those vertices with the same labeling of gadget and are connected in $\widehat{G}_j$. The only difficulties are the terminal gadgets, but these are easily determined since we only ever apply either the identity gate or a controlled not to the logical state of the corresponding input/output terminals. Hence, the Hamiltonian for the graph is $d_{\max}$-sparse and row-computable.

For the initial state, note that the construction of Section 4.2 only has non-zero amplitude on $2L+1$ vertices, which only depends on $\mathcal{C}$ in terms of the length. This is both efficiently specifiable and easily constructed.

Finally, we have that the states corresponding to an accepting computation are easy to check; they are simply those vertices on the final $(g+1)$ long paths with the first qubit in logical state 1.

Putting this together, we can then use the results of Section 4.2 to show that any Quantum Circuit Verificationinstance can be reduced to an instance of Quantum Walk Evolution. Hence, Quantum Walk Evolutionis **BQP**-hard.

4.3.2 Simulation of a quantum walk

Let us now show that Quantum Walk Evolutionis in **BQP**. It relatively easily follows from Theorem **??**, since we simply need to evolve a given Hamiltonian for the time T, and then measure in the computational basis.

In particular, the fact that the initial state is efficiently preparable means that there exists a quantum circuit $\mathcal{C}_{\text{prep}}$ that prepares the given initial state from the state $|0^n\rangle$, possibly including some ancilla states. Moreover, the quantum circuit only consists of $\text{poly}(|x|)$ one- and two-qubit gates, since the state is efficiently preparable. (Note that this bound depends on the efficiency of the given instance.)

From the initial state, we can then use Theorem **??** to evaluate the quantum walk Hamiltonian for the time T. Since the Hamiltonian is d-sparse, and since the Hamiltonian is an adjacency matrix, we have that its maximal eigenvalue is at most d. Assuming that we want to perform the simulation with error $1/10$, we can then simulate the evolution of the quantum walk in an efficient manner. (Again, the efficiency depends on the given instance.)

Finally, the quantum circuit can measure the state of the system in the vertex basis. If the measured vertex belongs to $\mathcal{K}$ (a post-processing procedure that can be done efficiently),

then the circuit accepts. Otherwise, the circuit rejects.

As the quantum walker fails with probability at most $\frac{1}{3}$ (i.e., accepts the state for a yes instance with probability at least $\frac{2}{3}$, and accepts a no-instance with probability at most $\frac{1}{3}$), with the error arising from the simulation we still have that the yes and no instances of our simulations have a constant acceptance gap. Hence, we have that QUANTUM WALK EVOLUTIONis in **BQP**.

Put together with our results using scattering, we then have that QUANTUM WALK EVOLUTIONis **BQP**-complete, or that quantum walks are universal for quantum computation.

4.4 Discussion and extensions

Note that these results are essentially already known. In particular, Childs gave a similar result using scattering theory, but where his time evolution arose from the theory of stationary phases.

One key point in this analysis is that, while we can reduce the graph to be degree-3, without changing much except the individual gadgets, the permutation of the underlying paths plays a key part in our encoded gates. However, these permutations are intrinsically non-planar (assuming that there are more than three non-identity 2-qubit gates). One might ask whether any planar graph could be used to encode a computation, or whether non-planarity is required for the computations.

Additionally, our current construction assumes no errors, and has no error-correction easily built in. We are unsure how error correction could be implemented in this scheme, since both non-local measurements and measurements in the middle of the computation seem rather difficult. This might also help us in the next chapter, where we use similar methods to show the universality of multi-qubit quantum walks.

Chapter 5

Universality of multi-particle scattering

[**TO DO:** *I should really give a broad overview of the technique. Maybe not in any great detail, but I should really explain why things are going to go the way they are.*]

In the previous chapter, we were able to show that the single-particle scattering on a large enough graph allowed for universal quantum computation. However, the graph had a number of vertices exponential in the number of simulated qubits. While the evolution was still time efficient, the underlying graph had to be a graph in the Hilbert space as opposed to an actual implementable graph.

To get around this, we need to somehow enlarge the Hilbert space while keeping the number of vertices of the graph small. If we use a vertex for each basis vector of the Hilbert space, we will not be able to shrink the graph down to any reasonable size. However, if we instead use some correlations in addition to the graph structure in order to encode computations we can reduce the size of the graph.

In particular, if we use multiple particles as opposed to a single particle, the resulting Hilbert space grows like V^N, where V is the number of vertices and N is the number of particles. Hence, if we encode computation using a number of particles that grows like the number of simulated qubits, we can keep the size of the underlying graph small.

The main ideas of this chapter follow [15], with various improvements from [14]. However, the proof of Theorem 4, while inspired by proofs in [15] is novel to this thesis.

[**TO DO:** *a lot more citations*]

5.1 Multi-particle quantum walk

We have already seen how a single particle moves on some given graph; the evolution proceeds with the Hamiltonian given by the adjacency matrix of the graph. If we want to extend this framework to multiple particles, we should ensure that each particle still has this single-particle evolution.

Namely, if we assume that N particles each move independently on a given graph G, we will want the Hamiltonian of this larger system to be as though each particle sees its own copy of G. To do this, we will have that the N particle quantum walk with no interaction

takes the form

$$H^N_{\text{mov}} = \sum_{w\in[N]} A(G)^{(w)} \tag{5.1}$$

where $B^{(w)}$ is the operator that acts on N particles as B on the wth particle and $\mathbb{I}$ on the rest, or

$$B^{(w)} = \mathbb{I}^{\otimes w-1}_{|V(G)|} \otimes B \otimes \mathbb{I}^{N-w}_{|V(G)|}. \tag{5.2}$$

With such a Hamiltonian, the evolution operator decomposes into a product of commuting terms, where each term acts as the single particle evolution for a different particle. This is exactly what we would want for the N-particle case.

However, the eigenstates of such a Hamiltonian are simply product states over the N particles, where each of the particles are an eigenstate of $A(G)$. Such a system is only as computationally powerful as that of a single-particle, since the individual particles cannot interact. As such, for our purposes we will want to include some interaction. We also want to ensure that we capture the intuitive structure of particle interactions in the continuum, where the interaction only depends on the distance between particles. This translation invariance can have several different abstractions to a general graph, but on a one dimensional lattice we would expect the interaction to only depend on the distance between the particles, as measured by the shortest path between vertices.

We will take this requirement on the infinite path and use it for all vertices. Futher, we will assume some finite range of interaction, so that particles with large physical separation don't interact. Namely, let us choose some $d_{\max} \in \mathbb{N}$ to be the finite range of the interaction, and then choose $d+1$ symmetric polynomials in two variables, U_d for $0 \leq d \leq d_{\max}$. Additionally, let $\hat{n}_v$ for $v \in V(G)$ be the operator that counts the number of particles at vertex v, explicitly given by

$$\hat{n}_v = \sum_{w\in[N]} |\, v\rangle\langle\, v\,|^{(w)}. \tag{5.3}$$

With these values, and if $d(u,v)$ is the distance function on the graph G given by the length of the shortest path between u and v, we can define the interaction

$$H_{\text{int}} = \sum_{d=0}^{d_{\max}} \sum_{\substack{u,v\in V(G)\\ d(u,v)=d}} U_d(\hat{n}_u, \hat{n}_v). \tag{5.4}$$

Note that on the infinite path (and in fact on any lattice), this interaction has the form we require.

With such a chosen interaction, (i.e., with $d_{\max}$ and the U_d well defined), we can then define the N-particle quantum walk on G with this interaction. Namely, we let

$$H^N_G = H^N_{\text{mov}} + H^N_{\text{int}} = \sum_{w\in[N]} A(G)^{(w)} + \sum_{d=0}^{d_{\max}} \sum_{\substack{u,v\in V(G)\\ d(u,v)=d}} U_d(\hat{n}_u, \hat{n}_v). \tag{5.5}$$

Hamiltonians of this form will be the study of this thesis.

As a particular example, if $d_{\max} = 0$, and

$$U(x, y) = \gamma \frac{x + y}{4}(x + y - 2) \tag{5.6}$$

we have an onsite interaction with strength γ, for which, if we restrict our attention to symmetric states, is the Bose-Hubbard Hamiltonian with strength $\frac{\gamma}{2}$. Similarly, if $d_{\max} = 0$, $U_0(x, y) = 0$ and $U_1(x, y) = \gamma xy$, we have a nearest-neighbor interaction with strength γ.

5.2 Two-particle scattering on an infinite path

With our chosen interactions, we now have a well defined N-particle quantum walk. However, we have very few analytic solutions to any problems with these Hamiltonians (as this is the purpose of this thesis). As such, we will attempt to understand these Hamiltonians in highly restricted systems, hoping that the results for these smaller systems will allow us to understand the N-particle states.

Since we already have an understanding of single-particle scattering, the next most simple case will be two-particle interactions on an infinite path. Let us assume that the interaction Hamiltonian has been chosen, such that there is a $d_{\max}$ and a set of functions U_d. We can then write the Hamiltonian (5.5) in the basis $|x, y\rangle$, where $x, y \in \mathbb{Z}$ are the positions of the first and second particles, as

$$H^2 = H^1_x \otimes \mathbb{I}_y + \mathbb{I}_x \otimes H^1_y + \sum_{x \in \mathbb{Z}} \sum_{d=0}^{d_{\max}} U_d(\hat{n}_x, \hat{n}_{x+d}), \tag{5.7}$$

where the single-particle Hamiltonian H^1 is simply the adjacency matrix for the infinite path, namely

$$H^1 = \sum_{x \in \mathbb{Z}} |x + 1\rangle\langle x| + |x\rangle\langle x + 1|. \tag{5.8}$$

Without the interaction term, the eigenstates for this Hamiltonian would simply by two independent scattering eigenstates, with amplitudes of the form $e^{ikx+ipy}$. However, the interaction causes there to be correlations between the two particles. These correlations will be similar to the single particle interactions scattering off of a graph with two attached semi-infinite paths.

As we are interested in the dynamics of two particles initially prepared in spatially separated wave packets moving toward each other along the path with momenta $k_1 \in (-\pi, 0)$ and $k_2 \in (0, \pi)$, we will need to understand these scattering eigenstates.

5.2.1 Scattering Eigenstates

Attempting to use the symmetry of these Hamiltonians to our advantage, we will derive scattering eigenstates of this Hamiltonian by transforming to the new variables $s = x + y$ and $r = x - y$. Here the allowed values (s, r) range over the pairs of integers where either

both are even or both are odd. Writing states in this basis as $|s;r\rangle$, the Hamiltonian (5.7) takes the form

$$H_s^{(1)} \otimes H_r^{(1)} + \mathbb{I}_s \otimes \sum_{r\in\mathbb{Z}} \mathcal{V}(|r|)\,|\,r\,\rangle\langle\,r\,|, \tag{5.9}$$

where $V(0) = U_0(2,2)$ and $V(r) = U_r(1,1)$ for $r > 0$. For each $p_1 \in (-\pi,\pi)$ and $p_2 \in (0,\pi)$ there is a scattering eigenstate $|\mathrm{sc}(p_1;p_2)\rangle$ of the form

$$\langle s;r|\mathrm{sc}(p_1;p_2)\rangle = e^{-ip_1 s/2}\langle r|\psi(p_1;p_2)\rangle, \tag{5.10}$$

where the state $|\psi(p_1;p_2)\rangle$ can be viewed as an effective single-particle scattering state of the Hamiltonian

$$2\cos\left(\frac{p_1}{2}\right) H_r^{(1)} + \sum_{r\in\mathbb{Z}} \mathcal{V}(|r|)\,|\,r\,\rangle\langle\,r\,| \tag{5.11}$$

with eigenvalue $4\cos(p_1/2)\cos(p_2)$. For a given $\mathcal{V}$, this is simply a single-particle scattering problem as described in Chapter 3, although the interior graph $\widehat{G}$ might be weighted. As such, we have that the state $|\,\psi(p_1;p_2)\,\rangle$ can be written as

$$\langle r|\psi(p_1;p_2)\rangle = \begin{cases} e^{-ip_2 r} + R(p_1,p_2)e^{ip_2 r} & \text{if } r \le -d_{\max} \\ f(p_1,p_2,r) & \text{if } |r| < d_{\max} \\ T(p_1,p_2)e^{-ip_2 r} & \text{if } r \ge d_{\max} \end{cases} \tag{5.12}$$

for $p_2 \in (0,\pi)$. Here the reflection and transmission coefficients R and T and the amplitudes of the scattering state for $|r| < d_{\max}$ (described by the function f) depend on both momenta as well as the interaction $\mathcal{V}$. With R, T, and f chosen appropriately, the state $|\mathrm{sc}(p_1;p_2)\rangle$ is an eigenstate of $H^{(2)}$ with eigenvalue $4\cos(p_1/2)\cos(p_2)$.

[**TO DO:** *if I want to give a better error bound, I'll need to talk about the dimer states*]

Since $\mathcal{V}(|r|)$ is an even function of r, we can also define scattering states for $p_2 \in (-\pi,0)$ by

$$\langle s;r|\mathrm{sc}(p_1;p_2)\rangle = \langle s;-r|\mathrm{sc}(p_1;-p_2)\rangle. \tag{5.13}$$

These other states are obtained by swapping x and y, corresponding to interchanging the two particles.

[**TO DO:** *double check this*] The construction of the symmetric and anti-symmetric scattering states follows as one would expect. For $p_1 \in (-\pi,\pi)$ and $p_2 \in (0,\pi)$, we define

$$|\,\mathrm{sc}(p_1;p_2)\,\rangle_\pm = \frac{1}{\sqrt{2}}\big(|\,\mathrm{sc}(p_1;p_2)\,\rangle \pm |\,\mathrm{sc}(p_1;-p_2)\,\rangle\big). \tag{5.14}$$

If we note that the unitarity of S and the fact that $V(|r|)$ being even in r forces $R(p_1,p_2) = R(p_1,-p_2)$ and $T(p_1,p_2) = T(p_1,-p_2)$ we can then see that the combinations

$$|T(p_1,p_2) \pm R(p_1,p_2)| = 1. \tag{5.15}$$

With this, we can then see that the symmeterized scattering states can be expanded as

$$\langle\,s;r\,|\,\mathrm{sc}(p_1;p_2)\,\rangle_\pm = \frac{1}{\sqrt{2}}e^{-ip_1 s/2}\begin{cases} e^{ip_2|r|} \pm e^{i\theta_\pm(p_1,p_2)}e^{-ip_2|r|} & \text{if } |r| \ge C \\ f(p_1,p_2,r) \pm f(p_1,p_2,-r) & \text{if } |r| < C \end{cases} \tag{5.16}$$

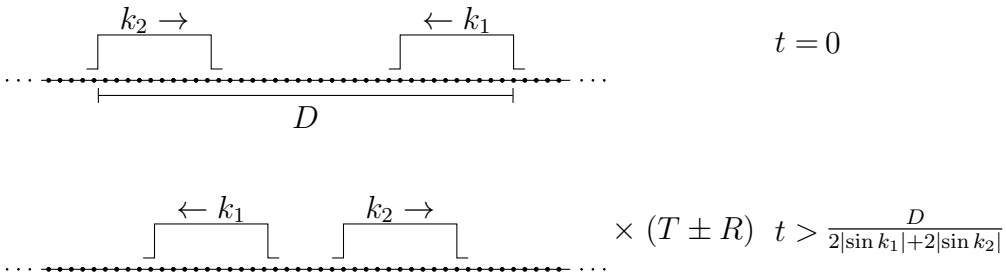

Figure 5.1: Scattering of two particles on an infinite path.

where $\theta_\pm(p_1, p_2)$ is a real function defined through

$$e^{i\theta_\pm(p_1,p_2)} = T(p_1, p_2) \pm R(p_1, p_2). \tag{5.17}$$

These eigenstates allow us to understand what happens when two particles with momenta $k_1 \in (-\pi, 0)$ and $k_2 \in (0, \pi)$ move toward each other. Here $p_1 = -k_1 - k_2$ and $p_2 = (k_2 - k_1)/2$. Similar to the scattering states of Chapter 3, we have that for $|r| \geq C$ the scattering state is a sum of two terms, one corresponding to the two particles moving toward each other and one corresponding to the two particles moving apart after scattering, but where the outgoing term has a phase of $T \pm R$ relative to the incoming term (as depicted in Figure 5.1). This phase arises from the interaction between the two particles.

5.2.2 Examples

[**TO DO:** *I don't like this section here. Find a place to put it*]

For example, consider the Bose-Hubbard model, where $\mathcal{V}(|r|) = U\delta_{r,0}$. Here $C = 0$ and $T = 1 + R$. In this case the scattering state $|\mathrm{sc}(p_1; p_2)\rangle_+$ is

$$\langle x, y|\mathrm{sc}(p_1; p_2)\rangle_+ = \frac{1}{\sqrt{2}} e^{-ip_1\left(\frac{x+y}{2}\right)} \left(e^{ip_2|x-y|} + e^{i\theta_+(p_1,p_2)} e^{-ip_2|x-y|}\right). \tag{5.18}$$

The first term describes the two particles moving toward each other and the second term describes them moving away from each other. To solve for the applied phase $e^{i\theta_+(p_1,p_2)}$ we look at the eigenvalue equation for $|\psi(p_1; p_2)\rangle$ at $r = 0$. This gives

$$R(p_1, p_2) = -\frac{U}{U - 4i\cos(p_1/2)\sin(p_2)}. \tag{5.19}$$

So for the Bose-Hubbard model,

$$e^{i\theta_+(p_1,p_2)} = T(p_1, p_2) + R(p_1, p_2) = -\frac{U + 4i\cos(p_1/2)\sin(p_2)}{U - 4i\cos(p_1/2)\sin(p_2)} = \frac{2\left(\sin(k_2) - \sin(k_1)\right) - iU}{2\left(\sin(k_2) - \sin(k_1)\right) + iU}. \tag{5.20}$$

For example, if $U = 2 + \sqrt{2}$ then two particles with momenta $k_1 = -\pi/2$ and $k_2 = \pi/4$ acquire a phase of $e^{-i\pi/2} = -i$ after scattering.

For a multi-particle quantum walk with nearest-neighbor interactions, $\mathcal{V}(|r|) = U\delta_{|r|,1}$ and $C = 1$. In this case the eigenvalue equations for $|\psi(p_1;p_2)\rangle$ at $r = -1$, $r = 1$, and $r = 0$ are

$$\begin{aligned}
4\cos\left(\frac{p_1}{2}\right)\cos(p_2)(e^{ip_2} + R(p_1,p_2)e^{-ip_2}) &= U(e^{ip_2} + R(p_1,p_2)e^{-ip_2}) \\
&\quad + 2\cos\left(\frac{p_1}{2}\right)\left(e^{2ip_2} + R(p_1,p_2)e^{-2ip_2} + f(p_1,p_2,0)\right) \\
4\cos\left(\frac{p_1}{2}\right)\cos(p_2)T(p_1,p_2)e^{-ip_2} &= UT(p_1,p_2)e^{-ip_2} \\
&\quad + 2\cos\left(\frac{p_1}{2}\right)\left(f(p_1,p_2,0) + T(p_1,p_2)e^{-2ip_2}\right) \\
2\cos(p_2)f(p_1,p_2,0) &= T(p_1,p_2)e^{-ip_2} + e^{ip_2} + R(p_1,p_2)e^{-ip_2},
\end{aligned}$$

respectively.

Solving these equations for R, T, and $f(p_1,p_2,0)$, we can construct the corresponding scattering states for bosons, fermions, or distinguishable particles (for more on the last case, see Section **??**). Unlike the case of the Bose-Hubbard model, we may not have $1 + R = T$. For example, when $U = -2 - \sqrt{2}$, $p_1 = \pi/4$, and $p_2 = 3\pi/8$, we get $R = 0$ and $T = i$ (see Section **??**).

5.2.3 Two-particle basis

[**TO DO:** *Can I bootstrap Andrew and David's basis result to decompose the identity?*]

The states $\{|\mathrm{sc}(p_1;p_2)\rangle : p_1 \in (-\pi,\pi),\ p_2 \in (-\pi,0)\cup(0,\pi)\}$ are (delta-function) orthonormal:

$$\begin{aligned}
\langle \mathrm{sc}(p_1';p_2')|\mathrm{sc}(p_1;p_2)\rangle &= \langle \mathrm{sc}(p_1';p_2')|\left(\sum_{r,\,s\text{ even}} |r\rangle\langle r|\otimes|s\rangle\langle s|\right)|\mathrm{sc}(p_1;p_2)\rangle \\
&\quad + \langle \mathrm{sc}(p_1';p_2')|\left(\sum_{r,\,s\text{ odd}} |r\rangle\langle r|\otimes|s\rangle\langle s|\right)|\mathrm{sc}(p_1;p_2)\rangle \\
&= \sum_{s\text{ even}} e^{-i(p_1-p_1')s/2}\sum_{r\text{ even}}\langle\psi(p_1';p_2')|r\rangle\langle r|\psi(p_1;p_2)\rangle \\
&\quad + \sum_{s\text{ odd}} e^{-i(p_1-p_1')s/2}\sum_{r\text{ odd}}\langle\psi(p_1';p_2')|r\rangle\langle r|\psi(p_1;p_2)\rangle \\
&= 2\pi\delta(p_1-p_1')\sum_{r=-\infty}^{\infty}\langle\psi(p_1;p_2')|r\rangle\langle r|\psi(p_1;p_2)\rangle \\
&= 4\pi^2\delta(p_1-p_1')\delta(p_2-p_2')
\end{aligned}$$

where in the last step we used the fact that $\langle\psi(p_1;p_2')|\psi(p_1;p_2)\rangle = 2\pi\delta(p_2-p_2')$.

5.2.4 Wavepacket Scattering

[**TO DO:** *go over section, ensure correct, and make equations all fit*]

Now that we have a thorough understanding of the two-particle scattering eigenstates on an infinite path, we will want to understand the time-evolution of wavepackets on the infinite path. In particular, if we initially have a product state corresponding to two Guassian wavepackets traveling towards each other, how does the time-evolved state look?

Along those lines, let $k \in (-\pi, \pi)$, and let $\mu \in \mathbb{N}$. We will define a Gaussian wavepacket centered at μ, with momentum k, standard deviation σ, and cutoff L as the state

$$|\chi_{\mu,k}\rangle = \gamma \sum_{x=\mu-L}^{\mu+L} e^{ikx} e^{-\frac{(x-\mu)^2}{2\sigma^2}} |x\rangle, \tag{5.21}$$

where γ^2 is a normalization factor given by $\gamma^{-2} = h_L^{\sigma/\sqrt{2}}(0)$. Note that this is nearly the same state as for single-particle scattering, but now we don't have to deal with the multiple semi-infinite paths and the graph $\widehat{G}$.

This section is focused on proving the following lemma discussing wavepacket propagation:

Theorem 4. *Let $H^{(2)}$ be a two-particle Hamiltonian of the form (??) with interaction range at most C. Let $\theta_\pm(p_1, p_2)$ be given by equation (??). Let $k_1 \in (-\pi, 0)$ and let $k_2 \in (0, \pi)$, let $L, \mu, \nu \in \mathbb{N}$ with $L > 0$ and $\mu < \nu - 2L$, and let $\sigma > 0$. Let us then define the states*

$$|\psi(0)\rangle_\pm = \frac{1}{\sqrt{2}}\big(|\chi_{\mu,k_1}\rangle|\chi_{\nu,k_2}\rangle \pm |\chi_{\nu,k_2}\rangle|\chi_{\mu,k_1}\rangle\big), \tag{5.22}$$

and

$$\begin{aligned} &|\alpha(t)\rangle_\pm \\ &\quad = \frac{e^{-2it(\cos(k_1)+\cos(k_2))}}{\sqrt{2}} e^{i\theta_\pm(t)}\big(|\chi_{\mu(t),k_1}\rangle|\chi_{\nu(t),k_2}\rangle \pm |\chi_{\nu(t),k_2}\rangle|\chi_{\mu(t),k_1}\rangle\big), \end{aligned} \tag{5.23}$$

where

$$\mu(t) = \mu - \lceil 2t \sin k_1 \rceil, \quad \nu(t) = \nu - \lceil 2t \sin k_2 \rceil, \quad \text{and} \quad \theta_\pm(t) = \begin{cases} 0 & t < \frac{\nu-\mu-2L}{2\sin k_2 - 2\sin k_1} \\ \theta_\pm(k_1, k_2) & t > \frac{\nu-\mu+2L}{2\sin k_2 - 2\sin k_1}. \end{cases} \tag{5.24}$$

If $\sigma = \frac{L}{2\sqrt{\log L}}$, and if $0 \leq t < \frac{\nu-\mu-2L}{2\sin k_2 - 2\sin k_1}$ or if $\frac{\nu-\mu+2L}{2\sin k_2 - 2\sin k_1} < t < cL$ for some constant c, then

$$\| e^{-iH^2 t} |\psi(0)\rangle_\pm - |\alpha(t)\rangle\|_\pm \leq \chi_2 \sqrt{\frac{\log L}{L}} \tag{5.25}$$

for some constant χ_2.

Note that we will use many of the tools used in the proof of Theorem 3.

Proof. The main idea behind this proof will be to show that $|\psi(0)\rangle$ and $|\alpha(t)\rangle$ are both well approximated by a Gaussian distribution over eigenstates of $H^{(2)}$ with momenta near k_1 and k_2, and then show that time evolving the Gaussian approximation for $|\psi(0)\rangle$ is well approximated by the Gaussian approximation for $|\alpha(t)\rangle$.

In particular, let us examine the inner product between an eigenstate $|\mathrm{sc}(p_1;p_2)\rangle_\pm$ and $|\alpha(t)\rangle_\pm$. Note that $|\mathrm{sc}(p_1;p_2)\rangle_\pm$ has no overlap with $|\alpha(t)\rangle_\mp$, and

$$\begin{aligned}
&{}_\pm\langle \mathrm{sc}(p_1;p_2)\,|\,\alpha(t)\rangle_\pm \\
&\quad = \frac{e^{-2it(\cos(k_1)+\cos(k_2))+i\theta_\pm(t)}}{\sqrt{2}}\big({}_\pm\langle \mathrm{sc}(p_1;p_2)\,|\,\chi_{\mu(t),k_1},\chi_{\nu(t),k_2}\rangle \pm {}_\pm\langle \mathrm{sc}(p_1;p_2)\,|\,\chi_{\nu(t),k_2},\chi_{\mu(t),k_1}\rangle\big).
\end{aligned} \tag{5.26}$$

We will then want to investigate the overlap between $|\mathrm{sc}(p_1;p_2)\rangle$ and the cut-off Gaussian approximations. In particular, if we assume that $s-r>2L$, then

$$\begin{aligned}
&{}_\pm\langle \mathrm{sc}(p_1;p_2)\,|\,\chi_{r,k_1},\chi_{s,k_2}\rangle \\
&\quad = \gamma^2\sum_{x=r-L}^{r+L}\sum_{y=s-L}^{L} e^{ik_1x}e^{-\frac{(x-r)^2}{2\sigma^2}}e^{ik_2y}e^{-\frac{(y-s)^2}{2\sigma^2}}\langle \mathrm{sc}(p_1;p_2)\,|\,x,y\rangle && (5.27)\\
&\quad = \gamma^2\sum_{x=r-L}^{r+L}\sum_{y=s-L}^{s+L} e^{i(k_1x+k_2y)}e^{-\frac{(x-r)^2+(y-s)^2}{2\sigma^2}}\frac{e^{ip_1\frac{x+y}{2}}}{\sqrt{2}}\left(e^{ip_2|x-y|}\pm e^{-i\theta_\pm(p_1,p_2)-ip_2|x-y|}\right) && (5.28)\\
&\quad = \gamma^2\frac{e^{i(k_1r+k_2s+p_1\frac{r+s}{2}+p_2(s-r))}}{\sqrt{2}}\sum_{x=-L}^{L}\sum_{y=-L}^{L} e^{-\frac{x^2+y^2}{2\sigma^2}}e^{i(k_1+\frac{p_1}{2}-p_2)x}e^{i(k_2+\frac{p_1}{2}+p_2)y} \\
&\qquad + \gamma^2\frac{e^{i(k_1r+k_2s+p_1\frac{r+s}{2}+p_2(r-s)-i\theta_\pm(p_1,p_2))}}{\sqrt{2}}\sum_{x=-L}^{L}\sum_{y=-L}^{L} e^{-\frac{x^2+y^2}{2\sigma^2}}e^{i(k_1+\frac{p_1}{2}+p_2)x}e^{i(k_2+\frac{p_1}{2}-p_2)y} && (5.29)\\
&\quad = \gamma^2\frac{e^{i(k_1+\frac{p_1}{2}-p_2)r+i(k_2+\frac{p_1}{2}+p_2)s}}{\sqrt{2}}h_L^\sigma\left(k_1+\frac{p_1}{2}-p_2\right)h_L^\sigma\left(k_2+\frac{p_1}{2}+p_2\right) \\
&\qquad + \gamma^2\frac{e^{i(k_1+\frac{p_1}{2}+p_2)r+i(k_2+\frac{p_1}{2}-p_2)s-i\theta_\pm(p_1,p_2)}}{\sqrt{2}}h_L^\sigma\left(k_1+\frac{p_1}{2}+p_2\right)h_L^\sigma\left(k_2+\frac{p_1}{2}-p_2\right). && (5.30)
\end{aligned}$$

If $s-r<-2L$, then nearly the same argument holds, and we find

$$\begin{aligned}
&{}_\pm\langle \mathrm{sc}(p_1;p_2)\,|\,\chi_{r,k_1},\chi_{s,k_2}\rangle \\
&\quad = \gamma^2\frac{e^{i(k_1+\frac{p_1}{2}+p_2)r+i(k_2+\frac{p_1}{2}-p_2)s}}{\sqrt{2}}h_L^\sigma\left(k_1+\frac{p_1}{2}+p_2\right)h_L^\sigma\left(k_2+\frac{p_1}{2}-p_2\right) \\
&\qquad + \gamma^2\frac{e^{i(k_1+\frac{p_1}{2}-p_2)r+i(k_2+\frac{p_1}{2}+p_2)s-i\theta_\pm(p_1,p_2)}}{\sqrt{2}}h_L^\sigma\left(k_1+\frac{p_1}{2}-p_2\right)h_L^\sigma\left(k_2+\frac{p_1}{2}+p_2\right).
\end{aligned} \tag{5.31}$$

Putting these bounds together, if we define $p_1 = -(k_1 + k_2)$ and $2p_2 = k_1 - k_2$, we find that for $t < \frac{\nu-\mu-2L}{2\sin k_2 - 2\sin k_1}$

$$
\begin{aligned}
&{}_{\pm}\langle \mathrm{sc}(p_1+\phi_1; p_2+\phi_2) \,|\, \alpha(t)\rangle_{\pm} \\
&\quad = \gamma^2 e^{-2it(\cos(k_1)+\cos(k_2))} e^{i\phi_1 \frac{\mu(t)+\nu(t)}{2}} \Bigg[e^{i\phi_2(\nu(t)-\mu(t))} h_L^{\sigma}\left(\frac{\phi_1}{2} - \phi_2\right) h_L^{\sigma}\left(\frac{\phi_1}{2} + \phi_2\right) \\
&\qquad \pm e^{i(2p_2+\phi_2)(\mu(t)-\nu(t)) - i\theta_{\pm}(p_1+\phi_1, p_2+\phi_2)} h_L^{\sigma}\left(\frac{\phi_1}{2} - 2p_2 - \phi_2\right) h_L^{\sigma}\left(\frac{\phi_1}{2} + 2p_2 + \phi_2\right) \Bigg].
\end{aligned} \tag{5.32}
$$

In nearly the same manner, if $t > \frac{\nu-\mu+2L}{2\sin k_2 - 2\sin k_1}$, we have

$$
\begin{aligned}
&{}_{\pm}\langle \mathrm{sc}(p_1+\phi_1; p_2+\phi_2) \,|\, \alpha(t)\rangle_{\pm} \\
&\quad = \gamma^2 e^{-2it(\cos(k_1)+\cos(k_2)) + i\theta_{\pm}(p_1,p_2)} e^{i\phi_1 \frac{\mu(t)+\nu(t)}{2}} \Bigg[e^{i\phi_2(\nu(t)-\mu(t)) - i\theta_{\pm}(p_1+\phi_1, p_2+\phi_2)} h_L^{\sigma}\left(\frac{\phi_1}{2} - \phi_2\right) h_L^{\sigma}\left(\frac{\phi_1}{2} + \phi_2\right) \\
&\qquad \pm e^{i(2p_2+\phi_2)(\mu(t)-\nu(t))} h_L^{\sigma}\left(\frac{\phi_1}{2} - 2p_2 - \phi_2\right) h_L^{\sigma}\left(\frac{\phi_1}{2} + 2p_2 + \phi_2\right) \Bigg].
\end{aligned} \tag{5.33}
$$

With these useful inner products, we can now define our Gaussian approximations. In particular, we will define the states

$$
|\, w(t)\rangle = \eta e^{-2it(\cos k_1 + \cos k_2)} \int_{-\delta}^{\delta}\int_{-\delta}^{\delta} \frac{d\phi_1 d\phi_2}{4\pi^2} e^{i\phi_1\left(\frac{\mu(t)+\nu(t)}{2}\right)} e^{i\phi_2(\nu(t)-\mu(t))} e^{-\frac{\sigma^2\phi_1^2}{4}} e^{-\sigma^2\phi_2^2} |\, \mathrm{sc}(p_1+\phi_1; p_2+\phi_2)\rangle_{\pm} \tag{5.34}
$$

where

$$
\eta^{-2} = \int_{-\infty}^{\infty}\int_{-\infty}^{\infty} \frac{d\phi_1 d\phi_2}{4\pi^2} e^{-\sigma^2\left(\frac{\phi_1^2}{2} + 2\phi_2^2\right)} = \frac{1}{4\pi\sigma^2}. \tag{5.35}
$$

While the states $|\, w(t)\rangle$ are not exactly normalized, we have that

$$
\langle\, w(t) \,|\, w(t)\rangle = \eta^2 \int_{-\delta}^{\delta}\int_{-\delta}^{\delta} \frac{d\phi_1 d\phi_2}{4\pi^2} e^{-\sigma^2\left(\frac{\phi_1^2}{2} + 2\phi_2^2\right)} \quad = 1 - \frac{\eta^2}{\pi^2}\int_{\delta}^{\infty}\int_{\delta}^{\infty} d\phi_1 d\phi_2 e^{-\sigma^2\left(\frac{\phi_1^2}{2} + 2\phi_2^2\right)} \tag{5.36}
$$

$$
\geq 1 - \frac{1}{\pi\delta^2\sigma^2} e^{-\frac{5\sigma^2\delta^2}{2}}, \tag{5.37}
$$

and as the second term on the right hand side is non-negative, we have that $\langle\, w(t) \,|\, w(t)\rangle \leq 1$.

As in the single-particle case, we will want to show that the overlap between $|\, w\rangle$ and

$|\alpha(t)\rangle_\pm$ is nearly 1. In particular, for $0 \le t < \frac{\nu(t)-\mu(t)-2L}{2\sin k_2 - 2\sin k_1}$, we then have that

$$\begin{aligned}
&\langle w(t)\,|\,\alpha(t)\rangle_\pm \\
&\quad= \eta\gamma^2 \int_{-\delta}^{\delta}\int_{-\delta}^{\delta} \frac{d\phi_1 d\phi_2}{4\pi^2} e^{-\frac{\sigma^2\phi_1^2}{4}} e^{-\sigma^2\phi_2^2} \Big[h_L^\sigma\big(\frac{\phi_1}{2}-\phi_2\big) h_L^\sigma\Big(\frac{\phi_1}{2}+\phi_2\Big) \\
&\qquad \pm e^{i\theta_\pm(p_1+\phi_1,p_2+\phi_2)} e^{2i(p_2+\phi_2)(\mu(t)-\nu(t))} h_L^\sigma\Big(\frac{\phi_1}{2}-2p_2-\phi_2\Big) h_L^\sigma\Big(\frac{\phi_1}{2}+2p_2+\phi_2\Big)\Big] \qquad (5.38)\\
&\quad= \eta\gamma^2 \int_{-\delta}^{\delta}\int_{-\delta}^{\delta} \frac{d\phi_1 d\phi_2}{4\pi^2} e^{-\frac{\sigma^2\phi_1^2}{4}} e^{-\sigma^2\phi_2^2} \Bigg[h_\infty^\sigma(\frac{\phi_1}{2}-\phi_2) h_\infty^\sigma(\frac{\phi_1}{2}+\phi_2) \\
&\qquad + \Big[h_L^\sigma\Big(\frac{\phi_1}{2}+\phi_2\Big) + h_\infty^\sigma\Big(\frac{\phi_1}{2}+\phi_2\Big)\Big]\Big[h_L^\sigma\Big(\frac{\phi_1}{2}-\phi_2\Big) - h_\infty^\sigma\Big(\frac{\phi_1}{2}-\phi_2\Big)\Big] \\
&\qquad \pm e^{i\theta_\pm(p_1+\phi_1,p_2+\phi_2)} e^{2i(p_2+\phi_2)(\mu(t)-\nu(t))} \Big[h_L^\sigma\Big(\frac{\phi_1}{2}+2p_2+\phi_2\Big) + h_\infty^\sigma\Big(\frac{\phi_1}{2}+2p_2+\phi_2\Big)\Big] \\
&\qquad\quad \times \Big[h_L^\sigma\Big(\frac{\phi_1}{2}-2p_2-\phi_2\Big) - h_\infty^\sigma\Big(\frac{\phi_1}{2}-2p_2-\phi_2\Big)\Big] \\
&\qquad \pm e^{i\theta_\pm(p_1+\phi_1,p_2+\phi_2)} e^{2i(p_2+\phi_2)(\mu(t)-\nu(t))} h_\infty^\sigma\Big(\frac{\phi_1}{2}+2p_2+\phi_2\Big) h_\infty^\sigma\Big(\frac{\phi_1}{2}-2p_2-\phi_2\Big)\Bigg]. \qquad (5.39)
\end{aligned}$$

While this expression looks rather complicated, most of the amplitude is a result of the first term in the integrand, and the rest of the terms are simply small error terms resulting from approximating h_L^σ by h_∞^σ or cross terms between the pre- and post-scattering amplitudes. As such, we will bound each term individually, giving upper and lower bounds on the first term, and only upper bounds on the norm of the latter terms.

For the first term, we have

$$\begin{aligned}
&\int_{-\delta}^{\delta}\int_{-\delta}^{\delta} \frac{d\phi_1 d\phi_2}{4\pi^2} e^{-\frac{\sigma^2\phi_1^2}{4}-\sigma^2\phi_2^2} h_\infty^\sigma\Big(\frac{\phi_1}{2}-\phi_2\Big) h_\infty^\sigma\Big(\frac{\phi_1}{2}+\phi_2\Big) \\
&\quad= \frac{\sigma^2}{2\pi}\int_{-\delta}^{\delta}\int_{-\delta}^{\delta} d\phi_1 d\phi_2 e^{-\frac{\sigma^2\phi_1^2}{2}-2\sigma^2\phi_2^2} h_\infty^{1/(2\pi\sigma)}\Big[2\pi i\sigma^2\Big(\frac{\phi_1}{2}-\phi_2\Big)\Big] h_\infty^{1/(2\pi\sigma)}\Big[2\pi i\sigma^2\Big(\frac{\phi_1}{2}+\phi_2\Big)\Big] \qquad (5.40)\\
&\quad\ge \frac{\sigma^2}{2\pi}\int_{-\delta}^{\delta}\int_{-\delta}^{\delta} d\phi_1 d\phi_2 e^{-\frac{\sigma^2\phi_1^2}{2}-2\sigma^2\phi_2^2} \qquad (5.41)\\
&\quad= \frac{1}{2}\langle w(t)\,|\,w(t)\rangle \qquad (5.42)
\end{aligned}$$

where we used the fact that $h^\sigma_\infty(i\phi) \geq 1$. Using the upper bounds on h, we also have that

$$\begin{aligned}
&\int_{-\delta}^{\delta}\int_{-\delta}^{\delta} \frac{d\phi_1 d\phi_2}{4\pi^2} e^{-\frac{\sigma^2\phi_1^2}{4}-\sigma^2\phi_2^2} h^\sigma_\infty\Big(\frac{\phi_1}{2}-\phi_2\Big) h^\sigma_\infty\Big(\frac{\phi_1}{2}+\phi_2\Big) \\
&\quad \leq \frac{\sigma^2}{2\pi}\int_{-\delta}^{\delta}\int_{-\delta}^{\delta} d\phi_1 d\phi_2 e^{-\frac{\sigma^2\phi_1^2}{2}-2\sigma^2\phi_2^2}\left[1+2\Big(1+\frac{1}{\pi\sigma^2}\frac{1}{4\pi-|\phi_1-2\phi_2|}\Big)e^{-2\pi^2\sigma^2+\pi\sigma^2(\phi_1-2\phi_2)}\right] \\
&\qquad \times\left[1+2\Big(1+\frac{1}{\pi\sigma^2}\frac{1}{4\pi-|\phi_1+2\phi_2|}\Big)e^{-2\pi^2\sigma^2+\pi\sigma^2(\phi_1+2\phi_2)}\right] \qquad (5.43)\\
&\quad \leq \frac{1}{2}\Big[1+3e^{-\pi^2\sigma^2\left(2\pi-3\delta\right)}\Big]^2 \langle\, w(t)\,|\,w(t)\,\rangle \qquad (5.44)
\end{aligned}$$

where we assumed that $2\pi > 3\delta$, and that $\sigma \geq 1$.

For the second term, note that for any φ_1, φ_2, and for any $L > \sigma \geq 1$, we have that

$$\begin{aligned}
&\big|\big(h^\sigma_L(\varphi_1)+h^\sigma_\infty(\varphi_1)\big)\big(h^\sigma_L(\varphi_2)-h^\sigma_\infty(\varphi_2)\big)\big| \\
&\qquad \leq \big|h^\sigma_L(\varphi_1)+h^\sigma_\infty(\varphi_1)\big|\frac{2\sigma^2}{L}e^{-\frac{L^2}{2\sigma^2}} \qquad (5.45)\\
&\qquad \leq \frac{2\sigma^2}{L}e^{-\frac{L^2}{2\sigma^2}}\Big[2+\big|h^\sigma_L(\varphi_2)-h^\sigma_\infty(\varphi_2)\big|+2\big|1-h^\sigma_\infty(\varphi_2)\big|\Big] \qquad (5.46)\\
&\qquad \leq \frac{2\sigma^2}{L}e^{-\frac{L^2}{2\sigma^2}}\Big[2+\frac{2\sigma^2}{L}e^{-\frac{L^2}{2\sigma^2}}+4(1+\sigma^2)e^{-\frac{1}{2\sigma^2}}\Big] \qquad (5.47)\\
&\qquad \leq \frac{24\sigma^4}{L}e^{-\frac{L^2}{2\sigma^2}}. \qquad (5.48)
\end{aligned}$$

If we then use this bound for the integrand, we have

$$\begin{aligned}
&\left|\int_{-\delta}^{\delta}\int_{-\delta}^{\delta}\frac{d\phi_1 d\phi_2}{4\pi^2}e^{-\frac{\sigma^2\phi_1^2}{4}}e^{-\sigma^2\phi_2^2}\Big[h^\sigma_L\Big(\frac{\phi_1}{2}+\phi_2\Big)+h^\sigma_\infty\Big(\frac{\phi_1}{2}+\phi_2\Big)\Big]\Big[h^\sigma_L\Big(\frac{\phi_1}{2}-\phi_2\Big)-h^\sigma_\infty\Big(\frac{\phi_1}{2}-\phi_2\Big)\Big]\right| \\
&\quad \leq \int_{-\delta}^{\delta}\int_{-\delta}^{\delta}\frac{d\phi_1 d\phi_2}{4\pi^2}e^{-\frac{\sigma^2\phi_1^2}{4}}e^{-\sigma^2\phi_2^2}\frac{24\sigma^4}{L}e^{-\frac{L^2}{2\sigma^2}} \qquad (5.49)\\
&\quad \leq \frac{6\sigma^4}{\pi^2 L}e^{-\frac{L^2}{2\sigma^2}}\int_{-\infty}^{\infty}\int_{-\infty}^{\infty}d\phi_1 d\phi_2 e^{-\frac{\sigma^2\phi_1^2}{4}}e^{-\sigma^2\phi_2^2} \qquad (5.50)\\
&\quad = \frac{12\sigma^2}{\pi L}e^{-\frac{L^2}{2\sigma^2}}. \qquad (5.51)
\end{aligned}$$

For the third term, we can use the same argument, and we have

$$\begin{aligned}
&\Bigg|\int_{-\delta}^{\delta}\int_{-\delta}^{\delta}\frac{d\phi_1 d\phi_2}{4\pi^2}e^{-\frac{\sigma^2\phi_1^2}{4}}e^{-\sigma^2\phi_2^2}e^{i\theta_\pm(p_1+\phi_1,p_2+\phi_2)}e^{2i(p_2+\phi_2)(\mu(t)-\nu(t))} \\
&\qquad \times\Big[h^\sigma_L\Big(\frac{\phi_1}{2}+2p_2+\phi_2\Big)+h^\sigma_\infty\Big(\frac{\phi_1}{2}+2p_2+\phi_2\Big)\Big] \\
&\qquad \times\Big[h^\sigma_L\Big(\frac{\phi_1}{2}-2p_2-\phi_2\Big)-h^\sigma_\infty\Big(\frac{\phi_1}{2}-2p_2-\phi_2\Big)\Big]\Bigg| \\
&\qquad\quad \leq \int_{-\delta}^{\delta}\frac{d\phi_1 d\phi_2}{4\pi^2}e^{-\frac{\sigma^2\phi_1^2}{4}}e^{-\sigma^2\phi_2^2}\frac{24\sigma^4}{L}e^{-\frac{L^2}{2\sigma^2}} \leq \frac{12\sigma^2}{\pi L}e^{-\frac{L^2}{2\sigma^2}}. \qquad (5.52)
\end{aligned}$$

For the fourth term, we instead need to use the fact that $h(\phi)$ rapidly decreases for large ϕ. In particular, if we assume that $\sigma^{-1} < 2\pi - |k_1| - |k_2|$, we have

$$\begin{aligned}
&\left| \int_{-\delta}^{\delta}\int_{-\delta}^{\delta} \frac{d\phi_1 d\phi_2}{4\pi^2} e^{-\frac{\sigma^2\phi_1^2}{4}} e^{-\sigma^2\phi_2^2} e^{i\theta_\pm(p_1+\phi_1,p_2+\phi_2)} e^{2i(p_2+\phi_2)(\mu(t)-\nu(t))} h_\infty^\sigma\Big(\frac{\phi_1}{2}+2p_2+\phi_2\Big) h_\infty^\sigma\Big(\frac{\phi_1}{2}-2p_2-\phi_2\Big)\right| \\
&\quad \le \int_{-\delta}^{\delta}\int_{-\delta}^{\delta} \frac{d\phi_1 d\phi_2}{4\pi^2} e^{-\frac{\sigma^2\phi_1^2}{4}} e^{-\sigma^2\phi_2^2} h_\infty^\sigma\Big(\frac{\phi_1}{2}+2p_2+\phi_2\Big) h_\infty^\sigma\Big(\frac{\phi_1}{2}-2p_2-\phi_2\Big) \qquad (5.53) \\
&\quad = \frac{\sigma^2}{2\pi}\int_{-\delta}^{\delta}\int_{-\delta}^{\delta} d\phi_1 d\phi_2 e^{-\sigma^2\phi_1^2} e^{-\sigma^2(\phi_2^2+(2p_2+\phi_2)^2)} \\
&\qquad\qquad \times h_\infty^{1/(2\pi\sigma)}\Big[2\pi i\sigma^2\Big(\frac{\phi_1}{2}+2p_2+\phi_2\Big)\Big] h_\infty^{1/(2\pi\sigma)}\Big[2\pi i\sigma^2\Big(\frac{\phi_1}{2}-2p_2-\phi_2\Big)\Big] \qquad (5.54) \\
&\le \frac{\sigma^2}{2\pi}\int_{-\delta}^{\delta}\int_{-\delta}^{\delta} d\phi_1 d\phi_2 e^{-\sigma^2\phi_1^2} e^{-\sigma^2(\phi_2^2+(2p_2+\phi_2)^2)} \big(1+3e^{-2\pi\sigma^2(\pi-|2p_2+\phi_2-\frac{\phi_1}{2}|)}\big)\big(1+3e^{-2\pi\sigma^2(\pi-|2p_2+\phi_2+\frac{\phi_1}{2}|)}\big) \\
&\qquad\qquad (5.55)
\end{aligned}$$

At this point, if $\pi > |k_1| + |k_2|$, we can choose δ so that $\pi > |k_1| + |k_2| + 2\delta$ and thus

$$\begin{aligned}
&\left| \int_{-\delta}^{\delta}\int_{-\delta}^{\delta} \frac{d\phi_1 d\phi_2}{4\pi^2} e^{-\frac{\sigma^2\phi_1^2}{4}} e^{-\sigma^2\phi_2^2} e^{i\theta_\pm(p_1+\phi_1,p_2+\phi_2)} e^{2i(p_2+\phi_2)(\mu(t)-\nu(t))} h_\infty^\sigma\Big(\frac{\phi_1}{2}+2p_2+\phi_2\Big) h_\infty^\sigma\Big(\frac{\phi_1}{2}-2p_2-\phi_2\Big)\right| \\
&\quad \le \frac{8\sigma^2}{\pi}\int_{-\delta}^{\delta}\int_{-\delta}^{\delta} d\phi_1 d\phi_2 e^{-\sigma^2\phi_1^2} e^{-\sigma^2(\phi_2^2+(2p_2+\phi_2)^2)} \qquad (5.56) \\
&\quad \le \frac{8\sigma}{\sqrt{\pi}}\int_{-\delta}^{\delta} d\phi_2 e^{-2\sigma^2(p_2^2+(p_2+\phi_2)^2)} \qquad (5.57) \\
&\quad \le 4\sqrt{2}e^{-2\sigma^2 p_2^2} = 4\sqrt{2}e^{-\frac{\sigma^2}{2}(k_2-k_1)^2}. \qquad (5.58)
\end{aligned}$$

However, if $\pi \le |k_1| + |k_2|$, we can instead bound the functions approximating h by their largest value, which is attained when $2\phi_2 \pm \phi_1 = 3\delta$. In particular, we have

$$\begin{aligned}
&\left| \int_{-\delta}^{\delta}\int_{-\delta}^{\delta} \frac{d\phi_1 d\phi_2}{4\pi^2} e^{-\frac{\sigma^2\phi_1^2}{4}} e^{-\sigma^2\phi_2^2} e^{i\theta_\pm(p_1+\phi_1,p_2+\phi_2)} e^{2i(p_2+\phi_2)(\mu(t)-\nu(t))} h_\infty^\sigma\Big(\frac{\phi_1}{2}+2p_2+\phi_2\Big) h_\infty^\sigma\Big(\frac{\phi_1}{2}-2p_2-\phi_2\Big)\right| \\
&\quad \le \frac{8\sigma^2}{\pi}\int_{-\delta}^{\delta}\int_{-\delta}^{\delta} d\phi_1 d\phi_2 e^{-\sigma^2\phi_1^2} e^{-\sigma^2(\phi_2^2+(2p_2+\phi_2)^2)} e^{4\pi\sigma^2(2|p_2|+\frac{3\delta}{2}-\pi)} \qquad (5.59) \\
&\quad \le \frac{8\sigma}{\sqrt{\pi}} e^{4\pi\sigma^2(2|p_2|+\frac{3}{2}\delta-\pi)-2\sigma^2 p_2^2}\int_{-\delta}^{\delta} d\phi_2 e^{-2\sigma^2(p_2+2p_2\phi_2+\phi_2^2)} \qquad (5.60) \\
&\quad \le \frac{16\delta}{\sqrt{\pi}} e^{-\sigma^2(4\pi^2-8\pi|p_2|+4\sigma^2 p_2^2-6\pi\delta+2\delta^2-4\delta|p_2|)} \qquad (5.61) \\
&\quad \le \frac{16\delta}{\sqrt{\pi}} e^{-\sigma^2(4[\pi-|p_2|]^2-(4|p_2|+6\pi)\delta)} \qquad (5.62) \\
&\quad \le \frac{16\delta}{\sqrt{\pi}} e^{-3\sigma^2\delta} \qquad (5.63)
\end{aligned}$$

where we assume that $\delta < \frac{(\pi-|p_2|)^2}{4|p_2|+6\pi}$. We can then put these two bounds together, if we assume that $\delta < p_2^2$ and that $\delta < \frac{(\pi-|p_2|)^2}{4|p_2|+6\pi}$, so that

$$\left| \int_{-\delta}^{\delta}\int_{-\delta}^{\delta} \frac{d\phi_1 d\phi_2}{4\pi^2} e^{-\frac{\sigma^2\phi_1^2}{4}} e^{-\sigma^2\phi_2^2} e^{i\theta_\pm(p_1+\phi_1,p_2+\phi_2)} e^{2i(p_2+\phi_2)(\mu(t)-\nu(t))} h_\infty^\sigma\Big(\frac{\phi_1}{2}+2p_2+\phi_2\Big) h_\infty^\sigma\Big(\frac{\phi_1}{2}-2p_2-\phi_2\Big)\right| \leq \frac{16}{\sqrt{\pi}} e^{-2\sigma^2\delta}. \tag{5.64}$$

We can now combine these results, and thus show that $|\,\alpha(t)\,\rangle_\pm$ is well approximated by $|\,w(t)\,\rangle$ for $0 \leq t < \frac{\nu(t)-\mu(t)-2L}{2\sin k_2 - 2\sin k_1}$. In particular, we have

$$\begin{aligned}
&\big\| |\,\alpha(t)\,\rangle_\pm - |\,w(t)\,\rangle \big\|^2 \\
&\quad \leq {}_\pm\langle \alpha(t)\,|\,\alpha(t)\,\rangle_\pm + \langle\, w(t)\,|\,w(t)\,\rangle - \langle\, w(t)\,|\,\alpha(t)\,\rangle_\pm - {}_\pm\langle \alpha(t)\,|\,w(t)\,\rangle && (5.65)\\
&\quad \leq 1 + \langle\, w(t)\,|\,w(t)\,\rangle - 2\eta\gamma^2\Big(\frac{1}{2}\langle\, w(t)\,|\,w(t)\,\rangle - \frac{12\sigma^2}{\pi L} e^{-\frac{L^2}{2\sigma^2}} - \frac{12\sigma^2}{\pi L} e^{-\frac{L^2}{2\sigma^2}} - \frac{16}{\sqrt{\pi}} e^{-2\sigma^2\delta}\Big). && (5.66)
\end{aligned}$$

For large enough σ, L, and small enough δ, we have that the term multiplying $\eta\gamma$ is negative, and thus we need to give a lower bound on $\eta\gamma^2$. We know the value of η, and as a lower bound on γ^2 we have

$$\gamma^2 = \frac{1}{h_L^{\sigma/\sqrt{2}}(0)} \geq \frac{1}{\sqrt{\pi}\sigma(1+3e^{-\pi^2\sigma^2})} \geq \frac{1}{\sqrt{\pi}\sigma}\big(1-3e^{-\pi^2\sigma^2}\big). \tag{5.67}$$

From this, and using our upper bounds on the norm of $\langle\, w(t)\,|\,w(t)\,\rangle$, we have

$$\begin{aligned}
&\big\| |\,\alpha(t)\,\rangle_\pm - |\,w(t)\,\rangle \big\|^2 \\
&\quad \leq 1 + \langle\, w(t)\,|\,w(t)\,\rangle - 4\big(1-3e^{-\pi^2\sigma^2}\big)\Big(\frac{1}{2}\langle\, w(t)\,|\,w(t)\,\rangle - \frac{24\sigma^2}{\pi L} e^{-\frac{L^2}{2\sigma^2}} - \frac{16}{\sqrt{\pi}} e^{-2\sigma^2\delta}\Big) && (5.68)\\
&\quad \leq 1 - \langle\, w(t)\,|\,w(t)\,\rangle(1-6e^{-\pi^2\sigma^2}) + \frac{96\sigma^2}{\pi L} e^{-\frac{L^2}{2\sigma^2}} + \frac{64}{\sqrt{\pi}} e^{-2\sigma^2\delta} && (5.69)\\
&\quad \leq 1 - \Big(1 - \frac{1}{\pi\delta^2\sigma^2} e^{-\frac{5\sigma^2\delta^2}{2}}\Big)(1-6e^{-\pi^2\sigma^2}) + \frac{96\sigma^2}{\pi L} e^{-\frac{L^2}{2\sigma^2}} + \frac{64}{\sqrt{\pi}} e^{-2\sigma^2\delta} && (5.70)\\
&\quad \leq \frac{1}{\pi\delta^2\sigma^2} e^{-\frac{5\sigma^2\delta^2}{2}} + 6e^{-\pi^2\sigma^2} + \frac{96\sigma^2}{\pi L} e^{-\frac{L^2}{2\sigma^2}} + \frac{64}{\sqrt{\pi}} e^{-2\sigma^2\delta} && (5.71)\\
&\quad \leq 44 e^{-2\sigma^2\delta} + \frac{32\sigma^2}{L} e^{-\frac{L^2}{2\sigma^2}}. && (5.72)
\end{aligned}$$

Let us now examine how close $|\,w(t)\,\rangle$ and $|\,\alpha(t)\,\rangle_\pm$ are for $t > \frac{\nu(t)-\mu(t)+2L}{2\sin k_2 - 2\sin k_1}$. In particular,

we have for these times that

$$
\begin{aligned}
&\langle w(t)\,|\,\alpha(t)\rangle_{\pm} \\
&\quad = \eta\gamma^2 e^{i\theta_{\pm}(p_1,p_2)} \int_{-\delta}^{\delta}\int_{-\delta}^{\delta} \frac{d\phi_1 d\phi_2}{4\pi^2} e^{-\frac{\sigma^2\phi_1^2}{4}} e^{-\sigma^2\phi_2^2} \Big[e^{-i\theta_{\pm}(p_1+\phi_1,p_2+\phi_2)} h_L^{\sigma}\Big(\frac{\phi_1}{2}-\phi_2\Big) h_L^{\sigma}\Big(\frac{\phi_1}{2}+\phi_2\Big) \\
&\qquad \pm e^{2i(p_2+\phi_2)(\mu(t)-\nu(t))} h_L^{\sigma}\Big(\frac{\phi_1}{2}-2p_2-\phi_2\Big) h_L^{\sigma}\Big(\frac{\phi_1}{2}+2p_2+\phi_2\Big)\Big] \qquad (5.73) \\
&\quad = \eta\gamma^2 e^{i\theta_{\pm}(p_1,p_2)} \int_{-\delta}^{\delta}\int_{-\delta}^{\delta} \frac{d\phi_1 d\phi_2}{4\pi^2} e^{-\frac{\sigma^2\phi_1^2}{4}} e^{-\sigma^2\phi_2^2} \Bigg[e^{-i\theta_{\pm}(p_1,p_2)} h_{\infty}^{\sigma}(\frac{\phi_1}{2}-\phi_2) h_{\infty}^{\sigma}(\frac{\phi_1}{2}+\phi_2) \\
&\qquad \Big(e^{-i\theta_{\pm}(p_1+\phi_1,p_2+\phi_2)} - e^{-i\theta_{\pm}(p_1,p_2)}\Big) h_{\infty}^{\sigma}(\frac{\phi_1}{2}-\phi_2) h_{\infty}^{\sigma}(\frac{\phi_1}{2}+\phi_2) \\
&\qquad + e^{-i\theta_{\pm}(p_1+\phi_1,p_2+\phi_2)} \Big[h_L^{\sigma}\Big(\frac{\phi_1}{2}+\phi_2\Big) + h_{\infty}^{\sigma}\Big(\frac{\phi_1}{2}+\phi_2\Big)\Big]\Big[h_L^{\sigma}\Big(\frac{\phi_1}{2}-\phi_2\Big) - h_{\infty}^{\sigma}\Big(\frac{\phi_1}{2}-\phi_2\Big)\Big] \\
&\qquad \pm e^{2i(p_2+\phi_2)(\mu(t)-\nu(t))} \Big[h_L^{\sigma}\Big(\frac{\phi_1}{2}+2p_2+\phi_2\Big) + h_{\infty}^{\sigma}\Big(\frac{\phi_1}{2}+2p_2+\phi_2\Big)\Big] \\
&\qquad\quad \times \Big[h_L^{\sigma}\Big(\frac{\phi_1}{2}-2p_2-\phi_2\Big) - h_{\infty}^{\sigma}\Big(\frac{\phi_1}{2}-2p_2-\phi_2\Big)\Big] \\
&\qquad \pm e^{2i(p_2+\phi_2)(\mu(t)-\nu(t))} h_{\infty}^{\sigma}\Big(\frac{\phi_1}{2}+2p_2+\phi_2\Big) h_{\infty}^{\sigma}\Big(\frac{\phi_1}{2}-2p_2-\phi_2\Big)\Bigg]. \qquad (5.74)
\end{aligned}
$$

This is nearly an identical overlap as for the small t case, except for the changing angle $\theta_{\pm}$. As such, we can bound most of the terms as before.

The first term in the bound is simply

$$
\begin{aligned}
&e^{i\theta_{\pm}(p_1,p_2)} \int_{-\delta}^{\delta}\int_{-\delta}^{\delta} \frac{d\phi_1 d\phi_2}{4\pi^2} e^{-\frac{\sigma^2\phi_1^2}{4}} e^{-\sigma^2\phi_2^2} e^{-i\theta_{\pm}(p_1,p_2)} h_{\infty}^{\sigma}(\frac{\phi_1}{2}-\phi_2) h_{\infty}^{\sigma}(\frac{\phi_1}{2}+\phi_2) \qquad (5.75) \\
&\quad = \int_{-\delta}^{\delta}\int_{-\delta}^{\delta} \frac{d\phi_1 d\phi_2}{4\pi^2} e^{-\frac{\sigma^2\phi_1^2}{4}} e^{-\sigma^2\phi_2^2} h_{\infty}^{\sigma}(\frac{\phi_1}{2}-\phi_2) h_{\infty}^{\sigma}(\frac{\phi_1}{2}+\phi_2) \qquad (5.76) \\
&\quad \geq \frac{1}{2}\langle w(t)\,|\,w(t)\rangle \qquad (5.77)
\end{aligned}
$$

as in the small t case.

The second term is slightly more complicated. However, remember from equation ?????? [**TO DO:** *find the correct equation*] that $\theta_{\pm}(p_1+\phi_1, p_2+\phi_2)$ are bounded rational functions of $e^{i\phi_1}$ and $e^{i\phi_2}$. As such, they are differentiable as functions of both ϕ_1 and ϕ_2 on some neighborhood U of $(0,0)$. Let us assume that δ is chosen so that $[-\delta,\delta]\times[-\delta,\delta] \subset U$, and now let

$$
\Gamma = \max_{[-\delta,\delta]\times[-\delta,\delta]} \Big|\nabla e^{i\theta_{\pm}(p_1+\phi_1,p_2+\phi_2)}\Big| \qquad (5.78)
$$

From this, we then have that

$$\left| \int_{-\delta}^{\delta}\int_{-\delta}^{\delta} \frac{d\phi_1 d\phi_2}{4\pi^2} e^{-\frac{\sigma^2\phi_1^2}{4}} e^{-\sigma^2\phi_2^2} \big(e^{-i\theta_\pm(p_1+\phi_1,p_2+\phi_2)} - e^{-i\theta_\pm(p_1,p_2)}\big) h_\infty^\sigma(\frac{\phi_1}{2}-\phi_2) h_\infty^\sigma(\frac{\phi_1}{2}+\phi_2) \right|$$

$$\leq \int_{-\delta}^{\delta}\int_{-\delta}^{\delta} \frac{d\phi_1 d\phi_2}{4\pi^2} e^{-\frac{\sigma^2\phi_1^2}{4}} e^{-\sigma^2\phi_2^2} \big(\phi_1^2+\phi_2^2\big)\Gamma h_\infty^\sigma(\frac{\phi_1}{2}-\phi_2) h_\infty^\sigma(\frac{\phi_1}{2}+\phi_2) \tag{5.79}$$

$$= \frac{\Gamma\sigma^2}{2\pi} \int_{-\delta}^{\delta}\int_{-\delta}^{\delta} d\phi_1 d\phi_2 e^{-\frac{\sigma^2\phi_1^2}{2}} e^{-2\sigma^2\phi_2^2} (\phi_1^2+\phi_2^2) h_\infty^{1/(2\pi\sigma)}\Big(2\pi i\sigma^2\Big[\frac{\phi_1}{2}-\phi_2\Big]\Big) h_\infty^{1/(2\pi\sigma)}\Big(2\pi i\sigma^2\Big[\frac{\phi_1}{2}+\phi_2\Big]\Big) \tag{5.80}$$

$$\leq \frac{\Gamma\sigma^2}{2\pi}(1+3e^{-\pi^2\sigma^2}) \int_{-\infty}^{\infty}\int_{-\infty}^{\infty} d\phi_1 d\phi_2 e^{-\frac{\sigma^2\phi_1^2}{2}} e^{-2\sigma^2\phi_2^2} (\phi_1^2+\phi_2^2) \tag{5.81}$$

$$\leq \frac{5\Gamma}{2\sigma^2}. \tag{5.82}$$

The third term can be bounded exactly as the second term for small t. In particular, we have bounds on the differences and sums of h, and thus

$$\left| \int_{-\delta}^{\delta}\int_{-\delta}^{\delta} \frac{d\phi_1 d\phi_2}{4\pi^2} e^{-\frac{\sigma^2\phi_1^2}{4}} e^{-\sigma^2\phi_2^2} e^{-i\theta_\pm(p_1+\phi_1,p_2+\phi_2)} \right.$$

$$\left. \times \Big[h_L^\sigma\Big(\frac{\phi_1}{2}+\phi_2\Big)+h_\infty^\sigma\Big(\frac{\phi_1}{2}+\phi_2\Big)\Big]\Big[h_L^\sigma\Big(\frac{\phi_1}{2}-\phi_2\Big)-h_\infty^\sigma\Big(\frac{\phi_1}{2}-\phi_2\Big)\Big] \right|$$

$$\leq \int_{-\delta}^{\delta}\int_{-\delta}^{\delta} \frac{d\phi_1 d\phi_2}{4\pi^2} e^{-\frac{\sigma^2\phi_1^2}{4}} e^{-\sigma^2\phi_2^2} \frac{24\sigma^4}{L} e^{-\frac{L^2}{2\sigma^2}} \tag{5.83}$$

$$\leq \frac{12\sigma^2}{\pi L} e^{-\frac{L^2}{2\sigma^2}}. \tag{5.84}$$

In a similar manner, we have that the fourth term can be bounded as the third for small t.

$$\left| \int_{-\delta}^{\delta}\int_{-\delta}^{\delta} \frac{d\phi_1 d\phi_2}{4\pi^2} e^{-\frac{\sigma^2\phi_1^2}{4}} e^{-\sigma^2\phi_2^2} e^{-2i(p_2+\phi_2)(\mu(t)-\nu(t))} \Big[h_L^\sigma\Big(\frac{\phi_1}{2}+2p_2+\phi_2\Big)+h_\infty^\sigma\Big(\frac{\phi_1}{2}+2p_2+\phi_2\Big)\Big] \right.$$

$$\left. \times \Big[h_L^\sigma\Big(\frac{\phi_1}{2}-2p_2-\phi_2\Big)-h_\infty^\sigma\Big(\frac{\phi_1}{2}-2p_2-\phi_2\Big)\Big] \right|$$

$$\leq \int_{-\delta}^{\delta}\int_{-\delta}^{\delta} \frac{d\phi_1 d\phi_2}{4\pi^2} e^{-\frac{\sigma^2\phi_1^2}{4}} e^{-\sigma^2\phi_2^2} \frac{24\sigma^4}{L} e^{-\frac{L^2}{2\sigma^2}} \tag{5.85}$$

$$\leq \frac{12\sigma^2}{\pi L} e^{-\frac{L^2}{2\sigma^2}}. \tag{5.86}$$

Finally, we have that the final term can be bounded as

$$\left| \int_{-\delta}^{\delta}\int_{-\delta}^{\delta} \frac{d\phi_1 d\phi_2}{4\pi^2} e^{-\frac{\sigma^2\phi_1^2}{4}} e^{-\sigma^2\phi_2^2} e^{2i(p_2+\phi_2)(\mu(t)-\nu(t))} h_\infty^\sigma\Big(\frac{\phi_1}{2}-2p_2-\phi_2\Big) h_\infty^\sigma\Big(\frac{\phi_1}{2}+2p_2+\phi_2\Big)\right|$$

$$\leq \int_{-\delta}^{\delta}\int_{-\delta}^{\delta} \frac{d\phi_1 d\phi_2}{4\pi^2} e^{-\frac{\sigma^2\phi_1^2}{4}} e^{-\sigma^2\phi_2^2} h_\infty^\sigma\Big(\frac{\phi_1}{2}-2p_2-\phi_2\Big) h_\infty^\sigma\Big(\frac{\phi_1}{2}+2p_2+\phi_2\Big) \tag{5.87}$$

$$\leq \frac{16}{\sqrt{\pi}} e^{-2\sigma^2\delta} \tag{5.88}$$

where we used the bounds for small t.

We can then use the bounds on all of the individual terms to show that $|\,w(t)\rangle$ and $|\,\alpha(t)\rangle$ are close. In particular, we have

$$\| |\,\alpha(t)\rangle_\pm - |\,w(t)\rangle\|^2$$

$$\leq {}_\pm\langle \alpha(t)\,|\,\alpha(t)\rangle_\pm + \langle\, w(t)\,|\,w(t)\,\rangle - \langle\, w(t)\,|\,\alpha(t)\rangle_\pm - {}_\pm\langle \alpha(t)\,|\,w(t)\rangle \tag{5.89}$$

$$\leq 1 + \langle\, w(t)\,|\,w(t)\,\rangle - 2\eta\gamma^2\Big(\frac{1}{2}\langle\, w(t)\,|\,w(t)\,\rangle - \frac{5\Gamma}{2\sigma^2} - \frac{12\sigma^2}{\pi L} e^{-\frac{L^2}{2\sigma^2}} - \frac{12\sigma^2}{\pi L} e^{-\frac{L^2}{2\sigma^2}} - \frac{16}{\sqrt{\pi}} e^{-2\sigma^2\delta}\Big). \tag{5.90}$$

If we again use our bounds on γ^2 and on $\langle\, w(t)\,|\,w(t)\,\rangle$, we find

$$\| |\,\alpha(t)\rangle_\pm - |\,w(t)\rangle\|^2$$

$$\leq 1 + \langle\, w(t)\,|\,w(t)\,\rangle - 4(1-3e^{-\pi^2\sigma^2})\Big(\frac{1}{2}\langle\, w(t)\,|\,w(t)\,\rangle - \frac{5\Gamma}{2\sigma^2} - \frac{24\sigma^2}{\pi L} e^{-\frac{L^2}{2\sigma^2}} - \frac{16}{\sqrt{\pi}} e^{-2\sigma^2\delta}\Big) \tag{5.91}$$

$$\leq 1 - \langle\, w(t)\,|\,w(t)\,\rangle(1-6e^{-\pi^2\sigma^2}) + \frac{5\Gamma}{2\sigma^2} + \frac{24\sigma^2}{\pi L} e^{-\frac{L^2}{2\sigma^2}} + \frac{16}{\sqrt{\pi}} e^{-2\sigma^2\delta} \tag{5.92}$$

$$\leq 1 - \Big(1 - \frac{1}{\pi\delta^2\sigma^2} e^{-\frac{5\sigma^2\delta^2}{2}}\Big)(1-6e^{-\pi^2\sigma^2}) + \frac{5\Gamma}{2\sigma^2} + \frac{24\sigma^2}{\pi L} e^{-\frac{L^2}{2\sigma^2}} + \frac{16}{\sqrt{\pi}} e^{-2\sigma^2\delta} \tag{5.93}$$

$$\leq \frac{1}{\pi\delta^2\sigma^2} e^{-\frac{5\sigma^2\delta^2}{2}} + 6e^{-\pi^2\sigma^2} + \frac{5\Gamma}{2\sigma^2} + \frac{24\sigma^2}{\pi L} e^{-\frac{L^2}{2\sigma^2}} + \frac{16}{\sqrt{\pi}} e^{-2\sigma^2\delta} \tag{5.94}$$

$$\leq 44e^{-2\sigma^2\delta} + \frac{32\sigma^2}{L} e^{-\frac{L^2}{2\sigma^2}} + \frac{5\Gamma}{2\sigma^2}. \tag{5.95}$$

With these good bounds on our approximations to the expected time-evolved states, it will now be useful to determine the overlap of the actual time-evolved state with our approximations. Note that $|\,\alpha(0)\rangle_\pm = |\,\psi(0)\rangle_\pm$, and thus we have that $|\,w(0)\rangle$ is a good approximation to the initial state. If we define the state

$$|\,v(t)\rangle = e^{-iH^{(2)}t}|\,w(0)\rangle \tag{5.96}$$

$$= \eta\int_{-\delta}^{\delta}\int_{-\delta}^{\delta} \frac{d\phi_1 d\phi_2}{4\pi^2} e^{i\phi_1\left(\frac{\mu+\nu}{2}\right)} e^{i\phi_2(\nu-\mu)} e^{-\frac{\sigma^2\phi_1^2}{4}} e^{-\sigma^2\phi_2^2} e^{-4it\cos\left(\frac{p_1+\phi_1}{2}\right)\cos(p_2+\phi_2)} |\,\mathrm{sc}(p_1+\phi_1; p_2+\phi_2)\rangle_\pm \tag{5.97}$$

we will have that this state does not change its overlap with $|\psi(t)\rangle$ over time (i.e., $\||v(t)\rangle - |\psi(t)\rangle\| = \||v(0)\rangle - |\psi(0)\rangle\|$). Additionally, we will have that $|v(t)\rangle$ and $|w(t)\rangle$ will be close in norm. As expected, we have

$$\begin{aligned}\langle v(t)|w(t)\rangle &= \eta^2 \int_{-\delta}^{\delta}\int_{-\delta}^{\delta} \frac{d\phi_1 d\phi_2}{4\pi^2} e^{i\phi_1\left(\frac{\mu(t)+\nu(t)}{2}-\frac{\mu+\nu}{2}\right)} e^{i\phi_2(\nu(t)-\mu(t)-\nu+\mu)} \\ &\quad \times e^{-\frac{\sigma^2\phi_1^2}{2}} e^{-2\sigma^2\phi_2^2} e^{2it\left(2\cos\left(\frac{p_1+\phi_1}{2}\right)\cos(p_2+\phi_2)-\cos(k_1)-\cos(k_2)\right)} \qquad (5.98)\\ &= \langle w(t)|w(t)\rangle - \eta^2 \int_{-\delta}^{\delta}\int_{-\delta}^{\delta} \frac{d\phi_1 d\phi_2}{4\pi^2} e^{-\frac{\sigma^2\phi_1^2}{2}} e^{-2\sigma^2\phi_2^2} \\ &\quad \times \left[1 - e^{i\phi_1\left(\frac{\mu(t)+\nu(t)}{2}-\frac{\mu+\nu}{2}\right)} e^{i\phi_2(\nu(t)-\mu(t)-\nu+\mu)} e^{2it\left(2\cos\left(\frac{p_1+\phi_1}{2}\right)\cos(p_2+\phi_2)-\cos(k_1)-\cos(k_2)\right)}\right]. \qquad (5.99)\end{aligned}$$

We can then bound the value of the integrand, using the fact that $|1-e^{i\theta}| \le \theta$. We then have

$$\begin{aligned}&\left|1 - e^{i\phi_1\left(\frac{\mu(t)+\nu(t)}{2}-\frac{\mu+\nu}{2}\right)} e^{i\phi_2(\nu(t)-\mu(t)-\nu+\mu)} e^{2it\left(2\cos\left(\frac{p_1+\phi_1}{2}\right)\cos(p_2+\phi_2)-\cos(k_1)-\cos(k_2)\right)}\right| \\ &\quad \le \Big| -\frac{\phi_1}{2}\big[\lceil 2t\sin k_1\rceil + \lceil 2t\sin k_2\rceil\big] - \phi_2\big[\lceil 2t\sin k_2\rceil - \lceil 2t\sin k_1\rceil\big] \\ &\qquad + 2t\Big[2\cos\Big(\frac{p_1+\phi_1}{2}\Big)\cos(p_2+\phi_2) - \cos(k_1) - \cos(k_2)\Big]\Big| \qquad (5.100)\\ &\quad \le |\phi_1| + 2|\phi_2| + 2t\Big|2\cos\Big(\frac{p_1+\phi_1}{2}\Big)\cos(p_2+\phi_2) - \cos(k_1) - \cos(k_2) \\ &\qquad - \frac{\phi_1}{2}\big[\sin k_1 + \sin k_2\big] - \phi_2\big[\sin k_2 - \sin k_1\big]\Big| \qquad (5.101)\\ &\quad \le |\phi_1| + 2|\phi_2| + 2t\Big|\cos\Big(-k_2 + \frac{\phi_1}{2} + \phi_2\Big) + \cos\Big(-k_1 + \frac{\phi_1}{2} - \phi_2\Big) - \cos(k_1) - \cos(k_2) \\ &\qquad - \Big(\frac{\phi_1}{2} + \phi_2\Big)\sin k_2 - \Big(\frac{\phi_1}{2} - \phi_2\Big)\sin k_1\Big| \qquad (5.102)\\ &\quad \le |\phi_1| + 2|\phi_2| + 2t\Big|\cos(k_2)\big[\cos\big(\frac{\phi_1}{2}+\phi_2\big) - 1\big] - \sin(k_2)\big[\big(\frac{\phi_1}{2}+\phi_2\big) - \sin\big(\frac{\phi_1}{2}+\phi_2\big)\big]\Big| \\ &\qquad + 2t\Big|\cos(k_1)\Big[\cos\Big(\frac{\phi_1}{2}-\phi_2\Big) - 1\Big] - \sin(k_1)\Big[\frac{\phi_1}{2} - \phi_2 - \sin\Big(\frac{\phi_1}{2}-\phi_2\Big)\Big]\Big| \qquad (5.103)\\ &\quad \le |\phi_1| + 2|\phi_2| + 2t\Big(\frac{\phi_1}{2}+\phi_2\Big)^2 + 2t\Big(\frac{\phi_1}{2}-\phi_2\Big)^2 \qquad (5.104)\\ &\quad \le |\phi_1| + \frac{t}{2}\phi_1^2 + 2|\phi_2| + 4t\phi_2^2. \qquad (5.105)\end{aligned}$$

We can then use this in the bound, so that

$$\begin{aligned}
&\left| \int_{-\delta}^{\delta}\int_{-\delta}^{\delta} \frac{d\phi_1 d\phi_2}{4\pi^2} e^{-\frac{\sigma^2\phi_1^2}{2}} e^{-2\sigma^2\phi_2^2} \Big[1 - e^{i\phi_1\left(\frac{\mu(t)+\nu(t)}{2} - \frac{\mu+\nu}{2}\right)} e^{i\phi_2(\nu(t)-\mu(t)-\nu+\mu)} \right. \\
&\qquad \left. \times e^{2it\left(2\cos\left(\frac{p_1+\phi_1}{2}\right)\cos(p_2+\phi_2)-\cos(k_1)-\cos(k_2)\right)}\Big]\right| \\
&\quad \leq \int_{-\delta}^{\delta}\int_{-\delta}^{\delta} \frac{d\phi_1 d\phi_2}{4\pi^2} e^{-\frac{\sigma^2\phi_1^2}{2}} e^{-2\sigma^2\phi_2^2} \Big[|\phi_1| + \frac{t}{2}\phi_1^2 + 2|\phi_2| + 4t\phi_2^2\Big] \qquad (5.106)\\
&\quad \leq \int_{0}^{\infty}\int_{0}^{\infty} \frac{d\phi_1 d\phi_2}{\pi^2} e^{-\frac{\sigma^2\phi_1^2}{2}} e^{-2\sigma^2\phi_2^2} \Big[\phi_1 + \frac{t}{2}\phi_1^2 + 2\phi_2 + 4t\phi_2^2\Big] \qquad (5.107)\\
&= \frac{3t}{8\pi\sigma^4} + \frac{\sqrt{2\pi}}{2\pi^2\sigma^3}. \qquad (5.108)
\end{aligned}$$

With this, we can then bound the difference between $|v(t)\rangle$ and $|w(t)\rangle$. In particular, we have

$$\begin{aligned}
\||v(t)\rangle - |w(t)\rangle\|^2 &= \langle v(t)|v(t)\rangle + \langle w(t)|w(t)\rangle - \langle v(t)|w(t)\rangle - \langle w(t)|v(t)\rangle \qquad (5.109)\\
&\leq 2\langle w(t)|w(t)\rangle - 2\Big[\langle w(t)|w(t)\rangle - \eta^2\frac{3t}{8\pi\sigma^4} - \eta^2\frac{\sqrt{2\pi}}{2\pi^2\sigma^3}\Big] \qquad (5.110)\\
&= \frac{3t}{\sigma^2} + \frac{4\sqrt{2}}{\sqrt{\pi}\sigma}. \qquad (5.111)
\end{aligned}$$

Finally, we can now bound the norm of the difference between the time evolved $|\psi(t)\rangle$ and the approximation $|\alpha(t)\rangle_\pm$. In particular, if we once again note that $|\alpha(0)\rangle_\pm = |\psi(0)\rangle_\pm$, and remember that $|v(t)\rangle = e^{-iH^{(2)}t}|v(0)\rangle$, we have

$$\begin{aligned}
&\||\psi(t)\rangle_\pm - |\alpha(t)\rangle_\pm\| \\
&\quad \leq \||\psi(t)_\pm\rangle - |v(t)\rangle\| + \||\alpha(t)\rangle_\pm - |w(t)\rangle\| + \||v(t)\rangle - |w(t)\rangle\| \qquad (5.112)\\
&\quad \leq \Big(44e^{-2\sigma^2\delta} + \frac{32\sigma^2}{L}e^{-\frac{L^2}{2\sigma^2}}\Big)^{1/2} + \Big(44e^{-2\sigma^2\delta} + \frac{32\sigma^2}{L}e^{-\frac{L^2}{2\sigma^2}} + \frac{5\Gamma}{2\sigma^2}\Big)^{1/2} + \Big(\frac{3t}{\sigma^2} + \frac{4\sqrt{2}}{\sqrt{\pi}\sigma}\Big)^{1/2}. \qquad (5.113)
\end{aligned}$$

If we have chosen $\sigma = \frac{L}{2\sqrt{\log(L)}}$, we then have that for L large enough, if $0 < t < \frac{\nu-\mu-2L}{2\sin k_2 - 2\sin k_1}$ or $\frac{\nu-\mu+2L}{2\sin k_2 - 2\sin k_1} < t < cL$

$$\begin{aligned}
&\||\psi(t)\rangle_\pm - |\alpha(t)\rangle_\pm\| \\
&\quad \leq \Big(\frac{9}{L\log(L)}\Big)^{1/2} + \Big(\frac{10}{L\log(L)}\Big)^{1/2} + \Big(\frac{12t\log L}{L^2} + \frac{16\sqrt{2\log L}}{\sqrt{\pi}L}\Big)^{1/2} \qquad (5.114)\\
&\quad \leq \chi_2\sqrt{\frac{\log L}{L}} \qquad (5.115)
\end{aligned}$$

where χ_2 is a constant. □

5.3 Encoding computation via scattering

At this point, we understand the time-evolution of single particle wave-packets on graphs with long paths, via Theorem 3, and we understand the time-evolution of two particle wave-packets traveling toward each other along a long path, via Theorem 4. Combining these results, along with the Lemma 1, will allow us to understand multi-particle scattering on relatively complicated graphs. We can then use this understanding to encode computation in the time evolution of initially separate wave-packets. Note that this idea of encoding qubits in the location of particles was originally used in [10], but the dual-rail encoding originally occured in [15].

Note that in this section, we will assume that the paths are either infinite, or semi-infinite. If the eventual goal is to have a graph with a number of vertices only polynomial in the number of encoded qubits, this might not be a valid assumption. However, Lemma 1 will allow us to approximate the evolution of the wave-packets on truncated graphs by the evolution on the semi-infinite paths. As such, our intuitive encoding scheme is appropriate.

[**TO DO:** *Find correct citations*]

5.3.1 Encoded qubits

The first thing that we will need to do to encode some computation using scattering, is to somehow encode the Hilbert space to be simulated. In Chapter 4, we were able to do this by having a number of (nearly) infinite paths equal to the dimension of the Hilbert space, and the encoded state corresponded to the path on which the particle was located. While this works, the fact that the number of paths grows exponentially in the number of encoded qubits makes this impractical for actually building a graph on which quantum walks can be built.

With our access to multiple particles, we will have a similar encoding to the single-particle case, in which each qubit is encoded in the location of a single particle. Namely, for each qubit, there will be two associated infinite paths, and a single particle wave-packet with momentum centered about some value k. The value of the encoded qubit will be $|0\rangle$ if the particle is located along the first (top) path, while the value of the encoded qubit will be $|1\rangle$ if the particle is located along the second (bottom) path.

Note that this is the same encoding as in Chapter 4 for a single qubit. The difference arises when encoding qubits, as the number of paths for the single particle encoding grows exponentially, while the number of paths for the multi-particle encoding grows linearly with the number of qubits. Additionally, we have that each encoded qubit has its own particle, with its own momentum. For our encoding, there will only be two possible momenta, namely k_{com} and k_{med}, corresponding to two different types of qubits. The qubits that are encoded at momentum k_{com} will be used as logical qubits, while those encoded at momentum k_{med} will be used as mediating qubits, for which we will need fewer gates. We will need two momenta, however, as our entangling gate will only work between qubits that are encoded at different momenta.

[**TO DO:** *Should I mention* $k_{com} = -\frac{\pi}{4}$ *and* $k_{med} = -\frac{\pi}{2}$*?*]

[**TO DO:** *Explicitly define wave-packets*]

Recall from Section **??** that for a given σ and cutoff length L, we defined the state

$$|\chi_{\mu,k}\rangle = \gamma \sum_{\mu-L}^{\mu+L} e^{ikx} e^{-\frac{(x-\mu)^2}{2\sigma^2}} |x\rangle, \tag{5.116}$$

and we used states of this form as our assumed wave-packets. We will use similar states for our encoded qubits, where σ and L will depend on the overall length of the computation.

5.3.2 Encoded single-qubit gates

Now that we have encoded qubits, we will want to know how to apply a single particle gate. For a single qubit, this will be done exactly as in Chapter 4. Namely, for a given qubit with momentum k, if we want to apply the unitary U, we will place a graph $\widehat{G}$ as an obstacle along the pair of infinite paths, where the scattering matrix at k of $\widehat{G}$ takes the form

$$S(k) = \begin{pmatrix} 0 & U^T \\ U & 0 \end{pmatrix} \tag{5.117}$$

where we assume that the labeling of the four terminal vertices proceeds as 0_{in}, 1_{in}, 0_{out}, and 1_{out}, as in [**TO DO:** *figure something*] .

While we cannot guarantee that the requisite graphs exist for all unitaries U at all momenta k, for specific momenta there exist a universal family of single-qubit gates. For example the graphs [**TO DO:** *draw graphs*] form a universal gate set for single-qubit unitaries at momentum $k = -\frac{\pi}{3}$, while those of [**TO DO:** *draw graphs*] for a universal gate set at $k = -\frac{2\pi}{3}$ (these were found in [9]). [**TO DO:** *determine universal gate set for $\pi/3$ and $2\pi/3$*]

The difference between the encoded single-qubit gates for the multi-particle encoding and the single-particle encoding is in the behavior for the paths not corresponding to the qubit on which the unitary acts. In the single-particle case, the set of paths was partitioned into sets of size two (corresponding to each basis state for the qubits not acted upon), where a copy of the obstacle graph was placed on each pair of paths. For the multi-particle encoding, only a single copy of the graph is placed as an obstacle; the remaining qubits' paths remain unimpeded.

[**TO DO:** *create figure*]

5.3.3 Encoded entangling gate

Now that we have encoded qubits and, at specific momenta, a universal set of single-qubit gates, we need to construct some kind of entangling gate. In the single-particle encoding, this gate was trivial, as a controlled-not gate (and in fact any permutation gate) simply corresponded to a relabelling of the encoding paths. For our multi-particle encoding, however, our encoding is rather more involved. Our entangling gate will necessarily involve a two-particle Hamiltonian, but we will arrange the graph (and the encoded initial states) in such a manner that the two-particles will only ever interact on a (long) path. As such, we can use Theorem **??** to see that the result of such scattering is simply an applied phase.

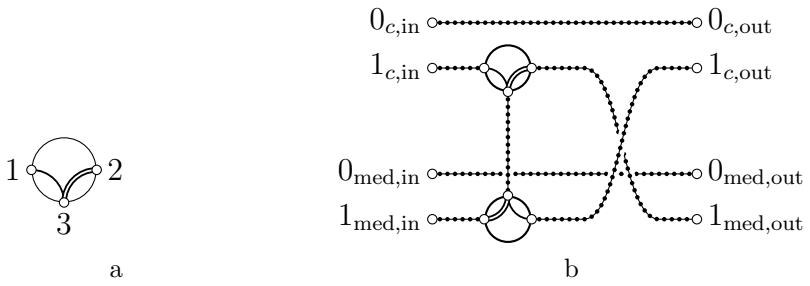

Figure 5.2: (a) Momentum switch schematic. (b) Cθ gate.

Explicitly, our entangling gate will be a controlled-θ gate, for some θ that depends on the interaction and the momenta used to encode the qubits. Further, our entangling gate will only be between qubits that are encoded with particles for which a momentum switch Section 3.4.2 exists. The main idea behind the gate is to place two momentum switches (represented schematically as Figure 5.2a) on the 1-paths of the qubits as obstacles, where the two switches are connected by a long path for their third terminals. In either particle is in the logical state 1, it will be routed along the long connecting path between the two paths, and then routed along 1_{out} for the opposite qubit. By arranging the lengths of the various paths correctly, we can ensure that if at most a single encoded qubit is in the logical 1 state, then an encoded identity operation occurs. However, if both encoded qubits are logically 1, then the two particles move past each other along the long connecting path, acquiring an additional phase that depends on their momenta and the interaction. As such, the graph in Figure 5.2b applies an encoded Cθ gate.

To see why this graph implements a Cθ gate, consider the movement of two particles as they pass through the graph. If either particle begins in the state $|\,0_{\text{in}}\,\rangle$, then it travels along a path to the output without interacting with the second particle. When the computational particle (qubit c in the figure) begins in the state $|\,1_{\text{in}}\,\rangle^{c}$, it is routed downward as it passes through the top momentum switch (following the single line). It travels down the vertical path and then is routed to the right (along the single line) as it passes through the bottom switch. Similarly, when the mediator particle begins in the state $|\,1_{\text{in}}\,\rangle^{\text{med}}$, it is routed upward (along the double line) through the vertical path at the bottom switch and then to the right (along the double line) at the top switch. If both particles begin in the state $|\,1_{\text{in}}\,\rangle$, then they interact on the vertical path. In this case, as the two particles move past each other, the wave function acquires a phase $e^{i\theta}$ arising from this interaction.

[**TO DO:** *combine previous two paragraphs*]

5.3.3.1 Momentum switch

Remember from Section 3.4.2 that momentum switches are three-terminal scattering gadgets that act like railroad switches, where at specific momenta the gadget has perfect transmission from terminal 3 to terminal 1, while at other momenta there is perfect transmission from terminal 3 to terminal 2. We will represent gadgets with this behavior schematically as in Figure 5.2a, where one set of momenta follow the single line while the other specified set follows the double line.

For our purposes, we will assume that the momentum switch splits the two momenta used to encode the different qubits k_{com} and k_{med}. Explicitly, we will assume that the S-matrix for the given momentum switch at k_1 and k_2 are given by

$$S_{\text{switch}}(k_{\text{com}}) = \begin{pmatrix} 0 & 0 & T_{\text{com}} \\ 0 & R_{\text{com}} & 0 \\ T_{\text{com}} & 0 & 0 \end{pmatrix} \qquad S_{\text{switch}}(k_{\text{med}}) = \begin{pmatrix} R_{\text{med}} & 0 & 0 \\ 0 & 0 & T_{\text{med}} \\ 0 & T_{\text{med}} & 0 \end{pmatrix}. \quad (5.118)$$

In other words, we will assume that the momentum switch has perfect transmission between terminals 1 and 3 at momentum k_{com}, and perfect transmission between terminals 2 and 3 at momentum k_{med}, possibly with an additional phase. With this, we have that a particle with momentum k_{com} follows the single line, while a particle with momentum k_{med} follows the double line.

5.3.3.2 Constructing the graph

We will now construct this graph, where we will assume that we know the encoded initial states. Note that this construction doe depend on the momenta of the encoded qubits in more than just the form of the momentum switch; the fact that the timing of the wave-packets is important forces us to change the length of the connecting paths depending on the initial momentum so that they arrive on the infinite path at the same time, while the requirement that the particles only interact along the path forces us to change the lengths depending on the size of the wave-packets.

The Cθ gate is implemented using the graph shown in Figure 5.3. In this section we specify the logical input states, the logical output states, the distances X, Z, and W appearing in the figure, and the total evolution time as functions of the momentum k_{com} and k_{med}. With these choices, we show that a Cθ gate is applied to the logical states at the end of the time evolution under the quantum walk Hamiltonian (up to error terms that are $\tilde{\mathcal{O}}(L^{-1/2})$). The results of this section pertain to the two-particle Hamiltonian $H^{(2)}_{G'}$ for the graph G' shown in Figure 5.3. [**TO DO:** *get correct error term*]

We first need to construct the assumed encoded initial states.

$$|0_{\text{in}}\rangle^{\text{com}} = \gamma \sum_{x=\mu-L}^{\mu+L} e^{ik_{\text{com}}x} e^{-\frac{(x-\mu)^2}{2\sigma^2}} |x,1\rangle \qquad |1_{\text{in}}\rangle^{c} = \gamma \sum_{x=\mu-L}^{\mu+L} e^{ik_{\text{com}}x} e^{-\frac{(x-\mu)^2}{2\sigma^2}} |x,2\rangle \quad (5.119)$$

for the computational qubit and

$$|0_{\text{in}}\rangle^{\text{med}} = \gamma \sum_{x=\nu-L}^{\nu+L} e^{ik_{\text{med}}x} e^{-\frac{(x-\nu)^2}{2\sigma^2}} |x,4\rangle \qquad |1_{\text{in}}\rangle^{\text{med}} = \gamma \sum_{x=\nu-L}^{\nu+L} e^{ik_{\text{med}}x} e^{-\frac{(x-\nu)^2}{2\sigma^2}} |x,3\rangle$$

for the mediator qubit. We can then define symmetrized (or antisymmetrized) logical input states for $a, b \in \{0,1\}$ as

$$|ab_{\text{in}}\rangle^{\text{com,med}}_{\pm} = \frac{1}{\sqrt{2}} \left(|a_{\text{in}}\rangle^{\text{com}} |b_{\text{in}}\rangle^{\text{med}} \pm |b_{\text{in}}\rangle^{\text{med}} |a_{\text{in}}\rangle^{\text{com}} \right).$$

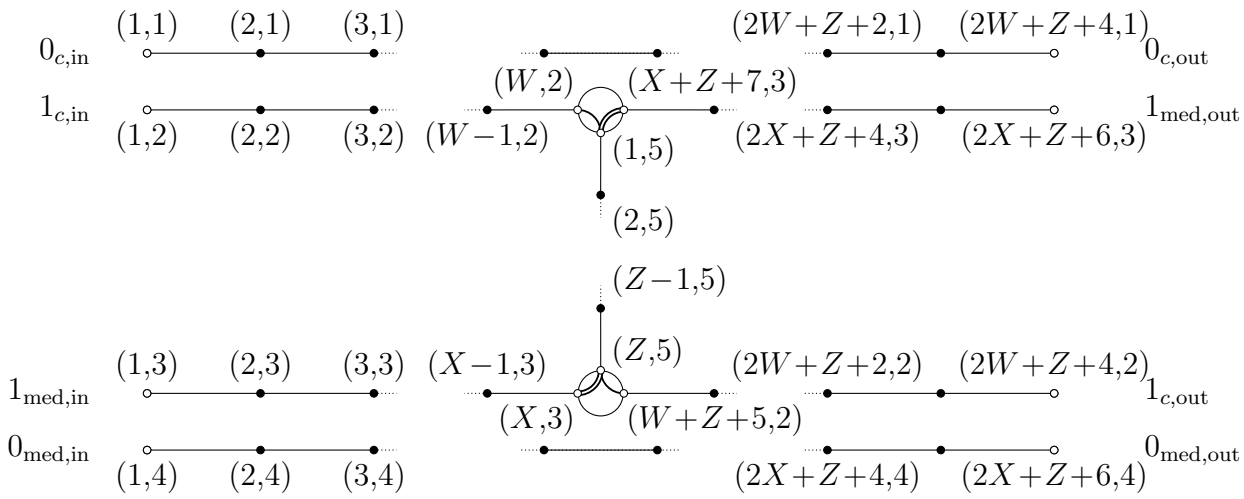

Figure 5.3: Graph G' used to implement the Cθ gate. The integers Z, X, and W are specified in equations (5.120), (5.121), and (5.122), respectively.

We choose the distances Z, X, and W from Figure **??** to be

$$Z = 4L \tag{5.120}$$

$$X = d_2 + L + M\left(-\frac{\pi}{2}\right) \tag{5.121}$$

$$W = d_1 + L + M\left(-\frac{\pi}{4}\right) \tag{5.122}$$

where

$$d_1 = M\left(-\frac{\pi}{4}\right)$$

$$d_2 = \left\lceil \frac{5L + 2d_1}{\sqrt{2}} - \frac{5}{2}L \right\rceil.$$

With these choices, a wave packet moving with speed $\sqrt{2}$ travels a distance $Z + 2d_1 + L = 5L + 2d_1$ in approximately the same time that a wave packet moving with speed 2 takes to travel a distance $Z + 2d_2 + L = 5L + 2d_2$, since

$$t_{\text{II}} = \frac{5L + 2d_1}{\sqrt{2}} \approx \frac{5L + 2d_2}{2}. \tag{5.123}$$

We claim that the logical input states evolve into logical output states (defined below) with a phase of $e^{i\theta}$ applied in the case where both particles are in the logical state 1. Specifically, let us define the output states as,

$$|0_{\text{out}}\rangle^c = \frac{e^{-it_{\text{II}}\sqrt{2}}}{\sqrt{L}} \sum_{x=Q_1+1}^{Q_1+L} e^{-i\frac{\pi}{4}x}|x,1\rangle \qquad |1_{\text{out}}\rangle^c = \frac{e^{-it_{\text{II}}\sqrt{2}}}{\sqrt{L}} \sum_{x=Q_1+1}^{Q_1+L} e^{-i\frac{\pi}{4}x}|x,2\rangle$$

$$|0_{\text{out}}\rangle^{\text{med}} = \frac{1}{\sqrt{L}} \sum_{y=Q_2+1}^{Q_2+L} e^{-i\frac{\pi}{2}y}|y,4\rangle \qquad |1_{\text{out}}\rangle^{\text{med}} = \frac{1}{\sqrt{L}} \sum_{y=Q_2+1}^{Q_2+L} e^{-i\frac{\pi}{2}y}|y,3\rangle$$

where $Q_1 = 2W + Z + 4 - M(-\pi/4) - L$ and $Q_2 = 2X + Z + 6 - M(-\pi/2) - L$,and $|ab_{\text{out}}\rangle^{c,\text{med}} = \text{Sym}\left(|a_{\text{out}}\rangle^{c}|b_{\text{out}}\rangle^{\text{med}}\right)$.

Note that the input states are wave packets located a distance $M(k)$ from the ends of the input paths on the left-hand side of the graph in Figure **??**. Similarly, the output logical states are wave packets located a distance $M(k)$ from the ends of the output paths on the right-hand side.

We then have the following lemma:

Lemma 11. *For the graph given in Figure 5.3, we have the following bounds for the time-evolved states:*

$$\left\| e^{-iH_{G'}^{(2)}t_{\text{II}}}|00_{in}\rangle^{c,med} - |00_{out}\rangle^{c,med} \right\| = \emptyset(L^{-1/4}) \tag{5.124}$$

$$\left\| e^{-iH_{G'}^{(2)}t_{\text{II}}}|01_{in}\rangle^{c,med} - |01_{out}\rangle^{c,med} \right\| = \emptyset(L^{-1/4}) \tag{5.125}$$

$$\left\| e^{-iH_{G'}^{(2)}t_{\text{II}}}|10_{in}\rangle^{c,med} - |10_{out}\rangle^{c,med} \right\| = \emptyset(L^{-1/4}) \tag{5.126}$$

$$\left\| e^{-iH_{G'}^{(2)}t_{\text{II}}}|11_{in}\rangle^{c,med} - e^{i\theta}|11_{out}\rangle^{c,med} \right\| = \emptyset(L^{-1/4}). \tag{5.127}$$

Proof. The first three bounds (5.124), (5.125), and (5.126) are relatively easy to show, since in each case the two particles are supported on disconnected subgraphs and therefore do not interact. In each of these three cases we can simply analyze the propagation of the one-particle starting states through the graph. The symmetrized (or antisymmetrized) starting state then evolves into the symmetrized (or antisymmetrized) tensor product of the two output states.

For example, with input state $|00_{\text{in}}\rangle^{c,\text{med}}$, the evolution of the particle with momentum $-\pi/4$ occurs only on the top path and the evolution of the particle with momentum $-\pi/2$ occurs only on the bottom path. Starting from the initial state $|0_{\text{in}}\rangle^{c}$ and evolving for time t_{II} with the single-particle Hamiltonian for the top path, we obtain the final state

$$|0_{\text{out}}\rangle^{c} + \emptyset(L^{-1/4}) \tag{5.128}$$

using the method of Section **??**. Similarly, starting from the initial state $|0_{\text{in}}\rangle^{\text{med}}$ and evolving for time t_{II} with the single-particle Hamiltonian for the bottom path of the graph we obtain the final state

$$|0_{\text{out}}\rangle^{\text{med}} + \emptyset(L^{-1/4}). \tag{5.129}$$

Putting these bounds together we get the bound (5.124).

In the case where the input state is $|10_{\text{in}}\rangle^{c,\text{med}}$ (or $|01_{\text{in}}\rangle^{c,\text{med}}$) the single-particle evolution for the particle with momentum $-\pi/4$ (or $-\pi/2$) is slightly more complicated, as in this case the particle moves through the momentum switches and the vertical path. The S-matrix of the momentum switch at the relevant momenta is given by equation (5.118). At momentum $-\pi/4$, the momentum switch has the same S-matrix as a path with 4 vertices (including the input and output vertices). At momentum $-\pi/2$, it has the same S-matrix as a path with 5 vertices (including input and output vertices). Note that our labeling of vertices on the output paths (in Figure **??**) takes this into account. The first vertices on the output

paths connected to the momentum switches are labeled $(X+Z+7,3)$ and $(W+Z+5,2)$, respectively, reflecting the fact that a particle with momentum $-\pi/4$ has traveled W vertices on the input path, Z vertices through the middle segment, and has effectively traveled an additional 4 vertices inside the two switches. Similarly, a particle with momentum $-\pi/2$ effectively sees an additional 6 vertices from the two momentum switches.

To get the bound (5.126) we have to analyze the single-particle evolution for the computational particle initialized in the state $|1_{\text{in}}\rangle^c$. We claim that, after time t_{II}, the time-evolved state is

$$|1_{\text{out}}\rangle^c + \emptyset(L^{-1/4}). \tag{5.130}$$

It is easy to see why this should be the case in light of our discussion above: when scattering at momentum $-\pi/4$, the graph in Figure **??** is equivalent to one where each momentum switch is replaced by a path with 2 internal vertices connecting the relevant input/output vertices.

To make this precise, we use the method described in Section **??** for analyzing scattering through sequences of overlapping graphs using the truncation lemma. Here we should choose subgraphs G_1 and G_2 of the graph G' in Figure **??** that overlap on the vertical path but where each subgraph contains only one of the momentum switches. A convenient choice is to take G_1 to be the subgraph containing the top switch and the paths connected to it (the vertices $(1,2),\dots,(W,2)$, $(1,5),\dots,(Z,5)$ and $(X+Z+7,3),\dots,(2X+Z+6,3)$). Similarly, choose G_2 to be the bottom switch along with the three paths connected to it. The graphs G_1 and G_2 both contain the vertices $(1,5),\dots,(Z,5)$ along the vertical path. Break up the total evolution time into two intervals $[0,t_\alpha]$ and $[t_\alpha,t_{\text{II}}]$. Choose t_α so that the wave packet, evolved for this time with $H^{(1)}_{G_1}$, travels through the top switch and ends up a distance $\Theta(L)$ from each switch, partway along the vertical path (up to terms bounded as $\emptyset(L^{-1/4})$, as in Section **??**). With this choice, the single-particle evolution with the Hamiltonian for the full graph is approximated by the evolution with $H^{(1)}_{G_1}$ on this time interval (see Section **??**). At time t_α, the particle is outgoing with respect to scattering from the graph G_1, but incoming with respect to G_2. On the interval $[t_\alpha,t_{\text{II}}]$ the time evolution is approximated by evolving the state with $H^{(1)}_{G_2}$. During this time interval the particle travels through the bottom switch onto the final path, and at t_{II} is a distance $M(-\pi/4)$ from the endpoint of the output path. Both switches have the same S-matrix (at momentum $-\pi/4$) as a path of length 4, so this analysis gives the output state $|10_{\text{out}}\rangle^{c,\text{med}}$ up to terms bounded as $\emptyset(L^{-1/4})$, establishing (5.126). For the bound (5.125), we apply a similar analysis to the trajectory of the mediator particle.

The case where the input state is $|11_{\text{in}}\rangle^{c,\text{med}}$ is more involved but proceeds similarly. In this case, to analyze the time evolution we divide the time interval $[0,t_{\text{II}}]$ into three segments $[0,t_A]$, $[t_A,t_B]$, and $[t_B,t_{\text{II}}]$. For each of these three time intervals we choose a subgraph G_A, G_B, G_C of the graph G' in Figure **??** and we approximate the time evolution by evolving with the Hamiltonian on the associated subgraph. We then use the truncation lemma to show that, on each time interval, the evolution generated by the Hamiltonian for the appropriate subgraph approximates the evolution generated by the full Hamiltonian, with error $\emptyset(L^{-1/4})$. Up to these error terms, at times $t=0$, $t=t_A$, $t=t_B$, and $t=t_{\text{II}}$ the time-evolved state

$$e^{-iH^{(2)}_{G'}t}|11_{\text{in}}\rangle^{c,\text{med}} \tag{5.131}$$

has both particles in square wave packet states, each with support only on L vertices of the graph, as depicted in Figure 5.4.

We take G_A to be the subgraph obtained from G' by removing the vertices labeled $(\lceil 1.85L \rceil, 5), \ldots, (\lceil 1.90L \rceil, 5)$ in the vertical path. By removing this interval of consecutive vertices, we disconnect the graph into two components where the initial state $|11_{\text{in}}\rangle^{c,\text{med}}$ has one particle in each component. This could be achieved by removing a single vertex, but instead we remove an interval of approximately $0.05L$ vertices to separate the components of G_A by more than the interaction range C (for sufficiently large L), simplifying our use of the truncation lemma.

We choose $t_A = 3L/2$. Consider the time evolution of the initial state $|11_{\text{in}}\rangle^{c,\text{med}}$ with the two-particle Hamiltonian $H^{(2)}_{G_A}$ for time t_A. The states $|1_{\text{in}}\rangle^{c}$ and $|1_{\text{in}}\rangle^{\text{med}}$ are supported on disconnected components of the graph G_A, so we can analyze the time evolution of the state $|11_{\text{in}}\rangle^{c,\text{med}}$ under $H^{(2)}_{G_A}$ by analyzing two single-particle problems, using the results of Section **??** for each particle. During the interval $[0, t_A]$, each particle passes through one switch, ending up a distance $\Theta(L)$ from the switch that it passed through and $\Theta(L)$ from the vertices that have been removed, as shown in Figure 5.4(b) (with error at most $\emptyset(L^{-1/4})$). Up to these error terms, the support of each particle remains at least $N_0 = \Theta(L)$ vertices from the endpoints of the graph, so we can apply the truncation lemma using $H = H^{(2)}_{G'}$, $W = \tilde{H} = H^{(2)}_{G_A}$, $T = t_{\text{A}}$, and $\delta = \emptyset(L^{-1/4})$. Here P is the projector onto states where both particles are located at vertices of G_A. We have $PH^{(2)}_{G'}P = H^{(2)}_{G_A}$ since the number of vertices in the removed segment is greater than the interaction range C. Applying the truncation lemma gives

$$\left\| e^{-iH^{(2)}_{G_A} t_A} |11_{\text{in}}\rangle^{c,\text{med}} - e^{-iH^{(2)}_{G'} t_A} |11_{\text{in}}\rangle^{c,\text{med}} \right\| = \emptyset(L^{-1/4}). \tag{5.132}$$

We approximate the evolution on the interval $[t_A, t_B]$ using the two-particle Hamiltonian $H^{(2)}_{G_B}$, where G_B is the vertical path $(1, 5), \ldots, (Z, 5)$. Using the result of Section **??**, we know that (up to terms bounded as $\emptyset(L^{-1/4})$) the wave packets move with their respective speeds and acquire a phase of $e^{i\theta}$ as they pass each other. We choose $t_B = 5L/2$ so that during the evolution the wave packets have no support on vertices within a distance $\Theta(L)$ from the endpoints of the vertical segment where the graph has been truncated (again up to terms bounded as $\emptyset(L^{-1/4})$). Using $H^{(2)}_{G_B}$ (rather than $H^{(2)}_{G'}$) to evolve the state on this interval, we incur errors bounded as $\emptyset(L^{-1/4})$ (using the truncation lemma with $N_0 = \Theta(L)$, $W = \tilde{H} = H^{(2)}_{G_B}$, $H = H^{(2)}_{G'}$, and $\delta = \emptyset(L^{-1/4})$).

We choose $G_C = G_A$; in the final interval $[t_B, t_{\text{II}}]$ we evolve using the Hamiltonian $H^{(2)}_{G_A}$ again, and we use the truncation lemma as we did for the first interval. The initial state is approximated by two wave packets supported on disconnected sections of G_A and the evolution of this initial state reduces to two single-particle scattering problems. During the interval $[t_B, t_{\text{II}}]$, each particle passes through a second switch, and at time t_{II} is a distance $M(k)$ from the end of the appropriate output path.

Our analysis shows that for the input state $|11_{\text{in}}\rangle^{c,\text{med}}$ the only effect of the interaction is to alter the global phase of the final state by a factor of $e^{i\theta}$ relative to the case where no interaction is present, up to error terms bounded as $\emptyset(L^{-1/4})$. This establishes equation

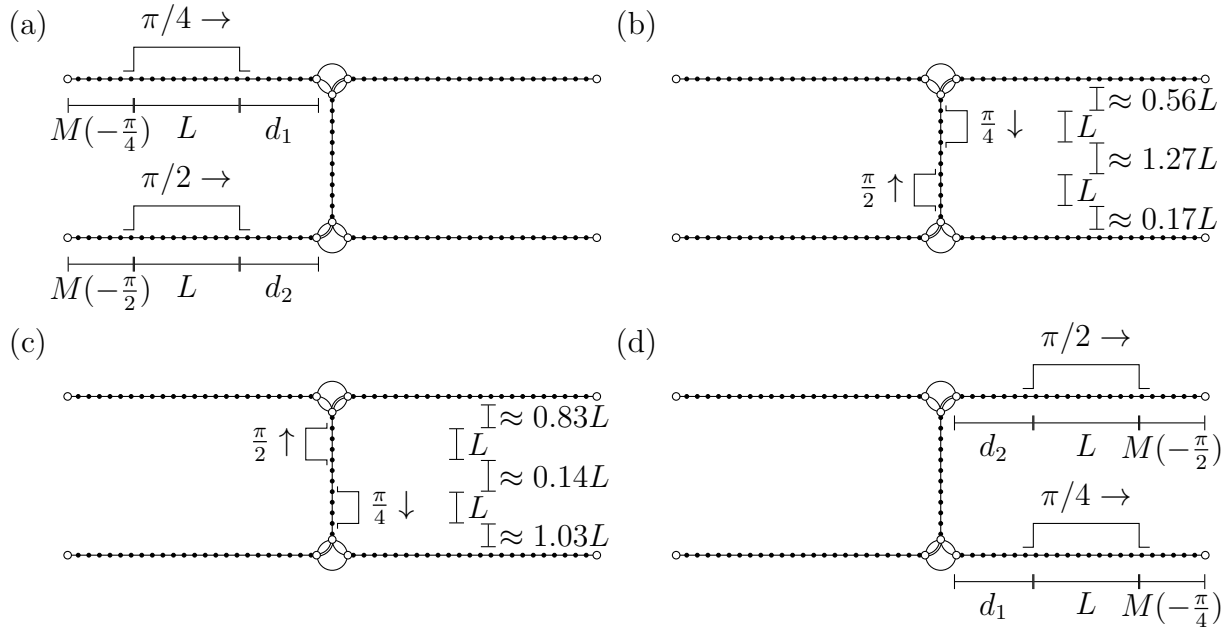

Figure 5.4: This picture illustrates the scattering process for two wave packets that are incident on the input paths as shown in figure (a) at time $t = 0$. Figure (b) shows the location of the two wave packets after a time $t_A = 3L/2$ and figure (c) shows the wave packets after a time $t_B = t_A + L$. After the particles pass one another they acquire an overall phase of $e^{i\theta}$. Figure (d) shows the final configuration of the wave packets after a total evolution time $t_{\text{II}} = (Z + 2d_1 + L)/\sqrt{2}$.

(5.127). In Figure 5.4 we illustrate the movement of the two wave packets through the graph when the initial state is $|11_{\text{in}}\rangle^{\text{c,med}}$.

□

[**TO DO:** *split 11_scattering_cartoon into several subfigures*]

5.4 Universal Computation

5.4.1 Two-qubit blocks

5.4.2 Combining blocks

5.5 Improvements and Modifications

What about long-range interactions, but where the interactions die off? Additionally, what about error correction?

Chapter 6

Ground energy of quantum walk

To get some flavor for **QMA**-completeness results.

Now that we have shown the universality of these Quantum Walk Hamiltonians via time evolution, we might want to ask related computational questions about these systems. In particular, once the computational universality of a system is shown, people often ask about the related ground energy problem. The reason for this is that many of these systems that allow for universal computation via time evolution also allow for the encoding of a computation in the ground space, which along with some energy penalties, allow one to show that the ground energy problem is **QMA**-hard.

The point of this chapter is to give a decent introduction to the flavor of **QMA**-hardness proofs, as well as providing a **QMA**-complete problem that might be more accessible to classical computer scientists.

6.1 The ground-energy problem

Essentially, we know that the single-particle quantum walk is governed by the adjacency matrix of the underlying graph. In particular, the Hamiltonian is exactly equal to the adjacency matrix, and thus asking questions about the ground energy of a single-particle quantum walk is simply asking a question about the smallest eigenvalue of a particular adjacency matrix.

However, the Hilbert space on which the quantum walk acts is necessarily exponential in size, with efficiently computable matrix entries. As such, this is a question about very specific types of matrices.

Problem 2 (d-sparse graph eigenvalue problem)**.** Given a d-sparse, row-computable graph G, and two constants $a < b$, is the smallest eigenvalue of $A(G)$ below a or above b, with the guarantee that one of these cases occur.

While this problem is definitely inspired from quantum walks, it actually makes no reference to quantum mechanics.

6.1.1 Containment in QMA

The proof that this problem is in **QMA**follows many other such Hamiltonian problems. In particular, this proof strategy works for any system in which we can evolve according to a particular Hamiltonian.

The main idea is to be given a particular state, and use phase estimation to determine the energy of the given state, up to some error. In the case that the smallest eigenvalue of the system is below a, the prover can provide the corresponding eigenvector encoded in a quantum state. The phase estimation algorithm will then (with high probability) find this eigenvalue, and the system will accept. If the smallest eigenvalue is above b, then no matter what state the prover provides, the phase estimation algorithm will project onto one of the eigenstates and determine the corresponding eigenvalue, which will necessarily be above b.

More concretely, we have

6.2 QMA-hardness

The main way that this works is that we will use the well known Kitaev Hamiltonian, with some particular changes so that we get taken to a Hamiltonian of a particular form. Once we have that form, we can easily see that the result we want.

6.2.1 Kitaev Hamiltonian

With the definition of the class **QMA**, the requirement is that for each input there exists some quantum circuit and some particular input state that the circuit either accepts or rejects. When attempting to prove that a particular Hamiltonian has a similar computational power, we need to construct a "circuit-to-Hamiltionian" map. The predominant (and really only) such map is the so-called Kitaev-Hamiltonian.

In this mapping, we attempt to encode the computation into the ground space of the Hamiltonian, in a similar manner to how the proof that 3-SAT is NP-Hard encodes the entire computation of a nondeterministic Turing Machine. [**TO DO:** *NP-hardness of 3-Sat reference*] However, we run into a problem on how to insure that neighboring time steps are only seperated by a single local unitary. In the classical case we can write down the entire state of the system at each timestep, or else only write down the changes that occur at each time step. In the first case we run into a problem in that information is copied between time steps, which is impossible for a general state by the no-cloning theorem [**TO DO:** *reference no-cloning*] while the second case quickly becomes infeasible as the changes to the quantum state might effect many basis states.

Kitaev worked around this problem by enlarging the Hilbert space on which the circuit acts, by having both a clock and a state register. The computation of the system was then encoded as an entangled state between these two registers. In this way, by having a projection into those states that evolve correctly for a particular time step, we can have a local check for the correctness of evolution.

In particular, if a given circuit $\mathcal{C}$ acts on $\mathbb{C}^{2^m}$ and can be written as $\mathcal{C} = U_T U_{T-1} \cdots U_1$, then the Kitaev Hamiltonian $H_{\mathcal{C}}$ acts on the Hilbert space $\mathbb{C}^{2^m} \otimes \mathbb{C}^{T+1}$, and can be written

as

$$H_{\mathcal{C}} = \sum_{t=0}^{T-1} \left(\mathbb{I}_{\mathbb{C}^{2^m}} \otimes |t\rangle - U_{t+1} \otimes |t+1\rangle\right)\left(\mathbb{I}_{\mathbb{C}^{2^m}} \otimes \langle t| - U_{t+1}^{\dagger} \otimes \langle t+1|\right) = \sum_{t=0}^{T-1} H_t \tag{6.1}$$

Note that each term H_t is a projector off those states of the form

$$|\psi\rangle \otimes |t\rangle + U_{t+1}|\psi\rangle \otimes |t+1\rangle. \tag{6.2}$$

Hence, we have that the ground state of H_C corresponds to the history states:

$$|\psi_{\text{hist}}\rangle = \sum_{t=0}^{T} U_t U_{t-1} \cdots U_1 |\psi\rangle \otimes |t\rangle. \tag{6.3}$$

These states encode the computation, as for a given initial state $|\psi\rangle$, the projection onto the time register gives the state of the computation at time t. Note that the energy gap for this Hamiltonian is exactly $1 - \cos(\pi/T)$, as the Hamiltonian is unitarily equivalent to a quantum walk on a line of length T.

With this mapping corresponding to a particular circuit, we can then force the initial state to have a particular form by adding in projectors tensored with a projection onto the $|t = 0\rangle$ state, with a similar projection for the requisite form of the final state. Putting everything together we then have a log-local Hamiltonian that will have a polynomial gap depending on whether the initial circuit accepted or rejected.

One can then show that this Hamiltonian will have a low energy eigenvector if and only if the corresponding circuit $\mathcal{C}$ has an accepting input.

6.2.2 Transformation to Adjacency Matrix

While the above prescription works well for the conversion to local-Hamiltonians in the general case, in the situation we are interested in we want all of the non-zero matrix elements to be the same value. As the matrix elements of $H_{\mathcal{C}}$ are related to the matrix values of the unitaries involved in the circuit $\mathcal{C}$, we thus want to force the matrix values of $\mathcal{C}$ to all be of the same form.

To enforce this, we suppose $\mathcal{C}$ implements a unitary

$$U_{\mathcal{C}_x} = U_M \ldots U_2 U_1 \tag{6.4}$$

where each U_i acts as

$$\mathcal{G} = \{H, HT, (HT)^{\dagger}, (H \otimes \mathbb{I})\,\text{CNOT}\} \tag{6.5}$$

on some qubits, and the identity on the rest.

Note that this gate set is universal, as we can easily simulate the gate set $\{H, T, \text{CNOT}\}$ with gates from $\mathcal{G}$ since $H^2 = \mathbb{I}$ and we can thus cancel the H terms before the interesting portion of the gates. Further, each non-zero matrix element of these unitaries has norm $2^{-1/2}$, as we wanted.

However, when we look at one of the local terms in the Hamiltonian, we find that not all of the matrix elements have the same norm. In particular, we find that

$$H_t = \big(\mathbb{I}_{\mathbb{C}^{2^m}} \otimes |t\rangle - U_{t+1} \otimes |t+1\rangle\big)\big(\mathbb{I}_{\mathbb{C}^{2^m}} \otimes \langle t| - U_{t+1}^\dagger \otimes \langle t+1|\big) \tag{6.6}$$

$$= \mathbb{I}_{\mathbb{C}^{2^m}} \otimes \big(|t\rangle\langle t| + |t+1\rangle\langle t+1|\big) - \big(U_{t+1} \otimes |t+1\rangle\langle t| + U_{t+1}^\dagger \otimes |t\rangle\langle t+1|\big). \tag{6.7}$$

While each off-diagonal term is either zero or has norm $2^{-1/2}$ in (6.7), the diagonal terms have norm 1. When each term is summed, we almost have that the sum of the diagonal terms are proportional to the identity, but unfortunately the boundary terms (with $t = 0$ or $t = T$) are only involved in one unitary. However, this problem can be avoided by having circular time, in which we both compute and uncompute the comptutation. With this, each timestep is involved in exactly two local terms, and thus the diagonal term is proportional to the identity.

With this, it will be convenient to consider

$$U_{\mathcal{C}}^\dagger U_{\mathcal{C}} = W_{2M} \dots W_2 W_1 \tag{6.8}$$

where

$$W_t = \begin{cases} U_t & 1 \le t \le M \\ U_{2M+1-t}^\dagger & M+1 \le t \le 2M. \end{cases} \tag{6.9}$$

As in Section 6.2.1 we start with a version of the Feynman-Kitaev Hamiltonian (with a different norm) [21, **?**] acting on the Hilbert space $\mathcal{H}_{\text{comp}} \otimes \mathcal{H}_{\text{clock}}$ where $\mathcal{H}_{\text{comp}} = (\mathbb{C}^2)^{\otimes m}$ is an m-qubit computational register and $\mathcal{H}_{\text{clock}} = \mathbb{C}^{2M}$ is a $2M$-level register with periodic boundary conditions (i.e., we let $|2M+1\rangle = |1\rangle$). However, we then subtract a term proportional to the identity, which yields the Hamiltonian

$$H_{\mathcal{C}} = -\sqrt{2}\sum_{t=1}^{2M} \left(W_t^\dagger \otimes |t\rangle\langle t+1| + W_t \otimes |t+1\rangle\langle t|\right). \tag{6.10}$$

Note that

$$V^\dagger H_{\mathcal{C}} V = -\sqrt{2}\sum_{t=1}^{2M} \left(\mathbb{I} \otimes |t\rangle\langle t+1| + \mathbb{I} \otimes |t+1\rangle\langle t|\right) \tag{6.11}$$

where

$$V = \sum_{t=1}^{2M} \left(\prod_{j=t-1}^{1} W_j\right) \otimes |t\rangle\langle t| \tag{6.12}$$

and $W_0 = 1$. Since V is unitary, the eigenvalues of H_x are the same as the eigenvalues of (6.11), namely

$$-2\sqrt{2}\cos\left(\frac{\pi\ell}{M}\right) \tag{6.13}$$

for $\ell = 0, \dots, 2M-1$. The ground energy of (6.11) is $-2\sqrt{2}$ and its ground space is spanned by

$$|\phi\rangle \frac{1}{\sqrt{2M}} \sum_{j=1}^{2M} |t\rangle, \quad |\phi\rangle \in \Lambda \tag{6.14}$$

where Λ is any orthonormal basis for $\mathcal{H}_{\text{comp}}$. A basis for the ground space of H_x is therefore

$$V\left(|\phi\rangle\frac{1}{\sqrt{2M}}\sum_{j=1}^{2M}|t\rangle\right) = \frac{1}{\sqrt{2M}}\sum_{t=1}^{2M} W_{t-1}W_{t-2}\ldots W_1|\phi\rangle|t\rangle \tag{6.15}$$

where $|\phi\rangle \in \Lambda$. The first excited energy of H_x is

$$\eta = -2\sqrt{2}\cos\left(\frac{\pi}{M}\right) \tag{6.16}$$

and the gap between ground and first excited energies is lower bounded as

$$\eta + 2\sqrt{2} \geq \sqrt{2}\frac{\pi^2}{M^2} \tag{6.17}$$

(using the fact that $1-\cos(x) \leq \frac{x^2}{2}$).

The universal set $\mathcal{G}$ is chosen so that each gate has nonzero entries that are integer powers of $\omega = e^{i\frac{\pi}{4}}$. Correspondingly, the nonzero standard basis matrix elements of $H_{\mathcal{C}}$ are also integer powers of $\omega = e^{i\frac{\pi}{4}}$. We consider the 8×8 shift operator

$$S = \sum_{j=0}^{7}|j+1 \bmod 8\rangle\langle j| \tag{6.18}$$

and note that ω is an eigenvalue of S with eigenvector

$$|\omega\rangle = \frac{1}{\sqrt{8}}\sum_{j=0}^{7}\omega^{-j}|j\rangle. \tag{6.19}$$

We modify $H_{\mathcal{C}}$ as follows. For each operator $-\sqrt{2}H$, $-\sqrt{2}HT$, $-\sqrt{2}(HT)^\dagger$, or $-\sqrt{2}\,(H\otimes\mathbb{I})\,\text{CNOT}$ appearing in equation (6.10), define another operator that acts on $\mathbb{C}^2\otimes\mathbb{C}^8$ or $\mathbb{C}^4\otimes\mathbb{C}^8$ (as appropriate) by replacing nonzero matrix elements with powers of the operator S:

$$\omega^k \mapsto S^k.$$

Matrix elements that are zero are mapped to the 8×8 all-zeroes matrix. Write $B(W)$ for the operators obtained by making this replacement, e.g.,

$$-\sqrt{2}HT = \begin{pmatrix}\omega^4 & \omega^5\\ \omega^4 & \omega\end{pmatrix} \mapsto B(HT) = \begin{pmatrix}S^4 & S^5\\ S^4 & S\end{pmatrix}.$$

Adjoining an 8-level ancilla as a third register and making this replacement in equation (**??**) gives

$$H_{\text{prop}} = \sum_{t=1}^{2M}\left(B(W_t)^\dagger_{13}\otimes|t\rangle\langle t+1|_2 + B(W_t)_{13}\otimes|t+1\rangle\langle t|_2\right) \tag{6.20}$$

which is a symmetric 0-1 matrix (the subscripts indicate which registers the operators act on). Note that H_{prop} commutes with S (acting on the 8-level ancilla) and therefore is block

diagonal with eight sectors. In the sector where S has eigenvalue ω, H_{prop} is identical to the Hamiltonian $H_{\mathcal{C}}$ that we started with (see equation (6.10)). There is also a sector (where S has eigenvalue ω^*) where the Hamiltonian is the element-wise complex conjugate of $H_{\mathcal{C}}$. We will add a term to H_{prop} that introduces an energy penalty for states in any of the other six sectors, ensuring that none of these states lie in the ground space.

To see what kind of energy penalty is needed, we lower bound the eigenvalues of H_{prop}. Note that for each $W \in \mathcal{G}$, $B(W)$ contains at most 2 ones in each row or column. Looking at equation (6.20) and using this fact, we see that each row and each column of H_{prop} contains at most four ones (with the remaining entries all zero). Therefore $\|H_{\text{prop}}\| \leq 4$, so every eigenvalue of H_{prop} is at least -4.

The matrix A_x associated with the circuit $\mathcal{C}_x$ acts on the Hilbert space

$$\mathcal{H}_{\text{comp}} \otimes \mathcal{H}_{\text{clock}} \otimes \mathcal{H}_{\text{anc}} \tag{6.21}$$

where $\mathcal{H}_{\text{anc}} = \mathbb{C}^8$ holds the 8-level ancilla. We define

$$A_x = H_{\text{prop}} + H_{\text{penalty}} + H_{\text{input}} + H_{\text{output}} \tag{6.22}$$

where

$$H_{\text{penalty}} = \mathbb{I} \otimes \mathbb{I} \otimes \left(S^3 + S^4 + S^5\right) \tag{6.23}$$

is the penalty ensuring that the ancilla register holds either $|\omega\rangle$ or $|\omega^*\rangle$ and the terms

$$H_{\text{input}} = \sum_{j=n_{\text{input}}+1}^{n} |1\rangle\langle 1|_j \otimes |1\rangle\langle 1| \otimes \mathbb{I}$$

$$H_{\text{output}} = |0\rangle\langle 0|_{\text{output}} \otimes |M+1\rangle\langle M+1| \otimes \mathbb{I}$$

ensure that the ancilla qubits are initialized in the state $|0\rangle$ when $t = 1$ and that the output qubit is in the state $|1\rangle\langle 1|$ when the circuit $\mathcal{C}_x$ has been applied (i.e., at time $t = M + 1$). Observe that A_x is a symmetric 0-1 matrix.

Now consider the ground space of the first two terms $H_{\text{prop}} + H_{\text{penalty}}$ in (6.22). Note that $[H_{\text{prop}}, H_{\text{penalty}}] = 0$, so these operators can be simultaneously diagonalized. Furthermore, H_{penalty} has smallest eigenvalue $-1-\sqrt{2}$, with eigenspace spanned by $|\omega\rangle$ and $|\omega^*\rangle$. One can also easily confirm that the first excited energy of H_{penalty} is -1.

The ground space of $H_{\text{prop}} + H_{\text{penalty}}$ lives in the sector where H_{penalty} has minimal eigenvalue $-1-\sqrt{2}$. To see this, note that within this sector H_{prop} has the same eigenvalues as H_x, and therefore has lowest eigenvalue $-2\sqrt{2}$. The minimum eigenvalue e_1 of $H_{\text{prop}} + H_{\text{penalty}}$ in this sector is

$$e_1 = -2\sqrt{2} + \left(-1 - \sqrt{2}\right) = -1 - 3\sqrt{2} = -5.24\ldots, \tag{6.24}$$

whereas in any other sector H_{penalty} has eigenvalue at least -1 and (using the fact that $H_{\text{prop}} \geq -4$) the minimum eigenvalue of $H_{\text{prop}} + H_{\text{penalty}}$ is at least -5. Thus, an orthonormal basis for the ground space of $H_{\text{prop}} + H_{\text{penalty}}$ is furnished by the states

$$\frac{1}{\sqrt{2M}} \sum_{t=1}^{2M} W_{t-1} W_{t-2} \ldots W_1 |\phi\rangle |t\rangle |\omega\rangle \tag{6.25}$$

$$\frac{1}{\sqrt{2M}} \sum_{t=1}^{2M} (W_{t-1} W_{t-2} \ldots W_1)^* |\phi^*\rangle |t\rangle |\omega^*\rangle \tag{6.26}$$

where $|\phi\rangle$ ranges over the basis Λ for $\mathcal{H}_{\text{comp}}$ and $*$ denotes (elementwise) complex conjugation.

At this point, we then have a symmetric 0-1 matrix whose ground-space is spanned by history states. While we have not yet shown that determining the ground energy of this matrix is **QMA**-hard, this graph is the result of our circuit-to-graph mapping.

6.2.3 Upper bound on the smallest eigenvalue for yes instances

Suppose x is a yes instance; then there exists some n_{input}-qubit state $|\psi_{\text{input}}\rangle$ satisfying $\text{AP}\left(\mathcal{C}_x, |\psi_{\text{input}}\rangle\right) \geq 1 - \frac{1}{2^{|x|}}$. Let

$$|\text{wit}\rangle = \frac{1}{\sqrt{2M}} \sum_{t=1}^{2M} W_{t-1} W_{t-2} \dots W_1 \left(|\psi_{\text{input}}\rangle |0\rangle^{\otimes n - n_{\text{input}}} \right) |t\rangle |\omega\rangle \tag{6.27}$$

and note that this state is in the e_1-energy ground space of $H_{\text{prop}} + H_{\text{penalty}}$ (since it has the form (6.25)). One can also directly verify that $|\text{wit}\rangle$ has zero energy for H_{input}. Thus

$$\begin{aligned}
\langle \text{wit}| A_x |\text{wit}\rangle &= e_1 + \langle \text{wit}| H_{\text{output}} |\text{wit}\rangle \\
&= e_1 + \frac{1}{2M} \langle \psi_{\text{input}}| \langle 0|^{\otimes n - n_{\text{input}}} U_{\mathcal{C}_x}^\dagger |0\rangle \langle 0|_{\text{output}} U_{\mathcal{C}_x} |\psi_{\text{input}}\rangle |0\rangle^{\otimes n - n_{\text{input}}} \\
&= e_1 + \frac{1}{2M} \left(1 - \text{AP}(\mathcal{C}_x, |\psi_{\text{input}}\rangle)\right) \\
&\leq e_1 + \frac{1}{2M} \frac{1}{2^{|x|}}.
\end{aligned}$$

6.2.4 Lower bound on the smallest eigenvalue for no instances

Now suppose x is a no instance. Then the verification circuit $\mathcal{C}_x$ has acceptance probability $\text{AP}\left(\mathcal{C}_x, |\psi\rangle\right) \leq \frac{1}{3}$ for all n_{input}-qubit input states $|\psi\rangle$.

We backtrack slightly to obtain bounds on the eigenvalue gaps of the Hamiltonians $H_{\text{prop}} + H_{\text{penalty}}$ and $H_{\text{prop}} + H_{\text{penalty}} + H_{\text{input}}$. We begin by showing that the energy gap of $H_{\text{prop}} + H_{\text{penalty}}$ is at least an inverse polynomial function of M. Subtracting a constant equal to the ground energy times the identity matrix sets the smallest eigenvalue to zero, and the smallest nonzero eigenvalue satisfies

$$\gamma(H_{\text{prop}} + H_{\text{penalty}} - e_1 \cdot \mathbb{I}) \geq \min \left\{ \sqrt{2} \frac{\pi^2}{M^2}, -5 - e_1 \right\} \geq \frac{1}{5M^2}. \tag{6.28}$$

since $-5 - e_1 \approx 0.24\ldots > \frac{1}{5}$. The first inequality above follows from the fact that every eigenvalue of H_{prop} in the range $[e_1, -5)$ is also an eigenvalue of H_x (as discussed above) and the bound (6.17) on the energy gap of H_x.

Now use the Nullspace Projection Lemma (Lemma **??**) with

$$H_A = H_{\text{prop}} + H_{\text{penalty}} - e_1 \cdot \mathbb{I} \qquad H_B = H_{\text{input}}. \tag{6.29}$$

Note that H_A and H_B are positive semidefinite. Let S_A be the ground space of H_A and consider the restriction $H_B|_{S_A}$. Here it is convenient to use the basis for S_A given by (6.25)

and (6.26) with $|\phi\rangle$ ranging over the computational basis states of n qubits. In this basis, $H_B|_{S_A}$ is diagonal with all diagonal entries equal to $\frac{1}{2M}$ times an integer, so $\gamma(H_B|_{S_A}) \geq \frac{1}{2M}$. We also have $\gamma(H_A) \geq \frac{1}{5M^2}$ from equation (6.28), and clearly $\|H_B\| \leq n$. Thus Lemma **??** gives

$$\gamma(H_{\text{prop}} + H_{\text{penalty}} + H_{\text{input}} - e_1 \cdot \mathbb{I}) \geq \frac{\left(\frac{1}{5M^2}\right)\left(\frac{1}{2M}\right)}{\frac{1}{5M^2} + \frac{1}{2M} + n} \geq \frac{1}{10M^3\,(1+n)} \geq \frac{1}{20M^3 n}. \tag{6.30}$$

Now consider adding the final term H_{output}. We use Lemma **??** again, now setting

$$H_A = H_{\text{prop}} + H_{\text{penalty}} + H_{\text{input}} - e_1 \cdot \mathbb{I} \qquad H_B = H_{\text{output}}. \tag{6.31}$$

Let S_A be the ground space of H_A. Note that it is spanned by states of the form (6.25) and (6.26) where $|\phi\rangle = |\psi\rangle|0\rangle^{\otimes n - n_{\text{input}}}$ and $|\psi\rangle$ ranges over any orthonormal basis of the n_{input}-qubit input register. The restriction $H_B|_{S_A}$ is block diagonal, with one block for states of the form

$$\frac{1}{\sqrt{2M}} \sum_{t=1}^{2M} W_{t-1} W_{t-2} \ldots W_1 \left(|\psi\rangle|0\rangle^{\otimes n - n_{\text{input}}}\right) |t\rangle|\omega\rangle \tag{6.32}$$

and another block for states of the form

$$\frac{1}{\sqrt{2M}} \sum_{t=1}^{2M} (W_{t-1} W_{t-2} \ldots W_1)^* \left(|\psi\rangle^*|0\rangle^{\otimes n - n_{\text{input}}}\right) |t\rangle|\omega^*\rangle. \tag{6.33}$$

We now show that the minimum eigenvalue of $H_B|_{S_A}$ is nonzero, and we lower bound it. We consider the two blocks separately. By linearity, every state in the first block can be written in the form (6.32) for some state $|\psi\rangle$. Thus the minimum eigenvalue within this block is the minimum expectation of H_{output} in a state (6.32), where the minimum is taken over all n_{input}-qubit states $|\psi\rangle$. This is equal to

$$\min_{|\psi\rangle} \frac{1}{2M} \left(1 - \text{AP}(\mathcal{C}_x, |\psi\rangle)\right) \geq \frac{1}{3M} \tag{6.34}$$

where we used the fact that $\text{AP}\left(\mathcal{C}_x, |\psi\rangle\right) \leq \frac{1}{3}$ for all $|\psi\rangle$. Likewise, every state in the second block can be written as (6.33) for some state $|\psi\rangle$, and the minimum eigenvalue within this block is

$$\min_{|\psi\rangle} \frac{1}{2M} \left(1 - \text{AP}(\mathcal{C}_x, |\psi\rangle)^*\right) \geq \frac{1}{3M} \tag{6.35}$$

(since $\text{AP}(\mathcal{C}_x, |\psi\rangle)^* = \text{AP}(\mathcal{C}_x, |\psi\rangle) \leq \frac{1}{3}$). Thus we see that $H_B|_{S_A}$ has an empty nullspace, so its smallest eigenvalue is equal to its smallest nonzero eigenvalue, namely

$$\gamma(H_B|_{S_A}) \geq \frac{1}{3M}. \tag{6.36}$$

Now applying Lemma **??** using this bound, the fact that $\|H_B\| = 1$, and the fact that $\gamma(H_A) \geq \frac{1}{20M^3 n}$ (from equation (6.30)), we get

$$\gamma(A_x - e_1 \cdot \mathbb{I}) \geq \frac{\frac{1}{60M^4 n}}{\frac{1}{20M^3 n} + \frac{1}{3M} + 1} \geq \frac{1}{120M^4 n}. \tag{6.37}$$

Since $H_B|_{S_A}$ has an empty nullspace, $A_x - e_1 \cdot \mathbb{I}$ has an empty nullspace, and this is a lower bound on its smallest eigenvalue.

6.3 Extensions and Discussion

While this result is interesting in its own right, as it shows that finding the ground energy of a sparse, row-computable matrix is **QMA**-complete, perhaps the most interesting result is that nothing particularly quantum is involved in the definition of the problem. In particular, the only condition we have on the matrix is that it is sparse, and row-computable. This condition might allow for a more natural understanding for more classically-minded computer scientists, as a **QMA**-complete problem could be stated without having to delve into any quantum computing.

As an additional problem, since the circuit-to-Hamiltonian map creates a 7-regular, simple graph, one might wonder if the removal of these conditions are necessary when the boundary terms are added. This is obviously going to be necessary, as otherwise we would have that determining the lowest eigenvalue of a Laplacian is **QMA**-complete, but it is a well known fact that the smallest eigenvalue of a Laplacian is zero.

[**TO DO:** *can I use the same techniques as the self-loop removal to remove self-loops from this system?*]

[**TO DO:** *Write more*]

Chapter 7

Ground energy of multi-particle quantum walk

With our proof that the ground state problem for a single-particle quantum walk is **QMA**-complete, we would now like to examine the corresponding problem for the multi-particle quantum walk. The similarities between the two systems make us expect that very similar results will hold for the multi-particle case, but we will again need to examine the problem in a lot of detail.

In particular, the **QMA**-completeness for the single particle walk was relatively straightforward, in that there is really only one particle to deal with. Because of this, we understand the dynamics and can exactly analyze the system on which things interact, leading to exact solutions for the energies of the resulting Hamiltonian. With the MPQW, a full analysis is currently beyond our knowledge, and our universality construction relied on a reduction to the cases with at most two interacting particles. In order to show that finding the ground energy of a MPQW is **QMA**-complete using our techniques, we'd need to again reduce to the case of a small number of particles.

To make this reduction, we will show that the problem is **QMA**-hard when restricted to the problem where the interaction term adds (almost) no energy to the ground state, so that the ground state is contained within the span of single-particle states that don't overlap. With this restriction, we will still have correlations between many particles, but we will be able to analyze the correlations and determine the corresponding ground energy.

7.1 MPQW Hamiltonian ground-energy problem

In order to make things precise, we will fix a particular finite-range interaction, and show that with this fixed interaction, the resulting question is **QMA**-complete to solve. In particular let $\mathcal{U}$ be an interaction with finite support and no negative coefficients. For a particular graph G, we can then define a Hamiltonian on such a graph as [**TO DO:** *find a correct way to define* $\mathcal{U}$]

$$H_{f,G} = \sum_{(i,j)\in E(G)} a_i a_j + a_j a_i + \sum_{i,j\in V(G)} U_{d(i,j)}(n_i, n_j) = H_{G,\text{move}} + H_{G,\text{int}}. \tag{7.1}$$

Note that because of the positivity restrictions placed on $\mathcal{U}$, we have that $H_{G,\text{int}}$ is positive semi-definite, and thus the ground energy of $H_{f,G}$ is at least the ground energy of $H_{G,\text{move}}$.

With this particular interaction, we can then construct the corresponding problem.

Note that these Hamiltonians actually act on an infinite dimensional Hilbert space, in that the number of particles is unbounded. In order to reduce the complexity of these problems to a reasonable amount, we restrict our attention to a particular number of particles. Once again, as each term in the Hamiltonian preserves the number of particles, we have that $H_{\mathcal{U},G}$ decomposes into blocks with a particular particle number, and we represent these blocks as $\overline{H}^N_{\mathcal{U},G}$.

Problem 3 ($\mathcal{U}$-interaction MPQW Hamiltonion)**.** Given as input a K-vertex graph G, a number of particles N, a real number c, and a precision parameter $\epsilon = 1/T$, where the positive integers N and T are given in unary, and the graph G is given as its adjacency matrix (a $K \times K$ symmetric 0-1 matrix), the $\mathcal{U}$-interaction MPQW Hamiltonian problem is to determine whether the smallest eigenvalue of $\overline{H}^N_{\mathcal{U},G}$ is at most c or is at least $c + \epsilon$, with a promise that one of these two cases hold.

7.1.1 MPQW Hamiltonian is contained in QMA

To prove that $\mathcal{U}$-interaction MPQW Hamiltonian problem is contained in **QMA**, we provide a verification algorithm satisfying the requirements of Definition **??**. In the Definition this algorithm is specified by a circuit involving only one measurement of the output qubit at the end of the computation. The procedure we describe below, which contains intermediate measurements in the computational basis, can be converted into a verification circuit of the desired form by standard techniques.

We are given an instance specified by G, N, c, and ϵ. We are also given an input state $|\phi\rangle$ of n_{input} qubits, where $n_{\text{input}} = \lceil \log_2 D_N \rceil$ and D_N is the dimension of $\mathcal{Z}_N(G)$ as given in equation (**??**). Note, using the inequality $\binom{a}{b} \leq a^b$ in equation (**??**), that $n_{\text{input}} = \mathcal{O}(K \log(N + K))$, where $K = |V|$ is the number of vertices in the graph G. We embed $\mathcal{Z}_N(G)$ into the space of n_{input} qubits straightforwardly as the subspace spanned by the first D_N standard basis vectors (with lexicographic ordering, say). The first step of the verification procedure is to measure the projector onto this space $\mathcal{Z}_N(G)$. If the measurement outcome is 1 then the resulting state $|\phi'\rangle$ is in $\mathcal{Z}_N(G)$ and we continue; otherwise we reject.

In the second step of the verification procedure, the goal is to measure $\bar{H}^N_G$ in the state $|\phi'\rangle$. The Hamiltonian $\bar{H}^N_G$ is sparse and efficiently row-computable, with norm

$$\left\|\bar{H}^N_G\right\| \leq \left\|H^N_G\right\| \leq N \left\|A(G)\right\| + \left\|\sum_{k \in V} \hat{n}_k \left(\hat{n}_k - 1\right)\right\| \leq NK + N^2. \tag{7.2}$$

We use phase estimation (see for example [**?**]) to estimate the energy of $|\phi'\rangle$, using sparse Hamiltonian simulation [1] to approximate evolution according to $\bar{H}^N_G$. We choose the parameters of the phase estimation so that, with probability at least $\frac{2}{3}$, it produces an approximation E of the energy with error at most $\frac{\epsilon}{4}$. This can be done in time $\text{poly}(N, K, \frac{1}{\epsilon})$. If $E \leq c + \frac{\epsilon}{2}$ then we accept; otherwise we reject.

We now show that this verification procedure satisfies the completeness and soundness requirements of Definition **??**. For a yes instance, an eigenvector of $\bar{H}_G^N$ with eigenvalue $e \leq c$ is accepted by this procedure as long as the energy E computed in the phase estimation step has the desired precision. To see this, note that we measure $|E - e| \leq \frac{\epsilon}{4}$, and hence $E \leq c + \frac{\epsilon}{4}$, with probability at least $\frac{2}{3}$. For a no instance, write $|\phi'\rangle \in \mathcal{Z}_N(G)$ for a state obtained after passing the first step. The value E computed by the subsequent phase estimation step satisfies $E \geq c + \frac{3\epsilon}{4}$ with probability at least $\frac{2}{3}$, in which case the state is rejected. From this we see that the probability of accepting a no instance is at most $\frac{1}{3}$.

7.1.2 Frustration-free

While showing that this problem is contained in **QMA**is relatively easy, in our proof of **QMA**-hardness we will want to impose additional structure on the problem. In particular, we will want the problem to have the extra promise that if the particular instance is a yes instance, then the interaction term will essentially add no energy to the ground state. In particular, we will want the ground state of the system to be a ground state for each term in the Hamilonian individually, which is usually a statement that the Hamiltonian is frustration-free.

The reason that this helps us is that it actually allows us to determine the actual ground energies of various Hamiltonians, and lets us convert the problem to one of adding positive semi-definite matrices. This allows us to use our Nullspace Projection Lemma (Lemma 2), and give strong bounds on the resulting eigenvalue gaps. Additionally, the guarantee that certain Hamilonians are frustration-free will allow us to give some additional results on various spin systems.

[**TO DO:** *does this work for both bosons and fermions?. I think it will, but I'm not sure. It might not be worth it to discuss fermions right now.*]

With all of this, let G be a graph, and let us assume that the interaction is $\mathcal{U}$. If we then restrict to the N-particle sector, we have that the Hamiltonian is given by

$$H_{\mathcal{U},G}^N = \sum_{(i,j)\in E(G)} (a_i^\dagger a_j + a_j^\dagger a_i) + \sum_{i,j\in V(G)} \mathcal{U}_{d(i,j)}(n_i, n_j) \tag{7.3}$$

$$= \sum_{w=1}^{N} A(G)^{(w)} + \sum_{i,j\in V(G)} \mathcal{U}_{d(i,j)}(\hat{n}_i, \hat{n}_j) \tag{7.4}$$

where

$$\hat{n}_i = \sum_{w=1}^{N} |\, i\,\rangle\langle\, i\,|^{(w)}. \tag{7.5}$$

Additionally, we will again assume that

$$H_{G,\text{move}}^N = \sum_{w=1}^{N} A(G)^{(w)} \tag{7.6}$$

is the movement term of the Hamiltonian, and that

$$H_{\mathcal{U},G,\text{int}}^N = \sum_{i,j\in V(G)} \mathcal{U}_{d(i,j)}(\hat{n}_i, \hat{n}_j) \tag{7.7}$$

is the interaction term of the Hamiltonian.

While $H^N_{\mathcal{U},G}$ acts on the entire $|V|^N$ dimensional system of distinguishable particles, we want to deal with indistinguishable particles (and in particular bosonic particles). As such, we will want to look at the restriction of $H^N_{\mathcal{U},G}$ to the bosonic subspace:

$$\overline{H}^N_{\mathcal{U},G} := H^N_{\mathcal{U},G}\big|_{\mathcal{Z}_N(G)} \tag{7.8}$$

[**TO DO:** *check boson/fermion*]

At this point, it will be extremely useful to add a term proportional to the identity in order to make a positive semidefinite operator. In particular, if we let $\mu(G)$ be the smallest eigenvalue of $A(G)$, we can consider

$$H_{\mathcal{U}}(G,N) = \overline{H}^n_{\mathcal{U},G} - N\mu(G) \tag{7.9}$$

which is a positive-semidefinite matrix. Additionally, as $\mu(G)$ can be efficiently computed using a classical polynomial-time algorithm, we have that the complexity of approximating the ground energy of $H_{\mathcal{U}}(G,N)$ is equivalent to the complexity of approximating the ground energy of $\overline{H}^N_{\mathcal{U},G}$.

We shall write

$$0 \leq \lambda^1_N(G) \leq \lambda^2_N(G) \leq \cdots \leq \lambda^{D_N}_N(G) \tag{7.10}$$

for the eigenvalues of $H_{\mathcal{U}}(G,N)$ and $\{|\lambda^j_N(G)\rangle\}$ for the associated eigenvectors.

Note that when $\lambda^1_N(G) = 1$, the ground energy of the N-particle MPQW Hamiltonian $\overline{H}^N_{\mathcal{U},G}$ is equal to N times the single-particle ground energy $\mu(G)$. In this case, we say that the N-particle MPQW Hamiltonian is frustration free, as the ground state minimizes both the movement term and the interaction term. We also define frustration freeness for N-particle states.

Definition 7 (Frustration-free state)**.** If $|\psi\rangle \in \mathcal{Z}_N(G)$ satisfies $H_{\mathcal{U}}(G,N)|\psi\rangle = 0$, then we say that $|\psi\rangle$ is an N-particle frustration-free state for $\mathcal{U}$ on G.

7.1.2.1 Basic properties

We now give some basic properties of $H_{\mathcal{U}}(G,N)$. In particular we will want to understand how the eigenvalues of the Hamiltonian change when we increase the number of particles, as well as understand such a system when looking at many disconnected copies of graphs.

Lemma 12. *For all $N > 1$, $\lambda^1_{N+1}(G) \geq \lambda^1_N(G)$.*

Proof. [**TO DO:** *Fix this for an arbitrary interaciton*] Let $\widehat{n}^N_i$ be the number operator (**??**) defined in the N-particle space and let $\widehat{n}^{N+1}_i$ be the corresponding operator in the $(N+1)$-particle space. Note that

$$\widehat{n}^{N+1}_i = \widehat{n}^N_i \otimes \mathbb{I} + |i\rangle\langle i|^{(N+1)} \geq \widehat{n}^N_i \otimes \mathbb{I}. \tag{7.11}$$

Using this and the fact that $A(G) \geq \mu(G)$, we get

$$H^{N+1}_G - (N+1)\,\mu(G) \geq \left(H^N_G - N\mu(G)\right) \otimes \mathbb{I}. \tag{7.12}$$

Hence

$$\lambda^1_{N+1}(G) = \min_{|\psi\rangle \in \mathcal{Z}_{N+1}(G):\ \langle\psi|\psi\rangle = 1} \langle\psi| H_G^{N+1} - (N+1)\,\mu(G) |\psi\rangle \tag{7.13}$$

$$\geq \min_{|\psi\rangle \in \mathcal{Z}_N(G)\otimes\mathbb{C}^{|V|}:\ \langle\psi|\psi\rangle = 1} \langle\psi| \left(H_G^N - N\mu(G)\right) \otimes \mathbb{I} |\psi\rangle \tag{7.14}$$

$$= \lambda^1_N(G) \tag{7.15}$$

(using the fact that $\mathcal{Z}_{N+1}(G) \subset \mathcal{Z}_N(G) \otimes \mathbb{C}^{|V|}$). □

We will encounter graphs G with more than one component. In the cases of interest, the smallest eigenvalue of the adjacency matrix for each component is the same. The following Lemma shows that the eigenvalues of $H(G,N)$ on such a graph can be written as sums of eigenvalues for the components. In this Lemma (and throughout the paper), we let $[k] = \{1, 2, \ldots, k\}$.

Lemma 13. *Suppose $G = \bigcup_{i=1}^k G_i$ with $\mu(G_1) = \mu(G_2) = \cdots = \mu(G_k)$. The eigenvalues of $H(G,N)$ are*

$$\sum_{i\in[k]:\ N_i \neq 0} \lambda^{y_i}_{N_i}(G_i) \tag{7.16}$$

where $N_1, \ldots, N_k \in \{0, 1, 2, \ldots\}$ with $\sum_i N_i = N$ and $y_i \in [D_{N_i}]$. The corresponding eigenvectors are (up to normalization)

$$\mathrm{Sym}\left(\prod_{i\in[k]:\ N_i \neq 0} |\lambda^{y_i}_{N_i}(G_i)\rangle \right). \tag{7.17}$$

Proof. Recall that the action of $H_G - N\mu(G)$ on the Hilbert space (**??**) is the same as the action of $H(G,N)$ on the Hilbert space $\mathcal{Z}_N(G)$. States in these Hilbert spaces are identified via the mapping described in equation (**??**). It is convenient to prove the Lemma by working with the second-quantized Hamiltonian H_G. We then translate our results into the first-quantized picture to obtain the stated claims.

For a graph with k components, equation (**??**) gives

$$H_G = \sum_{i=1}^k H_{G_i} \tag{7.18}$$

where $[H_{G_i}, H_{G_j}] = 0$. Label each vertex of G by (a,b) where $b \in [k]$ and $a \in [|V_b|]$, where V_b is the vertex set of the component G_b. An occupation number basis state (**??**) can be written

$$|l_{1,1}, \ldots, l_{|V_1|,1}\rangle |l_{1,2}, \ldots, l_{|V_2|,2}\rangle \ldots |l_{1,k}, \ldots, l_{|V_k|,k}\rangle. \tag{7.19}$$

The Hamiltonian $H_G - N\mu(G)$ conserves the number of particles N_b in each component b. Within the sector corresponding to a given set $N_1, \ldots, N_k$ with $\sum_{i\in[k]} N_i = N$, we have

$$\left(H_G - N\mu(G)\right) |l_{1,1}, \ldots, l_{|V_1|,1}\rangle |l_{1,2}, \ldots, l_{|V_2|,2}\rangle \ldots |l_{1,k}, \ldots, l_{|V_k|,k}\rangle \tag{7.20}$$

$$= \left(H_{G_1} - N_1\mu(G_1) |l_{1,1}, \ldots, l_{|V_1|,1}\rangle\right) |l_{1,2}, \ldots, l_{|V_2|,2}\rangle \ldots |l_{1,k}, \ldots, l_{|V_k|,k}\rangle \tag{7.21}$$

$$+ |l_{1,1}, \ldots, l_{|V_1|,1}\rangle \left(H_{G_2} - N_2\mu(G_2) |l_{1,2}, \ldots, l_{|V_2|,2}\rangle\right) \ldots |l_{1,k}, \ldots, l_{|V_k|,k}\rangle + \cdots \tag{7.22}$$

$$+ |l_{1,1}, \ldots, l_{|V_1|,1}\rangle |l_{1,2}, \ldots, l_{|V_2|,2}\rangle \ldots \left(H_{G_k} - N_k\mu(G_k) |l_{1,k}, \ldots, l_{|V_k|,k}\rangle\right), \tag{7.23}$$

where we used the fact that $\mu(G_i) = \mu(G)$ for $i \in [k]$. From this equation we see that the eigenstates of H_G can be obtained as product states with k factors in the basis (7.19). In each such product state, the ith factor is an eigenstate of $H_{G_i} - N_i\mu(G_i) = H_{G_i} - N_i\mu(G)$ in the N_i-particle sector, with eigenvalue $\lambda_{N_i}^{j_i}(G_i)$. Rewriting this result in the "first-quantized" language, we obtain the Lemma. □

7.1.2.2 QMA-hard problem

With all of these definitions floating around, it will then be useful to actually define the basic problem that we will show is **QMA**-hard. In particular, we have that for any positive integer α, the following problem:

Problem 4 (α-frustration-free$\mathcal{U}$-interaction MPQW Hamiltonian)**.** We are given as input a K-vertex simple graph G, a number of particles $N \leq K$, and a precision parameter $\epsilon = 1/T$, where the positive integers N and $T \geq 4K$ are given in unary, and the graph G is given as its adjacency matrix (a $K \times K$ symmetric 0-1 matrix). We arp promised that either $\lambda_N^1(G) \leq \epsilon^\alpha$ (a yes instance), or else that $\lambda_N^1(G) \geq \epsilon + \epsilon^\alpha$ (a no instance) and we are asked to decide which is the case.

Note that for each interaction type, this is an infinite family of problems. The positive integer α parameterizes how much the yes cases can deviate from a true frustration-free case. The reason that we define the problem in such a way is that it will facilitate the reduction found in Chapter 8.

Note that this is a special case of the $\mathcal{U}$-interaction MPQW Hamiltonian, with $c = N\mu(G) + \epsilon^\alpha$. As such, if we show that the α-frustration free $\mathcal{U}$-interaction MPQW Hamiltonian problem is **QMA**-hard, we will also show that the non-frustration-free problem is **QMA**-complete.

7.2 Useful graph primitives

At this point, we will want to construct a graph for which our **QMA**-hardness result will hold. As such, we will at this point restrict our attention to a particular interaction, $\mathcal{U}$. While the idea behind the construction of these graphs will not change, the exact graph will depend on both the largest distance for which there is a non-zero interaction. We will want to construct a foundational graph that does not have a two-particle ground state, and also we will want to ensure that our connections between these building blocks will not have multiple particles interacting except on specially chosen building blocks.

As such, let us assume that the minimum distance that the interaction $\mathcal{U}$ has non-zero interactions is $d_{\min}$, while the maximum distance is $d_{\max}$. Our graph will only depend on $d_{\max}$, but it will be useful to also know $d_{\min}$. We will also assume that $\mathcal{U}_{d_{\min}}^{(1,1)} > 0$, so that there is some energy penalty if two particles are at a distance $d_{\min}$ (assuming that $d_{\min} > 0$ — otherwise we will assume that $\mathcal{U}_0^2 > 0$).

Additionally, we will want the eventual graph to be a simple graph, so that there is always at most a single edge between two vertices and no self-loops. Unfortunately, our proof strategy will involve adding many positive semi-definite terms to the adjacency matrix, which

correspond to adding in edges and self-loops. As such, we will instead force every vertex in the graph to contain a self-loop, so that by removing all of the self loops we only shift the energy levels by a constant amount. Keep this in mind, as the eventual graph is defined.

With all of this said, however, this section will only define some useful foundational graphs that will be used in the final construction of the graph. All of these graphs will be constant sized, and we will show a spanning set for their single-particle and two-particle ground states. By construction, they will not have any three-particle frustration-free states.

7.2.1 Gate graphs

[**TO DO:** *rewrite this introduction*] In this section we define a class of graphs (*gate graphs*) and a diagrammatic notation for them (*gate diagrams*) that will allow us to construct the overall graph. We will also discuss the MPQW Hamiltonian acting on these graphs, with a particular emphasis on the low-energy states.

Every gate graph is constructed using a specific, finite-sized graph g_0 as a building block. This graph is shown in Figure 7.1 (for graphs with $d_{\min} <= 3$ and discussed in Section 7.2.1.1). These graphs are designed so that in the low energy sector, each copy of g_0 can only contain a single particle at a time, so that we can force particles to occupy certain states. Additionally, the low energy states correspond to the history states of simple single-qubit circuits, we can use these to encode simple computations as described in Section **??**.

In Section **??** we discuss the ground states of the Bose-Hubbard model on gate graphs. For any gate graph G, the smallest eigenvalue $\mu(G)$ of the adjacency matrix $A(G)$ satisfies $\mu(G) \geq -1 - 3\sqrt{2}$. It is convenient to define the constant

$$e_1 = -1 - 3\sqrt{2}. \tag{7.24}$$

When $\mu(G) = e_1$ we say G is an e_1-gate graph. We focus on the frustration-free states of e_1-gate graphs (recall from Definition **??** that $|\phi\rangle \in \mathcal{Z}_N(G)$ is frustration free iff $H(G,N)|\phi\rangle = 0$). We show that all such states live in a convenient subspace (called $\mathcal{I}(G,N)$) of the N-particle Hilbert space. This subspace has the property that no two (or more) particles ever occupy vertices of the same copy of g_0. The restriction to this subspace makes it easier to analyze the ground space.

In Section **??** we consider a class of subspaces that, like $\mathcal{I}(G,N)$, are defined by a set of constraints on the locations of N particles in an e_1-gate graph G. We state an "Occupancy Constraints Lemma" (proven in Appendix **??**) that relates a subspace of this form to the ground space of the Bose-Hubbard model on a graph derived from G.

7.2.1.1 The graph g_0

The graph g_0 shown in Figure 7.1 is constructed using the method of Chapter 6, with the single qubit circuit corresponding to a sequence of H and HT gates. The idea is to force the ground state of the resulting graph to correspond to these computations while also spreading the wave-function over most of the vertices. In this way, we can use the ground state to compute these single-particle unitaries while also forcing the graph to only have single-particle frustration free states.

In particular, let $k = 4 + 2\lceil \frac{d_{\max}}{2} \rceil$, and then let us look at the single-qubit circuit $\mathcal{C}_0$ with k gates U_j, for $j \in [k]$, where

$$U_1 = HT \qquad U_2 = (HT)^\dagger \tag{7.25}$$

and the rest of the $U_j = H$. We will eventually use the first four of these time steps as computations in the eventual gadgets, while the remaining time steps act as padding to ensure that this computational steps occur at a distance at least $d_{\max}$ from each other. As the circuit $\mathcal{C}_0$ implements an identity operation, we can easily concatenate these circuits and then output something using circular time as in the construction of Chapter 6. For our purposes, we will want to use 8 copies of the circuit in series, as the eventual gadgets we use will have 8 possible locations for interactions with other copies of g_0.

In particular, we will have that the 0-1 Hamiltonian corresponding to the eventual adjacency matrix of g_0 acts on the Hilbert space $\mathcal{H}(g_0) = \mathbb{C}^2 \otimes \mathbb{C}^{8k} \otimes \mathbb{C}^8$. If we then remember that $B(U)$ is the operator that takes $\omega \mapsto S$, where $\omega = e^{i\pi/4}$ and S is the shift operator acting on $\mathbb{C}^8$, we have that the component of the Hamiltonian corresponding to the circuit is

$$H_{\text{prop}} = -\sqrt{2} \sum_{t=0}^{8k} B(V_t)_{13} \otimes |t+1\rangle\langle t| + B(V_t^\dagger)_{13} \otimes |t\rangle\langle t+1|, \tag{7.26}$$

where

$$V_t = \begin{cases} HT & t = 0 \mod 8 \\ (HT)^\dagger & t = 1 \mod 8 \\ H & \text{otherwise.} \end{cases} \tag{7.27}$$

This term, along a penalty to the $\mathbb{C}^8$ Hilbert space given by

$$H_{\text{pen}} = \mathbb{I}_{\mathbb{C}^2} \otimes \mathbb{I}_{\mathbb{C}^{8k}} \otimes \left(S^3 + S^4 + S^3\right), \tag{7.28}$$

which forces the third register into a particularly useful form, allows us to guarantee that the ground state is a history state. Altogether, we then have that the adjacency matrix of $g(0)$ is given by

$$A(g_0) = H_{\text{prop}} + H_{\text{pen}}, \tag{7.29}$$

where each vertex is labeled by a computational basis state in the Hilbert space, namely (z, t, j) with $z \in \mathbb{F}_2$, $t \in [8k]$, and $j \in [8]$. The graph g_0 in the special case that $d_{\max} = 0$ is shown in Figure 7.1.

We can then use the results of Chapter 6 to calculate the smallest eigenvalue of $A(g_0)$, the corresponding eigenvectors, and the eigenvalue gap. In particular, we have that the smallest eigenvalue is

$$e_1 = -1 - 3\sqrt{2} = -5.24\ldots,, \tag{7.30}$$

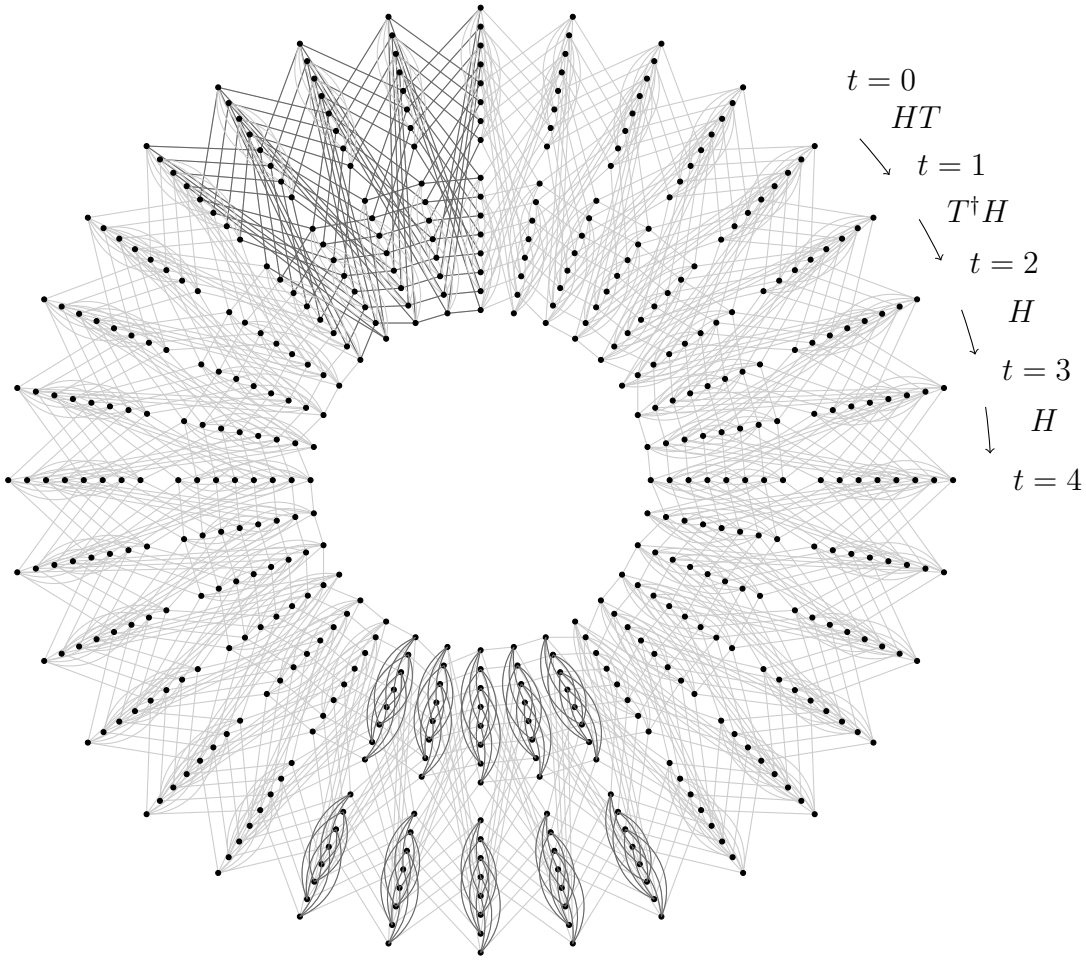

Figure 7.1: The graph g_0 for the case $d_{\max} = 0$. Vertices are arranged with each ray corresponding to a specific time t proceeding clockwise, with the outer 8 vertices corresponding to logical 0 and the inner 8 corresponding to logical 1, with the further breakdown into 8 vertices corresponding to the ancillary register. The difference in color for some edges is an attempt to highlight those edges corresponding to the penalty term (bottom of the figure) and the circuit (top left of the figure).

corresponding to a four dimensional ground space spanned by the states

$$|\psi_{z,0}\rangle = \frac{1}{\sqrt{8k}} \sum_{t=0}^{8k-1} \big(V_t V_{t-1} \cdots V_1\big)|z\rangle|t\rangle|\omega\rangle = \frac{1}{\sqrt{8k}} \sum_{t'=0}^{4k-1} |z\rangle|2t'\rangle|\omega\rangle + V_{2t'+1}|z\rangle|2t'+1\rangle|\omega\rangle \tag{7.31}$$

$$|\psi_{z,1}\rangle = \frac{1}{\sqrt{8k}} \sum_{t'=0}^{4k-1} |z\rangle|2t'\rangle|\overline{\omega}\rangle + V_{2t'+1} * |z\rangle|2t'+1\rangle|\overline{\omega}\rangle, \tag{7.32}$$

where

$$|\omega\rangle = \frac{1}{\sqrt{8}} \sum_{j=0}^{7} e^{i\pi j/4}|j\rangle \qquad \text{and} \qquad |\overline{\omega}\rangle = \frac{1}{\sqrt{8}} \sum_{j=0}^{7} e^{-i\pi j/4}|j\rangle.$$

Additionally, we have that the energy gap is at least

$$\lambda_1^2(g_0) \geq \sqrt{2}\cos\left(\frac{\pi}{4k}\right) \geq \frac{\pi\sqrt{2}}{16k^2} = c_k, \tag{7.33}$$

which is constant for constant interactions.

Note that the amplitudes of $|\psi_{z,0}\rangle$ in the above basis contain the result of computing either the identity, Hadamard, or HT gate acting on the "input" state $|z\rangle$, while the amplitudes $|\psi_{z,1}\rangle$ corresponds to the result of the identity, Hadamard or $\overline{HT}$ gate acting on the "input" state.

With these bounds on the single particle eigenstates, we can now show that the graph g_0 has no two-particle frustration-free states. By Lemma **??**, it follows that g_0 has no N-particle frustration-free states for $N \geq 2$. While we would like this to be true in general for all states, in the case of only onsite interactions ($d_{\max} = 0$) no anti-symmetric state is penalized by the interaction. As the ground space of $A(g_0)$ is degenerate, we then have that in this case there are two particle frustration-free states on g_0. However, we show that this is the only case for which this is true.

Lemma 14. *If $d_{max} > 0$, then $\lambda_2^1(g_0) > 0$ for all states. If $d_{max} = 0$, then when restricted to symmetric states, $\lambda_2^1(g_0) > 0$.*

Proof. Suppose (for a contradiction) that $|Q\rangle \in \mathcal{H}(g_0)^{\otimes 2}$ is a nonzero vector in the nullspace of $H(g_0, 2)$, so

$$H_{g_0}^2|Q\rangle = \left(A(g_0) \otimes \mathbb{I} + \mathbb{I} \otimes A(g_0) + \sum_{i,j \in g_0} \mathcal{U}_{d(i,j)}(\hat{n}_i, \hat{n}_j)\right)|Q\rangle = 2e_1|Q\rangle. \tag{7.34}$$

This implies

$$A(g_0) \otimes \mathbb{I}|Q\rangle = \mathbb{I} \otimes A(g_0)|Q\rangle = e_1|Q\rangle \tag{7.35}$$

since $A(g_0)$ has smallest eigenvalue e_1 and the interaction term is positive semidefinite. We can therefore write

$$|Q\rangle = \sum_{z,a,x,y \in \mathbb{F}_2} Q_{za,xy}|\psi_{z,a}\rangle|\psi_{x,y}\rangle \tag{7.36}$$

and

$$\mathcal{U}_{d(u,v)}(\hat{n}_u, \hat{n}_v)|Q\rangle = 0 \tag{7.37}$$

for all vertices $u, v \in g_0$.

We then have by assumption that $\mathcal{U}^{(1,1)}_{d_{\max}} > 0$ if $d_{\max} > 0$ or $\mathcal{U}^2_0 > 0$ if $d_{\max} = 0$, and thus for all vertices u, v of distance $d_{\max}$,

$$\langle u, v \,|\, Q \rangle = 0. \tag{7.38}$$

We will use this equation to show a contradiction, so that $|Q\rangle$ cannot exist.

Note that vertices of the form (x, T, j) and $(z, T + t, k)$ are at least a distance t apart for $t > 0$ and $t \leq d_{\max}$, since edges only exist between vertices corresponding to times that differ by at most 1. Further, as each unitary for $t \geq 2$ corresponds to a Hadamard, and only connects vertices with the same j or j's that differ by 4, we have that only vertices of the form $(x, 2, j)$ and $(z, 2 + t, j)$ or $(x, 2, j)$ and $(z, 2 + t, j + 4)$ can be a distance t apart; all other pairs of vertices must be at a distance of at least $t + 1$.

With all of this in mind, let us assume that $d_{\max}$ is an even integer greater than zero. We then have that the vertices $(0, 2, j)$ and $(0, 1 + d_{\max}, j + 4)$ are a distance $d_{\max} - 1$ apart. Further, we have that $(0, 1+d_{\max}, j+4)$ is also connected to the vertices $(0, 1+d_{\max}, j+1)$ and $(0, 1 + d_{\max}, j - 1)$, and thus we have that the vertices $u = (0, 2, j)$ and $v = (0, 1 + d_{\max}, j + \ell)$ are a distance $d_{\max}$ apart for all $j \in [8]$ and for $\ell = \pm 1$. Using (7.38) with these pairs of vertices we then have that

$$\begin{aligned}
\langle u, v \,|\, Q \rangle &= \sum_{x,a,z,b \in \mathbb{F}_2} Q_{xa,zb} \langle 0, 2, j \,|\, \psi_{x,a} \rangle \langle 0, 1 + d_{\max}, j + \ell \,|\, \psi_{zb} \rangle && (7.39) \\
&= \frac{1}{64k} \sum_{x,a,z,b \in \mathbb{F}_2} Q_{xa,zb} \langle 0 \,|\, x \rangle \langle 0 \,|H|\, z \rangle \omega^{(-1)^a j + (-1)^b (j+\ell)} && (7.40) \\
&= \frac{1}{128k} \big((Q_{00,00} + Q_{00,10}) \omega^{2j+\ell} + (Q_{00,01} + Q_{00,11}) \omega^{-\ell} \\
&\qquad + (Q_{01,00} + Q_{01,10}) \omega^{\ell} + (Q_{01,01} + Q_{01,11}) \omega^{-2j-\ell} \big), && (7.41)
\end{aligned}$$

and thus we have that $Q_{0a,0b} = -Q_{0a,1b}$ for all $a, b \in \mathbb{F}_2$. Using the same reasoning with vertices $u = (0, 2, j)$ and $v = (1, 1 + d_{\max}, j + \ell)$ with $\ell = \pm 1$ then gives us))

$$\begin{aligned}
\langle u, v \,|\, Q \rangle &= \sum_{x,a,z,b \in \mathbb{F}_2} Q_{xa,zb} \langle 0, 2, j \,|\, \psi_{x,a} \rangle \langle 1, d_{\max}, j + \ell \,|\, \psi_{zb} \rangle && (7.42) \\
&= \frac{1}{64k} \sum_{x,a,z,b \in \mathbb{F}_2} Q_{xa,zb} \langle 0 \,|\, x \rangle \langle 1 \,|H|\, z \rangle \omega^{(-1)^a j + (-1)^b (j+\ell)} && (7.43) \\
&= \frac{1}{128k} \big((Q_{00,00} - Q_{00,10} \omega^{2j+\ell} + (Q_{00,01} - Q_{00,11}) \omega^{-\ell} \\
&\qquad + (Q_{01,00} - Q_{01,10}) \omega^{\ell} + (Q_{01,01} - Q_{01,11}) \omega^{-2j-\ell} \big), && (7.44)
\end{aligned}$$

which combined with our previous results show that $Q_{0a,zb} = 0$ for all $a, b, z \in \mathbb{F}_2$. Again using the same reasoning with $u = (1, 2, j)$ and $v = (1, 1 + d_{\max}, j + \ell)$ for $\ell = 3$ or $\ell = 5$

gives us

$$\langle u, v \,|\, Q \rangle = \sum_{x,a,z,b \in \mathbb{F}_2} Q_{xa,zb} \langle 1, 2, j \,|\, \psi_{x,a} \rangle \langle 1, 1 + d_{\max}, j + \ell \,|\, \psi_{zb} \rangle \tag{7.45}$$

$$= \frac{1}{64k} \sum_{x,a,z,b \in \mathbb{F}_2} Q_{xa,zb} \langle 1 \,|\, x \rangle \langle 1 \,|H|\, z \rangle \omega^{(-1)^a j + (-1)^b (j+\ell)} \tag{7.46}$$

$$= \frac{1}{128k} \big((Q_{10,00} - Q_{10,10} \omega^{2j+\ell} + (Q_{10,01} - Q_{10,11}) \omega^{-\ell} + (Q_{11,00} - Q_{11,10}) \omega^{\ell} + (Q_{11,01} - Q_{11,11}) \omega^{-2j-\ell} \big), \tag{7.47}$$

which forces $Q_{1a,0b} = Q_{1a,1b}$ for all $a, b \in \mathbb{F}_2$. Finally, using this same technique for $u = (1, 2, j)$ and $v = (0, 1 + d_{\max}, j + \ell)$ with $\ell = \pm 1$ gives us

$$\langle u, v \,|\, Q \rangle = \sum_{x,a,z,b \in \mathbb{F}_2} Q_{xa,zb} \langle 1, 2, j \,|\, \psi_{x,a} \rangle \langle 0, 1 + d_{\max}, j + \ell \,|\, \psi_{zb} \rangle \tag{7.48}$$

$$= \frac{1}{64k} \sum_{x,a,z,b \in \mathbb{F}_2} Q_{xa,zb} \langle 1 \,|\, x \rangle \langle 0 \,|H|\, z \rangle \omega^{(-1)^a j + (-1)^b (j+\ell)} \tag{7.49}$$

$$= \frac{1}{128k} \big((Q_{10,00} + Q_{10,10} \omega^{2j+\ell} + (Q_{10,01} + Q_{10,11}) \omega^{-\ell} + (Q_{11,00} + Q_{11,10}) \omega^{\ell} + (Q_{11,01} + Q_{11,11}) \omega^{-2j-\ell} \big), \tag{7.50}$$

which combined with our previous results implies that $Q_{1a,zb} = 0$ for all $a, b, z \in \mathbb{F}_2$. Putting this together, we then have each $Q_{xa,zb} = 0$, and thus $|Q\rangle$ does not exist; in other words, if $d_{\max} > 0$ is even, then the nullspace of $H(g_0, 2)$ is empty.

Now let us assume that $d_{\max}$ is a positive odd integer. For all such $d_{\max}$, we can then use equation (7.38) with vertices $u = (y, 2, j)$ and $v = (y, 1 + d_{\max}, j + \ell)$ for $y \in \mathbb{F}_2$, $j \in [8]$, and $\ell = \pm 1$ to see

$$\langle u, v \,|\, Q \rangle = \sum_{x,a,z,b \in \mathbb{F}_2} Q_{xa,zb} \langle y, 2, j \,|\, \psi_{x,a} \rangle \langle y, 1 + d_{\max}, j + \ell \,|\, \psi_{zb} \rangle \tag{7.51}$$

$$= \frac{1}{64k} \sum_{x,a,z,b \in \mathbb{F}_2} Q_{xa,zb} \langle y \,|\, x \rangle \langle y \,|\, z \rangle \omega^{(-1)^a j + (-1)^b (j+\ell)} \tag{7.52}$$

$$= \frac{1}{64k} \big(Q_{y0,y0} \omega^{2j+\ell} + Q_{y0,y1} \omega^{-\ell} + Q_{y1,y0} \omega^{\ell} + Q_{y1,y1} \omega^{-2j-\ell} \big), \tag{7.53}$$

to see that $Q_{ya,yb} = 0$ for all $a, b, y \in \mathbb{F}_2$. With this result, let us now examine vertices at times that differ by $d_{\max}$. Using equation (7.38) with $u = (0, 2, j)$ and $v = (0, 2 + d_{\max}, j + 4)$

gives us

$$\langle u, v \,|\, Q \rangle = \sum_{x,a,z,b \in \mathbb{F}_2} Q_{xa,zb} \langle 0, 2, j \,|\, \psi_{x,a} \rangle \langle 0, 2 + d_{\max}, j + 4 \,|\, \psi_{zb} \rangle \tag{7.54}$$

$$= \frac{1}{64k} \sum_{x,a,z,b \in \mathbb{F}_2} Q_{xa,zb} \langle 0 \,|\, x \rangle \langle 0 \,|\, H \,|\, z \rangle \omega^{(-1)^a j + (-1)^b (j+4)} \tag{7.55}$$

$$= -\frac{1}{64k\sqrt{2}} \big((Q_{00,00} + Q_{00,10}) \omega^{2j} + (Q_{01,01} + Q_{01,11}) \omega^{-2j} + (Q_{01,00} + Q_{01,10} + Q_{00,01} + Q_{00,11}) \big) \tag{7.56}$$

$$= -\frac{1}{64k\sqrt{2}} \big(Q_{00,10} \omega^{2j} + Q_{01,11} \omega^{-2j} + (Q_{01,10} + Q_{00,11}) \big) \tag{7.57}$$

where in the last line we used the fact that $Q_{za,zb} = 0$. A similar result with $u = (0, 2, j)$ and $v = (1, 2 + d_{\max}, j + 4$ then gives us that $Q_{0a,zb} = 0$. Finally, repeating this same procedure with $u = (1, 2, j)$ and $v = (1, 2 + d_{\max}, j)$ and with $u = (1, 2, j)$ and $v = (0, 2 + d_{\max}, j + 4)$ gives us that $Q_{1a,zb} = 0$. Putting this all together, we have that each $Q_{xa,zb} = 0$ and thus $|Q\rangle$ does not exist if $d_{\max}$ is an odd integer.

Finally, let us assume that $d_{\max} = 0$, and that the state $|Q\rangle$ is symmetric (so that $Q_{xa,zb} = Q_{zb,xa}$). With these assumptions, let us examine equation (7.38) with $u = v = (y, 0, j)$ for $y \in \mathbb{F}_2$ and $j \in [8]$:

$$\langle u, v \,|\, Q \rangle = \sum_{x,a,z,b \in \mathbb{F}_2} Q_{xa,zb} \langle y, 0, j \,|\, \psi_{x,a} \rangle \langle y, 0, j \,|\, \psi_{zb} \rangle \tag{7.58}$$

$$= \frac{1}{64k} \sum_{x,a,z,b \in \mathbb{F}_2} Q_{xa,zb} \langle y \,|\, x \rangle \langle y \,|\, z \rangle \omega^{(-1)^a j + (-1)^b j} \tag{7.59}$$

$$= \frac{1}{64k} \big(Q_{y0,y0} \omega^{2j} + Q_{y1,y1} \omega^{-2j} + 2 Q_{y1,y0} \big). \tag{7.60}$$

Evaluating these equations together then gives us that $Q_{xa,xb} = 0$ for all $a, b, x \in \mathbb{F}_2$. If we now use equation (7.38) with $u = v = (0, 3, j)$ for all $j \in [8]$, we find that

$$\langle u, v \,|\, Q \rangle = \sum_{x,a,z,b \in \mathbb{F}_2} Q_{xa,zb} \langle 0, 3, j \,|\, \psi_{x,a} \rangle \langle 0, 3, j \,|\, \psi_{zb} \rangle \tag{7.61}$$

$$= \frac{1}{64k} \sum_{x,a,z,b \in \mathbb{F}_2} Q_{xa,zb} \langle 0 \,|\, H \,|\, x \rangle \langle 0 \,|\, H \,|\, z \rangle \omega^{(-1)^a j + (-1)^b j} \tag{7.62}$$

$$= \frac{1}{128k} \big(2 Q_{00,10} \omega^{2j} + 2 Q_{01,11} \omega^{-2j} + (2 Q_{01,10} + 2 Q_{00,11}) \big). \tag{7.63}$$

and thus $Q_{00,10} = Q_{01,11} = 0$ and $Q_{01,10} = -Q_{00,11}$. If we now use (7.38) with the only

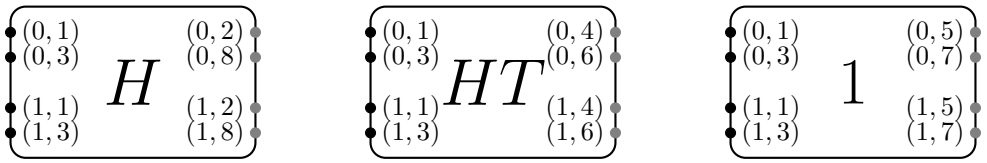

Figure 7.2: Diagram elements from which a gate diagram is constructed. Each diagram element is a schematic representation of the graph g_0 shown in Figure 7.1.

remaining vertices leading to novel restrictions, namely $u = v = (0, 1, 0)$, we find

$$\langle u, v \,|\, Q \rangle = \sum_{x,a,z,b \in \mathbb{F}_2} Q_{xa,zb} \langle 0, 1, j \,|\, \psi_{x,a} \rangle \langle 0, 1, j \,|\, \psi_{zb} \rangle \tag{7.64}$$

$$= \frac{1}{64k} \left(2Q_{01,10} \langle 0 | \overline{HT} | 0 \rangle \langle 0 | HT | 1 \rangle + 2Q_{00,11} \langle 0 | HT | 0 \rangle \langle 0 | \overline{HT} | 1 \rangle \right) \tag{7.65}$$

$$= \frac{1}{64k} \left(Q_{01,10} \omega + Q_{00,11} \omega^{-1} \right) \tag{7.66}$$

$$= \frac{Q_{01,10}}{64k} (\omega - \omega^{-1}) \tag{7.67}$$

must be zero, and thus each $Q_{xa,zb} = 0$. Hence, if $d_{\max} = 0$ no symmetric state $|Q\rangle$ is in the nullspace of $H(g_0, 2)$.

Combining all of this together, we have that if $d_{\max} > 0$, then the nullspace of $H(g_0, 2)$ is empty and thus $\lambda_2^1(g_0) > 0$, and if $d_{\max} = 0$ then no symmetric state is in the nullspace of $H(g_0, 2)$, and thus when restricted to symmetric states, $\lambda_2^1(g_0) > 0$. □

7.2.1.2 Diagram elements

We use several different graphs closely related to the graph g_0, with some depicted in Figure 7.2. We call these figures *diagram elements*, which are also the simplest examples of *gate diagram*, which we will define shortly. The idea behind these graphs is to encode a single qubit computation, complete with inputs and outputs.

[**TO DO:** *fix diagram element graphs*]

Each diagram element corresponds to two copies of the graph g_0, along with self-loops and edges between the two copies to force the ground space into a particular form while also ensuring that almost all of the vertices of the two copies will have self-loops. We need these additional self-loops and edges to ensure that the final graph that we construct has self-loops on all vertices.

In particular, each diagram element will be labeled by the unitary it computes, along with four numbers between zero and two, corresponding to the number of inputs "nodes" and output "nodes" of the diagram. Each such node will correspond to 16 vertices of the underlying graph representing one logical state and time of the two g_0 graphs. These nodes are constructed so that the distance between two vertices in separate nodes will be at least $d_{\max}$.

Explicitly, each diagram element will be labeled by a unitary $U \in \{\mathbb{I}, H, HT\}$, along with four integers $n_{0,\text{in}}$, $n_{0,\text{out}}$, $n_{1,\text{in}}$, and $n_{1,\text{out}}$ each between 0 and 2. These numbers correspond to the number of nodes for each particular input or output. We shall label such a diagram element a $U^{(n_{0,\text{in}},n_{1,\text{in}})}_{(n_{0,\text{out}},n_{1,\text{out}})}$ element. The vertex set for the corresponding diagram element corresponds to two copies of g_0 (namely, $2 \times 8k \times 8 \times 2$ vertices, labeled as (z, t, j, d) for $z, d \in \mathbb{F}_2$, $t \in [8k]$, and $j \in [8]$).

For each node of the gate diagram, we will associate a time for which the underlying history state has computed the correct unitary. Further, we will have these times each be a distance of at least $d_{\max}$ apart, to ensure that each node is at least a distance $d_{\max}$ apart. Namely, for each logical input and output, we will associate two times:

- 0-input: $t^{\text{in}}_{0,1} = 0$ and $t^{\text{in}}_{0,2} = k$,
- 1-input: $t^{\text{in}}_{1,1} = 2k$ and $t^{\text{in}}_{1,2} = 3k$,
- 0-output: $t^{\text{out}}_{0,1} = 4k + \ell$ and $t^{\text{out}}_{0,2} = 5k + \ell$,
- 1-output: $t^{\text{out}}_{1,1} = 4k + \ell$ and $t^{\text{out}}_{1,2} = 5k + \ell$,

where ℓ is 0, 1, or 3, depending on whether the labeled unitary is $\mathbb{I}$, HT, or H, respectively.

For a diagram element $U^{(n_{0,\text{in}},n_{1,\text{in}})}_{(n_{0,\text{out}},n_{1,\text{out}})}$, let us define the set of logical states and corresponding times that will be associated with the nodes as $T \subset \mathbb{F}_2 \times [8k]$. In particular, we have that

$$T = \cup_{z \in \mathbb{F}_2} \{(z, t^{\text{in}}_{z,j}) : j \leq n_{z,\text{in}}\} \cup \{(z, t^{\text{out}}_{z,j}) : j \leq n_{z,\text{out}}\}. \tag{7.68}$$

Note that $|S|$ corresponds to the number of nodes of the diagram element.

With S defined, the adjacency matrix for the diagram element $U^{(a,b)}_{(c,d)}$ will be

$$A(G_U^{(a,b),(c,d)}) = A(g_0) \otimes \mathbb{I}_2 + \sum_{(z,t) \notin T, j \in [8]} |\, z, t, j \,\rangle\langle\, z, t, j \,| \otimes \sum_{a,b \in \mathbb{F}_2} |\, a \,\rangle\langle\, b \,| \tag{7.69}$$

$$= A(g_0) \otimes \mathbb{I}_2 + 2\Pi_{\neg T} \otimes \mathbb{I}_8 \otimes |+\rangle\langle+| \tag{7.70}$$

In particular, the graph for $G_U^{(a,b),(c,d)}$ will simply correspond to two copies of g_0, along with a projector onto the equal superposition between the two graphs for each vertex not used as a node.

Because of the very similar form between $G_U^{(a,b),(c,d)}$ and g_0, their ground spaces and ground energies are closely related. As the second term in (7.70) is positive semi-definite, we have that the ground energy of $A(G_U^{(a,b),(c,d)})$ is at least that of $A(g_0)$. With more exact results, we have the following lemma:

Lemma 15. *Let $G_U^{(a,b),(c,d)}$ be the graph corresponding to a diagram element. The ground space of $A(G_U^{(a,b),(c,d)})$ is*

$$S = \text{span}\{|\, \psi_{z,a}, - \,\rangle : z, a \in \mathbb{F}_2\}. \tag{7.71}$$

Proof. Note that $A(G_U^{(a,b),(c,d)})$ commutes with $\mathbb{I}_2 \otimes \mathbb{I}_{8k} \otimes \mathbb{I}_8 \otimes |+\rangle\langle+|$, and thus there exists an eigenbasis for the adjacency matrix in which each vector is of the form $|\phi\rangle|+\rangle$ or $|\phi\rangle|-\rangle$. For states of this latter form, the second term in (7.70) vanishes, so $|\psi,-\rangle$ is in the ground space of $A(g_U^{(a,b),(c,d)})$ if and only if $|\psi\rangle$ is in the ground space of $A(g_0)$, and thus we have that S is a subspace of the nullspace.

Now let us examine $|\alpha,+\rangle$ for any state $|\alpha\rangle$. Since the first term of (7.70) has no dependence on the state $|+\rangle$, we have that the ground energy of $A(G_U^{(a,b),(c,d)})$ is at least e_1. Hence, if $|\alpha,+\rangle$ is in the ground space, then

$$\langle \alpha,+|A\big(G_U^{(a,b),(c,d)}\big)|\alpha,+\rangle = e_1 = \langle\alpha|A(g_0)|\alpha\rangle \tag{7.72}$$

and thus

$$\langle\alpha|\Pi_{\neg S}\otimes\mathbb{I}_8|\alpha\rangle = 0, \tag{7.73}$$

with $|\alpha\rangle$ in the ground space of $A(g_0)$.

However, let $t^* = 2$, and note that for all diagram elements (and all $d_{\max}$), (z,t^*) is not in T. We then have that

$$\Pi_{\neg S} \geq \mathbb{I}_2 \otimes |t^*\rangle\langle t^*| \otimes \mathbb{I}_8. \tag{7.74}$$

Note that this operator is strictly positive when restricted to the ground space of $A(g_0)$:

$$\langle\psi_{x,\gamma}|\mathbb{I}_2\otimes|t^*\rangle\langle t^*|\otimes\mathbb{I}_8|\psi_{z,\delta}\rangle = \frac{1}{8k}\delta_{\gamma,\delta}\delta_{x,z}. \tag{7.75}$$

Hence, $\Pi_{\neg S}$ is also strictly positive when restricted to the ground space of $A(g_0)$, and thus $|\alpha,+\rangle$ is not in the ground space of $A(G_U^{(a,b),(c,d)})$.

Putting this together, we have that the ground space of $A(G_U^{(a,b),(c,d)})$ is S. □

With this bound on the form of the ground space of $A(G_U^{(a,b),(c,d)})$, we can then use our knowledge of the two-particle interaction Hamiltonian on g_0 to relate this to the two-particle interaction Hamiltonian on $G_U^{(a,b),(c,d)}$. Namely, we show that since there does not exist a two-particle frustration-free state on g_0, there also does not exists a two-particle frustration-free state on $G_U^{(a,b),(c,d)}$.

Lemma 16. *If $d_{max} > 0$, then $\lambda_2^1(g_U^{(a,b),(c,d)}) > 0$ for all states. If $d_{max} = 0$, then when restricted to symmetric states, $\lambda_2^1(G_U^{(a,b),(c,d)}) > 0$.*

Proof. Note that using Lemma 15, the ground space of $A(G_U^{(a,b),(c,d)})$ is in one-to-one correspondence with the ground space of $A(g_0)$, by the transformation

$$|\phi_{x,a},-\rangle \leftrightarrow |\phi_{x,a}\rangle. \tag{7.76}$$

Namely, by attaching (or removing) a second register in the $|-\rangle$ state, corresponding to having equal and opposite amplitudes between the two copies of g_0 present in $g_U^{(a,b),(c,d)}$, we can transform between these two ground spaces.

We will use this relation, along with the fact that $\lambda_2^1(g_0) > 0$ from Lemma 14, to show that $\lambda_2^1(G_U^{(a,b),(c,d)}) > 0$ with the same assumptions.

Let us then look at any two-particle state that minimizes the movement term. In particular, it takes the form

$$|\overline{\phi}\rangle = \sum_{\alpha,\beta,x,z\in\mathbb{F}_2} Q^{x,z}_{\alpha,\beta} |\psi_{x,\alpha}, -\rangle |\psi_{z,\beta}, -\rangle. \tag{7.77}$$

Additionally, let us define the related two-particle state on g_0 as

$$|\phi\rangle = \sum_{\alpha,\beta,x,z\in\mathbb{F}_2} Q^{x,z}_{\alpha,\beta} |\psi_{x,\alpha}\rangle |\psi_{z,\beta}\rangle. \tag{7.78}$$

We can then see what the expectation of the interaction term of the Hamiltonian is under the state $|\overline{\phi}\rangle$:

$$\begin{aligned}
\langle\overline{\phi}|H_{\text{int}}|\overline{\phi}\rangle &= \sum_{u,v\in V(G_U^{(a,b),(c,d)})} \langle\overline{\phi}|U_{d(u,v)}(\hat{n}_u,\hat{n}_v)|\overline{\phi}\rangle &(7.79)\\
&= \sum_{u,v\in V(g_0),d_1,d_2\in\mathbb{F}_2} \langle\overline{\phi}|U_{d((u,d_1),(v,d_2))}(\hat{n}_{(u,d_1)},\hat{n}_{(v,d_2)})|\overline{\phi}\rangle &(7.80)\\
&\geq \sum_{u,v\in V(g_0),d_1\in\mathbb{F}_2} \langle\overline{\phi}|U_{d(u,v)}(\hat{n}_{(u,d_1)},\hat{n}_{(v,d_1)})|\overline{\phi}\rangle &(7.81)
\end{aligned}$$

where in the third line we only count the contributions to the interaction when both particles are in the same copy of g_0. As the interaction is positive-semidefinite, this can only decrease the expectation.

Now, from the form of $|\overline{\phi}\rangle$, we have that for any two $u, v \in V(g_0)$ and either copy of g_0,

$$\begin{aligned}
&\langle\overline{\phi}|U_{d(u,v)}(\hat{n}_{(u,d_1)},\hat{n}_{(v,d_1)})|\overline{\phi}\rangle\\
&\quad= \sum_{\substack{x_1,x_2,z_1,z_2\in\mathbb{F}_2\\ \alpha_1,\alpha_2,\beta_1,\beta_2\in\mathbb{F}_2}} (Q^{x_1,z_1}_{\alpha_1,\beta_1})^* Q^{x_2,z_2}_{\alpha_2,\beta_2} \langle\overline{\psi_{x_1,\alpha_1}}|\langle\overline{\psi_{z_1,\beta_1}}|U_{d(u,v)}(\hat{n}_{(u,d_1)},\hat{n}_{(v,d_1)})|\overline{\psi_{x_2,\alpha_2}}\rangle|\overline{\psi_{z_2,\beta_2}}\rangle &(7.82)\\
&\quad\geq |\langle d_1|-\rangle|^4 \sum_{\substack{x_1,x_2,z_1,z_2\in\mathbb{F}_2\\ \alpha_1,\alpha_2,\beta_1,\beta_2\in\mathbb{F}_2}} (Q^{x_1,z_1}_{\alpha_1,\beta_1})^* Q^{x_2,z_2}_{\alpha_2,\beta_2} \langle\psi_{x_1,\alpha_1}|\langle\psi_{z_1,\beta_2}|U_{d(u,v)}(\hat{n}_u,\hat{n}_v)|\psi_{x_2,\alpha_2}\rangle|\psi_{z_2,\beta_2}\rangle &(7.83)\\
&\quad= \frac{1}{4}\langle\phi|U_{d(u,v)}(\hat{n}_u,\hat{n}_v)|\phi\rangle. &(7.84)
\end{aligned}$$

Hence, we have that

$$\begin{aligned}
\langle\overline{\phi}|H_{\text{int}}|\overline{\phi}\rangle &\geq \sum_{u,v\in V(g_0),d_1\in\mathbb{F}_2} \langle\overline{\phi}|U_{d(u,v)}(\hat{n}_{(u,d_1)},\hat{n}_{(v,d_1)})|\overline{\phi}\rangle &(7.85)\\
&\geq \frac{1}{4}\sum_{u,v\in V(g_0),d_1\in\mathbb{F}_2} \langle\phi|U_{d(u,v)}(\hat{n}_u,\hat{n}_v)|\phi\rangle &(7.86)\\
&= \frac{1}{4}\sum_{d_1\in\mathbb{F}_2} \langle\phi|H_{\text{int}}|\phi\rangle &(7.87)\\
&= \frac{1}{2}\langle\phi|H_{\text{int}}|\phi\rangle. &(7.88)
\end{aligned}$$

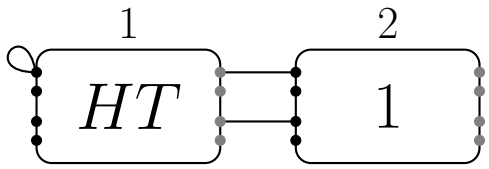

Figure 7.3: A gate diagram with two diagram elements labeled $q = 1$ (left) and $q = 2$ (right).

Using Lemma 14, we have that (7.88) is larger than zero for all states $|\phi\rangle$, and for all interactions that satisfy the conditions of Lemma 14, $\langle\overline{\phi}|H_{\text{int}}|\overline{\phi}\rangle > 0$. As such, there does not exist a two-particle frustration free state on the graph $g_U^{(a,b),(c,d)}$ for the same interactions as g_0.

□

7.2.1.3 Gate diagrams

While the diagram elements do have nice properties, we will eventually want to construct larger graphs using the diagram elements as basic elements. Further, as the diagram elements themselves are rather complicated graphs, it will be useful to have a diagrammatic construction for these graphs: these shall be the gate diagrams.

The rules for constructing gate diagrams are simple. A gate diagram consists of some number $R \in \{1, 2, \ldots\}$ of diagram elements, with self-loops attached to a subset $\mathcal{S}$ of the nodes and edges connecting a set $\mathcal{E}$ of pairs of nodes. A node may have a single edge or a single self-loop attached to it, but never more than one edge or self-loop and never both an edge and a self-loop. Each node in a gate diagram has a label (q, z, t) where $q \in [R]$ indicates the diagram element it belongs to. An example is shown in Figure 7.3.

Sometimes it is convenient to draw the input nodes on the right-hand side of a diagram element; e.g., in Figure 7.4 the node closest to the top left corner is labeled $(q, z, t) = (3, 0, 4k + 3)$.

To every gate diagram we associate a *gate graph* G with vertex set

$$\{(q, z, t, j, d) \colon q \in [R],\ z, d \in \mathbb{F}_2,\ t \in [8k],\ j \in [8]\} \tag{7.89}$$

and adjacency matrix

$$A(G) = \sum_{q \in [R]} |\,q\rangle\langle q\,| \otimes A(G_q) + h_{\mathcal{S}} + h_{\mathcal{E}} \tag{7.90}$$

$$A(G_q) = A(G_{U_q}^{(a_q,b_q),(c_q,d_q)}) \tag{7.91}$$

$$h_{\mathcal{S}} = \sum_{\mathcal{S}} |q, z, t\rangle\langle q, z, t| \otimes \mathbb{I}_8 \otimes \mathbb{I}_2 \tag{7.92}$$

$$h_{\mathcal{E}} = \sum_{\mathcal{E}} \left(|q, z, t\rangle + |q', z', t'\rangle\right)\left(\langle q, z, t| + \langle q', z', t'|\right) \otimes \mathbb{I}_8 \otimes \mathbb{I}_2. \tag{7.93}$$

The sums in equations (7.92) and (7.93) run over the set of nodes with self-loops $(q, z, t) \in \mathcal{S}$ and the set of pairs of nodes connected by edges $\{(q, z, t), (q', z', t')\} \in \mathcal{E}$, respectively. We

see from the above expression that each self-loop in the gate diagram corresponds to 16 self-loops in the graph G, and an edge in the gate diagram corresponds to 16 edges and 32 self-loops in G. Note that we can determine the type of each diagram element from the gate diagram, as the implemented unitary and number of nodes is encoded in the diagram.

As a node in a gate graph never has more than one edge or self-loop attached to it, equations (7.92) and (7.93) are sums of orthogonal Hermitian operators. Therefore

$$\|h_{\mathcal{S}}\| = \max_{\mathcal{S}} \||q,z,t\rangle\langle q,z,t| \otimes \mathbb{I}_j\| = 1 \quad \text{if } \mathcal{S} \neq \emptyset \tag{7.94}$$

$$\|h_{\mathcal{E}}\| = \max_{\mathcal{E}} \|(|q,z,t\rangle + |q',z',t'\rangle)\,(\langle q,z,t| + \langle q',z',t'|) \otimes \mathbb{I}_j\| = 2 \quad \text{if } \mathcal{E} \neq \emptyset \tag{7.95}$$

for any gate graph. (Of course, this also shows that $\|h_{\mathcal{S}'}\| = 1$ and $\|h_{\mathcal{E}'}\| = 2$ for any nonempty subsets $\mathcal{S}' \subseteq \mathcal{S}$ and $\mathcal{E}' \subseteq \mathcal{E}$.)

Consider the adjacency matrix $A(G)$ of a gate graph G, and note (from equation (7.90) that its smallest eigenvalue $\mu(G)$ satisfies

$$\mu(G) \geq e_1 \tag{7.96}$$

since $h_{\mathcal{S}}$ and $h_{\mathcal{E}}$ are positive semidefinite and $A(g_U^{(a,b),(c,d)})$ has smallest eigenvalue e_1. In the special case where $\mu(G) = e_1$, we say G is an e_1-gate graph.

Definition 8. An e_1-gate graph is a gate graph G such that the smallest eigenvalue of its adjacency matrix is $e_1 = -1 - 3\sqrt{2}$.

When G is an e_1-gate graph, a single-particle ground state $|\Gamma\rangle$ of $A(G)$ satisfies

$$\left(\sum_{q\in[R]} |q\rangle\langle q| \otimes A(G_q)\right)|\Gamma\rangle = e_1|\Gamma\rangle \tag{7.97}$$

$$h_{\mathcal{S}}|\Gamma\rangle = 0 \tag{7.98}$$

$$h_{\mathcal{E}}|\Gamma\rangle = 0. \tag{7.99}$$

Indeed, to show that a given gate graph G is an e_1-gate graph, it suffices to find a state $|\Gamma\rangle$ satisfying these conditions. Note that equation (7.97) implies that $|\Gamma\rangle$ can be written as a superposition of the states

$$|\overline{\psi^q_{z,a}}\rangle = |q\rangle|\overline{\psi_{z,a}}\rangle, \quad z,a \in \mathbb{F}_2, q \in [R] \tag{7.100}$$

where $|\overline{\psi_{z,a}}\rangle$ is given by equations (7.31) and (7.32) under the transform of (7.76). The coefficients in the superposition are then constrained by equations (7.98) and (7.99).

[**TO DO:** *fix frustration free stuff*]

7.2.2 Gadgets

In Example **??** we saw how a single-particle ground state can encode a single-qubit computation. In this Section we see how a two-particle frustration-free state on a suitably designed e_1-gate graph can encode a two-qubit computation. We design specific e_1-gate graphs (called

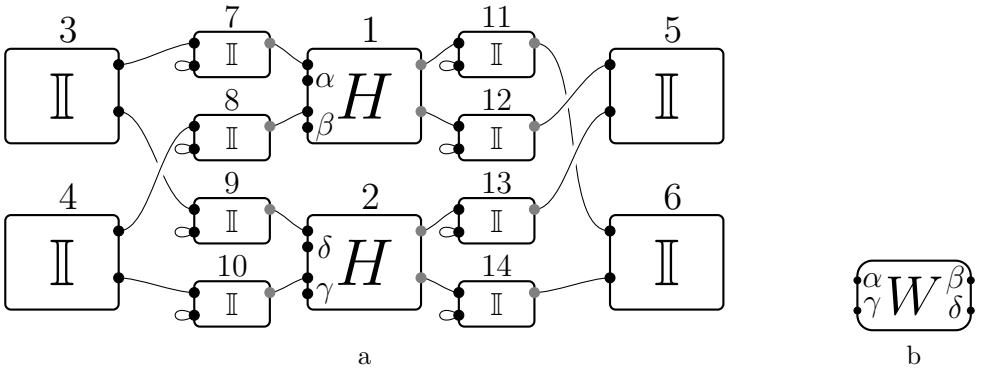

Figure 7.4: (a) The gate diagram for the move-together gadget. Note the four labeled nodes, α, β, γ, and δ, which have no attached edges. (b) A schematic representation for a move-together gadget, with the four labeled nodes corresponding to the four labeled nodes of (a).

gadgets) that we use in Section **??** to prove that these ground state problems for the MPQW are QMA-hard. For each gate graph we discuss, we show that the smallest eigenvalue of its adjacency matrix is e_1 and we solve for all of the frustration-free states.

We first design a gate graph where, in any two-particle frustration-free state, the locations of the particles are synchronized. We then design gadgets for two-qubit gates using four move-together gadgets, one for each two-qubit computational basis state. Finally, we describe a small modification of a two-qubit gate gadget called the "boundary gadget."

In important piece of these gadgets will be the inclusion of $\mathbb{I}^{(1,0)}_{(1,0)}$ diagram elements to separate the locations of particles. With these separations, we will only ever need to analyze the case when particles occupy the same diagram element, as these identity elements ensure that for the states that we care about, particles are always located at a distance of at least $d_{\max}$.

7.2.2.1 The move-together gadget

The gate diagram for the *move-together gadget* is shown in Figure 7.4. Using equation (7.90), we write the adjacency matrix of the corresponding gate graph G_W as

$$A(G_W) = \sum_{q=1}^{14} |q\rangle\langle q| \otimes A(G_q) + h_{\mathcal{E}} \tag{7.101}$$

where

$$G_q = \begin{cases} G_H^{(2,2),(1,1)} & q \in \{1,2\} \\ G_{\mathbb{I}}^{(1,1),(0,0)} & q \in \{3,4,5,6\} \\ G_{\mathbb{I}}^{(1,0),(1,0)} & q > 6, \end{cases} \tag{7.102}$$

$h_{\mathcal{E}}$ is given by (7.93), $h_{\mathcal{S}}$ is given by (7.92), $\mathcal{E}$ is the set of edges in the gate diagram, and $\mathcal{S}$ is the set of self-loops in the diagram.

We begin by solving for the single-particle ground states, i.e., the eigenvectors of (7.101) with eigenvalue $e_1 = -1 - 3\sqrt{2}$. As in Example **??**, we can solve for the states with $a = 0$

and $a = 1$ separately, since

$$\langle \psi^j_{x,1} | h_{\mathcal{E}} | \psi^i_{z,0} \rangle = 0 \tag{7.103}$$

for all $i, j \in [14]$ and $x, z \in \mathbb{F}_2$. We write a single-particle ground state as

$$\sum_{i=1}^{14} \left(\tau_i |\psi^i_{0,a}\rangle + \nu_i |\psi^i_{1,a}\rangle \right) \tag{7.104}$$

and solve for the coefficients τ_i and ν_i using equation (7.99). Enforcing (7.98) gives us that $\nu_i = 0$ for all $i > 6$. Enforcing (7.99) gives sixteen equations, one for each edge in the gate diagram:

$$\tau_3 = -\tau_7 \qquad \tau_7 = -\tau_1 \qquad \frac{1}{\sqrt{2}}(\tau_1 + \nu_1) = -\tau_{11} \qquad \tau_{11} = -\tau_6 \tag{7.105}$$

$$\nu_3 = -\tau_9 \qquad \tau_9 = -\tau_2 \qquad \frac{1}{\sqrt{2}}(\tau_2 + \nu_2) = -\tau_{13} \qquad \tau_{13} = -\nu_5 \tag{7.106}$$

$$\tau_4 = -\tau_8 \qquad \tau_8 = -\nu_1 \qquad \frac{1}{\sqrt{2}}(\tau_1 - \nu_1) = -\tau_{12} \qquad \tau_{12} = -\tau_5 \tag{7.107}$$

$$\nu_3 = -\tau_{10} \qquad \tau_{10} = -\nu_2 \qquad \frac{1}{\sqrt{2}}(\tau_2 - \nu_2) = -\tau_{14} \qquad \tau_{14} = -\nu_6. \tag{7.108}$$

Similarly, enforcing (7.98) gives eight equations, namely that $\nu_q = 0$ for $q > 6$. There are four linearly independent solutions to this set of equations, given by

$$\textit{Solution 1:} \quad \tau_1 = \tau_3 = -\tau_7 = 1 \quad \tau_5 = \tau_6 = -\tau_{11} = -\tau_{12} = \frac{1}{\sqrt{2}} \quad \text{all other coefficients } 0 \tag{7.109}$$

$$\textit{Solution 2:} \quad \nu_1 = \tau_4 = -\tau_8 = 1 \quad -\tau_5 = \tau_6 = -\tau_{11} = \tau_{12} = \frac{1}{\sqrt{2}} \quad \text{all other coefficients } 0 \tag{7.110}$$

$$\textit{Solution 3:} \quad \nu_2 = \nu_4 = -\tau_{10} = 1 \quad \nu_5 = -\nu_6 = -\tau_{13} = \tau_{14} = \frac{1}{\sqrt{2}} \quad \text{all other coefficients } 0 \tag{7.111}$$

$$\textit{Solution 4:} \quad \tau_2 = \nu_3 = -\tau_9 = 1 \quad \nu_5 = \nu_6 = -\tau_{13} = -\tau_{14} = \frac{1}{\sqrt{2}} \quad \text{all other coefficients } 0. \tag{7.112}$$

For each of these solutions, and for each $a \in \{0, 1\}$, we find a single-particle state with energy e_1. This result is summarized in the following Lemma.

Lemma 17. *G_W is an e_1-gate graph. A basis for the eigenspace of $A(G_W)$ with eigenvalue*

e_1 *is*

$$|\chi_{1,a}\rangle = \frac{1}{\sqrt{5}}\big(|\psi^1_{0,a}\rangle + |\psi^3_{0,a}\rangle - |\psi^7_{0,a}\rangle\big) + \frac{1}{\sqrt{10}}\big(|\psi^5_{0,a}\rangle + |\psi^6_{0,a}\rangle - |\psi^{11}_{0,a}\rangle - |\psi^{12}_{0,a}\rangle\big) \tag{7.113}$$

$$|\chi_{2,a}\rangle = \frac{1}{\sqrt{5}}\big(|\psi^1_{1,a}\rangle + |\psi^4_{0,a}\rangle - |\psi^8_{0,a}\rangle\big) + \frac{1}{\sqrt{10}}\big(-|\psi^5_{0,a}\rangle + |\psi^6_{0,a}\rangle - |\psi^{11}_{0,a}\rangle + |\psi^{12}_{0,a}\rangle\big) \tag{7.114}$$

$$|\chi_{3,a}\rangle = \frac{1}{\sqrt{5}}\big(|\psi^2_{1,a}\rangle + |\psi^4_{1,a}\rangle - |\psi^{10}_{0,a}\rangle\big) + \frac{1}{\sqrt{10}}\big(|\psi^5_{1,a}\rangle - |\psi^6_{1,a}\rangle - |\psi^{13}_{0,a}\rangle + |\psi^{14}_{0,a}\rangle\big) \tag{7.115}$$

$$|\chi_{4,a}\rangle = \frac{1}{\sqrt{5}}\big(|\psi^2_{0,a}\rangle + |\psi^3_{1,a}\rangle - |\psi^9_{0,a}\rangle\big) + \frac{1}{\sqrt{10}}\big(|\psi^5_{1,a}\rangle + |\psi^6_{1,a}\rangle - |\psi^{13}_{0,a}\rangle - |\psi^{14}_{0,a}\rangle\big) \tag{7.116}$$

where $a \in \mathbb{F}_2$.

In Figure 7.4 we have used a shorthand $\alpha, \beta, \gamma, \delta$ to identify four nodes of the move-together gadget; these are the nodes with labels $(q, z, t) = (1, 0, 0), (1, 1, 3k), (2, 1, 3k), (2, 0, 0)$, respectively. We view α and γ as "input" nodes and β and δ as "output" nodes for this gate diagram. It is natural to associate each single-particle state $|\chi_{i,a}\rangle$ with one of these four nodes. We also associate the set of 16 vertices represented by the node with the corresponding node, e.g.,

$$S_\alpha = \{(1, 0, 0, j, d) \colon j \in [8], d \in \mathbb{F}_2\}\,. \tag{7.117}$$

Looking at equation (7.113) (and perhaps referring back to equation (7.31)) we see that $|\chi_{1,a}\rangle$ has support on vertices in S_α but has no support on vertices in S_β, S_γ, or S_δ. Looking at the picture on the right-hand side of the equality sign in Figure 7.4, we think of $|\chi_{1,a}\rangle$ as localized at the node α, with no support on the other three nodes. The states $|\chi_{2,a}\rangle, |\chi_{3,a}\rangle, |\chi_{4,a}\rangle$ are similarly localized at nodes β, γ, δ. We view $|\chi_{1,a}\rangle$ and $|\chi_{3,a}\rangle$ as input states and $|\chi_{2,a}\rangle$ and $|\chi_{4,a}\rangle$ as output states for the move-together gadget.

Now we turn our attention to the two-particle frustration-free states of the move-together gadget, i.e., the states $|\Phi\rangle \in \mathcal{H}(G_W)^{\otimes 2}$ in the nullspace of $H(G_W, 2)$. As $\lambda_2^1(G_U) > 0$ for all U from Lemma 16, we have that any such state must take the form

$$|\Phi\rangle = \sum_{a,b\in\{0,1\},\, I,J\in[4]} C_{(I,a),(J,b)} |\chi_{I,a}\rangle |\chi_{J,b}\rangle \tag{7.118}$$

where

$$\langle\psi^q_{z,a}|\langle\psi^q_{x,b}|\Phi\rangle = 0 \tag{7.119}$$

for all $z, a, x, b \in \mathbb{F}_2$ and $q \in [14]$, and if $d_{\max} = 0$, where the coefficients are symmetric, i.e.,

$$C_{(I,a),(J,b)} = C_{(J,b),(I,a)},\,. \tag{7.120}$$

Note that this does not guarantee that the state is frustration-free, merely that these are necessary conditions for the state to be frustration free.

However, in the construction of the G_W gadget, we placed the $H^{(1,1)}_{(1,0)}$ elements specifically to ensure that the two-particle states were separated by a distance of at least $k > d_{\min}$. If we can ensure that the state $|\Phi\rangle$ has no support on pairs of diagram elements that are closer than $k > d_{\max}$, then we can guarantee that $|\Phi\rangle$ is frustration-free.

The move-together gadget is designed so that each solution $|\Phi\rangle$ to these equations is a superposition of a term where both particles are in input states and a term where both particles are in output states. The particles move from input nodes to output nodes together. We now solve equations (7.118)–(7.119) and prove the following.

Lemma 18. *A basis for the nullspace of $H(G_W, 2)$ is*

$$|\Phi^{\pm}_{a,b}\rangle = \frac{1}{2}\big(|\chi_{1,a}\rangle|\chi_{3,b}\rangle \pm |\chi_{3,b}\rangle|\chi_{1,a}\rangle + |\chi_{2,a}\rangle|\chi_{4,b}\rangle \pm |\chi_{4,b}\rangle|\chi_{2,a}\rangle\big), \quad a, b \in \mathbb{F}_2 \tag{7.121}$$

for $d_{max} > 0$, and if $d_{max} = 0$ a basis for the nullspace of $H(G_W, 2)$ when restricted to symmetric states is $|\Phi^{+}_{a,b}\rangle$ for $a, b \in \mathbb{F}_2$.

There are no N-particle frustration-free states on G_W for $N \geq 3$ for any d_{max}, i.e.,

$$\lambda^1_N(G_W) > 0 \quad \text{for } N \geq 3. \tag{7.122}$$

Proof. The states $|\Phi_{a,b}\rangle$ manifestly satisfy equations (7.118), and one can directly verify that they also satisfy (7.119) (the nontrivial cases to check are for $q = 5$, $q = 6$, and $q > 10$). Additionally, one can also directly verify that $|\Phi_{a,b}\rangle$ has no support on states for which the two particles are located on diagram elements closer than k, and thus the state is in the ground space of the interaction Hamiltonian.

To complete the proof that (7.121) is a basis for the nullspace of $H(G_W, 2)$, we verify that any state satisfying these conditions must be a linear combination of these four states. Applying equation (7.119) to the first 4 diagram elements gives

$$\langle\psi^1_{0,a}|\langle\psi^1_{0,b}|\Phi\rangle = \frac{1}{5}C_{(1,a),(1,b)} = 0 \qquad \langle\psi^1_{1,a}|\langle\psi^1_{1,b}|\Phi\rangle = \frac{1}{5}C_{(2,a),(2,b)} = 0 \tag{7.123}$$

$$\langle\psi^2_{1,a}|\langle\psi^2_{1,b}|\Phi\rangle = \frac{1}{5}C_{(3,a),(3,b)} = 0 \qquad \langle\psi^2_{0,a}|\langle\psi^2_{0,b}|\Phi\rangle = \frac{1}{5}C_{(4,a),(4,b)} = 0 \tag{7.124}$$

$$\langle\psi^1_{0,a}|\langle\psi^1_{1,b}|\Phi\rangle = \frac{1}{5}C_{(1,a),(2,b)} = 0 \qquad \langle\psi^2_{0,a}|\langle\psi^2_{1,b}|\Phi\rangle = \frac{1}{5}C_{(4,a),(3,b)} = 0 \tag{7.125}$$

$$\langle\psi^1_{1,a}|\langle\psi^1_{0,b}|\Phi\rangle = \frac{1}{5}C_{(2,a),(1,b)} = 0 \qquad \langle\psi^2_{1,a}|\langle\psi^2_{0,b}|\Phi\rangle = \frac{1}{5}C_{(3,a),(4,b)} = 0 \tag{7.126}$$

$$\langle\psi^3_{0,a}|\langle\psi^3_{1,b}|\Phi\rangle = \frac{1}{5}C_{(1,a),(4,b)} = 0 \qquad \langle\psi^4_{0,a}|\langle\psi^4_{1,b}|\Phi\rangle = \frac{1}{5}C_{(2,a),(3,b)} = 0 \tag{7.127}$$

$$\langle\psi^3_{1,a}|\langle\psi^3_{0,b}|\Phi\rangle = \frac{1}{5}C_{(4,a),(1,b)} = 0 \qquad \langle\psi^4_{1,a}|\langle\psi^4_{0,b}|\Phi\rangle = \frac{1}{5}C_{(3,a),(2,b)} = 0 \tag{7.128}$$

for all $a, b \in \{0, 1\}$. Using the fact that all of these coefficients are zero, we can then see that

$$|\Phi\rangle = \sum_{\substack{a,b\in\mathbb{F}_2 \\ j\in[4]}} C_{(j,a),(j+2,b)}|\chi_{j,a}\rangle|\chi_{j+2,b}\rangle. \tag{7.129}$$

Finally, applying equation (7.119) to diagram 6 gives

$$\langle\psi^6_{0,a}|\langle\psi^6_{1,b}|\Phi\rangle = \frac{1}{6}C_{(2,a),(4,b)} - \frac{1}{6}C_{(1,a),(3,b)} = 0 \tag{7.130}$$

$$\langle\psi^6_{1,a}|\langle\psi^6_{0,b}|\Phi\rangle = \frac{1}{6}C_{(4,a),(2,b)} - \frac{1}{6}C_{(3,a),(1,b)} = 0. \tag{7.131}$$

Hence

$$|\Phi\rangle = \sum_{\substack{a,b\in\mathbb{F}_2 \\ j\in[4]}} C_{(j,a),(j+2,b)}\big(|\chi_{j,a}\rangle|\chi_{j+2,b}\rangle + |\chi_{j+1,a}\rangle|\chi_{j+3,b}\rangle\big), \tag{7.132}$$

which is a superposition of the states $|\Phi^{\pm}_{a,b}\rangle$.

Note that the above analysis holds completely if we restrict ourselves to symmetric states, and thus if $d_{\max} = 0$, we end up with the same results except that we only care about the states $|\Phi^{+}_{a,b}\rangle$, as they span the symmetric nullspace.

Finally, we prove that there are no frustration-free ground states of the Bose-Hubbard model on G_W with more than two particles. By Lemma **??**, it suffices to prove that there are no frustration-free three-particle states.

Suppose (for a contradiction) that $|\Gamma\rangle \in \mathcal{H}(G_W)^{\otimes 3}$ is a normalized three-particle frustration-free state. Write

$$|\Gamma\rangle = \sum D_{(i,a),(j,b),(k,c)}|\chi_{i,a}\rangle|\chi_{j,b}\rangle|\chi_{k,c}\rangle. \tag{7.133}$$

Note that each reduced density matrix of $|\Gamma\rangle$ on two of the three subsystems must have all of its support on two-particle frustration-free states (see the remark following Lemma **??**), i.e., on the states $|\Phi_{a,b}\rangle$. Using this fact for the subsystem consisting of the first two particles, we see in particular that

$$(i,j) \notin \{(1,3),(3,1),(2,4),(4,2)\} \quad \Longrightarrow \quad D_{(i,a),(j,b),(k,c)} = 0 \tag{7.134}$$

(since $|\Phi_{a_1,a_2}\rangle$ only has support on vectors $|\chi_{i,a}\rangle|\chi_{j,b}\rangle$ with $i,j \in \{(1,3),(3,1),(2,4),(4,2)\}$).

Using this fact for subsystems consisting of particles $2,3$ and $1,3$, respectively, gives

$$(j,k) \notin \{(1,3),(3,1),(2,4),(4,2)\} \quad \Longrightarrow \quad D_{(i,a),(j,b),(k,c)} = 0 \tag{7.135}$$

$$(i,k) \notin \{(1,3),(3,1),(2,4),(4,2)\} \quad \Longrightarrow \quad D_{(i,a),(j,b),(k,c)} = 0. \tag{7.136}$$

Putting together equations (7.134), (7.135), and (7.136), we see that $|\Gamma\rangle = 0$. This is a contradiction, so no three-particle frustration-free states exist. □

With this gadget allowing us to entangle the locations of particles, we will be able to create a pseudo-history state, in which time is encoded in the location of particles. This is the large workhorse of the construction, as it allows us to understand the multi-particle ground space by understanding the simple two-particle ground states.

7.2.2.2 Two-qubit gate gadget

We can now use the W-gadget as a building block to encode graphs with more interesting ground-state behavior. In particular, we can use the W-gadget to force the two-particle state of a larger gadget to have entangled locations between the two particles. If we then place connections in a particular manner, we can use these guarantees to force the ground state to encode a computation corresponding to a permutation of the computational basis states (such as a controlled not operation). In particular, we will be to define a gate graph for each of the two-qubit unitaries

$$\{\mathrm{CNOT}_{12}, \mathrm{CNOT}_{21}, \mathrm{CNOT}_{12}\,(H\otimes\mathbb{I})\,, \mathrm{CNOT}_{12}\,(HT\otimes\mathbb{I})\}. \tag{7.137}$$

Here CNOT_{12} is the standard controlled-not gate with the second qubit as a target, whereas CNOT_{21} has the first qubit as target.

We define the gate graphs by exhibiting their gate diagrams. For the three cases

$$U = \mathrm{CNOT}_{12}(\tilde{U} \otimes \mathbb{I}) \tag{7.138}$$

with $\tilde{U} \in \{\mathbb{I}, H, HT\}$, we associate U with the gate diagram shown in Figure 7.5a. In Figure 7.5b we also indicate a shorthand used to represent this gate diagram. As one might expect, for the case $U = \mathrm{CNOT}_{21}$, we use the same gate diagram as for $U = \mathrm{CNOT}_{12}$; however, we use the slightly different shorthand shown in Figure 7.5c.

Roughly speaking, the two-qubit gate gadgets work as follows. We can ignore the 16 $\mathbb{I}_{(1,0)}^{(1,1)}$ diagram elements, as they exist to separate the locations of the particles, but otherwise there are four move-together gadgets, one for each two-qubit basis state $|00\rangle, |01\rangle, |10\rangle, |11\rangle$. These enforce the constraint that two particles must move through the graph together, while their connections to the four diagram elements labeled $1, 2, 3, 4$ ensure that most of the frustration-free two-particle states encode two-qubit computations, while the connections between diagram elements $1, 2, 3, 4$ and $5, 6, 7, 8$ ensure that the remaining frustration-free two-particle states are removed from the ground space.

To describe the frustration-free states of the gate graph depicted in Figure 7.5, first recall the definition of the states $|\chi_{j,a}\rangle$ for $j \in [4]$ from equations (7.113)–(7.116). For each of the move-together gadgets $xy \in \{00, 01, 10, 11\}$ in Figure 7.5b, write

$$|\chi_{j,a}^{xy}\rangle \tag{7.139}$$

for the state $|\chi_{j,a}\rangle$ with support (only) on the gadget labeled xy. Additionally, write

$$U^a = \begin{cases} U & \text{if } a = 0 \\ \overline{U} & \text{if } a = 1 \end{cases} \tag{7.140}$$

and similarly for $\tilde{U}$. This notation will help us to define the ground states of the resulting Hamiltonian, as the encoded computation will change depending on α.

We now show that G_U is an e_1-gate graph and solves for its frustration-free states.

Lemma 19. *Let $U = \mathrm{CNOT}_{12}(\tilde{U} \otimes \mathbb{I})$ where $\tilde{U} \in \{\mathbb{I}, H, HT\}$. The corresponding gate graph G_U is defined by its gate diagram shown in Figure 7.5a. The adjacency matrix $A(G_U)$ has ground energy e_1; a basis for the corresponding eigenspace is*

$$|\rho_{z,a}^{1,U}\rangle = \frac{1}{\sqrt{15}}\Big(|\psi_{z,a}^{1}\rangle + |\psi_{z,a}^{5+z}\rangle - |\psi_{z,a}^{25+z}\rangle + \sum_{x,y\in\mathbb{F}_2} \tilde{U}_{yz}^{a}\big(\sqrt{5}|\chi_{1,a}^{yx}\rangle - |\psi_{0,a}^{9+x+2y}\rangle\big)\Big) \tag{7.141}$$

$$|\rho_{z,a}^{2,U}\rangle = \frac{1}{\sqrt{15}}\Big(|\psi_{z,a}^{2}\rangle + |\psi_{z,a}^{6-z}\rangle - |\psi_{z,a}^{29+z}\rangle + \sum_{x\in\mathbb{F}_2} \big(\sqrt{5}|\chi_{2,a}^{zx}\rangle - |\psi_{0,a}^{17+2z+x}\rangle\big)\Big) \tag{7.142}$$

$$|\rho_{z,a}^{3,U}\rangle = \frac{1}{\sqrt{15}}\Big(|\psi_{z,a}^{3}\rangle + |\psi_{z,a}^{7}\rangle - |\psi_{z,a}^{27+z}\rangle + \sum_{x\in\mathbb{F}_2} \big(\sqrt{5}|\chi_{3,a}^{xz}\rangle - |\psi_{0,a}^{17+2z+x}\rangle\big)\Big) \tag{7.143}$$

$$|\rho_{z,a}^{4,U}\rangle = \frac{1}{\sqrt{15}}\Big(|\psi_{z,a}^{4}\rangle + |\psi_{z,a}^{8}\rangle - |\psi_{z,a}^{31+z}\rangle + \sum_{x\in\mathbb{F}_2} \big(\sqrt{5}|\chi_{4,a}^{x(z\oplus x)}\rangle - |\psi_{0,a}^{21+2z+x}\rangle\big)\Big) \tag{7.144}$$

where $z, a \in \mathbb{F}_2$.

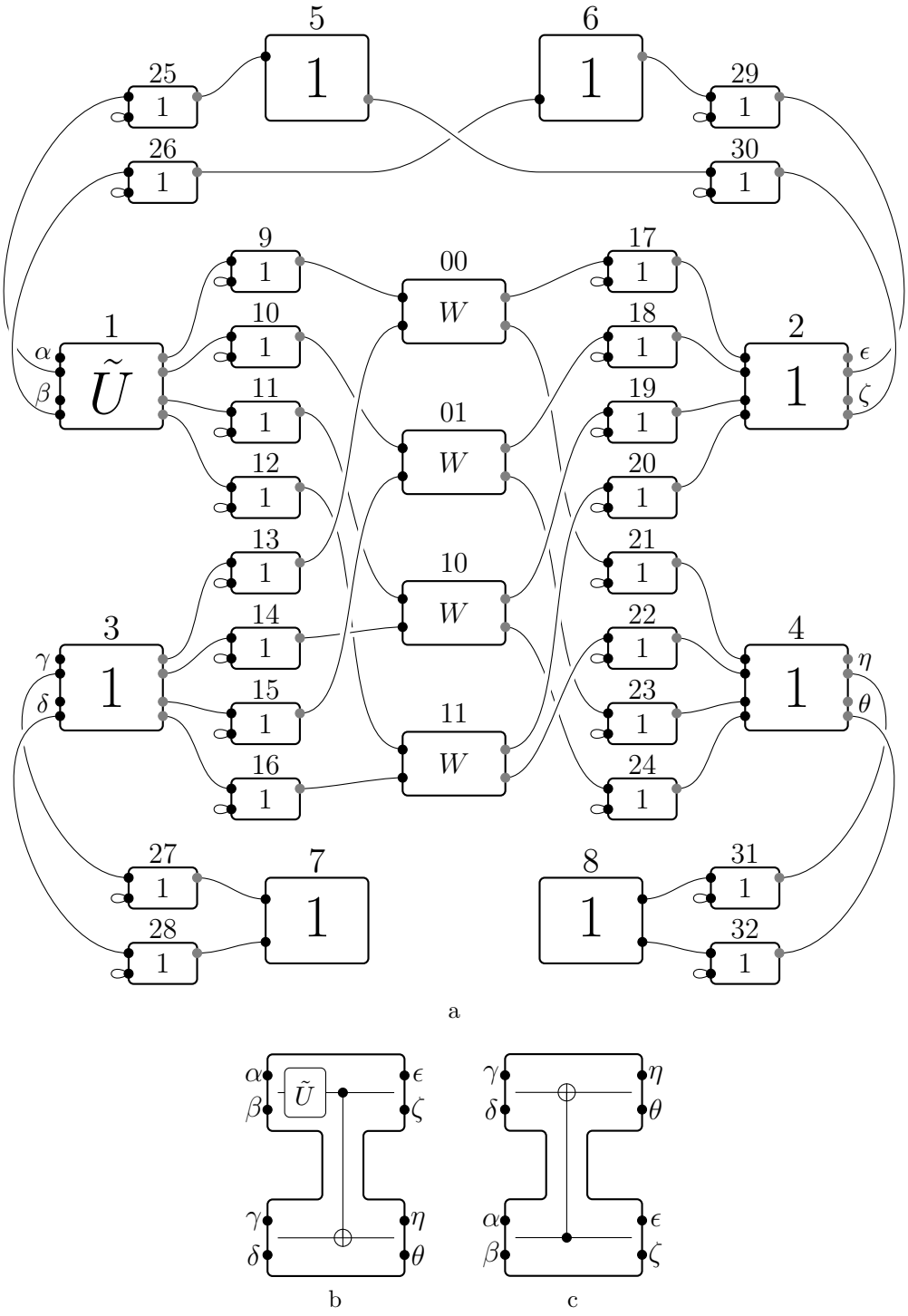

Figure 7.5: (a) Gadget for the two-qubit unitary $U = \mathrm{CNOT}_{12}(\tilde{U} \otimes \mathbb{I})$ with $\tilde{U} \in \{1, H, HT\}$. (b) A schematic encoding for $U = \mathrm{CNOT}_{12}(\tilde{U} \otimes \mathbb{I})$, where the eight labeled nodes correspond to the eight labeled nodes of (a). (c) For the $U = \mathrm{CNOT}_{21}$ gate (first qubit is the target), we use the same gate graph as in (b) with $\tilde{U} = 1$, but with a different location for the eight labeled nodes.

Proof. As the gate graph G_U is specified by its gate diagram, shown in Figure 7.5a, the adjacency matrix of the gate graph G_U is of the form in equation (7.90). There are 14 diagram elements for each of the move-together gadgets, so there are 88 diagram elements in total. We will need to refer to those diagram elements labeled $q \in [32]$ in Figure 7.5a (i.e., those not contained in the move-together gadgets).

Write

$$A(G_U) = A(G'_U) + h_{\mathcal{E}'} \tag{7.145}$$

where G'_U is the gate graph obtained from G_U by removing all 48 edges shown in Figure 7.5b (G'_U does include the edges within each of the move-together gadgets along with the selfloops of G_U). Here $h_{\mathcal{E}'}$ is given by equation (7.93) with $\mathcal{E}'$ the set of 48 edges shown in Figure 7.5b.

One basis for the e_1-energy ground space of $A(G'_U)$ is given by the 112 states

$$|\psi^q_{z,a}\rangle, \quad q \in [32],\, z, a \in \mathbb{F}_2 \tag{7.146}$$

$$|\chi^{xy}_{j,a}\rangle, \quad x, y, a \in \mathbb{F}_2,\, j \in [4], \tag{7.147}$$

where we exclude $|\psi^q_{1,a}\rangle$ if $q > 8$ (as these states encounter a self-loop). It will be convenient to work with the following slightly rotated basis for this space:

$$|\psi^q_{z,a}\rangle \qquad q \in [8],\, z, a \in \mathbb{F}_2 \tag{7.148}$$

$$\sum_{x \in \mathbb{F}_2} \tilde{U}^a_{xz} |\psi^{j+2x}_{0,a}\rangle \qquad a, z \in \mathbb{F}_2, j \in \{9, 10\} \tag{7.149}$$

$$|\psi^q_{0,a}\rangle \qquad a \in \mathbb{F}_2, 13 \le q \le 32 \tag{7.150}$$

$$\sum_{x \in \mathbb{F}_2} \tilde{U}^a_{xz} |\chi^{xy}_{1,a}\rangle \qquad y, z, a \in \mathbb{F}_2 \tag{7.151}$$

$$|\chi^{xy}_{j,a}\rangle \qquad x, y, a \in \mathbb{F}_2,\, j \in \{2, 3, 4\}. \tag{7.152}$$

In this basis, some of the states are in a superposition corresponding to the output of the single-qubit unitary $\tilde{U}$.

We are interested in the intersection of the ground space of $A(G'_U)$ with the nullspace of $h_{\mathcal{E}'}$, so we compute the matrix elements of $h_{\mathcal{E}'}$ in the above basis. The resulting 112×112 matrix is block diagonal with sixteen 7×7 blocks. Each block is identical, with entries

$$\frac{1}{8k} \begin{pmatrix} 3 & 1 & 1 & 1 & 0 & 0 & 0 \\ 1 & 2 & 0 & 0 & \frac{1}{\sqrt{5}} & 0 & 0 \\ 1 & 0 & 2 & 0 & 0 & \frac{1}{\sqrt{5}} & 0 \\ 1 & 0 & 0 & 2 & 0 & 0 & 1 \\ 0 & \frac{1}{\sqrt{5}} & 0 & 0 & \frac{1}{5} & 0 & 0 \\ 0 & 0 & \frac{1}{\sqrt{5}} & 0 & 0 & \frac{1}{5} & 0 \\ 0 & 0 & 0 & 1 & 0 & 0 & 1 \end{pmatrix}. \tag{7.153}$$

The seven states involved in each block are given by (in order from left to right as in the

matrix above):

$$|\psi^1_{z,a}\rangle, \sum_{x\in\mathbb{F}_2} \tilde{U}^a_{xz}|\psi^{9+2x}_{0,a}\rangle, \sum_{x\in\mathbb{F}_2} \tilde{U}^a_{xz}|\psi^{10+2x}_{0,a}\rangle, |\psi^{25+z}_{0,a}\rangle, \sum_{x\in\mathbb{F}_2} \tilde{U}^a_{xz}|\chi^{x0}_{1,a}\rangle, \sum_{x\in\mathbb{F}_2} \tilde{U}^a_{xz}|\chi^{x1}_{1,a}\rangle, |\psi^{5+z}_{z,a}\rangle \tag{7.154}$$

$$|\psi^2_{z,a}\rangle, |\psi^{17+2z}_{0,a}\rangle, |\psi^{18+2z}_{0,a}\rangle, |\psi^{29+z}_{0,a}\rangle, |\chi^{z0}_{2,a}\rangle, |\chi^{z1}_{2,a}\rangle, |\psi^{6-z}_{z,a}\rangle \tag{7.155}$$

$$|\psi^3_{z,a}\rangle, |\psi^{13+2z}_{0,a}\rangle, |\psi^{14+2z}_{0,a}\rangle, |\psi^{27+z}_{0,a}\rangle, |\chi^{0z}_{3,a}\rangle, |\chi^{1z}_{3,a}\rangle, |\psi^{7}_{z,a}\rangle \tag{7.156}$$

$$|\psi^4_{z,a}\rangle, |\psi^{21+2z}_{0,a}\rangle, |\psi^{22+2z}_{0,a}\rangle, |\psi^{31+z}_{0,a}\rangle, |\chi^{0z}_{4,a}\rangle, |\chi^{1(z\oplus 1)}_{4,a}\rangle, |\psi^{8}_{z,a}\rangle. \tag{7.157}$$

The unique zero eigenvector of the matrix (7.153) is

$$\frac{1}{\sqrt{15}}\begin{pmatrix}1 & -1 & -1 & -1 & \sqrt{5} & \sqrt{5} & 1\end{pmatrix}^T. \tag{7.158}$$

Constructing this vector within each of the 16 blocks, we get the states found in the lemma. □

With this understanding of the ground states of $A(G_U)$, we can then give some meaning to the nodes of the graph. In particular, we view the nodes labeled $\alpha, \beta, \gamma, \delta$ in Figure **??** as "input" nodes and those labeled $\epsilon, \zeta, \eta, \theta$ as "output nodes". Each of the states $|\rho^{i,U}_{z,a}\rangle$ is associated with one of the nodes, depending on the values of $i \in [4]$ and $z \in \mathbb{F}_2$. For example, the states $|\rho^{1,U}_{0,0}\rangle$ and $|\rho^{1,U}_{0,1}\rangle$ are associated with input node α since they both have nonzero amplitude on vertices of the gate graph that are associated with α (and zero amplitude on vertices associated with other labeled nodes).

With the single particle states found, we now turn our attention to the two-particle states. It will turn out that the two particle eigenstates of the move-together gadget found in Lemma 18 will play a critical part in our construction.

Lemma 20. *A basis for the nullspace of $H(G_U, 2)$ is*

$$|T^{U,\pm}_{z_1,a,z_2,b}\rangle = \frac{1}{2}\Big(|\rho^{1,U}_{z_1,a}\rangle|\rho^{3,U}_{z_2,b}\rangle \pm |\rho^{3,U}_{z_2,b}\rangle|\rho^{1,U}_{z_1,a}\rangle + \sum_{x_1,x_2=0}^{1} U(a)_{x_1x_2,z_1z_2}\big(|\rho^{2,U}_{x_1,a}\rangle|\rho^{4,U}_{x_2,b}\rangle \pm |\rho^{4,U}_{x_2,b}\rangle|\rho^{2,U}_{x_1,a}\rangle\big)\Big) \tag{7.159}$$

for $z_1, z_2, a, b \in \mathbb{F}_2$ when $d_{max} > 0$, and if $d_{max} = 0$ a basis for the nullspace of $H(G_U, 2)$ when restricted to symmetric states is $|T^{U,+}_{z_1,a,z_2,b}\rangle$ for $z_1, z_2, a, b \in \mathbb{F}_2$. For any $N \geq 3$, there are no N-particle frustration-free states on G_U for any $d_{max} > 0$ and there are no N-particle symmetric frustration-free states on G_U when $d_{max} = 0$, i.e.,

$$\lambda^1_N(G_U) > 0 \quad \textit{for } N \geq 3. \tag{7.160}$$

Proof. Let us first show that the states $|T^{U,\pm}_{z_1,a,z_2,b}\rangle$ are contained within the nullspace of $H(G_U, 2)$. We we can expand these states in terms of the $|\psi^q_{z,a}\rangle$ for $q \in [32]$ and $|\chi^{xy}_{j,a}\rangle$, and see that the state $|T^{U,\pm}_{z_1,a,z_2,b}\rangle$ has no support on diagram elements for which particles are located closer than $k > d_{\max}$, unless possibly both particles are contained in a single move-together gadget. In particular, whenever one particle is in state $|\psi^q_{z,a}\rangle$ (and thus localized to the diagram element q), the other particle is located on a diagram element separated from

the first by at least one additional diagram element. As the nodes of a diagram element are located on vertices of at least $d_{\max}$ distance, these states do not cause an energy penalty. The only difficult case to check is when both particles are in move-together gadgets, but the structure of the states $|T^{U,\pm}_{z_1,a,z_2,b}\rangle$ is such that either the particles are in separate move-together gadgets (and thus on states with support at a distance much larger than k), or the two particles are in a state within the span of $|\Phi^{\pm}_{a,b}\rangle$ and thus by Lemma 18 are not penalized by the interaction term. Altogether, we have that the states $|T^{U,\pm}_{z_1,a,z_2,b}\rangle$ are contained in the nullspace of the interaction Hamiltonian, and thus are frustration-free.

Now let us show that any state in the nullspace of $H(G_U, 2)$ are within the span of the states $|T^{U,\pm}_{z_1,a,z_2,b}\rangle$. Using Lemma **??** we can write any two-particle frustration-free state as

$$|\Theta\rangle = \sum_{z,a,x,b\in\{0,1\}} \sum_{I,J\in[4]} B_{(z,a,I),(x,b,J)} |\rho^{I,U}_{z,a}\rangle |\rho^{J,U}_{x,b}\rangle \tag{7.161}$$

where

$$\langle\psi^{q}_{x,a}|\langle\psi^{q}_{z,b}|\Theta\rangle = 0 \tag{7.162}$$

for all $x, z, a, b \in \{0, 1\}$ and $q \in [88]$, and if $d_{\max} = 0$ we want

$$B_{(z,a,I),(x,b,J)} = B_{(x,b,J),(z,a,I)}. \tag{7.163}$$

To enforce equation (7.162) we consider the diagram elements $q \in [32]$ (as labeled in Figure 7.5a) separately from the other 56 diagram elements (those inside the move-together gadgets).

Using equation (7.162) with $q \in \{1, 2, 3, 4, 7, 8\}$ and $x, z, a, b \in \mathbb{F}_2$ gives

$$B_{(x,a,I),(z,b,I)} = 0 \quad I \in [4],\ x, z, a, b \in \mathbb{F}_2. \tag{7.164}$$

Using $q = 5$, $x = 0$, and $z = 1$ in equation (7.162) gives

$$\langle\psi^{5}_{0,a}|\langle\psi^{5}_{1,b}|\Theta\rangle = \frac{1}{15} B_{(0,a,1),(1,b,2)} = 0, \tag{7.165}$$

for $a, b \in \{0, 1\}$, while $q = 6$, $x = 0$, and $z = 1$ gives

$$\langle\psi^{6}_{0,a}|\langle\psi^{6}_{1,b}|\Theta\rangle = \frac{1}{15} B_{(0,a,2),(1,b,1)} = 0. \tag{7.166}$$

Note that we can use the same equations with $x = 1$ and $z = 0$ to see that $B_{(1,a,2),(0,b,1)} = B_{(1,a,1),(0,b,2)} = 0$ as well. If we then apply equation (7.162) with $q = 5$ or $q = 6$ and other choices for x and z, or for any or $9 \le q \le 32$, we find that the equation does not lead to any additional independent constraints on the state $|\Theta\rangle$.

Now consider the constraint (7.162) for diagram elements inside the move-together gadgets in Figure 7.5a. Let Π_{xy} be the projector onto two-particle states where both particles are located at vertices contained within the move-together gadget labeled $xy \in \{00, 01, 10, 11\}$. Using the results of Lemma 18, we see that for diagram elements inside the move-together gadgets, (7.162) is satisfied if and only if

$$\Pi_{xy}|\Theta\rangle \in \mathrm{span}\big\{|\chi^{xy}_{1,a}\rangle|\chi^{xy}_{3,b}\rangle \pm |\chi^{xy}_{3,b}\rangle|\chi^{xy}_{1,a}\rangle + |\chi^{xy}_{2,a}\rangle|\chi^{xy}_{4,b}\rangle \pm |\chi^{xy}_{4,b}\rangle|\chi^{xy}_{2,a}\rangle,\ a, b \in \{0, 1\}\big\}. \tag{7.167}$$

Since we already know

$$\Pi_{xy}|\Theta\rangle \in \mathrm{span}\big\{|\chi^{xy}_{i,a}\rangle|\chi^{xy}_{j,b}\rangle,\ i,j\in[4], a,b\in\mathbb{F}_2\big\}, \tag{7.168}$$

we get

$$\langle\chi^{xy}_{K,a}|\langle\chi^{xy}_{K,b}|\Theta\rangle = 0 \quad K\in[4] \tag{7.169}$$

$$\langle\chi^{xy}_{K,a}|\langle\chi^{xy}_{L,b}|\Theta\rangle = 0 \quad |K-L|\neq 2 \tag{7.170}$$

$$\big(\langle\chi^{xy}_{1,a}|\langle\chi^{xy}_{3,b}| - \langle\chi^{xy}_{2,a}|\langle\chi^{xy}_{4,b}|\big)|\Theta\rangle = 0 \tag{7.171}$$

$$\big(\langle\chi^{xy}_{3,a}|\langle\chi^{xy}_{1,b}| - \langle\chi^{xy}_{4,a}|\langle\chi^{xy}_{2,b}|\big)|\Theta\rangle = 0 \tag{7.172}$$

for all $a,b\in\{0,1\}$. Note that (7.169) is automatically satisfied whenever (7.164) holds.

Applying equation (7.170) with $(K,L)=(1,2)$ and $a,b,x,y\in\mathbb{F}_2$, we get

$$\langle\chi^{xy}_{1,a}|\langle\chi^{xy}_{2,b}|\Theta\rangle = \frac{1}{3}\sum_{z\in\mathbb{F}_2}\tilde{U}^a_{xz}B_{(z,a,1),(x,b,2)} = \frac{1}{3}\tilde{U}^a_{xx}B_{(x,a,1),(x,b,2)} = 0. \tag{7.173}$$

In the second equality we used the fact that $B_{(z,a,1),(x,b,2)}$ is zero whenever $z\neq x$ (from equations (7.163), (7.165), and (7.166)). Since $\tilde{U}\in\{1,H,HT\}$ we have $\tilde{U}^a_{xx}\neq 0$, and it follows that

$$B_{(x,a,1),(x,b,2)} = 0 \tag{7.174}$$

for all $x,a,b\in\mathbb{F}_2$, while the same argument for $(K,L)=(2,1)$ gives $B_{(x,a,2),(x,b,1)}=0$ for all $x,a,b\in\mathbb{F}_2$.

Applying equation (7.170) with $(K,L)=(1,4)$ gives

$$\langle\chi^{xy}_{1,a}|\langle\chi^{xy}_{4,b}|\Theta\rangle = \frac{1}{3}\sum_{z\in\mathbb{F}_2}\tilde{U}(a)_{xz}B_{(z,a,1),(x\oplus y,b,4)} = 0 \qquad x,y,a,b\in\mathbb{F}_2. \tag{7.175}$$

By taking appropriate combinations of these equations, we have

$$\sum_{x\in\mathbb{F}_2}\tilde{U}^{a,\dagger}_{wx}\langle\chi^{x(y\oplus x)}_{1,a}|\langle\chi^{x(y\oplus x)}_{4,b}|\Theta\rangle = \frac{1}{3}B_{(w,a,1),(y,b,4)} = 0 \qquad w,y,a,b\in\mathbb{F}_2, \tag{7.176}$$

while the same argument with $(K,L)=(4,1)$ gives $B_{(x,a,4),(z,b,1)}=0$ for $x,z,a,b\in\mathbb{F}_2$

Applying equation (7.170) with $(K,L)\in\{(2,3),(3,2),(3,4),(4,3)\}$ gives

$$\langle\chi^{xy}_{2,a}|\langle\chi^{xy}_{3,b}|\Theta\rangle = \frac{1}{3}B_{(x,a,2),(y,b,3)} = 0 \qquad \langle\chi^{xy}_{3,a}|\langle\chi^{xy}_{2,b}|\Theta\rangle = \frac{1}{3}B_{(x,a,3),(y,b,2)} = 0 \tag{7.177}$$

$$\langle\chi^{xy}_{3,a}|\langle\chi^{xy}_{4,b}|\Theta\rangle = \frac{1}{3}B_{(x,a,3),(x\oplus y,b,4)} = 0 \qquad \langle\chi^{xy}_{4,a}|\langle\chi^{xy}_{3,b}|\Theta\rangle = \frac{1}{3}B_{(x,a,4),(x\oplus y,b,3)} = 0 \tag{7.178}$$

for all $x,y,a,b\in\mathbb{F}_2$.

Now putting together equations (7.164), (7.165), (7.166), (7.174), (7.176), (7.177), and (7.178), we get

$$B_{(x,a,I),(z,b,J)} = 0 \quad \text{for all } x,z,a,b\in\mathbb{F}_2, \text{ where } |I-J|\neq 2, \tag{7.179}$$

and thus we have

$$|\Theta\rangle = \sum_{\substack{z,c,w,d\in\mathbb{F}_2 \\ j\in[4]}} B_{(z,c,j),(w,d,j+2)} |\rho^{j,U}_{z,c}\rangle |\rho^{j+2,U}_{w,d}\rangle. \tag{7.180}$$

Now

$$\langle\chi^{xy}_{1,a}|\langle\chi^{xy}_{3,b}|\rho^{1,U}_{z,c}\rangle|\rho^{3,U}_{w,d}\rangle = \frac{1}{3}\delta_{a,c}\delta_{b,d}\tilde{U}(a)_{xz}\delta_{y,w} = \langle\chi^{xy}_{3,b}|\langle\chi^{xy}_{1,a}|\rho^{3,U}_{z,d}\rangle|\rho^{1,U}_{w,c}\rangle \tag{7.181}$$

$$\langle\chi^{xy}_{2,a}|\langle\chi^{xy}_{4,b}|\rho^{2,U}_{z,c}\rangle|\rho^{4,U}_{w,d}\rangle = \frac{1}{3}\delta_{a,c}\delta_{b,d}\delta_{x,z}\delta_{y,w\oplus x} = \langle\chi^{xy}_{4,a}|\langle\chi^{xy}_{2,b}|\rho^{4,U}_{z,c}\rangle|\rho^{2,U}_{w,d}\rangle, \tag{7.182}$$

so enforcing equation (7.171) gives

$$\sum_{z\in\mathbb{F}_2} \tilde{U}^a_{xz} B_{(z,a,1),(y,b,3)} = B_{(x,a,2),(x\oplus y,b,4)}, \tag{7.183}$$

while enforcing equation (7.172) gives

$$\sum_{z\in\mathbb{F}_2} \tilde{U}^a_{xz} B_{(y,b,3),(z,a,1)} = B_{(x\oplus y,b,4),(x,a,2)}, \tag{7.184}$$

for each $x, y, a, b \in \mathbb{F}_2$. In other words

$$B_{(z,c,2),(w,d,4)} = \sum_{x\in\mathbb{F}_2} \tilde{U}^c_{zx} B_{(x,c,1),(z\oplus w,d,3)} = \sum_{x,y\in\mathbb{F}_2} U^c_{zw,xy} B_{(x,c,1),(y,d,3)}, \tag{7.185}$$

and

$$B_{(w,d,4),(z,c,2)} = \sum_{x,y\in\mathbb{F}_2} U^c_{zw,xy} B_{(y,d,3),(x,c,1)}, \tag{7.186}$$

where we used $U^a = \mathrm{CNOT}_{12}(\tilde{U}^a \otimes 1)$. Plugging this into (7.180) gives

$$\begin{aligned}
|\Theta\rangle = \sum_{z,a,w,b\in\mathbb{F}_2} \Big[& B_{(z,a,1),(w,b,3)} |\rho^{1,U}_{z,a}\rangle|\rho^{3,U}_{w,b}\rangle + B_{(z,a,3),(w,b,1)} |\rho^{3,U}_{z,a}\rangle|\rho^{1,U}_{w,b}\rangle \\
& + \sum_{x,y\in\mathbb{F}_2} U^a_{zw,xy} B_{(x,a,1),(y,b,3)} |\,\rho^{2,U}_{z,a}\,\rangle|\,\rho^{4,U}_{w,b}\,\rangle + U^b_{wz,yx} B_{(x,a,3),(y,b,1)} |\,\rho^{4,U}_{z,a}\,\rangle|\,\rho^{2,U}_{w,b}\,\rangle \Big] \qquad (7.187) \\
= \sum_{z,a,w,b\in\mathbb{F}_2} \Big[& B_{(z,a,1),(w,b,3)} \Big(|\rho^{1,U}_{z,a}\rangle|\rho^{3,U}_{w,b}\rangle + \sum_{x,y\in\mathbb{F}_2} U^a_{xy,zw} |\,\rho^{2,U}_{x,a}\,\rangle|\,\rho^{4,U}_{y,b}\,\rangle \Big) \\
& + B_{(z,a,3),(w,b,1)} \Big(|\,\rho^{3,U}_{z,a}\,\rangle|\rho^{1,U}_{w,b}\rangle + \sum_{x,y\in\mathbb{F}_2} U^b_{yx,wz} |\,\rho^{4,U}_{x,a}\,\rangle|\,\rho^{2,U}_{y,b}\,\rangle \Big) \Big] \qquad (7.188) \\
= \sum_{z,a,w,b\in\mathbb{F}_2} & B_{(z,a,1),(w,b,3)} \big(|\,T^{U,+}_{z,a,w,b}\,\rangle + |\,T^{U,-}_{z,a,w,b}\,\rangle \big) - B_{(z,a,3),(w,b,1)} \big(|\,T^{U,+}_{w,b,z,a}\,\rangle - |\,T^{U,-}_{w,b,z,a}\,\rangle \big) \qquad (7.189)
\end{aligned}$$

This is the general solution to equations (7.161)–(7.162), so the space of two-particle frustration-free states for G_U is spanned by the 32 orthonormal states (7.159).

Note that the above analysis only uses Lemma 18, and thus if $d_{\max} = 0$ and we restrict ourselves to the symmetric states, the entire computation follows. Further, we also have that only the states $|T^{U,+}_{z,a,w,b}\rangle$ are symmetric, and thus these states span the symmetric subspace.

Finally, we show that there are no three-particle frustration-free states (for any $d_{\max}$). By Lemma **??**, this implies that there are no frustration-free states for more than two particles. Suppose (to reach a contradiction) that $|\Gamma\rangle$ is a normalized three-particle frustration-free state. Write

$$|\Gamma\rangle = \sum E_{(x,a,q),(y,b,r),(z,c,s)} |\rho^q_{x,a}\rangle |\rho^r_{y,b}\rangle |\rho^s_{z,c}\rangle \tag{7.190}$$

and note that each reduced density matrix of $|\Gamma\rangle$ on two of the three subsystems must have all of its support on two-particle frustration-free states (see the remark following Lemma **??**). As the two-particle ground space is supported on states of the form

$$|\,\rho^r_{x,a}\,\rangle |\,\rho^q_{z,b}\,\rangle \tag{7.191}$$

for $|r-q| = 2$, we have that each two-particle reduced state must also exist in this subspace. We then find that

$$\{q,r\} \notin \{\{1,3\},\{2,4\}\} \implies E_{(x,a,q),(y,b,r),(z,c,s)} = 0 \tag{7.192}$$
$$\{q,s\} \notin \{\{1,3\},\{2,4\}\} \implies E_{(x,a,q),(y,b,r),(z,c,s)} = 0 \tag{7.193}$$
$$\{r,s\} \notin \{\{1,3\},\{2,4\}\} \implies E_{(x,a,q),(y,b,r),(z,c,s)} = 0 \tag{7.194}$$

which together imply that $|\Gamma\rangle = 0$ (a contradiction). Hence no three-particle frustration-free state exists. □

The two-particle state $|T^{U,\pm}_{z_1,a,z_2,b}\rangle$ is a superposition of a term

$$\frac{1}{2}\big(|\rho^{1,U}_{z_1,a}\rangle |\rho^{3,U}_{z_2,b}\rangle \pm |\,\rho^{3,U}_{z_2,b}\,\rangle |\,\rho^{1,U}_{z_1,a}\,\rangle\big) \tag{7.195}$$

with both particles located on vertices corresponding to input nodes and a term

$$\frac{1}{2}\Big(\sum_{x_1,x_2\in\{0,1\}} U^a_{x_1x_2,z_1z_2}\big(|\rho^{2,U}_{x_1,a}\rangle |\rho^{4,U}_{x_2,b}\rangle \pm |\,\rho^{4,U}_{x_2,b}\,\rangle |\,\rho^{2,U}_{x_1,a}\,\rangle\big)\Big) \tag{7.196}$$

with both particles on vertices corresponding to output nodes. The two-qubit gate U^a is applied as the particles move from input nodes to output nodes. Note that we have essentially constructed a graph such that the ground states correspond to the history states. Assuming that we can guarantee that particles will have the correct locations, we will be able to combine these gadgets together to construct a history state.

7.2.2.3 Boundary gadget

In addition to the gadgets that will allow us to implement two-qubit gates, it will be useful to also have gadgets with similar ground states, but without the ability to move through the gadget. In particular, we will need to have gadgets that act as boundaries on where the particles can move. In practice, we will simply use a slightly modified version of the

two-qubit gate gadget, but with additional self loops placed so that the gadget only has single-particle self-loops.

We will actually need two types of boundary gadgets, corresponding to whether or not we will want to force the state of a particular qubit into the zero state, such as initializing ancilla or forcing the output qubit to accept.

The most simple type of *boundary gadget* will be one without penalties. The gate diagram is nearly the same as in Figure 7.5a (with $\tilde{U} = \mathbb{I}$) by adding self-loops to eight of the labeled vertices. In particular, the adjacency matrix is given by

$$A(G_{\text{bnd}}) = A(G_{\text{CNOT}_{12}}) + h_{\mathcal{S}} \tag{7.197}$$

$$h_{\mathcal{S}} = \sum_{z\in\mathbb{F}_2} (|1,z,2kz\rangle\langle 1,z,2kz|\otimes\mathbb{I}_8\otimes\mathbb{I}_2 + |2,z,4k+2kz\rangle\langle 2,z,4k+2kz|\otimes\mathbb{I}_j + |3,z,2kz\rangle\langle 3,z,2kz|\otimes\mathbb{I}_j). \tag{7.198}$$

The second type of boundary gadget with penalties, is shown in Figure **??**. Again the gate diagram is obtained from Figure 7.5a by adding self-loops, but we also change the $q = 8$ element from a $\mathbb{I}^{(1,1)}_{(0,0)}$ element to a $\mathbb{I}^{(1,1)}_{(0,1)}$ diagram element. In particular, we have that its adjacency matrix is

$$A(G_{\text{bnd,pen}}) = A(G_{\text{bnd}}) - 2\sum_{j\in[8]} |\,8,1,6k,j,+\rangle\langle 8,1,6k,j,+\,| \tag{7.199}$$

Note that $A(G_{\text{bnd,pen}})$ is still a positive semidefinite matrix, as the subtracted terms correspond to changing the $q = 8$ element from a $\mathbb{I}^{(1,1)}_{(0,0)}$ element to a $\mathbb{I}^{(1,1)}_{(1,1)}$ element. This does not affect any of our previous results on the single- or two- particle eigenstates, but will allow us to have an additional node for that logical state.

For both types of boundary gadgets, the single-particle ground states (with energy e_1) are superpositions of the states $|\rho^{i,U}_{z,a}\rangle$ from Lemma 19 that are in the nullspace of $h_{\mathcal{S}}$. Note that

$$\langle\rho^{j,U}_{x,b}|h_{\mathcal{S}}|\rho^{i,U}_{z,a}\rangle = \delta_{a,b}\delta_{x,z}\left(\delta_{i,1}\delta_{j,1} + \delta_{i,2}\delta_{j,2} + \delta_{i,3}\delta_{j,3}\right)\frac{1}{15}\cdot\frac{1}{8k} \tag{7.200}$$

and thus we have that the only single-particle ground states are

$$|\rho^{\text{bnd}}_{z,a}\rangle = |\rho^{4,U}_{z,a}\rangle \tag{7.201}$$

with $z, a \in \mathbb{F}_2$. Additionally, there are no two- (or more) particle frustration-free states, because no superposition of the states (7.159) lies in the subspace

$$\text{span}\{|\rho^{4,U}_{z,a}\rangle|\rho^{4,U}_{x,b} : z,a,x,b \in \mathbb{F}_2\} \tag{7.202}$$

of states with single-particle reduced density matrices in the ground space of $A(G_{\text{bnd}})$. We summarize these results as follows.

Lemma 21. *The smallest eigenvalue of $A(G_{bnd})$ and of $A(G_{bnd,pen})$ is e_1, with corresponding eigenvectors*

$$|\rho^{bnd}_{z,a}\rangle = \frac{1}{\sqrt{15}}\Big(|\psi^4_{z,a}\rangle + |\psi^8_{z,a}\rangle - |\,\psi^{31+z}_{z,a}\rangle + \sum_{x\in\mathbb{F}_2}\left(\sqrt{5}|\chi^{x(z\oplus x)}_{4,a}\rangle - |\,\psi^{21+2z+x}_{0,a}\rangle\right)\Big). \tag{7.203}$$

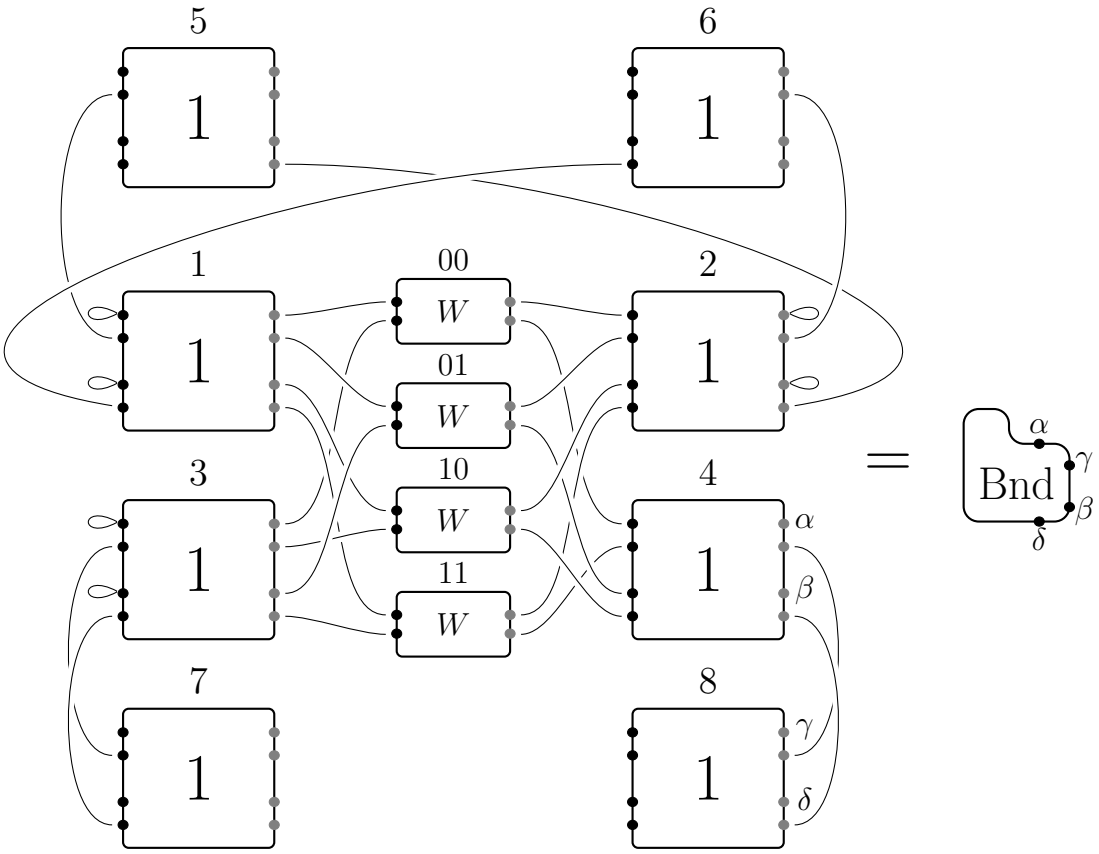

Figure 7.6: The gate diagram for the boundary gadget is obtained from Figure 7.5b by setting $\tilde{U} = 1$ and adding 6 self-loops.

For any $N \geq 2$, there are no N-particle frustration-free states on G_{bnd} or $G_{bnd,pen}$ for any $d_{max} > 0$ and there are no N-particle symmetric frustration-free states on G_{bnd} or $G_{bnd,pen}$ when $d_{max} = 0$, i.e.,

$$\lambda_N^1(G_{bnd}) \geq \lambda_N^1(G_{bnd,pen}) > 0 \quad \textit{for } N \geq 2. \tag{7.204}$$

7.3 The occupancy constraints lemma

While the graphs defined in Section 7.2 have many useful features, such as simple single- and two-particle states and a constant energy gap, they do require that the particles are located in very specific locations. In particular, in order for the two-particle gadgets to encode a computation we require that two-particles have non-zero amplitude on the particle. While this is simple to achieve if the number of particles is larger than the number of gadgets, the final gate graph that we construct will have many more gate graphs than particles, which will result in the existence of many unwanted states remaining in the n-particle ground space.

To get around this problem, we will need to ensure that certain two-particle states are removed from the ground space. In particular, if we want to encode each logical qubit via a single particle, we will want to ensure that only one particle corresponds to a specific qubit. If we encode time in a spatial manner, this will require that two particles don't correspond to the same qubit at different times.

We will get around this problem via a lemma that we call the *occupancy constraints lemma*. The basic idea is that it will take in a gate graph, and a set of two-particle states that we don't want to occur, and then construct a larger graph that has related n-particle ground states but without the unwanted states.

7.3.1 Occupancy constraints

With the idea of excluding certain two-particle states from the ground space of the quantum walk on a gate graph, we will somehow need to encode these constraints. To do so, let us assume that G is a gate graph with R diagram elements (of some type). We will then define G^{occ} to be a graph with R vertices, where the vertices of G^{occ} correspond to the diagram elements of G. The edge set of G^{occ} is then defined to encode the occupancy constraints of G, namely there exists an edge between two vertices of G^{occ} if and only if we want to exclude those states from the ground-space of G where two particles are located on the corresponding diagram elements of G. In this way, we can easily encode our requisite occupancy constraints: simply add an edge in the graph G^{occ}.

[**TO DO:** *find whatever section we defined frustration-free stuff, and reference*]

With these occupancy constraints well defined, it will also be useful to define the frustration-free ground space that also respects these constraints. In particular, remember that for a particular gate graph G, we defined the N-particle frustration-free ground space of the gate graph without edges between the diagram elements and without self-loops as

$$\mathcal{I}(G,N) = \text{span}\left\{ |\psi^{q_1}_{z_1,a_1}\rangle \cdots |\psi^{q_N}_{z_N,a_N}\rangle : \forall i,j \in [N], z_i, a_i \in \mathbb{F}_2, q_i \in [R], i \neq j \Rightarrow q_i \neq q_j \right\}. \tag{7.205}$$

In particular, this subspace guarantees that each individual particle is in the ground state of a diagram element, and further that no two particles are located on the same element.

To also ensure that the particles satisfy a particular pair of occupancy constraints, we can restrict this subspace even farther. Once again, if G is a gate graph, and if G^{occ} is a set of occupancy constraints for G, then we can define

$$\mathcal{I}(G, G^{\text{occ}}, N) := \text{span}\left\{ |\psi^{q_1}_{z_1,a_1}\rangle \cdots |\psi^{q_N}_{z_N,a_N}\rangle : \right. \\ \left. \forall i,j \in [N], z_i, a_i \in \mathbb{F}_2, q_i \in [R], i \neq j \Rightarrow q_i \neq q_j \text{ and } (i,j) \notin E(G^{\text{occ}}) \right\}. \tag{7.206}$$

This subspace explicitly excludes those states that violate the occupancy constraints of G^{occ}, and thus will be useful for when we want to assume that the occupancy constraints are satisfied.

Now that we have a subspace that satisfy our occupancy constraints, we will want to understand how the eigenvalues change when we add in the various edges and self-loops of the original gate graph. In particular, we will define

$$H(G, G^{\text{occ}}, N) = H(G, N)\big|_{\mathcal{I}(G,G^{\text{occ}},N)} \tag{7.207}$$

to be the MPQW Hamiltonian when restricted to the subspace that satisfies the occupancy constraints. We then define $\lambda^1_N(G, G^{\text{occ}})$ for the smallest eigenvalue of this Hamiltonian. Note that if the system is exactly frustration-free, $\lambda^1_N(G, G^{\text{occ}}) = 0$.

7.3.2 Occupancy Constraints Lemma statement

Now that we can easily encode our occupancy constraints, we would like to have the technical results that our transformation allows us to perform. Specifically, while our transform might raise certain states out of the ground space, it might also drastically reduce the energy gap of the Hamiltonian as well. As our eventual goal is to show that the MPQW-ground state problem is **QMA**-complete, we need to bound this reduction in the gap.

[**TO DO:** *correct occupancy constraints bounds*]

With this in mind, we can state the explicit bounds for our lemma:

Lemma 22 (**Occupancy Constraints Lemma**). *Let G be an e_1-gate graph specified as a gate diagram with $R \geq 2$ diagram elements. Let $N \in [R]$, let G^{occ} specify a set of occupancy constraints on G, and suppose the subspace $\mathcal{I}(G, G^{occ}, N)$ is nonempty. Then there exists an efficiently computable e_1-gate graph $G^{\square}$ with at most $7R^2$ diagram elements such that*

1. *If $\lambda^1_N(G, G^{occ}) \leq a$ then $\lambda^1_N(G^{\square}) \leq \frac{a}{R}$.*
2. *If $\lambda^1_N(G, G^{occ}) \geq b$ with $b \in [0,1]$, then $\lambda^1_N(G^{\square}) \geq \frac{\gamma_{\square} b}{R^{9+\nu}}$, where $\gamma_{\square}$ is a constant that depends only on the interaction $\mathcal{U}$, and ν is the bound on the maximum strength of the interaction potential.*

In the next subsection we give the explicit transformation of the graph G to the graph $G^{\square}$. While the actual transformation itself is not particularly complicated, in order to show how the energy gap transforms we will need to define several intermediate graphs in which not all of the edges are added. Thus our proof of the occupancy constraints lemma will also be rather iterative, and will be done later in this section.

7.3.2.1 Definition of $G^{\square}$

We will now show how to construct $G^{\square}$ from G and an occupancy constraints graph G^{occ}. To ensure that the ground space has the appropriate form, the construction of $G^{\square}$ differ slightly for even and odd R is even or odd as a result of the edges in gate diagrams adding an additional sign between connected diagram elements. The following description handles both cases.

In order to ease the definition of $G^{\square}$, let us first fix notation for the gate graph G and the occupancy constraints graph G^{occ}. Write the adjacency matrix of G as (see equation (7.90))

$$A(G) = \sum_{q=1}^{R} |q\rangle\langle q| \otimes A(g_q) + h_{\mathcal{E}^G} + h_{\mathcal{S}^G} \tag{7.208}$$

where $h_{\mathcal{E}^G}$ and $h_{\mathcal{S}^G}$ are determined (through equations (7.93) and (7.92)) by the sets $\mathcal{E}^G$ and $\mathcal{S}^G$ of edges and self-loops in the gate diagram for G, and where g_q is the $128k$-vertex graph corresponding to the diagram element labeled q.

1. For each diagram element $q \in [R]$ in the gate diagram for G, construct a gadget as shown in Figure 7.7, with diagram elements labeled $q_{\text{in}}, q_{\text{out}}$ and $d(q,s)$ where $q, s \in [R]$ and $q \neq s$ if R is even. In particular, if the diagram element labeled q is a $U^{(a,b)}_{(c,d)}$ diagram element, then q_{in} is a $\mathbb{I}^{(a,b)}_{(1,1)}$ diagram element, q_{out} is a $U^{(1,1)}_{(c,d)}$ diagram element, and each $d(q,s)$ is a $\mathbb{I}^{(2,2)}_{(2,2)}$ diagram element. Each node (q,z,t) in the gate diagram for G is mapped to a new node $\text{new}(q,z,t)$ as shown by the black and grey arrows, i.e.,

$$\text{new}(q,z,t) = \begin{cases} (q_{\text{in}}, z, t) & \text{if } (q,z,t) \text{ is an input node} \\ (q_{\text{out}}, z, t) & \text{if } (q,z,t) \text{ is an output node.} \end{cases} \tag{7.209}$$

   Edges and self-loops in the gate diagram for G are replaced by edges and self-loops between the corresponding nodes in the modified diagram.

2. For each edge $\{q_1, q_2\} \in E(G^{\text{occ}})$ in the occupancy constraints graph we add four $\mathbb{I}^{(1,1)}_{(0,0)}$ diagram elements. We refer to these diagram elements by labels $e_{ij}(q_1, q_2)$ with $i, j \in \mathbb{F}_2$. For these diagram elements the labeling function is symmetric, i.e., $e_{ij}(q_1, q_2) = e_{ji}(q_2, q_1)$ whenever $\{q_1, q_2\} \in E(G^{\text{occ}})$.

3. For each non-edge $\{q_1, q_2\} \notin E(G^{\text{occ}})$ with $q_1, q_2 \in [R]$ and $q_1 \neq q_2$ we add 8 $\mathbb{I}^{(1,1)}_{(0,0)}$ diagram elements. We refer to these diagram elements as $e_{ij}(q_1, q_2)$ and $e_{ij}(q_2, q_1)$ with $i, j \in \mathbb{F}_2$; when $\{q_1, q_2\} \notin E(G^{\text{occ}})$ the labeling function is not symmetric, i.e., $e_{ij}(q_1, q_2) \neq e_{ji}(q_2, q_1)$. If R is odd we also add $4R$ $\mathbb{I}^{(1,1)}_{(0,0)}$ diagram elements labeled $e_{ij}(q, q)$ with $i, j \in \mathbb{F}_2$ and $q \in [R]$.

4. Finally, we add edges and self-loops to the gate diagram as shown in Figure 7.8. This gives the gate diagram for $G^{\square}$.

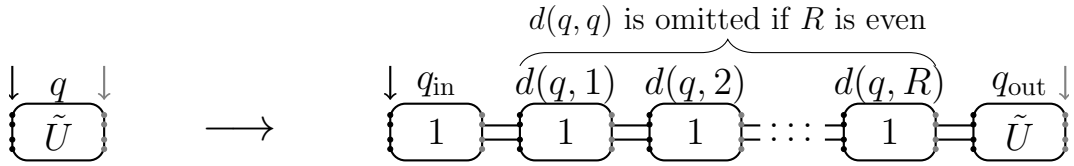

Figure 7.7: The first step in constructing the gate diagram of $G^{\square}$ from that of G is to replace each diagram element as shown. The four input nodes (black arrow) and four output nodes (grey arrow) on the left-hand side are identified with nodes on the right-hand side as shown.

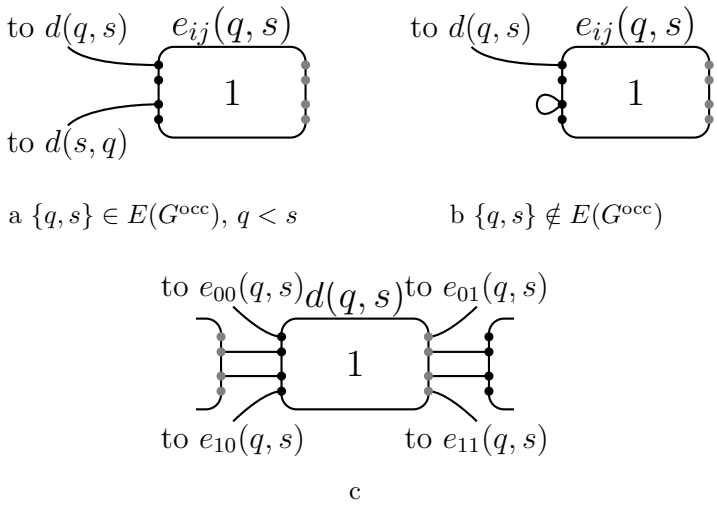

Figure 7.8: Edges and self-loops added in step 4 of the construction of the gate diagram of $G^{\square}$. When $\{q,s\} \in E(G^{\text{occ}})$ with $q < s$, we add two outgoing edges to $e_{ij}(q,s)$ as shown in (a). Note that if $q > s$ and $\{q,s\} \in E(G^{\text{occ}})$ then $e_{ij}(q,s) = e_{ji}(s,q)$. When $\{q,s\} \notin E(G^{\text{occ}})$ we add a self-loop and a single outgoing edge from $e_{ij}(q,s)$ as shown in (b). Each diagram element $d(q,s)$ has eight outgoing edges (four of which are added in step 4), as shown in (c).

[**TO DO:** *fix these graphs*]

The set of diagram elements in the gate graph for $G^{\square}$ is indexed by

$$L^{\square} = Q_{\text{in}} \cup D \cup E_{\text{edges}} \cup E_{\text{non-edges}} \cup Q_{\text{out}} \tag{7.210}$$

where

$$\begin{aligned} Q_{\text{in}} &= \{q_{\text{in}} : q \in [R]\} && (7.211)\\ D &= \{d(q,s) : q,s \in [R] \text{ and } q \neq s \text{ if } R \text{ is even}\} && (7.212)\\ E_{\text{edges}} &= \{e_{ij}(q,s) : i,j \in \{0,1\},\ \{q,s\} \in E(G^{\text{occ}}) \text{ and } q < s\} \\ E_{\text{non-edges}} &= \{e_{ij}(q,s) : i,j \in \{0,1\},\ \{q,s\} \notin E(G^{\text{occ}}) \text{ and } q \neq s \text{ if } R \text{ is even}\} \\ Q_{\text{out}} &= \{q_{\text{out}} : q \in [R]\}\,. && (7.213) \end{aligned}$$

The total number of diagram elements in $G^{\square}$ is

$$\begin{aligned} |L^{\square}| &= |Q_{\text{in}}| + |D| + |E_{\text{edges}}| + |E_{\text{non-edges}}| + |Q_{\text{out}}| && (7.214)\\ &= \begin{cases} R + R^2 + 4|E(G^{\text{occ}})| + 4\left(R^2 - 2|E(G^{\text{occ}})|\right) + R & R \text{ odd} \\ R + R\left(R-1\right) + 4|E(G^{\text{occ}})| + 4\left(R(R-1) - 2|E(G^{\text{occ}})|\right) + R & R \text{ even} \end{cases} && (7.215)\\ &= \begin{cases} 5R^2 + 2R - 4|E(G^{\text{occ}})| & R \text{ odd} \\ 5R^2 - 3R - 4|E(G^{\text{occ}})| & R \text{ even.} \end{cases} && (7.216) \end{aligned}$$

In both cases this is upper bounded by $7R^2$ as claimed in the statement of the Lemma. Write

$$A(G^{\square}) = \sum_{l \in L^{\square}} |l\rangle\langle l| \otimes A(g_l) + h_{\mathcal{S}^{\square}} + h_{\mathcal{E}^{\square}} \tag{7.217}$$

where g_l corresponds to the diagram element labeled $l \in L^{\square}$, $\mathcal{S}^{\square}$ and $\mathcal{E}^{\square}$ are the sets of self-loops and edges in the gate diagram for $G^{\square}$.

We now focus on the input nodes of diagram elements in Q_{in} and the output nodes of the diagram elements in Q_{out}. These are the nodes indicated by the black and grey arrows in Figure 7.7. Write $\mathcal{E}^0 \subset \mathcal{E}^{\square}$ and $\mathcal{S}^0 \subset \mathcal{S}^{\square}$ for the sets of edges and self-loops that are incident on these nodes in the gate diagram for $G^{\square}$. Note that the sets $\mathcal{E}^0$ and $\mathcal{S}^0$ are in one-to-one correspondence with (respectively) the sets $\mathcal{E}^G$ and $\mathcal{S}^G$ of edges and self-loops in the gate diagram for G (by definition). The other edges and self-loops in $G^{\square}$ do not depend on the sets of edges and self-loops in G, as they are created in our effort to enforce the occupancy constraints. Writing

$$\mathcal{S}^{\triangle} = \mathcal{S}^{\square} \setminus S^0 \qquad \mathcal{E}^{\triangle} = \mathcal{E}^{\square} \setminus \mathcal{E}^0, \tag{7.218}$$

we have

$$h_{\mathcal{S}^{\square}} = h_{\mathcal{S}^0} + h_{\mathcal{S}^{\triangle}} \qquad h_{\mathcal{E}^{\square}} = h_{\mathcal{E}^0} + h_{\mathcal{E}^{\triangle}}. \tag{7.219}$$

With these edges and self-loops that are only affected by the occupancy constraints, it will be useful to define a couple of graphs slightly more simple than $G^{\square}$. In particular, it will be useful to first examine the gate graph that only has the self-loops added during the transformation from G to $G^{\square}$, namely the self-loops on nodes in $\mathcal{S}^{\triangle}$, as this graph has a

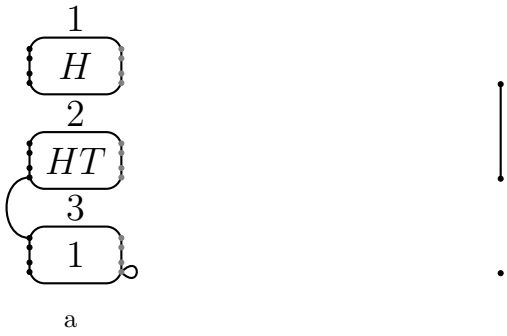

Figure 7.9: An example (a) Gate diagram for a gate graph G and (b) Occupancy constraints graph G^{occ}. In the text we describe how these two ingredients are mapped to a gate graph $G^{\square}$; the gate diagram for $G^{\square}$ is shown in Figure 7.10.

particularly simple ground space, and we will label this graph $G^{\diamondsuit}$. We will then be able to more easily analyze the graph that arises by adding in the edges of $\mathcal{E}^{\triangle}$, and we will label this graph by $G^{\triangle}$. With these foundational graphs understood (and in particular understanding their N-particle frustration-free ground states), we will then easily understand the ground states and ground energies of $G^{\square}$ in term of the ground energies of G.

In particular, we will define the gate diagram for $G^{\diamondsuit}$ to be the diagram on the elements labeled by $L^{\square}$ and including the self-loops in $\mathcal{S}^{\triangle}$. We then have that the adjacency matrix for $G^{\diamondsuit}$ is

$$A(G^{\diamondsuit}) = \sum_{\ell \in L^{\square}} |\ell\rangle\langle\ell| \otimes A(g_{\ell}) + h_{\mathcal{S}^{\triangle}}. \tag{7.220}$$

We can also define the gate diagram for $G^{\triangle}$ to be the same as for $G^{\diamondsuit}$, but including the edges in $\mathcal{E}^{\triangle}$. We can then define the adjacency matrix for $G^{\triangle}$ as

$$A(G^{\triangle}) = \sum_{l \in L^{\square}} |l\rangle\langle l| \otimes A(g_l) + h_{\mathcal{S}^{\triangle}} + h_{\mathcal{E}^{\triangle}}. \tag{7.221}$$

Note that $G^{\triangle} = G^{\square}$ whenever the gate diagram for G contains no edges or self-loops.

We provide an example of this construction in Figure 7.9 (which shows a gate graph and an occupancy constraints graph) and Figure 7.10 (which describes the derived gate graphs $G^{\square}$, $G^{\triangle}$, and $G^{\diamondsuit}$).

[**TO DO:** *completely fix these example graphs*]

7.3.3 The gate graph $G^{\diamondsuit}$

With the various graphs well defined, let us now find the ground states of $A(G^{\diamondsuit})$. We know from (7.220) that each component of $G^{\diamondsuit}$ is a diagram element g_l, with self-loops on some of the nodes. Using Lemma 15, we can then see that each component of $G^{\diamond}$ suit has at most 4 orthonormal e_1-energy eigenstates, and that this is the minimum energy.

More concretely, for each diagram element labeled by $l \in L^{\square}$ in $A(G^{\diamondsuit})$, we can write g'_l for the graph with adjacency matrix

$$A(g'_l) = A(g_l) + |1, 2k\rangle\langle 1, 2k| \otimes \mathbb{I}_{16} \tag{7.222}$$

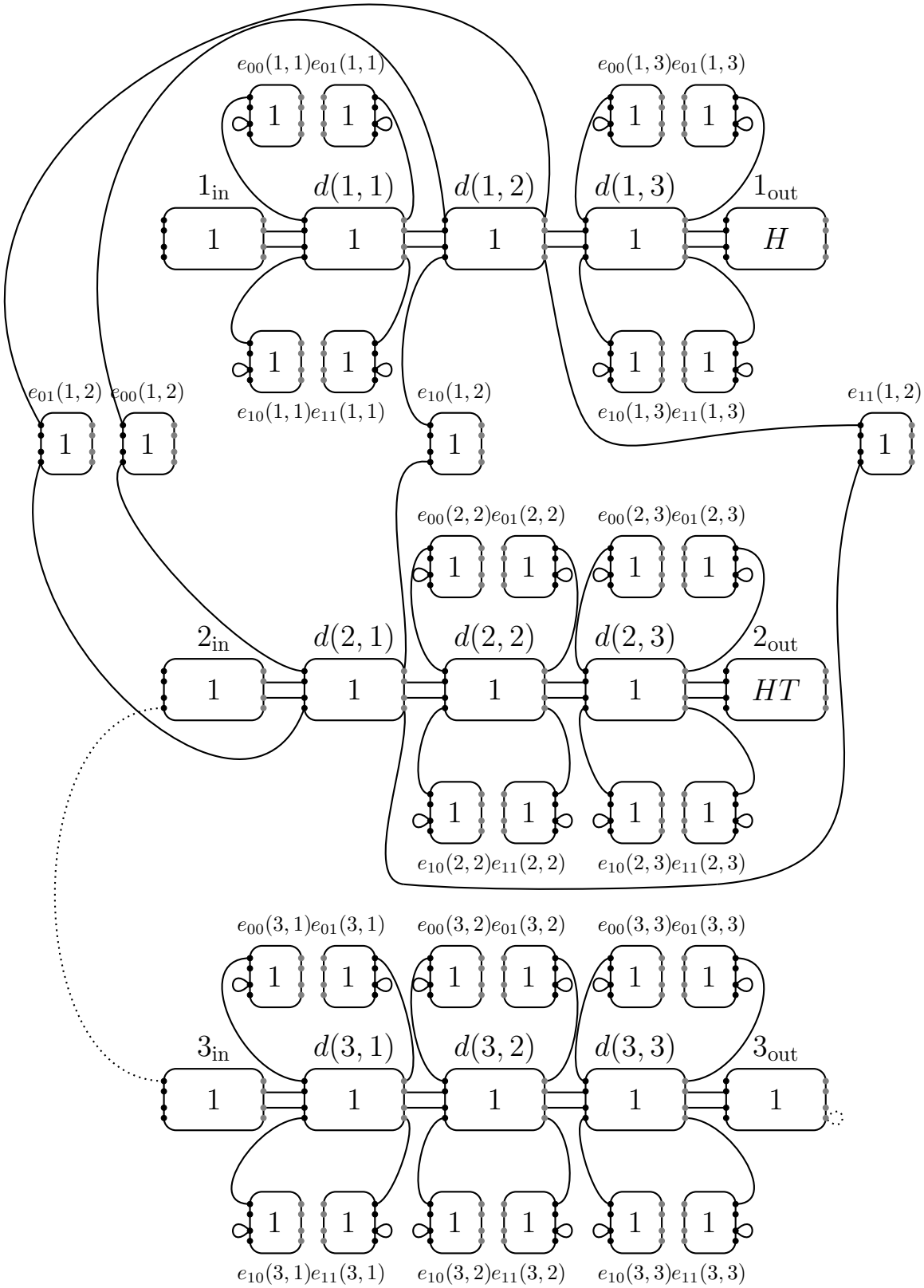

Figure 7.10: The gate diagram for $G^{\triangle}$ (only solid lines) and $G^{\square}$ (including dotted lines) derived from the example gate graph G and occupancy constraints graph G^{occ} from Figure 7.9. The gate diagram for $G^{\diamondsuit}$ is obtained from that of $G^{\triangle}$ by removing all edges (but leaving the self-loops).

(i.e., g_l with 16 self-loops added), and thus each component of $G^\diamondsuit$ is either g_l or g'_l.

We can then use Lemma 15 to see that $A(g_\ell)$ has four orthonormal e_1-energy ground states for each ℓ namely $|\overline{\psi_{z,a}}\rangle$ for $z, a \in \mathbb{F}_2$, as defined in (7.31), (7.32), using the transform of (7.76). As the states with $z = 0$ are in the nullspace of $|1, 2k\rangle\langle 1, 2k| \otimes \mathbb{I}_{16}$, while the operator is strictly positive for the states with $z = 1$, we se that the ground space of $A(g'_l)$ is spanned by the states $|\overline{\psi_{0,a}}\rangle$ for $a \in \mathbb{F}_2$. If we now label the states by the $l \in L^\square$, (i.e., $|\psi^l_{z,a}\rangle = |l\rangle|\overline{\psi_{z,a}}\rangle$, we can choose a basis $\mathcal{W}$ for the e_1-energy ground space of $A(G^\diamondsuit)$ where each basis vector is supported on one of the components:

$$\mathcal{W} = \left\{|\psi^l_{0,a}\rangle : a \in \mathbb{F}_2,\, l \in E_{\text{non-edges}}\right\} \bigcup \left\{|\psi^l_{z,a}\rangle : z, a \in \mathbb{F}_2,\, l \in L^\square \setminus E_{\text{non-edges}}\right\}. \tag{7.223}$$

The eigenvalue gap of $A(G^\diamondsuit)$ is equal to that of either $A(g_l)$ or $A(g'_l)$ for some l. Since g_l and g'_l are constant-sized $256k$-vertex graphs, there exists a constant sized gap for each; let $c_\diamondsuit$ be the minimum value of this gap for all possible diagram elements, both with and without the added self-loops. We then have that

$$\gamma(A(G^\diamondsuit) - e_1) \geq c_\diamondsuit \tag{7.224}$$

The ground space of $A(G^\diamondsuit)$ has dimension

$$|\mathcal{W}| = 4\left|L^\square\right| - 2\,|E_{\text{non-edges}}| \tag{7.225}$$

$$= \begin{cases} 4\left(5R^2 + 2R - 4|E(G^{\text{occ}})|\right) - 2\left(4R^2 - 8|E(G^{\text{occ}})|\right) & R \text{ odd} \\ 4\left(5R^2 - 3R - 4|E(G^{\text{occ}})|\right) - 2\left(4R(R-1) - 8|E(G^{\text{occ}})|\right) & R \text{ even} \end{cases} \tag{7.226}$$

$$= \begin{cases} 12R^2 + 8R & R \text{ odd} \\ 12R^2 - 4R & R \text{ even.} \end{cases} \tag{7.227}$$

We now consider the N-particle Hamiltonian $H(G^\diamondsuit, N)$ and characterize its nullspace.

Lemma 23. *If $d_{max} > 0$ and if $|L^\square| geq N$, then the nullspace of $H(G^\diamondsuit, N)$ is*

$$\mathcal{I}_\diamondsuit = \text{span}\left\{|\psi^{q_1}_{z_1,a_1}\rangle|\psi^{q_2}_{z_2,a_2}\rangle\cdots|\psi^{q_N}_{z_N,a_N}\rangle \;:\; |\psi^{q_i}_{z_i,a_i}\rangle \in \mathcal{W} \text{ and } \forall i,j \in [N], i \neq j \Rightarrow q_i \neq q_j\right\} \tag{7.228}$$

where $\mathcal{W}$ is given in equation (7.223). If $d_{max} = 0$ and if $|L^\square| \geq N$, then when restricted to symmetric states, then nullspace of $H(G^\diamondsuit, N)$ is given by

$$\mathcal{I}^{\text{Sym}}_\diamondsuit = \text{span}\{\text{Sym}(|\Phi\rangle) : |\Phi\rangle \in \mathcal{I}_\diamondsuit\}. \tag{7.229}$$

When $d_{max} > 0$ (and when restricted to symmetric states for $d_{max} = 0$), the smallest nonzero eigenvalue satisfies

$$\gamma(H(G^\diamondsuit, N)) > \gamma_\diamondsuit, \tag{7.230}$$

where $\gamma_\diamondsuit$ is a constant that depends only on the interaction $\mathcal{U}$.

Proof. The main tool used in this proof is our characterization of the 2-particle ground states on diagram elements from Lemma 16, namely that they don't exist. Combined with our results for interactions on disconnected graphs from Lemma 13, we essentially have the proof.

In particular, we have from Lemma 16 that in the N-particle ground space, no component of $G^{\diamondsuit}$ supports a two-particle frustration-free state (i.e., $\lambda_2^1(g_l) > 0$ for each $l \in L^{\square}$), while $\lambda_1^1(g_l) = 0$. If we assume that $L^{\square} \geq N$ and $d_{\max} > 0$, we then have from Lemma 13 that the N-particle nullspace for $G^{\diamondsuit}$ is exactly $\mathcal{I}_{\diamondsuit}$. If we restrict our attention to symmetric states, the same argument holds for all $d_{\max}$.

Additionally, we have from Lemma 13 that the smallest nonzero eigenvector of $H(G^{\diamondsuit}, N)$ is either the smallest eigenvalue of a single-particle excited state for some diagram element g_l, or else the smallest energy of a two-particle state on some diagram element g_l (where we used the fact that adding the self-loops can only increase the energy of a state). As such, we can then bound the eigenvalue gap for the N-particle sector on $G^{\diamondsuit}$ as

$$\gamma(H(G^{\diamondsuit}, N)) \geq \min_{l \in L^{\square}} \{\min\{\lambda_2^1(g_l), \gamma(H(g_l, 1))\}\} \tag{7.231}$$

$$\geq \min_{\substack{U \in \{\mathbb{I}, H, HT\} \\ 0 \leq a,b,c,d \leq 2}} \min\{\lambda_2^1(G_U^{(a,b),(c,d)}), \gamma(H(G_U^{(a,b),(c,d)}, 1))\} = \gamma_{\diamondsuit}. \tag{7.232}$$

Note that $\gamma_{\diamondsuit}$ depends only on $d_{\max}$ (from the size of the graph g_0) and on the 2-particle energy (from the two-particle ground energy), and thus $\gamma_{\diamondsuit}$ is some constant that depends only on the interaction. □

At this point, we have a foundational graph with a constant eigenvalue gap, upon which we can add edges and see how the eigenvalue gap changes.

7.3.4 The adjacency matrix of the gate graph $G^{\triangle}$

With the graph $G^{\diamondsuit}$ defined and its ground-states defined and energy gaps bounded, we now want to examine the graph with the edges that enforce the occupancy constraints. In particular, we now want to examine $G^{\triangle}$.

We begin by solving for the ground space of the adjacency matrix $A(G^{\triangle})$. From equation (7.221) and we have

$$A(G^{\triangle}) = A(G^{\diamondsuit}) + h_{\mathcal{E}^{\triangle}}. \tag{7.233}$$

We already know that the e_1-energy ground space of $A(G^{\diamondsuit})$ is spanned by $\mathcal{W}$ from equation (7.223). Since $h_{\mathcal{E}^{\triangle}} \geq 0$ it follows that $A(G^{\triangle}) \geq e_1$. If we then want to find the e_1-energy groundspace of $A(G^{\triangle})$, we construct superpositions of vectors from $\mathcal{W}$ that are in the nullspace of $h_{\mathcal{E}^{\triangle}}$. To this end we consider the restriction

$$h_{\mathcal{E}^{\triangle}}\big|_{\mathrm{span}(\mathcal{W})}, \tag{7.234}$$

and we will show that it is block diagonal in the basis $\mathcal{W}$.

Recall from equation (7.93) that

$$h_{\mathcal{E}^{\triangle}} = \sum_{\{(l,z,t),(l',z',t')\} \in \mathcal{E}^{\triangle}} (|l,z,t\rangle + |l',z',t'\rangle)(\langle l,z,t| + \langle l',z',t'|) \otimes \mathbb{I}_{16}. \tag{7.235}$$

The edges $\{(l,z,t),(l',z',t')\} \in \mathcal{E}^{\triangle}$ can be read off from Figure 7.7 and Figure 7.8, where we refer back to Figure 7.2 for the labeling convention of nodes on a diagram element. The

edges from Figure 7.7 are

$$\big\{(q_{\text{in}}, z, (5+z)k), (d(q,1), z, (1+z)k)\big\}, \tag{7.236}$$
$$\big\{(d(q,i), z, (5+z)k), (d(q,i+1), z, (1+z)k)\big\}, \tag{7.237}$$
$$\big\{(d(q,R), z, (5+z)k), (q_{\text{out}}, z, (1+z)k)\big\}, \tag{7.238}$$

with $q \in [R]$, $i \in [R-1]$ and $z \in \mathbb{F}_2$, and where $d(q,q)$ does not appear if R is even (i.e., $d(q,q-1)$ is followed by $d(q,q+1)$). The edges from Figure 7.8 take the form

$$\left\{(d(q,s), z, k(3z+4x)), (e_{zx}(q,s), \alpha(q,s), 2k\alpha(q,s))\right\}, \tag{7.239}$$

with $q, s \in [R]$, $q \neq s$ if R is even, $z, x \in \mathbb{F}_2$, and where

$$\alpha(q,s) = \begin{cases} 1 & q > s \text{ and } \{q,s\} \in E(G^{\text{occ}}) \\ 0 & \text{otherwise.} \end{cases} \tag{7.240}$$

The set $\mathcal{E}^{\triangle}$ consists of all edges in equations (7.236)–(7.239).

It will turn out that (7.234) is block diagonal, with blocks $\mathcal{W}_{(z,a,q)} \subseteq \mathcal{W}$ of size

$$\left|\mathcal{W}_{(z,a,q)}\right| = \begin{cases} 3R+2 & R \text{ odd} \\ 3R-1 & R \text{ even} \end{cases} \tag{7.241}$$

for each for each triple (z,a,q) with $z, a \in \mathbb{F}_2$ and $q \in [R]$. Using equation (7.227) we can confirm that $|\mathcal{W}| = 4R\left|\mathcal{W}_{(z,a,q)}\right|$, so this accounts for all basis vectors in $\mathcal{W}$. The subset of basis vectors for a given block is

$$\begin{aligned} \mathcal{W}_{(z,a,q)} = &\left\{|\psi_{z,a}^{q_{\text{in}}}\rangle, |\psi_{z,a}^{q_{\text{out}}}\rangle\right\} \cup \left\{|\psi_{z,a}^{d(q,s)}\rangle : s \in [R],\ s \neq q \text{ if } R \text{ even}\right\} \\ &\cup \left\{|\psi_{\alpha(q,s),a}^{e_{zx}(q,s)}\rangle : x \in \{0,1\},\ s \in [R],\ s \neq q \text{ if } R \text{ even}\right\}. \end{aligned} \tag{7.242}$$

Using equation (7.235) and the description of $\mathcal{E}^{\triangle}$ from using the edges of equations (7.236)–(7.239), we can check by direct inspection that (7.234) only has nonzero matrix elements between basis vectors in $\mathcal{W}$ from the same block. The graph $G^{\triangle}$ was designed to expand the states $|\overline{\psi_{z,a}}\rangle$, and block structure reflects this idea.

We can now compute the matrix elements between states from the same block. For example, if R is odd there are edges $\{(q_{\text{in}}, 0, 5k), (d(q,1), 0, k)\}$ and $\{(q_{\text{in}}, 1, 6k), (d(q,1), 1, 2k)\}$ in $\mathcal{E}^{\triangle}$. Using the fact that $|\psi_{z,a}^{l}\rangle = |l\rangle|\psi_{z,a}, -\rangle$ where $|\psi_{z,a}\rangle$ is given by (7.31) and (7.32), we can then compute the relevant matrix elements:

$$\langle \psi_{z,a}^{q_{\text{in}}} | h_{\mathcal{E}^{\triangle}} | \psi_{z,a}^{d(q,1)} \rangle \tag{7.243}$$
$$= \langle \psi_{z,a}^{q_{\text{in}}} | \Bigg(\sum_{x \in \mathbb{F}_2} \big(|q_{\text{in}}, x, 5(k+x)\rangle + |d(q,1), (1+x)k, 1\rangle\big) \otimes \big(\langle q_{\text{in}}, x, (5+x)k| + \langle d(q,1), (1+x)k, 1|\big) \otimes \mathbb{I} \Bigg) |\psi_{z,a}^{d(q,1)}\rangle \tag{7.244}$$
$$= \sum_{x \in \mathbb{F}_2} \langle \overline{\psi_{z,a}}| \left(|x, (5+x)k\rangle\langle x, (1+x)k| \otimes \mathbb{I}\right) |\overline{\psi_{z,a}}\rangle = \frac{1}{8k}. \tag{7.245}$$

Continuing in this manner, we can compute the principal submatrix of (7.234) corresponding to the set $\mathcal{W}_{(z,a,q)}$. This matrix is shown in Figure 7.11a. In the figure each vertex is associated with a state in the block and the weight on a given edge is the matrix element between the two states associated with vertices joined by that edge. The diagonal matrix elements are described by the weights on the self-loops. The matrix described by Figure 7.11a is the same for each block. [**TO DO:** *fix this figure for the correct values* $1/8k$]

For each triple (z, a, q) with $z, a \in \mathbb{F}_2$ and $q \in [R]$, define

$$|\phi^q_{z,a}\rangle = \begin{cases} \frac{1}{\sqrt{3R+2}}\Big[|\psi^{q_{\text{in}}}_{z,a}\rangle + |\psi^{q_{\text{out}}}_{z,a}\rangle + \sum_{j\in[R]}(-1)^j \left(|\psi^{d(q,j)}_{z,a}\rangle - |\psi^{e_{z0}(q,j)}_{\alpha(q,j),a}\rangle - |\psi^{e_{z1}(q,j)}_{\alpha(q,j),a}\rangle\right)\Big] & R \text{ odd} \\ \frac{1}{\sqrt{3R-1}}\Big[|\psi^{q_{\text{in}}}_{z,a}\rangle + |\psi^{q_{\text{out}}}_{z,a}\rangle + \sum_{j<q}(-1)^j \left(|\psi^{d(q,j)}_{z,a}\rangle - |\psi^{e_{z0}(q,j)}_{\alpha(q,j),a}\rangle - |\psi^{e_{z1}(q,j)}_{\alpha(q,j),a}\rangle\right) \\ \qquad - \sum_{j<q}(-1)^j \left(|\psi^{d(q,j)}_{z,a}\rangle - |\psi^{e_{z0}(q,j)}_{\alpha(q,j),a}\rangle - |\psi^{e_{z1}(q,j)}_{\alpha(q,j),a}\rangle\right)\Big] & R \text{ even.} \end{cases} \tag{7.246}$$

The choice to omit $d(q, q)$ for R even ensures that $|\psi^{q_{\text{in}}}_{z,a}\rangle$ and $|\psi^{q_{\text{out}}}_{z,a}\rangle$ have the same sign in these ground states, similar to the original gate diagram this gate graph replaced. We now show that these states span the ground space of $A(G^{\triangle})$.

Lemma 24. *An orthonormal basis for the e_1-energy ground space of $A(G^{\triangle})$ is given by the states*

$$\left\{|\phi^q_{z,a}\rangle : z, a \in \{0, 1\}, q \in [R]\right\} \tag{7.247}$$

defined by equation (7.246). The eigenvalue gap is bounded as

$$\gamma(A(G^{\triangle}) - e_1) > \frac{c_{\triangle}}{R^2}, \tag{7.248}$$

where $c_{\triangle}$ is a constant that only depends on the interaction $\mathcal{U}$.

Proof. The e_1-energy ground space of $A(G^{\triangle})$ is equal to the nullspace of (7.234). Since this operator is block diagonal in the basis $\mathcal{W}$, we can solve for the eigenvectors in the nullspace of each block. Thus, to prove the first part of the lemma, we will analyze the $|\mathcal{W}_{(z,a,q)}| \times |\mathcal{W}_{(z,a,q)}|$ matrix described by Figure 7.11a and show that (7.246) is the unique vector in its nullspace.

We first rewrite the matrix in a slightly different basis obtained by multiplying some of the basis vectors by a phase of -1. Specifically, we use the basis

$$\left\{|\psi^{q_{\text{in}}}_{z,a}\rangle, -|\psi^{d(q,1)}_{z,a}\rangle, |\psi^{e_{z0}(q,1)}_{\alpha(q,1),a}\rangle, |\psi^{e_{z1}(q,1)}_{\alpha(q,1),a}\rangle, |\psi^{d(q,2)}_{z,a}\rangle, -|\psi^{e_{z0}(q,2)}_{\alpha(q,2),a}\rangle, -|\psi^{e_{z1}(q,2)}_{\alpha(q,2),a}\rangle, \ldots, |\psi^{q_{\text{out}}}_{z,a}\rangle\right\} \tag{7.249}$$

where the state associated with each vertex on one side of a bipartition of the graph is multiplied by -1; these are the phases appearing in equation (7.246). Changing to this basis replaces the weight $\frac{1}{8k}$ on each edge in Figure 7.11a by $-\frac{1}{8k}$ and does not change the weights on the self-loops. The resulting matrix is $\frac{1}{8k}L_0$, where L_0 is the Laplacian matrix of the graph shown in Figure 7.11b.

Now we use the fact that the Laplacian of any connected graph has smallest eigenvalue zero, with a unique eigenvector equal to the all-ones vector. [**TO DO:** *Find a citation for this claim*] . Hence for each block we get an eigenvector in the nullspace of (7.234)) given by (7.246). Ranging over all $z, a \in \mathbb{F}_2$ and $q \in [R]$ gives the claimed basis for the e_1-energy ground space of $A(G^{\triangle})$.

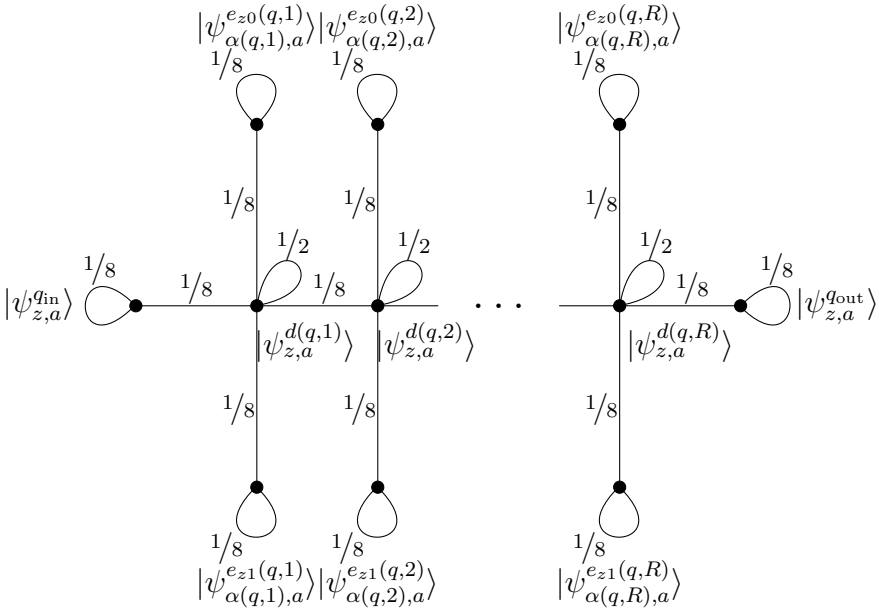

a The matrix $h^{\triangle}_{\mathcal{E}}|_{\mathrm{span}(\mathcal{W})}$ is block diagonal in the basis $\mathcal{W}$, with a block $\mathcal{W}_{(z,a,q)}$ for each $z, a \in \{0,1\}$ and $q \in \{1,\ldots,R\}$. The states involved in a given block and the matrix elements between them are depicted.

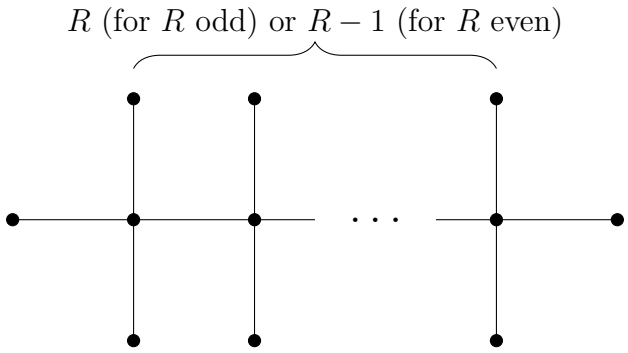

b After multiplying some of the basis vectors by -1, the matrix depicted in (a) is transformed into 1/8 times the Laplacian matrix of this graph.

Figure 7.11

To prove the lower bound on the eigenvalue gap, we use the Nullspace Projection Lemma (Lemma **??**) with

$$H_A = A(G^{\diamondsuit}) - e_1 \qquad H_B = h_{\mathcal{E}^{\triangle}} \tag{7.250}$$

and where $S = \text{span}(\mathcal{W})$ is the nullspace of H_A as shown in Section 7.3.3. Since the restriction of H_B to $\mathcal{S}$ is block diagonal in the basis $\mathcal{W}$, the smallest nonzero eigenvalue of (7.234) is equal to the smallest nonzero eigenvalue of one of its blocks. The matrix for each block is $\frac{1}{8k}L_0$. Thus we can lower bound the smallest nonzero eigenvalue of $H_B|_S$ using standard bounds on the smallest nonzero eigenvalue of the Laplacian L of a graph G. In particular, Theorem 4.2 of reference [24] shows that

$$\gamma(L) \geq \frac{4}{|V(G)|\,\text{diam}(G)} \geq \frac{4}{|V(G)|^2}$$

(where $\text{diam}(G)$ is the diameter of G). Since the size of the graph in Figure 7.11b is either $3R-1$ or $3R+2$, we have

$$\gamma(H_B|_S) = \frac{1}{8k}\gamma(L_0) \geq \frac{1}{8k}\frac{4}{(3R+2)^2} \geq \frac{1}{32kR^2}$$

since $R \geq 2$.

Using this bound and the fact that $\gamma(H_A) > c_{\diamondsuit}$ (from equation (7.224)) and $\|H_B\| = 2$ (from equation (7.95)) and plugging into Lemma **??** gives

$$\gamma(A(G^{\triangle}) - e_1) \geq \frac{c_{\diamondsuit} \cdot \frac{1}{32kR^2}}{c_{\diamondsuit} + 2} > \frac{c_{\diamondsuit}}{94kR^2} = \frac{c_{\triangle}}{R^2}. \tag{7.251}$$

where we used the fact that $c_{\diamondsuit} \leq 1$, and we define $c_{\triangle} = c_{\diamondsuit}/(96k)$. As $c_{\diamondsuit}$ is a constant that only depends on the interaction, so too is $c_{\triangle}$. □

7.3.5 The Hamiltonian $H(G^{\triangle}, N)$

With the previous sections results about the graph $G^{\triangle}$, and in particular knowing its ground states and eigenvalue gap, we can now analyze the multi-particle Hamiltonian. Namely, we can now consider the N-particle Hamiltonian $H(G^{\triangle}, N)$ and solve for its nullspace.

In preparation for understanding the N-particle states, it will be useful to note the following fact about the subsets $\mathcal{W}_{(z,a,q)} \subset \mathcal{W}$ defined in equation (7.242).

Definition 9. We say $\mathcal{W}_{(z_1,a_1,q_1)}$ and $\mathcal{W}_{(z_2,a_2,q_2)}$ *overlap on a diagram element* if there exists $l \in L^{\square}$ such that $|\psi^l_{x_1,b_1}\rangle \in \mathcal{W}_{(z_1,a_1,q_1)}$ and $|\psi^l_{x_2,b_2}\rangle \in \mathcal{W}_{(z_2,a_2,q_2)}$ for some $x_1, x_2, b_1, b_2 \in \mathbb{F}_2$.

Fact 2 (Key property of $\mathcal{W}_{(z,a,q)}$)**.** *Sets $\mathcal{W}_{(z_1,a_1,q_1)}$ and $\mathcal{W}_{(z_2,a_2,q_2)}$ overlap on a diagram element if and only if $q_1 = q_2$ or $\{q_1, q_2\} \in E(G^{occ})$.*

This fact can be confirmed by direct inspection of the sets $\mathcal{W}_{(z,a,q)}$. If $q_1 = q_2 = q$ the diagram element l on which they overlap can be chosen to be $l = q_{\text{in}}$; if $q_1 \neq q_2$ and $\{q_1, q_2\} \in E(G^{\text{occ}})$ then $l = e_{z_1 z_2}(q_1, q_2) = e_{z_2 z_1}(q_2, q_1)$. Conversely, if $\{q_1, q_2\} \notin E(G^{\text{occ}})$ with $q_1 \neq q_2$, then there is no overlap. This fact is the intuitive reason behind our construction of $G^{\square}$; we designed the graph $G^{\triangle}$ so that Fact 2 held.

We will show that the nullspace $\mathcal{I}_\triangle$ of $H(G^\triangle, N)$ is

$$\mathcal{I}_\triangle = \text{span}\left\{|\phi^{q_1}_{z_1,a_1}\rangle|\phi^{q_2}_{z_2,a_2}\rangle \dots |\phi^{q_N}_{z_N,a_N}\rangle \colon z_i, a_i \in \mathbb{F}_2,\ q_i \in [R],\ q_i \neq q_j, \text{ and } \{q_i, q_j\} \notin E(G^{\text{occ}})\right\}, \tag{7.252}$$

for $d_{\max} > 0$, and if $d_{\max} = 0$ we will show that when restricted to symmetric states, the nullspace of $H(G^\triangle, N)$ is

$$\mathcal{I}^{\text{Sym}}_\triangle = \left\{ \text{Sym}(|\,\Phi\rangle) \ :\ |\,\Phi\rangle \in \mathcal{I}_\triangle \right\}. \tag{7.253}$$

Note that $\mathcal{I}_\triangle$ is very similar to $\mathcal{I}(G, G^{\text{occ}}, N)$ (from equation (**??**)) but with each single-particle state $|\psi^q_{z,a}\rangle \in \mathcal{Z}_N(G)$ replaced by $|\phi^q_{z,a}\rangle \in \mathcal{Z}_N(G^\triangle)$ (with the same similarity for the symmetric states).

[**TO DO:** *Change from $\mathcal{Z}$ to something else*]

Lemma 25. *The nullspace of $H(G^\triangle, N)$ is $\mathcal{I}_\triangle$ as defined in equation (7.252) for $d_{max} > 0$, or when restricted to symmetric states the nullspace of $H(G^\triangle, N)$ is $\mathcal{I}^{\text{Sym}}_\triangle$. In either case, its smallest nonzero eigenvalue is*

$$\gamma(H(G^\triangle, N)) > \frac{\gamma_\triangle}{R^7}, \tag{7.254}$$

where $\gamma_\triangle$ is a constant that only depends on $\mathcal{U}$.

In addition to Fact 2, we use the following simple fact in the proof of the Lemma.

Fact 3. *Let $|p\rangle = c|\alpha_0\rangle + \sqrt{1-c^2}|\alpha_1\rangle$ with $\langle\alpha_i|\alpha_j\rangle = \delta_{ij}$ and $c \in [0,1]$. Then*

$$|p\rangle\langle p| = c^2|\alpha_0\rangle\langle\alpha_0| + M \tag{7.255}$$

where $\|M\| \leq 1 - \frac{3}{4}c^4$.

To prove this Fact, one can calculate $\|M\| = \frac{1}{2}(1-c^2) + \frac{1}{2}\sqrt{1+2c^2-3c^4}$ and use the inequality $\sqrt{1+x} \leq 1 + \frac{x}{2}$ for $x \geq -1$.

Proof of Lemma 25. Using equation (7.233) and the fact that the smallest eigenvalues of $A(G^\diamondsuit)$ and $A(G^\triangle)$ are the same (equal to e_1, from Section 7.3.3 and Lemma 24), we can break the MPQW-Hamiltonian on $G^\triangle$ into three terms. Namely, we have

$$H(G^\triangle, N) = H(G^\diamondsuit, N) + \sum_{w=1}^{N} h^{(w)}_{\mathcal{E}^\triangle} + B, \tag{7.256}$$

where B is the change in interaction terms resulting from vertices changing distance. It is important to realize that B only adds terms to the Hamiltonian, as any vertices that were originally at a distance less than $d_{\max}$ remain at the same distance when adding the edges in $\mathcal{E}^\triangle$, and thus B is positive semi-definite. Recall from Lemma 23 that the nullspace of $H(G^\diamondsuit, N)$ is $\mathcal{I}_\diamondsuit$ (or $\mathcal{I}^{\text{Sym}}_\diamondsuit$ if we are restricting to symmetric states). We consider

$$\sum_{w=1}^{N} h^{(w)}_{\mathcal{E}^\triangle}\Big|_{\mathcal{I}_\diamondsuit}. \tag{7.257}$$

We show that its nullspace is equal to $\mathcal{I}_\triangle$, and we lower bound its smallest nonzero eigenvalue. Specifically, we prove

$$\gamma\left(\sum_{w=1}^{N} h_{\mathcal{E}^\triangle}^{(w)}\Big|_{\mathcal{I}_\diamond}\right) > \frac{12c_\triangle}{(4R)^6}. \tag{7.258}$$

Additionally, we will show that B annihilates those states in $\mathcal{I}_\triangle$, so that $\mathcal{I}_\triangle$ is the nullspace of $H(G^\triangle, N)$ as claimed.

We will first prove equation (7.254) using this bound on the added movement terms (equation (7.258)) and the fact that B annihilates $\mathcal{I}_\triangle$. We apply the Nullspace Projection Lemma (Lemma **??**) with H_A and H_B given by the first and second terms in equation (7.256); in this case the nullspace of H_A is $S = \mathcal{I}_\diamond$ (from Lemma 23). Now applying Lemma **??** and using the bounds $\gamma(H_A) > \frac{1}{300}$ (from Lemma 23), $\|H_B\| \leq N\|h_{\mathcal{E}^\triangle}\| = 2N \leq 2R$ (from equation (7.95) and the fact that $N \leq R$), and the bound (7.258) on $\gamma(H_B|_S)$, we find

$$\gamma(H(G^\triangle, N) - M) \geq \frac{\frac{12c_\triangle\gamma_\diamond}{(4R)^6}}{\gamma_\diamond + 2R} \geq \frac{16\gamma_\diamond c_\triangle}{(4R)^7} = \frac{\gamma_\triangle}{R^7}. \tag{7.259}$$

If we then remember the fact that M annihilates all states in $\mathcal{I}_\triangle$, we can use a variational argument to show that the same bound holds for the entire MPQW Hamiltonian (i.e., adding M to the Hamiltonian does not reduce the gap):

$$\gamma(H(G^\triangle, N)) \geq \frac{\gamma_\triangle}{R^7}. \tag{7.260}$$

With the final reductions for the proof completed, we must now establish that B annihilates all terms in $\mathcal{I}_\triangle$, the nullspace of (7.257) is $\mathcal{I}_\triangle$, and prove the lower bound (7.258). Let us first show that each state in $\mathcal{I}_\triangle$ has no energy penalty due to new interactions arising from the addition of edges in the graph $G^\triangle$. By definition, note that the only vertices in $G^\triangle$ that have vertices at a distance closer than $d_{\max}$ either belong to the same diagram element, belong to diagram elements corresponding to $\{q_{\text{in}}, q_{\text{out}}, d(q,s)\}$ for some $q \in [R]$, or else belong to diagram elements labeled $\{d(q,s), e_{z_1,z_2}(q,s)\}$ for some $q, s \in [R]$, and $z_1, z_2 \in \mathbb{F}_2$. As such, if any state has energy penalties resulting from the added edges (i.e., is not annihilated by the operator B,), then it must have at least two particles located on one of these pairs of diagram elements. However, each state $|\,\Phi\,\rangle \in \mathcal{I}_\triangle$ is guaranteed to only have a single particle on each such pair of diagram elements, by construction. Hence, $B|\,\Phi\,\rangle = 0$.

To analyze (7.257) we use the fact (established in Section 7.3.4) that (7.234) is block diagonal with a block $\mathcal{W}_{(z,a,q)} \subset \mathcal{W}$ for each triple (z,a,q) with $z, a \in \mathbb{F}_2$ and $q \in [R]$, as the operator (7.257) inherits a block structure from this fact. For any basis vector

$$\text{Sym}(|\psi_{z_1,a_1}^{q_1}\rangle|\psi_{z_2,a_2}^{q_2}\rangle \ldots |\psi_{z_N,a_N}^{q_N}\rangle) \in \mathcal{I}_\diamond, \tag{7.261}$$

we define a set of occupation numbers that correspond to the number of particles in each block. Namely, we will define

$$\mathcal{N} = \left\{N_{(x,b,r)} \colon x, b \in \{0,1\},\, r \in [R]\right\} \tag{7.262}$$

where

$$N_{(x,b,r)} = |\{j \colon |\psi_{z_j,a_j}^{q_j}\rangle \in \mathcal{W}_{(x,b,r)}\}|. \tag{7.263}$$

Observe that (7.257) conserves the set of occupation numbers (due to the inherited block structure) and is therefore block diagonal with a block for each possible set $\mathcal{N}$.

For a given block corresponding to a set of occupation numbers $\mathcal{N}$, we write $\mathcal{I}_\diamondsuit(\mathcal{N}) \subset \mathcal{I}_\diamondsuit$ for the subspace spanned by basis vectors (7.261) in the block. We classify the blocks into three categories depending on $\mathcal{N}$.

Classification of the blocks of (7.257) according to $\mathcal{N}$

Consider the following two conditions on a set $\mathcal{N} = \{N_{(x,b,r)} \colon x, b \in \{0,1\},\, r \in [R]\}$ of occupation numbers:

(a) $N_{(x,b,r)} \in \{0,1\}$ for all $x, b \in \{0,1\}$ and $r \in [R]$. If this holds, write (y_i, c_i, s_i) for the nonzero occupation numbers (with some arbitrary ordering), i.e., $N_{(y_i,c_i,s_i)} = 1$ for $i \in [N]$.

(b) The sets $\mathcal{W}_{(y_i,c_i,s_i)}$ and $\mathcal{W}_{(y_j,c_j,s_j)}$ do not overlap on a diagram element for all distinct $i, j \in [N]$.

We say a block is of type 1 if $\mathcal{N}$ satisfies (a) and (b). We say it is of type 2 if $\mathcal{N}$ does not satisfy (a). We say it is of type 3 if $\mathcal{N}$ satisfies (a) but does not satisfy (b).

Note that every block must be of type 1, 2, or 3. We will show that each block of type 1 contains one state in the nullspace of (7.257) and, ranging over all blocks of this type, we will obtain a basis for $\mathcal{I}_\triangle$. We will also show that the smallest nonzero eigenvalue within a block of type 1 is at least $\frac{\gamma_\diamondsuit}{R^2}$. We will then show that blocks of type 2 and 3 do not contain any states in the nullspace of (7.257) and that the smallest eigenvalue within any block of type 2 or 3 is greater than [**TO DO:** *get correct bound*] $\frac{12 c_\triangle}{(4R)^6}$. Hence, the nullspace of (7.257) is $\mathcal{I}_\triangle$ and its smallest nonzero eigenvalue is lower bounded as in equation (7.258).

Type 1

Let us first investigate those blocks of type 1. Note (from Definition 9) that requirement (b) implies $q \neq r$ whenever

$$|\psi^q_{x,b}\rangle \in \mathcal{W}_{(y_i,c_i,s_i)} \text{ and } |\psi^r_{z,a}\rangle \in \mathcal{W}_{(y_j,c_j,s_j)} \tag{7.264}$$

for distinct $i, j \in [N]$. Hence, we can remove the requirement that $q_i \neq q_j$:

$$\mathcal{I}_\diamondsuit(\mathcal{N}) = \operatorname{span}\{\operatorname{Sym}(|\psi^{q_1}_{z_1,a_1}\rangle |\psi^{q_2}_{z_2,a_2}\rangle \dots |\psi^{q_N}_{z_N,a_N}\rangle) \colon q_i \neq q_j \text{ and } |\psi^{q_j}_{z_j,a_j}\rangle \in \mathcal{W}_{(y_j,c_j,s_j)}\} \tag{7.265}$$

$$= \operatorname{span}\{\operatorname{Sym}(|\psi^{q_1}_{z_1,a_1}\rangle |\psi^{q_2}_{z_2,a_2}\rangle \dots |\psi^{q_N}_{z_N,a_N}\rangle) \colon |\psi^{q_j}_{z_j,a_j}\rangle \in \mathcal{W}_{(y_j,c_j,s_j)}\}. \tag{7.266}$$

From this we see that

$$\dim(\mathcal{I}_\diamondsuit(\mathcal{N})) = \prod_{j=1}^{N} \left|\mathcal{W}_{(y_j,c_j,s_j)}\right| = \begin{cases} (3R+2)^N & R \text{ odd} \\ (3R-1)^N & R \text{ even.} \end{cases} \tag{7.267}$$

We now solve for all the eigenstates of (7.257) within the block.

As we need only understand the eigenvectors of each individual block, it will be useful to remember Lemma 24 as we have already determined all of the single-particle eigenstates.

It will convenient to write an orthonormal basis of eigenvectors of the $|\mathcal{W}_{(z,a,q)}| \times |\mathcal{W}_{(z,a,q)}|$ matrix described by Figure 7.11a as

$$|\phi^q_{z,a}(u)\rangle, \quad u \in [|\mathcal{W}_{(z,a,q)}|] \tag{7.268}$$

and their ordered eigenvalues as

$$\theta_1 \leq \theta_2 \leq \ldots \leq \theta_{|\mathcal{W}_{(z,a,q)}|}. \tag{7.269}$$

From the proof of Lemma 24, the eigenvector with smallest eigenvalue $\theta_1 = 0$ is $|\phi^q_{z,a}\rangle = |\phi^q_{z,a}(1)\rangle$ and $\theta_2 \geq \frac{c_\diamondsuit}{R^2}$. For any $u_1, u_2, \ldots, u_N \in [|\mathcal{W}_{(z,a,q)}|]$, the state

$$\mathrm{Sym}(|\phi^{s_1}_{y_1,c_1}(u_1)\rangle|\phi^{s_2}_{y_2,c_2}(u_2)\rangle \ldots |\phi^{s_N}_{y_N,c_N}(u_N)\rangle) \tag{7.270}$$

is an eigenvector of (7.257) with eigenvalue $\sum_{j=1}^N \theta_{u_j}$. Furthermore, states corresponding to different choices of $u_1, \ldots, u_N$ are orthogonal, and ranging over all $\dim(\mathcal{I}_\diamondsuit(\mathcal{N}))$ choices we get every eigenvector in the block. The smallest eigenvalue within the block is $N\theta_1 = 0$ and there is a unique vector in the nullspace, given by

$$|\,\Phi_{\mathcal{N}}\rangle := \mathrm{Sym}(|\phi^{s_1}_{y_1,c_1}\rangle|\phi^{s_2}_{y_2,c_2}\rangle \ldots |\phi^{s_N}_{y_N,c_N}\rangle) \tag{7.271}$$

(recall $|\phi^q_{z,a}\rangle = |\phi^q_{z,a}(1)\rangle$). The smallest nonzero eigenvalue of (7.257) within the block is $(N-1)\theta_1 + \theta_2 = \theta_2 \geq \frac{c_\diamondsuit}{R^2}$.

With the knowledge that each state of the form (7.271) minimizes the energy of (7.257), and is in fact the unique ground state within a particular type 1 block, we will now show that the collection of all such states span the space $\mathcal{I}_\triangle$. As the second requirement on type 1 blocks requires that the sets $\mathcal{W}_{(y_i,c_i,s_i)}$ no not pairwise overlap, we can use Fact 2 to see that this is equivalent to the sets satisfying $s_i \neq s_j$ and $\{s_i, s_j\} \notin E(G^{\mathrm{occ}})$ for distinct $i, j \in [N]$ (as well as arbitrary y_i and c_i). Hence the set of states (7.271) obtained from of all blocks of type 1 is

$$\begin{aligned}
&\big\{|\,\Phi_{\mathcal{N}}\rangle : \mathcal{N} \text{ is a type 1 block}\big\} \\
&\quad = \big\{ \mathrm{Sym}(|\phi^{s_1}_{y_1,c_1}\rangle|\phi^{s_2}_{y_2,c_2}\rangle \ldots |\phi^{s_N}_{y_N,c_N}\rangle) : \\
&\qquad \forall i,j \in [N], y_i, c_i \in \mathbb{F}_2,\ s_i \in [R],\ i \neq j \Rightarrow s_i \neq s_j \text{ and } \{s_i, s_j\} \notin E(G^{\mathrm{occ}})\big\}
\end{aligned} \tag{7.272}$$

which by definition spans $\mathcal{I}_\triangle$.

Type 2

Now let $\mathcal{N}$ be of type 2. We then have that there exist $x, b \in \mathbb{F}_2$ and $r \in [R]$ such that $N_{(x,b,r)} \geq 2$. We will show there are no eigenvectors in the nullspace of (7.257) within a block of this type and we lower bound the smallest eigenvalue within the block. Specifically, we show

$$\min_{|\kappa\rangle \in \mathcal{I}_\diamondsuit(\mathcal{N})} \langle\kappa| \sum_{w=1}^N h^{(w)}_{\mathcal{E}^\triangle} |\kappa\rangle > \frac{12 c_\triangle}{(4R)^6}. \tag{7.273}$$

First note that all $|\kappa\rangle \in \mathcal{I}_\diamondsuit$ satisfy $(A(G^\diamondsuit) - e_1)^{(w)}|\kappa\rangle = 0$ for each $w \in [N]$, which can be seen using the definition of $\mathcal{I}_\diamondsuit$ and the fact that $\mathcal{W}$ spans the nullspace of $A(G^\diamondsuit) - e_1$. We can then add these terms to equation (7.233), so that

$$\min_{|\kappa\rangle \in \mathcal{I}_\diamondsuit(\mathcal{N})} \langle\kappa| \sum_{w=1}^{N} h^{(w)}_{\mathcal{E}^\triangle} |\kappa\rangle = \min_{|\kappa\rangle \in \mathcal{I}_\diamondsuit(\mathcal{N})} \langle\kappa| \sum_{w=1}^{N} \left(A(G^\triangle) - e_1\right)^{(w)} |\kappa\rangle. \tag{7.274}$$

If we then examine only the ground space of this operator, we can see that

$$\begin{aligned}\sum_{w=1}^{N} \left(A(G^\triangle) - e_1\right)^{(w)} &\geq \gamma \left(\sum_{w=1}^{N} \left(A(G^\triangle) - e_1\right)^{(w)} \right) \cdot \left(1 - \Pi^\triangle\right) \\ &= \gamma (A(G^\triangle) - e_1) \cdot \left(1 - \Pi^\triangle\right) > \frac{c_\triangle}{R^2} \left(1 - \Pi^\triangle\right), \end{aligned} \tag{7.275}$$

where $\Pi^\triangle$ is the projector onto the nullspace of $\sum_{w=1}^{N} \left(A(G^\triangle) - e_1\right)^{(w)}$, and where in the last step we used Lemma 24. Plugging equation (7.275) into equation (7.274) gives

$$\min_{|\kappa\rangle \in \mathcal{I}_\diamondsuit(\mathcal{N})} \langle\kappa| \sum_{w=1}^{N} h^{(w)}_{\mathcal{E}^\triangle} |\kappa\rangle > \frac{c_\triangle}{R^2} \Big(1 - \max_{|\kappa\rangle \in \mathcal{I}_\diamondsuit(\mathcal{N})} \langle\kappa|\Pi^\triangle|\kappa\rangle\Big). \tag{7.276}$$

Using Lemma 24 we can write $\Pi^\triangle$ explicitly as

$$\Pi^\triangle = \sum_{(\vec{z},\vec{a},\vec{q}) \in \mathcal{Q}} \mathcal{P}_{(\vec{z},\vec{a},\vec{q})} \tag{7.277}$$

where

$$\mathcal{P}_{(\vec{z},\vec{a},\vec{q})} = |\phi^{q_1}_{z_1,a_1}\rangle\langle\phi^{q_1}_{z_1,a_1}| \otimes |\phi^{q_2}_{z_2,a_2}\rangle\langle\phi^{q_2}_{z_2,a_2}| \otimes \cdots \otimes |\phi^{q_N}_{z_N,a_N}\rangle\langle\phi^{q_N}_{z_N,a_N}| \tag{7.278}$$

$$\mathcal{Q} = \{(z_1, \ldots z_N, a_1, \ldots, a_N, q_1, \ldots, q_N) : \; z_i, a_i \in \mathbb{F}_2 \text{ and } q_i \in [R]\}. \tag{7.279}$$

Essentially, each particle is projected onto the ground state of a block, where the blocks are labeled by the elements of $\mathcal{Q}$ and there are no correlations between the particles. For each $(\vec{z},\vec{a},\vec{q}) \in \mathcal{Q}$ we also define a space

$$S_{(\vec{z},\vec{a},\vec{q})} = \text{span}(\mathcal{W}_{(z_1,a_1,q_1)}) \otimes \text{span}(\mathcal{W}_{(z_2,a_2,q_2)}) \otimes \cdots \otimes \text{span}(\mathcal{W}_{(z_N,a_N,q_N)}). \tag{7.280}$$

Note that $\mathcal{P}_{(\vec{z},\vec{a},\vec{q})}$ has all of its support in $S_{(\vec{z},\vec{a},\vec{q})}$, and that

$$S_{(\vec{z},\vec{a},\vec{q})} \perp S_{(\vec{z}',\vec{a}',\vec{q}')} \text{ for distinct } (\vec{z},\vec{a},\vec{q}), (\vec{z}',\vec{a}',\vec{q}') \in \mathcal{Q}. \tag{7.281}$$

Therefore $\mathcal{P}_{(\vec{z},\vec{a},\vec{q})}\mathcal{P}_{(\vec{z}',\vec{a}',\vec{q}')} = 0$ for distinct $(\vec{z},\vec{a},\vec{q}), (\vec{z}',\vec{a}',\vec{q}') \in \mathcal{Q}$. (Below we use similar reasoning to obtain a less obvious result.) Note that $\mathcal{P}_{(\vec{z},\vec{a},\vec{q})}$ is orthogonal to $\mathcal{I}_\diamondsuit(\mathcal{N})$ unless

$$|\{j : (z_j, a_j, q_j) = (w, u, v)\}| = N_{(w,u,v)} \text{ for all } w, u \in \{0, 1\},\ v \in [R]. \tag{7.282}$$

We restrict our attention to the projectors that are not orthogonal to $\mathcal{I}_\diamondsuit(\mathcal{N})$. Letting $\mathcal{Q}(\mathcal{N}) \subset \mathcal{Q}$ be the set of $(\vec{z},\vec{a},\vec{q})$ satisfying equation (7.282), we have

$$\langle\kappa| \sum_{(\vec{z},\vec{a},\vec{q}) \in \mathcal{Q}} \mathcal{P}_{(\vec{z},\vec{a},\vec{q})} |\kappa\rangle = \langle\kappa| \sum_{(\vec{z},\vec{a},\vec{q}) \in \mathcal{Q}(\mathcal{N})} \mathcal{P}_{(\vec{z},\vec{a},\vec{q})} |\kappa\rangle \quad \text{for all } |\kappa\rangle \in \mathcal{I}_\diamondsuit(\mathcal{N}). \tag{7.283}$$

Since $N_{(x,b,r)} \geq 2$, note that in each term $\mathcal{P}_{(\vec{z},\vec{a},\vec{q})}$ with $(\vec{z},\vec{a},\vec{q}) \in \mathcal{Q}(\mathcal{N})$, the operator

$$|\phi^r_{x,b}\rangle\langle\phi^r_{x,b}| \otimes |\phi^r_{x,b}\rangle\langle\phi^r_{x,b}| \tag{7.284}$$

appears between two of the N registers (tensored with rank-1 projectors on the other $N-2$ registers). Using equation (7.246) we may expand $|\phi^r_{x,b}\rangle$ as a sum of states from $\mathcal{W}_{(x,b,r)}$. This gives

$$|\phi^r_{x,b}\rangle|\phi^r_{x,b}\rangle = c_0|\psi^{r_{\text{in}}}_{x,b}\rangle|\psi^{r_{\text{in}}}_{x,b}\rangle + \left(1-c_0^2\right)^{\frac{1}{2}}|\Phi^r_{x,b}\rangle \tag{7.285}$$

where c_0 is either $\frac{1}{3R+2}$ (if R is odd) or $\frac{1}{3R-1}$ (if R is even), and where $|\psi^{r_{\text{in}}}_{x,b}\rangle|\psi^{r_{\text{in}}}_{x,b}\rangle$ is orthogonal to $|\Phi^r_{x,b}\rangle$. Note that each of the states $|\phi^r_{x,b}\rangle|\phi^r_{x,b}\rangle$, $|\psi^{r_{\text{in}}}_{x,b}\rangle|\psi^{r_{\text{in}}}_{x,b}\rangle$, and $|\Phi^r_{x,b}\rangle$ lie in the space

$$\text{span}(\mathcal{W}_{(x,b,r)}) \otimes \text{span}(\mathcal{W}_{(x,b,r)}). \tag{7.286}$$

Now applying Fact 3 gives

$$|\phi^r_{x,b}\rangle\langle\phi^r_{x,b}| \otimes |\phi^r_{x,b}\rangle\langle\phi^r_{x,b}| = c_0^2|\psi^{r_{\text{in}}}_{x,b}\rangle\langle\psi^{r_{\text{in}}}_{x,b}| \otimes |\psi^{r_{\text{in}}}_{x,b}\rangle\langle\psi^{r_{\text{in}}}_{x,b}| + M^r_{x,b} \tag{7.287}$$

where $M^r_{x,b}$ is a Hermitian operator with all of its support on the space (7.286) and

$$\left\|M^r_{x,b}\right\| \leq 1 - \frac{3}{4}c_0^4 \leq 1 - \frac{3}{4}\left(\frac{1}{3R+2}\right)^4 \leq 1 - \frac{3}{4}\frac{1}{(4R)^4} \tag{7.288}$$

since $R \geq 2$. For each $(\vec{z},\vec{a},\vec{q}) \in \mathcal{Q}(\mathcal{N})$ we define $\mathcal{P}^M_{(\vec{z},\vec{a},\vec{q})}$ to be the operator obtained from $\mathcal{P}_{(\vec{z},\vec{a},\vec{q})}$ by replacing

$$|\phi^r_{x,b}\rangle\langle\phi^r_{x,b}| \otimes |\phi^r_{x,b}\rangle\langle\phi^r_{x,b}| \mapsto M^r_{x,b} \tag{7.289}$$

on two of the registers (if $N_{(x,b,r)} > 2$ there is more than one way to do this; we fix one choice for each $(\vec{z},\vec{a},\vec{q}) \in \mathcal{Q}(\mathcal{N})$). Note that $\mathcal{P}^M_{(\vec{z},\vec{a},\vec{q})}$ has all of its support in the space $S_{(\vec{z},\vec{a},\vec{q})}$. Using (7.281) gives

$$\mathcal{P}^M_{(\vec{z},\vec{a},\vec{q})}\mathcal{P}^M_{(\vec{z}',\vec{a}',\vec{q}')} = 0 \text{ for distinct } (\vec{z},\vec{a},\vec{q}),(\vec{z}',\vec{a}',\vec{q}') \in \mathcal{Q}(\mathcal{N}). \tag{7.290}$$

Using equation (7.287) and the fact that

$$\langle\kappa|\left(|\psi^{r_{\text{in}}}_{x,b}\rangle\langle\psi^{r_{\text{in}}}_{x,b}|^{(w_1)}\right)\left(|\psi^{r_{\text{in}}}_{x,b}\rangle\langle\psi^{r_{\text{in}}}_{x,b}|^{(w_2)}\right)|\kappa\rangle = 0 \quad \text{for all } |\kappa\rangle \in \mathcal{I}_\diamond(\mathcal{N}) \text{ and distinct } w_1,w_2 \in [N] \tag{7.291}$$

(which can be seen from the definition of $\mathcal{I}_\diamond$), we have

$$\langle\kappa|\mathcal{P}_{(\vec{z},\vec{a},\vec{q})}|\kappa\rangle = \langle\kappa|\mathcal{P}^M_{(\vec{z},\vec{a},\vec{q})}|\kappa\rangle \quad \text{for all } |\kappa\rangle \in \mathcal{I}_\diamond(\mathcal{N}). \tag{7.292}$$

Hence, letting

$$\Pi^\triangle_{\mathcal{N}} = \sum_{(\vec{z},\vec{a},\vec{q})\in\mathcal{Q}(\mathcal{N})} \mathcal{P}^M_{(\vec{z},\vec{a},\vec{q})}, \tag{7.293}$$

we have $\langle\kappa|\Pi^\triangle|\kappa\rangle = \langle\kappa|\Pi^\triangle_{\mathcal{N}}|\kappa\rangle$ for all $|\kappa\rangle \in \mathcal{I}_\diamond(\mathcal{N})$. To obtain the desired bound (**??**) on the norm of $\Pi^\triangle_{\mathcal{N}}$, we use the fact that the norm of a sum of pairwise orthogonal Hermitian operators is upper bounded by the maximum norm of an operator in the sum, so

$$\left\|\Pi^\triangle_{\mathcal{N}}\right\| = \left\|\sum_{(\vec{z},\vec{a},\vec{q})\in\mathcal{Q}(\mathcal{N})} \mathcal{P}^M_{(\vec{z},\vec{a},\vec{q})}\right\| = \max_{(\vec{z},\vec{a},\vec{q})\in\mathcal{Q}(\mathcal{N})} \left\|\mathcal{P}^M_{(\vec{z},\vec{a},\vec{q})}\right\| = \left\|M^r_{x,b}\right\| \leq 1 - \frac{3}{4}\frac{1}{(4R)^4}. \tag{7.294}$$

Putting this together, we then have that

$$\max_{|\kappa\rangle\in\mathcal{I}_\diamond(\mathcal{N})} \langle\kappa|\Pi^{\triangle}|\kappa\rangle = \max_{|\kappa\rangle\in\mathcal{I}_\diamond(\mathcal{N})} \langle\kappa|\Pi^{\triangle}_{\mathcal{N}}|\kappa\rangle \leq \|\Pi^{\triangle}_{\mathcal{N}}\| \leq 1 - \frac{3}{4(4R)^4}. \tag{7.295}$$

If we then use (7.276), we have that

$$\min_{|\kappa\rangle\in\mathcal{I}_\diamond(\mathcal{N})} \langle\kappa| \sum_{w=1}^{N} h^{(w)}_{\mathcal{E}^{\triangle}} |\kappa\rangle > \frac{c_{\triangle}}{R^2}\Big(1 - \max_{|\kappa\rangle\in\mathcal{I}_\diamond(\mathcal{N})} \langle\kappa|\Pi^{\triangle}|\kappa\rangle\Big) \geq \frac{12c_{\triangle}}{(4R)^6}. \tag{7.296}$$

Type 3

Let us finally examine the case where $\mathcal{N}$ is of type 3 then $N_{(x,b,r)} \in \{0,1\}$ for all $x, b \in \mathbb{F}_2$ and $r \in [R]$, and

$$N_{(y,c,s)} = N_{(t,d,u)} = 1 \tag{7.297}$$

for some $(y,c,s) \neq (t,d,u)$ with either $u = s$ or $\{u,s\} \in E(G^{\text{occ}})$ (using property (b) and Fact 2). We show there are no eigenvectors in the nullspace of (7.257) within a block of this type and we lower bound the smallest eigenvalue within the block. We establish the same bound (7.273) as for blocks of Type 2.

The proof is very similar to that given above for blocks of Type 2. In fact, the first part of proof is identical, from equation (7.274) up to and including equation (7.283). That is to say, as in the previous case we have

$$\langle\kappa| \sum_{(\vec{z},\vec{a},\vec{q})\in\mathcal{Q}} \mathcal{P}_{(\vec{z},\vec{a},\vec{q})} |\kappa\rangle = \langle\kappa| \sum_{(\vec{z},\vec{a},\vec{q})\in\mathcal{Q}(\mathcal{N})} \mathcal{P}_{(\vec{z},\vec{a},\vec{q})} |\kappa\rangle \quad \text{for all } |\kappa\rangle \in \mathcal{I}_\diamond(\mathcal{N}). \tag{7.298}$$

In this case, since $N_{(y,c,s)} = N_{(t,d,u)} = 1$, in each term $\mathcal{P}_{(\vec{z},\vec{a},\vec{q})}$ with $(\vec{z},\vec{a},\vec{q}) \in \mathcal{Q}(\mathcal{N})$, the operator

$$|\phi^s_{y,c}\rangle\langle\phi^s_{y,c}| \otimes |\phi^u_{t,d}\rangle\langle\phi^u_{t,d}| \tag{7.299}$$

appears between two of the N registers (tensored with rank 1 projectors on the other $N-2$ registers). Using equation (7.246) we may expand $|\phi^s_{y,c}\rangle$ and $|\phi^u_{t,d}\rangle$ as superpositions (with amplitudes $\pm\frac{1}{\sqrt{3R+2}}$ if R is odd or $\pm\frac{1}{\sqrt{3R-1}}$ if R is even) of the basis states from $\mathcal{W}_{(y,c,s)}$ and $\mathcal{W}_{(t,d,u)}$ respectively. Since $\mathcal{W}_{(y,c,s)}$ and $\mathcal{W}_{(t,d,u)}$ overlap on some diagram element, there exists $l \in L^{\square}$ such that $|\psi^l_{x_1,b_1}\rangle \in \mathcal{W}_{(y,c,s)}$ and $|\psi^l_{x_2,b_2}\rangle \in \mathcal{W}_{(t,d,u)}$ for some $x_1, x_2, b_1, b_2 \in \{0,1\}$. Hence

$$|\phi^s_{y,c}\rangle|\phi^u_{t,d}\rangle = c_0\left(\pm|\psi^l_{x_1,b_1}\rangle|\psi^l_{x_2,b_2}\rangle\right) + \left(1-c_0^2\right)^{\frac{1}{2}} |\Phi^{s,u}_{y,c,t,d}\rangle \tag{7.300}$$

where c_0 is either $\frac{1}{3R+2}$ (if R is odd) or $\frac{1}{3R-1}$ (if R is even). Now applying Fact 3 we get

$$|\phi^s_{y,c}\rangle\langle\phi^s_{y,c}| \otimes |\phi^u_{t,d}\rangle\langle\phi^u_{t,d}| = c_0^2 |\psi^l_{x_1,b_1}\rangle\langle\psi^l_{x_1,b_1}| \otimes |\psi^l_{x_2,b_2}\rangle\langle\psi^l_{x_2,b_2}| + M^{s,u}_{y,c,t,d} \tag{7.301}$$

where $\|M^{s,u}_{y,c,t,d}\| \leq 1 - \frac{3}{4}\left(\frac{1}{4R}\right)^4$. For each $(\vec{z},\vec{a},\vec{q}) \in \mathcal{Q}(\mathcal{N})$ we define $\mathcal{P}^M_{(\vec{z},\vec{a},\vec{q})}$ to be the operator obtained from $\mathcal{P}_{(\vec{z},\vec{a},\vec{q})}$ by replacing

$$|\phi^s_{y,c}\rangle\langle\phi^s_{y,c}| \otimes |\phi^u_{t,d}\rangle\langle\phi^u_{t,d}| \mapsto M^{s,u}_{y,c,t,d} \tag{7.302}$$

on two of the registers and we let $\Pi^{\triangle}_{\mathcal{N}}$ be given by (7.293). Then, as in the previous case, $\langle\kappa|\Pi^{\triangle}|\kappa\rangle = \langle\kappa|\Pi^{\triangle}_{\mathcal{N}}|\kappa\rangle$ for all $|\kappa\rangle \in \mathcal{I}_{\diamond}(\mathcal{N})$ and using the same reasoning as before, we get the bound (7.294) on $\|\Pi^{\triangle}_{\mathcal{N}}\|$. Using these two facts we get the same bound on the smallest eigenvalue within a block of type 3 as the bound we obtained for blocks of type 2:

$$\min_{|\kappa\rangle\in\mathcal{I}_{\diamond}(\mathcal{N})} \langle\kappa| \sum_{w=1}^{N} h^{(w)}_{\mathcal{E}^{\triangle}} |\kappa\rangle > \frac{c_{\triangle}}{R^2}\Big(1 - \max_{|\kappa\rangle\in\mathcal{I}_{\diamond}(\mathcal{N})} \langle\kappa|\Pi^{\triangle}|\kappa\rangle\Big) \geq \frac{12c_{\triangle}}{(4R)^6}. \qquad \square$$

7.3.6 The gate graph $G^{\square}$

With all of the intermediate graphs characterized, we now consider the gate graph $G^{\square}$ and prove Lemma 22. We first show that $G^{\square}$ is an e_1-gate graph. From equations (7.217), (7.219), and (7.221) we have

$$A(G^{\square}) = A(G^{\triangle}) + h_{\mathcal{E}^0} + h_{\mathcal{S}^0}. \tag{7.303}$$

Lemma 24 characterizes the e_1-energy ground space of $G^{\triangle}$ and gives an orthonormal basis $\{|\phi^q_{z,a}\rangle \colon z, a \in \{0,1\},\, q \in [R]\}$ for it. To solve for the e_1-energy ground space of $A(G^{\square})$, we solve for superpositions of the states $\{|\phi^q_{z,a}\rangle\}$ in the nullspace of $h_{\mathcal{E}^0} + h_{\mathcal{S}^0}$.

Recall the definition of the sets $\mathcal{E}^0$ and $\mathcal{S}^0$, as these are the edges and self-loops that are inherited from the graph G. From Section 7.3.2.1, each node (q,z,t) in the gate diagram for G is associated with a node $\text{new}(q,z,t)$ in the gate diagram for $G^{\square}$ as described by (7.209). This mapping is depicted in Figure 7.7 by the black and grey arrows. Applying this mapping to each pair of nodes in the edge set $\mathcal{E}^G$ and each node in the self-loop set $\mathcal{S}^G$ of the gate diagram for G, we get the sets $\mathcal{E}^0$ and $\mathcal{S}^0$. Hence, using equations (7.92) and (7.93),

$$h_{\mathcal{S}^0} = \sum_{(q,z,t)\in\mathcal{S}^G} |\text{new}(q,z,t)\rangle\langle\text{new}(q,z,t)| \otimes \mathbb{I} \tag{7.304}$$

$$h_{\mathcal{E}^0} = \sum_{\{(q,z,t),(q',z',t')\}\in\mathcal{E}^G} \left(|\text{new}(q,z,t)\rangle + |\text{new}(q',z',t')\rangle\right)\left(\langle\text{new}(q,z,t)| + \langle\text{new}(q',z',t')|\right) \otimes \mathbb{I}. \tag{7.305}$$

Using equation (7.246), we see that for all nodes (q,z,t) in the gate diagram for G and for all $j \in [8]$, $x,b,d \in \mathbb{F}_2$, and $r \in [R]$,

$$\begin{aligned}\langle\text{new}(q,z,t),j,d|\phi^r_{x,b}\rangle &= \sqrt{c_0}\begin{cases}\langle q_{\text{in}},z,t,j,d|\psi^{r_{\text{in}}}_{x,b}\rangle & \text{if } (q,z,t) \text{ is an input node}\\ \langle q_{\text{out}},z,t,j,d|\psi^{r_{\text{out}}}_{x,b}\rangle & \text{if } (q,z,t) \text{ is an output node}\end{cases}\\ &= \sqrt{c_0}\delta_{r,q}\langle z,t,j,d|\psi_{x,b}\rangle\end{aligned} \tag{7.306}$$

where c_0 is $\frac{1}{3R+2}$ if R is odd or $\frac{1}{3R-1}$ if R is even, and where $|\psi_{x,b}\rangle$ is defined by equations (7.31) and (7.32). The matrix element on the left-hand side of this equation is evaluated in the Hilbert space $\mathcal{Z}_1(G^{\square})$ where each basis vector corresponds to a vertex of the graph $G^{\square}$; these vertices are labeled (l,z,t,j,d) with $l \in L^{\square}$, $z,d \in \mathbb{F}_2$, $t \in [2k]$, and $j \in [8]$. However, from (7.306) we see that

$$\underbrace{\langle\text{new}(q,z,t),j,d|\phi^r_{x,b}\rangle}_{\text{in } \mathcal{Z}_1(G^{\square})} = \sqrt{c_0}\,\underbrace{\langle q,z,t,j,d|\psi^r_{x,b}\rangle}_{\text{in } \mathcal{Z}_1(G)} \tag{7.307}$$

where the right-hand side is evaluated in the Hilbert space $\mathcal{Z}_1(G)$.

Putting together equations (7.304), (7.305), and (7.307) gives

$$\langle \phi^q_{z,a}|h_{\mathcal{E}^0} + h_{\mathcal{S}^0}|\phi^r_{x,b}\rangle = \langle \psi^q_{z,a}|h_{\mathcal{E}^G} + h_{\mathcal{S}^G}|\psi^r_{x,b}\rangle \cdot \begin{cases} \frac{1}{3R+2} & R \text{ odd} \\ \frac{1}{3R-1} & R \text{ even} \end{cases} \tag{7.308}$$

for all $z, a, x, b \in \mathbb{F}_2$ and $q, r \in [R]$. On the left-hand side of this equation, the Hilbert space is $\mathcal{Z}_1(G^\square)$; on the right-hand side it is $\mathcal{Z}_1(G)$.

We use equation (7.308) to relate the e_1-energy ground states of $A(G)$ to those of $A(G^\square)$. Since G is an e_1-gate graph, there is a state

$$|\Gamma\rangle = \sum_{z,a,q} \alpha_{z,a,q}|\psi^q_{z,a}\rangle \in \mathcal{Z}_1(G) \tag{7.309}$$

that satisfies $A(G)|\Gamma\rangle = e_1|\Gamma\rangle$ and hence $h_{\mathcal{E}^G}|\Gamma\rangle = h_{\mathcal{S}^G}|\Gamma\rangle = 0$. Letting

$$|\Gamma'\rangle = \sum_{z,a,q} \alpha_{z,a,q}|\phi^q_{z,a}\rangle \in \mathcal{Z}_1(G^\square) \tag{7.310}$$

and using equation (7.308), we see that $\langle\Gamma'|h_{\mathcal{E}^0} + h_{\mathcal{S}^0}|\Gamma'\rangle = 0$ and therefore $\langle\Gamma'|A(G^\square)|\Gamma'\rangle = e_1$. Hence $G^\square$ is an e_1-gate graph. Moreover, the linear mapping from $\mathcal{Z}_1(G)$ to $\mathcal{Z}_1(G^\square)$ defined by

$$|\psi^q_{z,a}\rangle \mapsto |\phi^q_{z,a}\rangle \tag{7.311}$$

maps each e_1-energy eigenstate of $A(G)$ to an e_1-energy eigenstate of $A(G^\square)$.

Now consider the N-particle Hamiltonian $H(G^\square, N)$. Using equation (7.303) and the fact that both $A(G^\square)$ and $A(G^\triangle)$ have smallest eigenvalue e_1, we have

$$H(G^\square, N) = H(G^\triangle, N) + \sum_{w=1}^{N} (h_{\mathcal{E}^0} + h_{\mathcal{S}^0})^{(w)}\Big|_{\mathcal{Z}_N(G^\square)} + C', \tag{7.312}$$

where C corresponds to the added interactions resulting from the additional edges. IRecall from Lemma 24 that the nullspace of the first term is $\mathcal{I}_\triangle$. The N-fold tensor product of the mapping (7.311) acts on basis vectors of $\mathcal{I}(G, G^{\text{occ}}, N)$ as

$$\text{Sym}(|\psi^{q_1}_{z_1,a_1}\rangle|\psi^{q_2}_{z_2,a_2}\rangle \dots |\psi^{q_N}_{z_N,a_N}\rangle) \mapsto \text{Sym}(|\phi^{q_1}_{z_1,a_1}\rangle|\phi^{q_2}_{z_2,a_2}\rangle \dots |\phi^{q_N}_{z_N,a_N}\rangle), \tag{7.313}$$

where $z_i, a_i \in \mathbb{F}_2$, $q_i \neq q_j$, and $\{q_i, q_j\} \notin E(G^{\text{occ}})$. Clearly this defines an invertible linear map between the two spaces $\mathcal{I}(G, G^{\text{occ}}, N)$ and $\mathcal{I}_\triangle$. Let $|\Theta\rangle \in \mathcal{I}(G, G^{\text{occ}}, N)$ and write $|\Theta'\rangle \in \mathcal{I}_\triangle$ for its image under the map (7.313). Then

$$\langle\Theta'|H(G^\square, N) - C'|\Theta'\rangle = \langle\Theta'|\sum_{w=1}^{N} (h_{\mathcal{E}^0} + h_{\mathcal{S}^0})^{(w)}\,|\Theta'\rangle \tag{7.314}$$

$$= \langle\Theta|\sum_{w=1}^{N} (h_{\mathcal{E}^G} + h_{\mathcal{S}^G})^{(w)}\,|\Theta\rangle \cdot \begin{cases} \frac{1}{3R+2} & R \text{ odd} \\ \frac{1}{3R-1} & R \text{ even} \end{cases} \tag{7.315}$$

where in the first equality we used the fact that $|\Theta'\rangle$ is in the nullspace $\mathcal{I}_\triangle$ of $H(G^\triangle, N)$ and in the second equality we used equation (7.308) and the fact that $\langle \phi^q_{z,a} | \phi^r_{x,b} \rangle = \langle \psi^q_{z,a} | \psi^r_{x,b} \rangle$.

Understanding how C' relates to the added interactions in the original gate-graph G is slightly more tricksome, as an arbitrary state we might have N-particle interactions which under our transformation would require a factor of $(3R)^{-N}$ to the energy. However, the fact that each state in $\mathcal{I}_\triangle$ and each state in $\mathcal{I}(G, G^{\text{occ}}, N)$ satisfy the occupancy constraints implies that at most a single particle ever occupies a single vertex (and thus $C' = 0$ if $d_{\max} = 0$). Using this, we have that when restricted to those states in $\mathcal{I}_\triangle$, C' only affects two-particles at a time and the requisite change to the energy penalty will only be $(3R)^{-2}$.

[**TO DO:** *probably I should make this more coherent*] As such, let $\mathcal{V}^\square \subset V(G^\square) \times V(G^\square)$ consist of those pairs of vertices that could be affected by the new interactions caused by the added edges. Since each node of every diagram element is separated by a distance at least $d_{\max}$, we have that each pair of vertices must come from diagram elements labeled q_{in} or q_{out}. Further, if we let $\mathcal{V} \subset V(G) \times V(G)$ be the similar set of vertices that can have interactions caused by the added edges in G, we have that $\mathcal{V}^\square$ is in one-to-one correspondence to those of $\mathcal{V}$, since we have added the same number of edges. In particular, we have that the vertices on [**TO DO:** *actually figure out this mapping*]

With this in mind, along with the fact that we have at most a single particle located on each vertex and the relation between $|\phi^q_{z,a}\rangle$ and $|\psi^q_{z,a}\rangle$, we have that

$$\langle \Theta' | C' | \Theta' \rangle = \sum_{(u',v') \in \mathcal{V}^\square} \sum_{w_1 \neq w_2 \in [N]} \langle \Theta' | \big(|u'\rangle\langle u'|^{(w_1)} \otimes |v'\rangle\langle v'|^{(w_2)} \big) | \Theta' \rangle \tag{7.316}$$

$$= \sum_{(u,v) \in \mathcal{V}} \sum_{w_1 \neq w_2 \in [N]} \langle \Theta | \big(|u\rangle\langle u|^{(w_1)} \otimes |v\rangle\langle v|^{(w_2)} \big) | \Theta \rangle \begin{cases} \frac{1}{(3R+2)^2} & R \text{ odd} \\ \frac{1}{(3R-1)^2} & R \text{ even} \end{cases} \tag{7.317}$$

$$= \langle \Theta | C | \Theta \rangle \begin{cases} \frac{1}{(3R+2)^2} & R \text{ odd} \\ \frac{1}{(3R-1)^2} & R \text{ even} \end{cases} \tag{7.318}$$

We now complete the proof of Lemma 22 using equation (7.315) and (7.318).

Case 1: $\lambda_N(G, G^{\text{occ}}) \leq a$

In this case there exists a state $|\Theta\rangle \in \mathcal{I}(G, G^{\text{occ}}, N)$ satisfying

$$\langle \Theta | \sum_{w=1}^{N} \left(h_{\mathcal{E}^G} + h_{\mathcal{S}^G} \right)^{(w)} + C | \Theta \rangle = a_{\text{adj}} + a_{\text{int}} \leq a, \tag{7.319}$$

From equation (7.315) we see that the state $|\Theta'\rangle \in \mathcal{I}_\triangle$ satisfies $\langle \Theta' | | \Theta' \rangle \leq \frac{a_{\text{adj}}}{3R-1}$, and from (7.318) that it also satisfies $\langle \Theta' | C' | \Theta \rangle' \leq \frac{a_{\text{int}}}{(3R-1)^2}$.

Putting this together, (along with the fact that $|\Theta'\rangle \in \mathcal{I}_\triangle$ and thus is in the nullspace of $H(G^\triangle, N)$),

$$\langle \Theta' | H(G^\square, N) | \Theta' \rangle \leq \frac{a_{\text{adj}}}{3R-1} + \frac{a_{\text{int}}}{(3R-1)^2} < \frac{a_{\text{adj}}}{R} + \frac{a_{\text{int}}}{R} = \frac{a}{R}. \tag{7.320}$$

Case 2: $\lambda_N(G, G^{\mathbf{occ}}) \geq b$

In this case

$$\lambda_N(G, G^{\text{occ}}) = \min_{|\Theta\rangle \in \mathcal{I}(G, G^{\text{occ}}, N)} \langle \Theta | H(G, G^{\text{occ}}, N) | \Theta \rangle \tag{7.321}$$

$$= \min_{|\Theta\rangle \in \mathcal{I}(G, G^{\text{occ}}, N)} \langle \Theta | \sum_{w=1}^{N} \left(h_{\mathcal{E}^G} + h_{\mathcal{S}^G}\right)^{(w)} | \Theta \rangle + \langle \Theta | C | \Theta \rangle \tag{7.322}$$

$$= b_{\text{adj}} + b_{\text{int}} \geq b. \tag{7.323}$$

Now applying equation (7.315) and (7.318) gives

$$\min_{|\Theta'\rangle \in \mathcal{I}_\triangle} \langle \Theta' | H(G^\square, N) | \Theta' \rangle = \min_{|\Theta'\rangle \in \mathcal{I}_\triangle} \langle \Theta' | \sum_{w=1}^{N} \left(h_{\mathcal{E}^0} + h_{\mathcal{S}^0}\right)^{(w)} | \Theta' \rangle + \langle \Theta' | C' | \Theta' \rangle \tag{7.324}$$

$$\geq \frac{b_{\text{adj}}}{3R+2} + \frac{b_{\text{int}}}{(3R+2)^2} \tag{7.325}$$

$$\geq \frac{1}{(3R+2)^2} b, \tag{7.326}$$

This establishes that the nullspace of $H(G^\square, N)$ is empty, i.e., $\lambda_N^1(G^\square) > 0$, so $\lambda_N^1(G^\square) = \gamma(H(G^\square, N))$. We lower bound $\lambda_N^1(G^\square)$ using the Nullspace Projection Lemma (Lemma **??**) with

$$H_A = H(G^\triangle, N) \qquad H_B = \sum_{w=1}^{N} \left(h_{\mathcal{E}^0} + h_{\mathcal{S}^0}\right)^{(w)} \Big|_{\mathcal{Z}_N(G^\square)} + C' \tag{7.327}$$

and where the nullspace of H_A is $S = \mathcal{I}_\triangle$. We apply Lemma **??** and use the bounds $\gamma(H_A) > \frac{\gamma_\triangle}{R^7}$ (from Lemma 25), $\gamma(H_B|_S) \geq \frac{b}{(3R+2)^2}$ (from equation (7.326)), and

$$\|H_B\| \leq N \|h_{\mathcal{E}^0} + h_{\mathcal{S}^0}\| + \|H_{\text{int}}\| \leq 3N + d_{\mathcal{U}} N^\nu \leq d_{\mathcal{U}} R^{\nu_{\mathcal{U}}} \tag{7.328}$$

(using equations (7.95) and (7.94), the bounds on H_{int}, and the fact that $N \leq R$) to find

$$\lambda_N^1(G^\square) = \gamma(H(G^\square, N)) \tag{7.329}$$

$$\geq \frac{\gamma_\triangle b}{(3R+2)^2 R^7} \frac{1}{\frac{\gamma_\triangle}{R^7} + d_{\mathcal{U}} R^{\nu_{\mathcal{U}}}} \tag{7.330}$$

$$> \frac{\gamma_\square b}{R^{9+\nu}} \tag{7.331}$$

where $\gamma_\square$ depends only on the interaction $\mathcal{U}$.

7.4 Constructing the graph for QMA-completeness

With the graphs defined in Section 7.2 and the ability to ensure that certain states are excluded from the ground space via the occupancy constraints lemma Section 7.3.1, we will now be able to construct the graph that will be used in our **QMA**-completeness proof. In

particular, we will show how to transform a given circuit into a graph, such that the n-particle ground-energy will correspond to whether the circuit has an accepting state when certain states are excluded from the ground space.

The main idea will be to use the graph primitives of Section 7.2 to construct a gate graph replacing circuits of a particular form. We will use a single particle for each qubit, and use the location of a single qubit to encode the current "time" of the occupation. Using our two-particle graph gadgets, we can then ensure that the particles move together through the entire computation (assuming that they start in the correct possitions).

7.4.1 Verification circuits

[**TO DO:** *Show that the circuit can be written in the requisite form.*]

7.4.2 Gate graph for a given circuit

For any n-qubit, M-gate verification circuit $\mathcal{C}_X$ of the form described above, we associate a gate graph G_X. The gate diagram for G_X is built using the gadgets described in Section **??**; specifically, we use M two-qubit gadgets and $2(n-1)$ boundary gadgets. Since each two-qubit gadget and each boundary gadget contains 32 diagram elements, the total number of diagram elements in G_X is $R = 32(M + 2n - 2)$.

We now present the construction of the gate diagram for G_X. We also describe some gate graphs obtained as intermediate steps that are used in our analysis in Section **??**. The reader may find this description easier to follow by looking ahead to Figure 7.12, which illustrates this construction for a specific 3-qubit circuit.

1. **Draw a grid** with columns labeled $j = 0, 1, \ldots, M+1$ and rows labeled $i = 1, \ldots, n$ (this grid is only used to help describe the diagram).

2. **Place gadgets in the grid to mimic the quantum circuit.** For each $j = 1, \ldots, M$, place a gadget for the two-qubit gate U_j between rows 1 and $s(j)$ in the jth column. Place boundary gadgets in rows $i = 2, \ldots, n$ of column 0 and in the same rows of column $M+1$. Write G_1 for the gate graph associated with the resulting diagram.

3. **Connect the nodes within each row.** First add edges connecting the nodes in rows $i = 2, \ldots, n$; call the resulting gate graph G_2. Then add edges connecting the nodes in row 1; call the resulting gate graph G_3.

4. **Add self-loops to the boundary gadgets.** In this step we add self-loops to enforce initialization of ancillas (at the beginning) and the proper output of the circuit (at the end). For each row $k = n_{\text{in}}+1, \ldots, n$, add a self-loop to node δ (as shown in Figure 7.6) of the corresponding boundary gadget in column $r = 0$, giving the gate diagram for G_4. Finally, add a self-loop to node α of the boundary gadget (as in Figure 7.6) in row 2 and column $M+1$, giving the gate diagram for G_X.

Figure 7.12 illustrates the step-by-step construction of G_X using a simple 3-qubit circuit with four gates

$$\text{CNOT}_{12}\,(\text{CNOT}_{13}HT \otimes \mathbb{I})\,\text{CNOT}_{21}\text{CNOT}_{13}. \tag{7.332}$$

In this example, two of the qubits are input qubits (so $n_{\text{in}} = 2$), while the third qubit is an ancilla initialized to $|0\rangle$. Following the convention described in Section **??**, we take qubit 2 to be the output qubit. (In this example the circuit is not meant to compute anything interesting; its only purpose is to illustrate our method of constructing a gate graph).

We made some choices in designing this circuit-to-gate graph mapping that may seem arbitrary (e.g., we chose to place boundary gadgets in each row except the first). We have tried to achieve a balance between simplicity of description and ease of analysis, but we expect that other choices could be made to work.

7.4.2.1 Notation for G_X

We now introduce some notation that allows us to easily refer to a subset $\mathcal{L}$ of the diagram elements in the gate diagram for G_X.

Recall from Section **??** that each two-qubit gate gadget and each boundary gadget is composed of 64 diagram elements. This can be seen by looking at Figure 7.5b and noting (from Figure 7.4) that each move-together gadget comprises 14 diagram elements.

For each of the two-qubit gate gadgets in the gate diagram for G_X, we focus our attention on the four diagram elements labeled 1–4 in Figure 7.5b. In total there are $4M$ such diagram elements in the gate diagram for G_X: in each column $j \in \{1, \ldots, M\}$ there are two in row 1 and two in row $s(j)$. When $U_j \in \{\text{CNOT}_{1s(j)}, \text{CNOT}_{1s(j)}\,(H \otimes \mathbb{I})\,, \text{CNOT}_{1s(j)}\,(HT \otimes \mathbb{I})\}$ the diagram elements labeled $1, 2$ are in row 1 and those labeled $3, 4$ are in row $s(j)$; when $U_j = \text{CNOT}_{s(j)1}$ those labeled $1, 2$ are in row $s(j)$ and those labeled $3, 4$ are in row 1. We denote these diagram elements by triples (i, j, d). Here i and j indicate (respectively) the row and column of the grid in which the diagram element is found, and d indicates whether it is the leftmost ($d = 0$) or rightmost ($d = 1$) diagram element in this row and column. We define

$$\mathcal{L}_{\text{gates}} = \{(i, j, d) : i \in \{1, s(j)\},\ j \in [M],\ d \in \{0, 1\}\} \tag{7.333}$$

to be the set of all such diagram elements.

For example, in Figure 7.12 the first gate is

$$U_1 = \text{CNOT}_{13}, \tag{7.334}$$

so the gadget from Figure 7.5b (with $\tilde{U} = 1$) appears between rows 1 and 3 in the first column. The diagram elements labeled $1, 2, 3, 4$ from Figure 7.5b are denoted by $(1, 1, 0), (1, 1, 1), (3, 1, 0), (3, 1, 1)$, respectively. The second gate in Figure 7.12 is $U_2 = \text{CNOT}_{21}$, so the gadget from Figure 7.5c (with $\tilde{U} = 1$) appears between rows 2 and 1; in this case the diagram elements labeled $1, 2, 3, 4$ in Figure 7.5b are denoted by $(2, 2, 0), (2, 2, 1), (1, 2, 0), (1, 2, 1)$, respectively.

We also define notation for the boundary gadgets in G_X. For each boundary gadget. we focus on a single diagram element, labeled 4 in Figure 7.6. For the left hand-side and right-hand side boundary gadgets, respectively, we denote these diagram elements as

$$\mathcal{L}_{\text{in}} = \{(i, 0, 1) \colon i \in \{2, \ldots, n\}\} \tag{7.335}$$

$$\mathcal{L}_{\text{out}} = \{(i, M + 1, 0) \colon i \in \{2, \ldots, n\}\}\,. \tag{7.336}$$

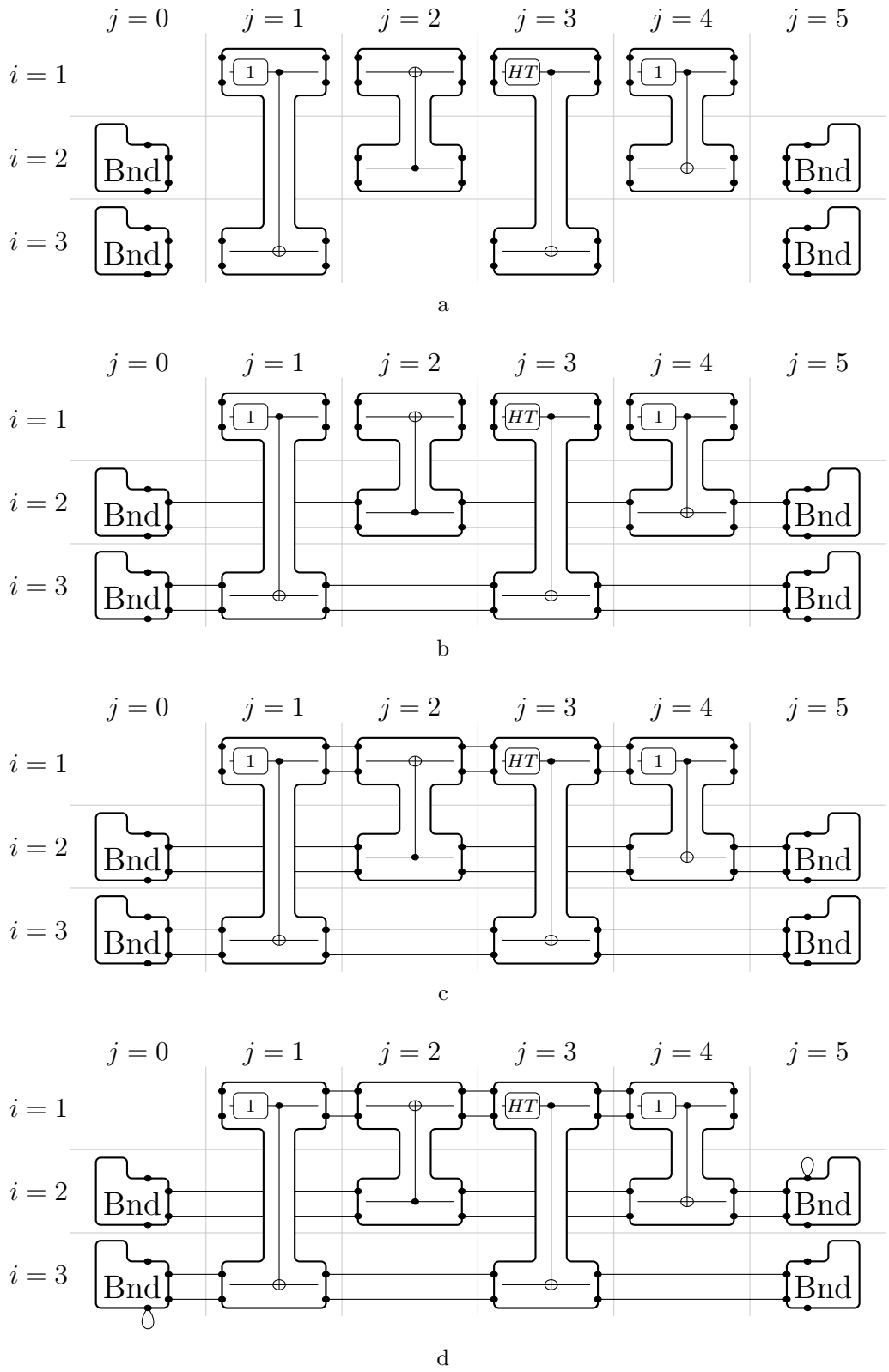

Figure 7.12: Step-by-step construction of the gate diagram for G_X for the three-qubit example circuit described in the text. (a) The gate diagram for G_1. (b) Add edges in all rows except the first to obtain the gate diagram for G_2. (c) Add edges in the first row to obtain the gate diagram for G_3. (d) Add self-loops to the boundary gadgets to obtain the gate diagram for G_X (the diagram for G_4 in this case differs from (d) by removing the self-loop in column 5; this diagram is not shown).

Definition 10. Let $\mathcal{L}$ be the set of diagram elements

$$\mathcal{L} = \mathcal{L}_{\text{in}} \cup \mathcal{L}_{\text{gates}} \cup \mathcal{L}_{\text{out}} \tag{7.337}$$

where $\mathcal{L}_{\text{in}}$, $\mathcal{L}_{\text{gates}}$, and $\mathcal{L}_{\text{out}}$ are given by equations (7.335), (7.333), and (7.336), respectively.

Finally, it is convenient to define a function F that describes horizontal movement within the rows of the gate diagram for G_X. The function F takes as input a two-qubit gate $j \in [M]$, a qubit $i \in \{2, \ldots, n\}$, and a single bit and outputs a diagram element from the set $\mathcal{L}$. If the bit is 0 then F outputs the diagram element in row i that appears in a column $0 \leq k < j$ with k maximal (i.e., the closest diagram element in row i to the left of column j):

$$F(i, j, 0) = \begin{cases} (i, k, 1) & \text{where } 1 \leq k < j \text{ is the largest } k \text{ such that } s(k) = i, \text{ if it exists} \\ (i, 0, 1) & \text{otherwise.} \end{cases} \tag{7.338}$$

On the other hand, if the bit is 1, then F outputs the diagram element in row i that appears in a column $j < k \leq M + 1$ with k minimal (i.e., the closest diagram element in row i to the right of column j).

$$F(i, j, 1) = \begin{cases} (i, k, 0) & \text{where } j < k \leq M \text{ is the smallest } k \text{ such that } s(k) = j, \text{ if it exists} \\ (i, M + 1, 0) & \text{otherwise.} \end{cases} \tag{7.339}$$

7.4.2.2 Occupancy constraints graph

In this Section we define an occupancy constraints graph $G_X oc$. Along with G_X and the number of particles n, this determines a subspace $\mathcal{I}(G_X, G_X oc, n) \subset \mathcal{Z}_n(G_X)$ through equation (**??**). We will see in Section **??** how low-energy states of the Bose-Hubbard model that live entirely within this subspace encode computations corresponding to the quantum circuit $\mathcal{C}_X$. This fact is used in the proof of Theorem **??**, which shows that the smallest eigenvalue $\lambda_n^1(G_X, G_X oc)$ of

$$H(G_X, G_X oc, n) = H(G_X, n)\big|_{\mathcal{I}(G_X, G_X oc, n)} \tag{7.340}$$

is related to the maximum acceptance probability of the circuit.

We encode quantum data in the locations of n particles in the graph G_X as follows. Each particle encodes one qubit and is located in one row of the graph G_X. Since all two-qubit gates in $\mathcal{C}_X$ involve the first qubit, the location of the particle in the first row determines how far along the computation has proceeded. We design the occupancy constraints graph to ensure that low-energy states of $H(G_X, G_X oc, n)$ have exactly one particle in each row (since there are n particles and n rows), and so that the particles in rows $2, \ldots, n$ are not too far behind or ahead of the particle in the first row. To avoid confusion, we emphasize that not *all* states in the subspace $\mathcal{I}(G_X, G_X oc, n)$ have the desired properties—for example, there are states in this subspace with more than one particle in a given row. We see in the next Section that states with low energy for $H(G_X, n)$ that also satisfy the occupancy constraints (i.e., low-energy states of $H(G_X, G_X oc, n)$) have the desired properties.

We now define $G_X oc$, which is a simple graph with a vertex for each diagram element in G_X. Each edge in $G_X oc$ places a constraint on the locations of particles in G_X. The graph $G_X oc$ only has edges between diagram elements in the set $\mathcal{L}$ from Definition 10; we define the edge set $E(G_X oc)$ by specifying pairs of diagram elements $L_1, L_2 \in \mathcal{L}$. We also indicate (in bold) the reason for choosing the constraints, which will become clearer in Section **??**.

1. **No two particles in the same row.** For each $i \in [n]$ we add constraints between diagram elements $(i, j, c) \in \mathcal{L}$ and $(i, k, d) \in \mathcal{L}$ in row i but in different columns, i.e.,

$$\{(i, j, c), (i, k, d)\} \in E(G_X oc) \text{ whenever } j \neq k. \tag{7.341}$$

2. **Synchronization with the particle in the first row.** For each $j \in [M]$ we add constraints between row 1 and row $s(j)$:

$$\{(1, j, c), (s(j), k, d)\} \in E(G_X oc) \text{ whenever } k \neq j \text{ and } (s(j), k, d) \neq F(s(j), j, c). \tag{7.342}$$

For each $j \in [M]$ we also add constraints between row 1 and rows $i \in [n] \setminus \{1, s(j)\}$:

$$\{(1, j, c), (i, k, d)\} \in E(G_X oc) \text{ whenever } (i, k, d) \notin \{F(i, j, 0), F(i, j, 1)\}. \tag{7.343}$$

7.5 Proof of QMA-hardness for MPQW ground energy

Theorem **??** bounds the smallest eigenvalue $\lambda_n^1(G_X, G_X oc)$ of $H(G_X, G_X oc, n)$. To prove the Theorem, we investigate a sequence of Hamiltonians starting with $H(G_1, n)$ and $H(G_1, G_X oc, n)$ and then work our way up to the Hamiltonian $H(G_X, G_X oc, n)$ by adding positive semidefinite terms.

For each Hamiltonian we consider, we solve for the nullspace and the smallest nonzero eigenvalue. To go from one Hamiltonian to the next, we use the following "Nullspace Projection Lemma," which was used (implicitly) in reference [**?**]. The Lemma bounds the smallest nonzero eigenvalue $\gamma(H_A + H_B)$ of a sum of positive semidefinite Hamiltonians H_A and H_B using knowledge of the smallest nonzero eigenvalue $\gamma(H_A)$ of H_A and the smallest nonzero eigenvalue $\gamma(H_B|_S)$ of the restriction of H_B to the nullspace S of H_A.

We prove the Lemma in Section **??**. When we apply this Lemma, we are usually interested in an asymptotic limit where $c, d \ll \|H_B\|$ and the right-hand side of (**??**) is $\Omega(\frac{cd}{\|H_B\|})$.

Our proof strategy, using repeated applications of the Nullspace Projection Lemma, is analogous to that of reference [**?**], where the so-called Projection Lemma was used similarly. Our technique has the advantage of not requiring the terms we add to our Hamiltonian to have "unphysical" problem-size dependent coefficients (it also has this advantage over the method of perturbative gadgets [**?**, **?**]). This allows us to prove results about the "physically realistic" Bose-Hubbard Hamiltonian. A similar technique based on Kitaev's Geometric Lemma was used recently in reference [**?**] (however, that method is slightly more computation intensive, requiring a lower bound on $\gamma(H_B)$ as well as bounds on $\gamma(H_A)$ and $\gamma(H_B|_S)$).

7.5.1 Single-particle ground-states

We begin by discussing the graphs

$$G_1, G_2, G_3, G_4, G_X \tag{7.344}$$

(as defined in Section **??**; see Figure 7.12) in more detail and deriving some properties of their adjacency matrices.

The graph G_1 has a component for each of the two-qubit gates $j \in [M]$, for each of the boundary gadgets $i = 2, \ldots, n$ in column 0, and for each of the boundary gadgets $i = 2, \ldots, n$ in column $M + 1$. In other words

$$G_1 = \underbrace{\left(\bigcup_{i=2}^{n} G_{\text{bnd}}\right)}_{\text{left boundary}} \cup \underbrace{\left(\bigcup_{j=1}^{M} G_{U_j}\right)}_{\text{two-qubit gates}} \cup \underbrace{\left(\bigcup_{i=2}^{n} G_{\text{bnd}}\right)}_{\text{right boundary}}. \tag{7.345}$$

We use our knowledge of the adjacency matrices of the components G_{bnd} and G_{U_j} to understand the ground space of $A(G_1)$. Recall (from Section **??**) that the smallest eigenvalue of $A(G_{U_j})$ is

$$e_1 = -1 - 3\sqrt{2} \tag{7.346}$$

(with degeneracy 16) which is also the smallest eigenvalue of $A(G_{\text{bnd}})$ (with degeneracy 4). For each diagram element $L \in \mathcal{L}$ and pair of bits $z, a \in \{0, 1\}$ there is an eigenstate $|\rho^L_{z,a}\rangle$ of $A(G_1)$ with this minimal eigenvalue e_1. In total we get sixteen eigenstates

$$|\rho^{(1,j,0)}_{z,a}\rangle, |\rho^{(1,j,1)}_{z,a}\rangle, |\rho^{(s(j),j,0)}_{z,a}\rangle, |\rho^{(s(j),j,1)}_{z,a}\rangle, \quad z, a \in \{0, 1\} \tag{7.347}$$

for each two-qubit gate $j \in [M]$, four eigenstates

$$|\rho^{(i,0,1)}_{z,a}\rangle, \quad z, a \in \{0, 1\} \tag{7.348}$$

for each boundary gadget $i \in \{2, \ldots, n\}$ in column 0, and four eigenstates

$$|\rho^{(i,M+1,0)}_{z,a}\rangle, \quad z, a \in \{0, 1\} \tag{7.349}$$

for each boundary gadget $i \in \{2, \ldots, n\}$ in column $M + 1$. The set

$$\left\{|\rho^L_{z,a}\rangle \colon z, a \in \{0, 1\},\ L \in \mathcal{L}\right\} \tag{7.350}$$

is an orthonormal basis for the ground space of $A(G_1)$.

We write the adjacency matrices of G_2, G_3, G_4, and G_X as

$$A(G_2) = A(G_1) + h_1 \qquad A(G_4) = A(G_3) + \sum_{i=n_{\text{in}}+1}^{n} h_{\text{in},i} \tag{7.351}$$

$$A(G_3) = A(G_2) + h_2 \qquad A(G_X) = A(G_4) + h_{\text{out}}. \tag{7.352}$$

From step 3 of the construction of the gate diagram in Section **??**, we see that h_1 and h_2 are both sums of terms of the form

$$(|q, z, t\rangle + |q', z, t'\rangle)\,(\langle q, z, t| + \langle q', z, t'|) \otimes \mathbb{I}_j, \tag{7.353}$$

where h_1 contains a term for each edge in rows $2, \ldots, n$ and h_2 contains a term for each of the $2(M-1)$ edges in the first row. The operators

$$h_{\text{in},i} = |(i,0,1),1,7\rangle\langle(i,0,1),1,7| \otimes \mathbb{I} \quad h_{\text{out}} = |(2,M+1,0),0,5\rangle\langle(2,M+1,0),0,5| \otimes \mathbb{I} \tag{7.354}$$

correspond to the self-loops added in the gate diagram in step 4 of Section **??**.

We prove that G_1, G_2, G_3, G_4, and G_X are e_1-gate graphs.

Lemma 26. *The smallest eigenvalues of G_1, G_2, G_3, G_4 and G_X are*

$$\mu(G_1) = \mu(G_2) = \mu(G_3) = \mu(G_4) = \mu(G_X) = e_1. \tag{7.355}$$

Proof. We showed in the above discussion that $\mu(G_1) = e_1$. The adjacency matrices of G_2, G_3, G_4, and G_X are obtained from that of G_1 by adding positive semidefinite terms (h_1, h_2, $h_{\text{in},i}$, and h_{out} are all positive semidefinite). It therefore suffices to exhibit an eigenstate $|\varrho\rangle$ of $A(G_1)$ with

$$h_1|\varrho\rangle = h_2|\varrho\rangle = h_{\text{in},i}|\varrho\rangle = h_{\text{out}}|\varrho\rangle = 0 \tag{7.356}$$

(for each $i \in \{n_{\text{in}}+1, \ldots, n\}$). There are many states $|\varrho\rangle$ satisfying these conditions; one example is

$$|\varrho\rangle = |\rho_{0,0}^{(1,1,0)}\rangle \tag{7.357}$$

which is supported on vertices where h_1, h_2, $h_{\text{in},i}$, and h_{out} have no support. □

7.5.1.1 Multi-particle Hamiltonian

We now outline the sequence of Hamiltonians considered in the following Sections and describe the relationships between them. As a first step, in Section **??** we exhibit a basis $\mathcal{B}_n$ for the nullspace of $H(G_1, n)$ and we prove that its smallest nonzero eigenvalue is lower bounded by a positive constant. We then discuss the restriction

$$H(G_1, G_X oc, n) = H(G_1, n)\big|_{\mathcal{I}(G_1, G_X oc, n)} \tag{7.358}$$

in Section **??**, where we prove that a subset $\mathcal{B}_{\text{legal}} \subset \mathcal{B}_n$ is a basis for the nullspace of (7.358), and that its smallest nonzero eigenvalue is also lower bounded by a positive constant.

For the remainder of the proof we use the Nullspace Projection Lemma (Lemma **??**) four times, using the decompositions

$$H(G_2, G_X oc, n) = H(G_1, G_X oc, n) + H_1\big|_{\mathcal{I}(G_2, G_X oc, n)} \tag{7.359}$$

$$H(G_3, G_X oc, n) = H(G_2, G_X oc, n) + H_2\big|_{\mathcal{I}(G_3, G_X oc, n)} \tag{7.360}$$

$$H(G_4, G_X oc, n) = H(G_3, G_X oc, n) + \sum_{i=n_{\text{in}}+1}^{n} H_{\text{in},i}\big|_{\mathcal{I}(G_4, G_X oc, n)} \tag{7.361}$$

$$H(G_X, G_X oc, n) = H(G_4, G_X oc, n) + H_{\text{out}}\big|_{\mathcal{I}(G_X, G_X oc, n)} \tag{7.362}$$

where

$$H_1 = \sum_{w=1}^{n} h_1^{(w)} \qquad H_{\text{in},i} = \sum_{w=1}^{n} h_{\text{in},i}^{(w)} \qquad H_2 = \sum_{w=1}^{n} h_2^{(w)} \qquad H_{\text{out}} = \sum_{w=1}^{n} h_{\text{out}}^{(w)}$$

are all positive semidefinite, with $h_1, h_2, h_{\text{in},i}, h_{\text{out}}$ as defined in Section **??**. Note that in writing equations (7.359), (7.360), (7.361), and (7.362), we have used the fact (from Lemma 26) that the adjacency matrices of the graphs we consider all have the same smallest eigenvalue e_1. Also note that

$$\mathcal{I}\left(G_i, G_X oc, n\right) = \mathcal{I}\left(G_X, G_X oc, n\right) \tag{7.363}$$

for $i \in [4]$ since the gate diagrams for each of the graphs G_1, G_2, G_3, G_4 and G_X have the same set of diagram elements.

Let S_k be the nullspace of $H(G_k, G_X oc, n)$ for $k = 1, 2, 3, 4$. Since these positive semidefinite Hamiltonians are related by adding positive semidefinite terms, their nullspaces satisfy

$$S_4 \subseteq S_3 \subseteq S_2 \subseteq S_1 \subseteq \mathcal{I}\left(G_X, G_X oc, n\right). \tag{7.364}$$

We solve for $S_1 = \text{span}(\mathcal{B}_{\text{legal}})$ in Section **??** and we characterize the spaces S_2, S_3, and S_4 in Section **??** in the course of applying our strategy.

For example, to use the Nullspace Projection Lemma to lower bound the smallest nonzero eigenvalue of $H(G_2, G_X oc, n)$, we consider the restriction

$$\left(H_1\big|_{\mathcal{I}(G_2, G_X oc, n)}\right)\Big|_{S_1} = H_1\big|_{S_1}. \tag{7.365}$$

We also solve for S_2, which is equal to the nullspace of (7.365). To obtain the corresponding lower bounds on the smallest nonzero eigenvalues of $H(G_k, G_X oc, n)$ for $k = 2, 3, 4$ and $H(G_X, G_X oc, n)$, we consider restrictions

$$H_2\big|_{S_2}, \quad \sum_{i=n_{\text{in}}+1}^{n} H_{\text{in},i}\big|_{S_3}, \quad \text{and} \quad H_{\text{out}}\big|_{S_4}. \tag{7.366}$$

Analyzing these restrictions involves extensive computation of matrix elements. To simplify and organize these computations, we first compute the restrictions of each of these operators to the space S_1. We present the results of this computation in Section **??**; details of the calculation can be found in Section **??**. In Section **??** we proceed with the remaining computations and apply the Nullspace Projection Lemma three times using equations (7.359), (7.360), and (7.361). Finally, in Section **??** we apply the Lemma again using equation (7.362) and we prove Theorem **??**.

7.5.2 Configurations

In this Section we use Lemma 13 to solve for the nullspace of $H(G_1, n)$, i.e., the n-particle frustration-free states on G_1. Lemma 13 describes how frustration-free states for G_1 are built out of frustration-free states for its components.

To see how this works, consider the example from Figure 7.12a. In this example, with $n = 3$, we construct a basis for the nullspace of $H(G_1, 3)$ by considering two types of eigenstates. First, there are frustration-free states

$$\text{Sym}(|\rho^{L_1}_{z_1,a_1}\rangle |\rho^{L_2}_{z_2,a_2}\rangle |\rho^{L_3}_{z_3,a_3}\rangle) \tag{7.367}$$

where $L_k = (i_k, j_k, d_k) \in \mathcal{L}$ belong to different components of G_1. That is to say, $j_w \neq j_t$ unless $j_w = j_t \in \{0, 5\}$, in which case $i_w \neq i_t$ (in this case the particles are located either at the left or right boundary, in different rows of G_1). There are also frustration-free states where two of the three particles are located in the same two-qubit gadget $J \in [M]$ and one of the particles is located in a diagram element L_1 from a different component of the graph. These states have the form

$$\mathrm{Sym}(|T^J_{z_1,a_1,z_2,a_2}\rangle |\rho^{L_1}_{z_3,a_3}\rangle) \tag{7.368}$$

where

$$|T^J_{z_1,a_1,z_2,a_2}\rangle = \frac{1}{\sqrt{2}}|\rho^{(1,J,0)}_{z_1,a_1}\rangle|\rho^{(s(J),J,0)}_{z_2,a_2}\rangle + \frac{1}{\sqrt{2}} \sum_{x_1,x_2\in\{0,1\}} U_J(a_1)_{x_1x_2,z_1z_2}|\rho^{(1,J,1)}_{x_1,a_1}\rangle|\rho^{(s(J),J,1)}_{x_2,a_2}\rangle \tag{7.369}$$

and $L_1 = (i, j, k) \in \mathcal{L}$ satisfies $j \neq J$. Each of the states (7.367) and (7.368) is specified by 6 "data" bits $z_1, z_2, z_3, a_1, a_2, a_3 \in \{0, 1\}$ and a "configuration" indicating where the particles are located in the graph. The configuration is specified either by three diagram elements $L_1, L_2, L_3 \in \mathcal{L}$ from different components of G_1 or by a two-qubit gate $J \in [M]$ along with a diagram element $L_1 \in \mathcal{L}$ from a different component of the graph.

We now define the notion of a configuration for general n. Informally, we can think of an n-particle configuration as a way of placing n particles in the graph G_1 subject to the following restrictions. We first place each of the n particles in a component of the graph, with the restriction that no boundary gadget may contain more than one particle and no two-qubit gadget may contain more than two particles. For each particle on its own in a component (i.e., in a component with no other particles), we assign one of the diagram elements $L \in \mathcal{L}$ associated to that component. We therefore specify a configuration by a set of two-qubit gadgets $J_1, \ldots, J_Y$ that contain two particles, along with a set of diagram elements $L_k \in \mathcal{L}$ that give the locations of the remaining $n - 2Y$ particles. We choose to order the Js and the Ls so that each configuration is specified by a unique tuple $(J_1, \ldots, J_Y, L_1, \ldots, L_{n-2Y})$. For concreteness, we use the lexicographic order on diagram elements in the set $\mathcal{L}$: $L_A = (i_A, j_A, d_A)$ and $L_B = (i_B, j_B, d_B)$ satisfy $L_A < L_B$ iff either $i_A < i_B$, or $i_A = i_B$ and $j_A < j_B$, or $(i_A, j_A) = (i_B, j_B)$ and $d_A < d_B$.

Definition 11 (Configuration). An n-particle configuration on the gate graph G_1 is a tuple

$$(J_1, \ldots, J_Y, L_1, \ldots, L_{n-2Y}) \tag{7.370}$$

with $Y \in \{0, \ldots, \lfloor \frac{n}{2} \rfloor\}$, ordered integers

$$1 \leq J_1 < J_2 < \cdots < J_Y \leq M, \tag{7.371}$$

and lexicographically ordered diagram elements

$$L_1 < L_2 < \cdots < L_{n-2Y}, \qquad L_k = (i_k, j_k, d_k) \in \mathcal{L}. \tag{7.372}$$

We further require that each L_k is from a different component of G_1, i.e.,

$$j_w = j_t \quad \Longrightarrow \quad j_w \in \{0, M + 1\} \text{ and } i_w \neq i_t, \tag{7.373}$$

and we require that $j_u \neq J_v$ for all $u \in [n - 2Y]$ and $v \in [Y]$.

In Figure **??** we give some examples of configurations (for the example from Figure 7.12a with $n = 3$) and we introduce a diagrammatic notation for them.

For any configuration and n-bit strings $\vec{z}$ and $\vec{a}$, there is a state in the nullspace of $H(G_1, n)$, given by

$$\mathrm{Sym}(|T^{J_1}_{z_1,a_1,z_2,a_2}\rangle \dots |T^{J_Y}_{z_{2Y-1},a_{2Y-1},z_{2Y},a_{2Y}}\rangle |\rho^{L_1}_{z_{2Y+1},a_{2Y+1}}\rangle \dots |\rho^{L_{n-2Y}}_{z_n,a_n}\rangle). \tag{7.374}$$

The ordering in the definition of a configuration ensures that each distinct choice of configuration and n-bit strings $\vec{z}, \vec{a}$ gives a different state.

Definition 12. Let $\mathcal{B}_n$ be the set of all states of the form (7.374), where $(J_1, \dots, J_Y, L_1, \dots, L_{n-2Y})$ is a configuration and $\vec{z}, \vec{a} \in \{0,1\}^n$.

Lemma 27. *The set $\mathcal{B}_n$ is an orthonormal basis for the nullspace of $H(G_1, n)$. Furthermore,*

$$\gamma(H(G_1, n)) \geq \mathcal{K}_0 \tag{7.375}$$

where $\mathcal{K}_0 \in (0, 1]$ is an absolute constant.

Proof. Each component of G_1 is either a two-qubit gadget or a boundary gadget (see equation (7.345)). The single-particle states of $A(G_1)$ with energy e_1 are the states $|\rho^L_{z,a}\rangle$ for $L \in \mathcal{L}$ and $z, a \in \{0,1\}$, as discussed in Section **??**. Each of these states has support on only one component of G_1. In addition, G_1 has a two-particle frustration-free state for each two-qubit gadget $J \in [M]$ and bits z, a, x, b, namely $\mathrm{Sym}(|T^J_{z,a,x,b}\rangle)$. Furthermore, no component of G_1 has any three- (or more) particle frustration-free states. Using these facts and applying Lemma 13, we see that $\mathcal{B}_n$ spans the nullspace of $H(G_1, n)$.

Lemma 13 also expresses each eigenvalue of $H(G_1, n)$ as a sum of eigenvalues for its components. We use this fact to obtain the desired lower bound on the smallest nonzero eigenvalue. Our analysis proceeds on a case-by-case basis, depending on the occupation numbers for each component of G_1 (the values $N_1, \dots, N_k$ in Lemma 13).

First consider any set of occupation numbers where some two-qubit gate gadget $J \in [M]$ contains 3 or more particles. By Lemma **??** and Lemma 13, any such eigenvalue is at least $\lambda^1_3(G_{U_J})$, which is a positive constant by Lemma 19. Next consider a case where some boundary gadget contains more than one particle. The corresponding eigenvalues are similarly lower bounded by $\lambda^1_2(G_{\mathrm{bnd}})$, which is also a positive constant by Lemma 21. Finally, consider a set of occupation numbers where each two-qubit gadget contains at most two particles and each boundary gadget contains at most one particle. The smallest eigenvalue with such a set of occupation numbers is zero. The smallest nonzero eigenvalue is either

$$\gamma(H(G_{U_J}, 1)),\ \gamma(H(G_{U_J}, 2)) \text{ for some } J \in [M], \text{ or } \gamma(H(G_{\mathrm{bnd}}, 1)). \tag{7.376}$$

However, these quantities are at least some positive constant since $H(G_{U_J}, 1)$, $H(G_{U_J}, 2)$, and $H(G_{\mathrm{bnd}}, 1)$ are nonzero constant-sized positive semidefinite matrices.

Now combining the lower bounds discussed above and using the fact that, for each $J \in [M]$, the two-qubit gate U_J is chosen from a fixed finite gate set (given in (**??**)), we see that $\gamma(H(G_1, n))$ is lower bounded by the positive constant

$$\min\{\lambda^1_3(G_U), \lambda^1_2(G_{\mathrm{bnd}}), \gamma(H(G_U, 1)), \gamma(H(G_U, 2)), \gamma(H(G_{\mathrm{bnd}}, 1)) \colon U \text{ is from the gate set } (\mathbf{??})\}. \tag{7.377}$$

The condition $\mathcal{K}_0 \leq 1$ can be ensured by setting $\mathcal{K}_0$ to be the minimum of 1 and (7.377). □

Note that the constant $\mathcal{K}_0$ can in principle be computed using (7.377): each quantity on the right-hand side can be evaluated by diagonalizing a specific finite-dimensional matrix.

7.5.2.1 Legal configurations

In this section we define a subset of the n-particle configurations that we call legal configurations, and we prove that the subset of the basis vectors in $\mathcal{B}_n$ that have legal configurations spans the nullspace of $H(G_1, G_X oc, n)$.

We begin by specifying the set of legal configurations. Every legal configuration

$$(J_1, \ldots, J_Y, L_1, \ldots, L_{n-2Y}) \tag{7.378}$$

has $Y \in \{0, 1\}$. The legal configurations with $Y = 0$ are

$$((1, j, d_1), F(2, j, d_2), F(3, j, d_3), \ldots, F(n, j, d_n)) \tag{7.379}$$

where $j \in [M]$ and where $\vec{d} = (d_1, \ldots, d_n)$ satisfies $d_i \in \{0, 1\}$ and $d_1 = d_{s(j)}$. (Recall that the function F, defined in equations (7.338) and (7.339), describes horizontal movement of particles.) The legal configurations with $Y = 1$ are

$$(j, F(2, j, d_2), \ldots, F(s(j) - 1, j, d_{s(j)-1}), F(s(j) + 1, j, d_{s(j)+1}), \ldots, F(n, j, d_n)) \tag{7.380}$$

where $j \in \{1, \ldots, M\}$ and $d_i \in \{0, 1\}$ for $i \in [n] \setminus \{1, s(j)\}$. Although the values d_1 and $d_{s(j)}$ are not used in equation (7.380), we choose to set them to

$$d_1 = d_{s(j)} = 2 \tag{7.381}$$

for any legal configuration with $Y = 1$. In this way we identify the set of legal configurations with the set of pairs $j, \vec{d}$ with $j \in [M]$ and

$$\vec{d} = (d_1, d_2, d_3, \ldots, d_n) \tag{7.382}$$

satisfying

$$d_1 = d_{s(j)} \in \{0, 1, 2\} \quad \text{and} \quad d_i \in \{0, 1\} \text{ for } i \notin \{1, s(j)\}. \tag{7.383}$$

The legal configuration is given by equation (7.379) if $d_1 = d_{s(j)} \in \{0, 1\}$ and equation (7.380) if $d_1 = d_{s(j)} = 2$.

The examples in Figures **??**, **??**, and **??** show legal configurations whereas the examples in Figures **??**, **??**, and **??** are illegal. The legal examples correspond to $j = 1$, $\vec{d} = (1, 1, 1)$; $j = 2$, $\vec{d} = (2, 2, 0)$; and $j = 1$, $\vec{d} = (1, 0, 1)$, respectively. We now explain why the other examples are illegal. Looking at (7.380), we see that the configuration $(3, (2, 0, 1))$ depicted in Figure **??** is illegal since $F(2, 3, 0) = (2, 2, 1) \neq (2, 0, 1)$ and $F(2, 3, 1) = (2, 4, 0) \neq (2, 0, 1)$. The configuration in Figure **??** is illegal since there are two particles in the same row. Looking at equation (7.379), we see that the configuration $((1, 1, 1), (2, 2, 0), (3, 5, 0))$ in Figure **??** is illegal since $(3, 5, 0) \notin \{F(3, 1, 0), F(3, 1, 1)\} = \{(3, 0, 1), (3, 3, 0)\}$.

We now identify the subset of basis vectors $\mathcal{B}_{\text{legal}} \subset \mathcal{B}_n$ that have legal configurations. We write each such basis vector as

$$|j, \vec{d}, \vec{z}, \vec{a}\rangle = \begin{cases} \text{Sym}\left(|\rho^{(1,j,d_1)}_{z_1,a_1}\rangle \bigotimes_{i=2}^{n} |\rho^{F(i,j,d_i)}_{z_i,a_i}\rangle\right) & d_1 = d_{s(j)} \in \{0,1\} \\ \text{Sym}\left(|T^{j}_{z_1,a_1,z_{s(j)},a_{s(j)}}\rangle \bigotimes_{\substack{i=2 \\ i\neq s(j)}}^{n} |\rho^{F(i,j,d_i)}_{z_i,a_i}\rangle\right) & d_1 = d_{s(j)} = 2 \end{cases} \tag{7.384}$$

where $j, \vec{d}$ specifies the legal configuration and $\vec{z}$,$\vec{a} \in \{0,1\}^n$. (Note that the bits in $\vec{z}$ and $\vec{a}$ are ordered slightly differently than in equation (7.374); here the labeling reflects the indices of the encoded qubits).

Definition 13. Let

$$\mathcal{B}_{\text{legal}} = \left\{|j, \vec{d}, \vec{z}, \vec{a}\rangle : j \in [M],\ d_1 = d_{s(j)} \in \{0,1,2\} \text{ and } d_i \in \{0,1\} \text{ for } i \notin \{1, s(j)\},\ \vec{z}, \vec{a} \in \{0,1\}^n\right\} \tag{7.385}$$

and $\mathcal{B}_{\text{illegal}} = \mathcal{B}_n \setminus \mathcal{B}_{\text{illegal}}$.

The basis $\mathcal{B}_n = \mathcal{B}_{\text{legal}} \cup \mathcal{B}_{\text{illegal}}$ is convenient when considering the restriction to the subspace $\mathcal{I}(G_1, G_X oc, n)$. Letting Π_0 be the projector onto $\mathcal{I}(G_1, G_X oc, n)$, the following Lemma (proven in Section **??**) shows that the restriction

$$\Pi_0\big|_{\text{span}(\mathcal{B}_n)} \tag{7.386}$$

is diagonal in the basis $\mathcal{B}_n$. The Lemma also bounds the diagonal entries.

Lemma 28. *Let Π_0 be the projector onto $\mathcal{I}(G_1, G_X oc, n)$. For any $|j, \vec{d}, \vec{z}, \vec{a}\rangle \in \mathcal{B}_{legal}$, we have*

$$\Pi_0 |j, \vec{d}, \vec{z}, \vec{a}\rangle = |j, \vec{d}, \vec{z}, \vec{a}\rangle. \tag{7.387}$$

Furthermore, for any two distinct basis vectors $|\phi\rangle, |\psi\rangle \in \mathcal{B}_{illegal}$, we have

$$\langle\phi|\Pi_0|\phi\rangle \leq \frac{255}{256} \tag{7.388}$$

$$\langle\phi|\Pi_0|\psi\rangle = 0. \tag{7.389}$$

We use this Lemma to characterize the nullspace of $H(G_1, G_X oc, n)$ and bound its smallest nonzero eigenvalue.

Lemma 29. *The nullspace S_1 of $H(G_1, G_X oc, n)$ is spanned by the orthonormal basis $\mathcal{B}_{legal}$. Its smallest nonzero eigenvalue is*

$$\gamma(H(G_1, G_X oc, n)) \geq \frac{\mathcal{K}_0}{256} \tag{7.390}$$

where $\mathcal{K}_0 \in (0,1]$ is the absolute constant from Lemma 27.

Proof. Recall from Section **??** that

$$H(G_1, G_X oc, n) = H(G_1, n)|_{\mathcal{I}(G_1, G_X oc, n)}. \tag{7.391}$$

Its nullspace is the space of states $|\kappa\rangle$ satisfying

$$\Pi_0|\kappa\rangle = |\kappa\rangle \quad \text{and} \quad H(G_1, n)|\kappa\rangle = 0 \tag{7.392}$$

(recall that Π_0 is the projector onto $\mathcal{I}(G_1, G_X oc, n)$, the states satisfying the occupancy constraints). Since $\mathcal{B}_n$ is a basis for the nullspace of $H(G_1, n)$, to solve for the nullspace of $H(G_1, G_X oc, n)$ we consider the restriction (7.386) and solve for the eigenspace with eigenvalue 1. This calculation is simple because (7.386) is diagonal in the basis $\mathcal{B}_n$, according to Lemma 28. We see immediately from the Lemma that $\mathcal{B}_{\text{legal}}$ spans the nullspace of $H(G_1, G_X oc, n)$; we now show that Lemma 28 also implies the lower bound (7.390). Note that

$$\gamma(H(G_1, G_X oc, n)) = \gamma(\Pi_0 H(G_1, n)\Pi_0). \tag{7.393}$$

Let Π_{legal} and Π_{illegal} project onto the spaces spanned by $\mathcal{B}_{\text{legal}}$ and $\mathcal{B}_{\text{illegal}}$ respectively, so $\Pi_{\text{legal}} + \Pi_{\text{illegal}}$ projects onto the nullspace of $H(G_1, n)$. The operator inequality

$$H(G_1, n) \geq \gamma(H(G_1, n)) \cdot (1 - \Pi_{\text{legal}} - \Pi_{\text{illegal}}) \tag{7.394}$$

implies

$$\Pi_0 H(G_1, n)\Pi_0 \geq \gamma(H(G_1, n)) \cdot \Pi_0(1 - \Pi_{\text{legal}} - \Pi_{\text{illegal}})\Pi_0. \tag{7.395}$$

Since the operators on both sides of this inequality are positive semidefinite and have the same nullspace, their smallest nonzero eigenvalues are bounded as

$$\gamma(\Pi_0 H(G_1, n)\Pi_0) \geq \gamma(H(G_1, n)) \cdot \gamma(\Pi_0(1 - \Pi_{\text{legal}} - \Pi_{\text{illegal}})\Pi_0). \tag{7.396}$$

Hence

$$\gamma(H(G_1, G_X oc, n)) = \gamma(\Pi_0 H(G_1, n)\Pi_0) \geq \mathcal{K}_0 \cdot \gamma(\Pi_0(1 - \Pi_{\text{legal}} - \Pi_{\text{illegal}})\Pi_0) \tag{7.397}$$

where we used Lemma 27. From equations (7.388) and (7.389) we see that

$$\Pi_0|g\rangle = |g\rangle \quad \text{and} \quad \Pi_{\text{illegal}}|f\rangle = |f\rangle \qquad \Longrightarrow \qquad \langle f|g\rangle\langle g|f\rangle \leq \frac{255}{256}. \tag{7.398}$$

The nullspace of

$$\Pi_0 \left(1 - \Pi_{\text{legal}} - \Pi_{\text{illegal}}\right) \Pi_0 \tag{7.399}$$

is spanned by

$$\mathcal{B}_{\text{legal}} \cup \{|\tau\rangle \colon \Pi_0|\tau\rangle = 0\}. \tag{7.400}$$

To see this, note that (7.399) commutes with Π_0, and the space of $+1$ eigenvectors of Π_0 that are annihilated by (7.399) is spanned by $\mathcal{B}_{\text{legal}}$ (by Lemma 28). Any eigenvector $|g_1\rangle$ corresponding to the smallest nonzero eigenvalue of this operator therefore satisfies $\Pi_0|g_1\rangle = |g_1\rangle$ and $\Pi_{\text{legal}}|g_1\rangle = 0$, so

$$\gamma(\Pi_0(1 - \Pi_{\text{legal}} - \Pi_{\text{illegal}})\Pi_0) = 1 - \langle g_1|\Pi_{\text{illegal}}|g_1\rangle \geq \frac{1}{256} \tag{7.401}$$

using equation (7.398). Plugging this into equation (7.397) gives the lower bound (7.390). □

We now consider

$$H_1|_{S_1}, H_2|_{S_1}, H_{\text{in},i}|_{S_1}, H_{\text{out}}|_{S_1} \tag{7.402}$$

where these operators are defined in Section 7.5.1.1 and

$$S_1 = \text{span}(\mathcal{B}_{\text{legal}}) \tag{7.403}$$

is the nullspace of $H(G_1, G_X oc, n)$.

We specify the operators (7.402) by their matrix elements in an orthonormal basis for S_1. Although the basis $\mathcal{B}_{\text{legal}}$ was convenient in Section **??**, here we use a different basis in which the matrix elements of H_1 and H_2 are simpler. We define

$$|j, \vec{d}, \text{In}(\vec{z}), \vec{a}\rangle = \sum_{\vec{x}\in\{0,1\}^n} \big(\langle \vec{x}|\bar{U}_{j,d_1}(a_1)|\vec{z}\rangle\big)|j, \vec{d}, \vec{x}, \vec{a}\rangle \tag{7.404}$$

where

$$\bar{U}_{j,d_1}(a_1) = \begin{cases} U_{j-1}(a_1)U_{j-2}(a_1)\dots U_1(a_1) & \text{if } d_1 \in \{0,2\} \\ U_j(a_1)U_{j-1}(a_1)\dots U_1(a_1) & \text{if } d_1 = 1. \end{cases} \tag{7.405}$$

In each of these states the quantum data (represented by the $\vec{x}$ register on the right-hand side) encodes the computation in which the unitary $\bar{U}_{j,d_1}(a_1)$ is applied to the initial n-qubit state $|\vec{z}\rangle$ (the notation $\text{In}(\vec{z})$ indicates that $\vec{z}$ is the input). The vector $\vec{a}$ is only relevant insofar as its first bit a_1 determines whether or not each two-qubit unitary is complex conjugated; the other bits of $\vec{a}$ go along for the ride. Letting $\vec{z}, \vec{a} \in \{0,1\}^n$, $j \in [M]$, and

$$\vec{d} = (d_1, \dots, d_n) \quad \text{with} \quad d_1 = d_{s(j)} \in \{0,1,2\} \quad \text{and} \quad d_i \in \{0,1\},\ i \notin \{1, s(j)\}, \tag{7.406}$$

we see that the states (7.404) form an orthonormal basis for S_1. In Section **??** we compute the matrix elements of the operators (7.402) in this basis, which are reproduced below.

Roughly speaking, the nonzero off-diagonal matrix elements of the operator H_1 in the basis (7.404) occur between states $|j, \vec{d}, \text{In}(\vec{z}), \vec{a}\rangle$ and $|j, \vec{c}, \text{In}(\vec{z}), \vec{a}\rangle$ where the legal configurations $j, \vec{d}$ and $j, \vec{c}$ are related by horizontal motion of a particle in one of the rows $i \in \{2, \dots, n\}$.

Matrix elements of H_1

$$\langle k, \vec{c}, \text{In}(\vec{x}), \vec{b}|H_1|j, \vec{d}, \text{In}(\vec{z}), \vec{a}\rangle = \delta_{k,j}\delta_{\vec{a},\vec{b}}\delta_{\vec{z},\vec{x}} \cdot \begin{cases} \frac{n-1}{64} & \vec{c} = \vec{d} \\ \frac{1}{64}\prod_{\substack{r=1 \\ r\neq i}}^{n} \delta_{d_r,c_r} & d_i \neq c_i \text{ for some } i \in [n] \setminus \{1, s(j)\} \\ \frac{1}{64\sqrt{2}}\prod_{\substack{r=2 \\ r\neq s(j)}}^{n} \delta_{d_r,c_r} & (c_1, d_1) \in \{(2,0),(0,2),(1,2),(2,1)\} \\ 0 & \text{otherwise.} \end{cases} \tag{7.407}$$

From this expression we see that $H_1|_{S_1}$ is block diagonal in the basis (7.404), with a block for each $\vec{z}, \vec{a} \in \{0,1\}^n$ and $j \in [M]$. Moreover, the submatrix for each block is the same. In Figure **??** we illustrate some of the off-diagonal matrix elements of $H_1|_{S_1}$ for the example from Figure 7.12.

Next, we present the matrix elements of H_2.

Matrix elements of H_2

$$\begin{aligned}\langle k, \vec{c}, \mathrm{In}(\vec{x}), \vec{b}|H_2|j, \vec{d}, \mathrm{In}(\vec{z}), \vec{a}\rangle = f_{\mathrm{diag}(\vec{d},j)\cdot\delta_{j,k}\delta_{\vec{a},\vec{b}}\delta_{\vec{z},\vec{x}}\delta_{\vec{c},\vec{d}}} \\ + \left(f_{\text{off-diag}}(\vec{c},\vec{d},j)\cdot\delta_{k,j-1} + f_{\text{off-diag}}(\vec{d},\vec{c},k)\cdot\delta_{k-1,j}\right)\delta_{\vec{a},\vec{b}}\delta_{\vec{z},\vec{x}}\end{aligned} \tag{7.408}$$

where

$$f_{\mathrm{diag}}(\vec{d},j) = \begin{cases} 0 & d_1 = 0 \text{ and } j = 1, \text{ or } d_1 = 1 \text{ and } j = M \\ \frac{1}{128} & d_1 = 2 \text{ and } j \in \{1, M\} \\ \frac{1}{64} & \text{otherwise} \end{cases} \tag{7.409}$$

and

$$f_{\text{off-diag}}(\vec{c},\vec{d},j) = \left(\prod_{\substack{r=2 \\ r\notin\{s(j-1),s(j)\}}}^{n} \delta_{d_r,c_r}\right) \cdot \begin{cases} \frac{1}{64\sqrt{2}} & (c_1, c_{s(j)}, d_1, d_{s(j-1)}) \in \{(2,0,0,0),(1,1,2,1)\} \\ \frac{1}{64} & (c_1, c_{s(j)}, d_1, d_{s(j-1)}) = (1,0,0,1) \\ \frac{1}{128} & (c_1, c_{s(j)}, d_1, d_{s(j-1)}) = (2,1,2,0) \\ 0 & \text{otherwise.} \end{cases} \tag{7.410}$$

This shows that $H_2|_{S_1}$ is block diagonal in the basis (7.404), with a block for each $\vec{z}, \vec{a} \in \{0,1\}^n$. Also note that (in contrast with H_1) H_2 connects states with different values of j. In Figure **??** we illustrate some of the off-diagonal matrix elements of $H_2|_{S_1}$, for the example from Figure 7.12.

Finally, we present the matrix elements of $H_{\mathrm{in},i}$ (for $i \in \{n_{\mathrm{in}}+1, \ldots, n\}$) and H_{out}:

Matrix elements of $H_{\mathbf{in},i}$

For each ancilla qubit $i \in \{n_{\mathrm{in}}+1, \ldots, n\}$, define $j_{\min,i} = \min\{j \in [M] \colon s(j) = i\}$ to be the index of the first gate in the circuit that involves this qubit (recall from Section **??** that we consider circuits where each ancilla qubit is involved in at least one gate). The operator $H_{\mathrm{in},i}$ is diagonal in the basis (7.404), with entries

$$\langle j, \vec{d}, \mathrm{In}(\vec{z}), \vec{a}|H_{\mathrm{in},i}|j, \vec{d}, \mathrm{In}(\vec{z}), \vec{a}\rangle = \begin{cases} \frac{1}{64} & j \le j_{\min,i},\ z_i = 1, \text{ and } d_i = 0 \\ 0 & \text{otherwise.} \end{cases} \tag{7.411}$$

Matrix elements of $H_{\mathbf{out}}$

Let $j_{\max} = \max\{j \in [M] \colon s(j) = 2\}$ be the index of the last gate $U_{j_{\max}}$ in the circuit

that acts between qubits 1 and 2 (the output qubit). Then

$$\langle k, \vec{c}, \mathrm{In}(\vec{x}), \vec{b}|H_{\mathrm{out}}|j, \vec{d}, \mathrm{In}(\vec{z}), \vec{a}\rangle = \delta_{j,k}\delta_{\vec{c},\vec{d}}\delta_{\vec{a},\vec{b}} \begin{cases} \langle \vec{x}|U^\dagger_{\mathcal{C}_X}(a_1)|0\rangle\langle 0|_2 U_{\mathcal{C}_X}(a_1)|\vec{z}\rangle \frac{1}{64} & j \geq j_{\max} \text{ and } d_2 = 1 \\ 0 & \text{otherwise.} \end{cases} \tag{7.412}$$

7.5.3 Frustration-Free states

Define the $(n-2)$-dimensional hypercubes

$$\mathcal{D}^j_k = \left\{(d_1, \ldots, d_n) \colon d_1 = d_{s(j)} = k,\ d_i \in \{0,1\} \text{ for } i \in [n] \setminus \{1, s(j)\}\right\} \tag{7.413}$$

for $j \in \{1, \ldots, M\}$ and $k \in \{0,1,2\}$, and the superpositions

$$|\mathrm{Cube}_k(j, \vec{z}, \vec{a})\rangle = \frac{1}{\sqrt{2^{n-2}}} \sum_{\vec{d} \in \mathcal{D}^j_k} (-1)^{\sum_{i=1}^n d_i} |j, \vec{d}, \mathrm{In}(\vec{z}), \vec{a}\rangle \tag{7.414}$$

for $k \in \{0,1,2\}$, $j \in [M]$, and $\vec{z}, \vec{a} \in \{0,1\}^n$. For each $j \in [M]$ and $\vec{z}, \vec{a} \in \{0,1\}^n$, let

$$|C(j, \vec{z}, \vec{a})\rangle = \frac{1}{2}|\mathrm{Cube}_0(j, \vec{z}, \vec{a})\rangle + \frac{1}{2}|\mathrm{Cube}_1(j, \vec{z}, \vec{a})\rangle - \frac{1}{\sqrt{2}}|\mathrm{Cube}_2(j, \vec{z}, \vec{a})\rangle. \tag{7.415}$$

We prove

Lemma 30. *The Hamiltonian $H(G_2, G_X oc, n)$ has nullspace S_2 spanned by the states*

$$|C(j, \vec{z}, \vec{a})\rangle \tag{7.416}$$

for $j \in [M]$ and $\vec{z}, \vec{a} \in \{0,1\}^n$. Its smallest nonzero eigenvalue is

$$\gamma(H(G_2, G_X oc, n)) \geq \frac{\mathcal{K}_0}{35000n} \tag{7.417}$$

where $\mathcal{K}_0 \in (0,1]$ is the absolute constant from Lemma 27.

Proof. Recall from the previous section that $H_1|_{S_1}$ is block diagonal in the basis (7.404), with a block for each $j \in [M]$ and $\vec{z}, \vec{a} \in \{0,1\}^n$. That is to say, $\langle k, \vec{c}, \mathrm{In}(\vec{x}), \vec{b}|H_1|j, \vec{d}, \mathrm{In}(\vec{z}), \vec{a}\rangle$ is zero unless $\vec{a} = \vec{b}$, $k = j$, and $\vec{z} = \vec{x}$. Equation (7.407) gives the nonzero matrix elements within a given block, which we use to compute the frustration-free ground states of $H_1|_{S_1}$.

Looking at equation (7.407), we see that the matrix for each block can be written as a sum of n commuting matrices: $\frac{n-1}{64}$ times the identity matrix (case 1 in equation (7.407)), $n-2$ terms that each flip a single bit $i \notin \{1, s(j)\}$ of $\vec{d}$ (case 2), and a term that changes the value of the "special" components $d_1 = d_{s(j)} \in \{0,1,2\}$ (case 3). Thus

$$\langle j, \vec{c}, \mathrm{In}(\vec{z}), \vec{a}|H_1|j, \vec{d}, \mathrm{In}(\vec{z}), \vec{a}\rangle = \langle j, \vec{c}, \mathrm{In}(\vec{z}), \vec{a}|\frac{1}{64}(n-1) + \frac{1}{64}\sum_{i \in [n]\setminus\{1,s(j)\}} H_{\mathrm{flip},i} + \frac{1}{64}H_{\mathrm{special},j}|j, \vec{d}, \mathrm{In}(\vec{z}), \vec{a}\rangle \tag{7.418}$$

where

$$\langle j, \vec{c}, \mathrm{In}(\vec{z}), \vec{a}|H_{\mathrm{flip},i}|j, \vec{d}, \mathrm{In}(\vec{z}), \vec{a}\rangle = \delta_{c_i, d_i \oplus 1} \prod_{r \in [n]\setminus\{i\}} \delta_{c_r, d_r} \tag{7.419}$$

and

$$\langle j, \vec{c}, \mathrm{In}(\vec{z}), \vec{a}|H_{\mathrm{special},j}|j, \vec{d}, \mathrm{In}(\vec{z}), \vec{a}\rangle = \begin{cases} \frac{1}{\sqrt{2}} & (c_1, d_1) \in \{(2,0),(0,2),(1,2),(2,1)\} \\ & \text{and } d_r = c_r \text{ for } r \in [n] \setminus \{1, s(j)\} \\ 0 & \text{otherwise.} \end{cases} \tag{7.420}$$

Note that these n matrices are mutually commuting, each eigenvalue of $H_{\mathrm{flip},i}$ is ± 1, and each eigenvalue of $H_{\mathrm{special},j}$ is equal to one of the eigenvalues of the matrix

$$\frac{1}{\sqrt{2}} \begin{pmatrix} 0 & 0 & 1 \\ 0 & 0 & 1 \\ 1 & 1 & 0 \end{pmatrix}, \tag{7.421}$$

which are $\{-1, 0, 1\}$. Thus we see that the eigenvalues of $H_1|_{S_1}$ within a block for some $j \in [M]$ and $\vec{z}, \vec{a} \in \{0,1\}^n$ are

$$\frac{1}{64}\left(n - 1 + \sum_{i \notin \{1, s(j)\}} y_i + w\right) \tag{7.422}$$

where $y_i \in \pm 1$ for each $i \in [n] \setminus \{1, s(j)\}$ and $w \in \{-1, 0, 1\}$. In particular, the smallest eigenvalue within the block is zero (corresponding to $y_i = w = -1$). The corresponding eigenspace is spanned by the simultaneous -1 eigenvectors of each $H_{\mathrm{flip},i}$ for $i \in [n]\setminus\{1, s(j)\}$ and $H_{\mathrm{special},j}$. The space of simultaneous -1 eigenvectors of $H_{\mathrm{flip},i}$ for $i \in [n] \setminus \{1, s(j)\}$ within the block is spanned by $\{|\mathrm{Cube}_0(j, \vec{z}, \vec{a})\rangle, |\mathrm{Cube}_1(j, \vec{z}, \vec{a})\rangle, |\mathrm{Cube}_2(j, \vec{z}, \vec{a})\rangle\}$. The state $|C(j, \vec{z}, \vec{a})\rangle$ is the unique superposition of these states that is a -1 eigenvector of $H_{\mathrm{special},j}$. Hence, for each block we obtain a unique state $|C(j, \vec{z}, \vec{a})\rangle$ in the space S_2. Ranging over all blocks $j \in [M]$ and $\vec{z}, \vec{a} \in \{0,1\}^n$, we get the basis described in the Lemma.

The smallest nonzero eigenvalue within each block is $\frac{1}{64}$ (corresponding to $y_i = -1$ and $w = 0$ in equation (7.422)), so

$$\gamma(H_1|_{S_1}) = \frac{1}{64}. \tag{7.423}$$

To get the stated lower bound, we use Lemma **??** with $H(G_2, G_X oc, n) = H_A + H_B$ where

$$H_A = H(G_1, G_X oc, n) \qquad H_B = H_1|_{\mathcal{I}(G_2, G_X oc, n)} \tag{7.424}$$

(as in equation (7.359)), along with the bounds

$$\gamma(H_A) \geq \frac{\mathcal{K}_0}{256} \qquad \gamma(H_B|_{S_1}) = \gamma(H_1|_{S_1}) = \frac{1}{64} \qquad \|H_B\| \leq \|H_1\| \leq n\,\|h_1\| = 2n \tag{7.425}$$

from Lemma 29, equations (7.365) and (7.423), and the fact that $\|h_1\| = 2$ from (7.95). This gives

$$\gamma(H(G_2, G_X oc, n)) \geq \frac{\mathcal{K}_0}{64\mathcal{K}_0 + 256 + 2n \cdot 64 \cdot 256} \geq \frac{\mathcal{K}_0}{35000n} \tag{7.426}$$

where we used the facts that $\mathcal{K}_0 \leq 1$ and $n \geq 1$. □

For each $\vec{z}, \vec{a} \in \{0,1\}^n$ define the uniform superposition

$$|\mathcal{H}(\vec{z},\vec{a})\rangle = \frac{1}{\sqrt{M}} \sum_{j=1}^{M} |C\,(j,\vec{z},\vec{a})\rangle. \tag{7.427}$$

that encodes (somewhat elaborately) the history of the computation that consists of applying either $U_{\mathcal{C}_X}$ or $U^*_{\mathcal{C}_X}$ to the state $|\vec{z}\rangle$. The first bit of $\vec{a}$ determines whether the circuit $\mathcal{C}_X$ or its complex conjugate is applied.

Lemma 31. *The Hamiltonian $H(G_3, G_X oc, n)$ has nullspace S_3 spanned by the states*

$$|\mathcal{H}(\vec{z},\vec{a})\rangle \tag{7.428}$$

for $\vec{z}, \vec{a} \in \{0,1\}^n$. Its smallest nonzero eigenvalue is

$$\gamma(H(G_3, G_X oc, n)) \geq \frac{\mathcal{K}_0}{10^7 n^2 M^2} \tag{7.429}$$

where $\mathcal{K}_0 \in (0,1]$ is the absolute constant from Lemma 27.

Proof. Recall that

$$H(G_3, G_X oc, n) = H(G_2, G_X oc, n) + H_2|_{\mathcal{I}(G_3, G_X oc, n)} \tag{7.430}$$

with both terms on the right-hand side positive semidefinite. To solve for the nullspace of $H(G_3, G_X oc, n)$, it suffices to restrict our attention to the space

$$S_2 = \mathrm{span}\{|C(j,\vec{z},\vec{a})\rangle \colon j \in [M],\ \vec{z},\vec{a} \in \{0,1\}^n\} \tag{7.431}$$

of states in the nullspace of $H(G_2, G_X oc, n)$. We begin by computing the matrix elements of H_2 in the basis for S_2 given above. We use equations (7.408) and (7.415) to compute the diagonal matrix elements:

$$\langle C\,(j,\vec{z},\vec{a})\,|H_2|C\,(j,\vec{z},\vec{a})\rangle = \frac{1}{4}\langle \mathrm{Cube}_0(j,\vec{z},\vec{a})|H_2|\mathrm{Cube}_0(j,\vec{z},\vec{a})\rangle + \frac{1}{4}\langle \mathrm{Cube}_1(j,\vec{z},\vec{a})\rangle|H_2|\mathrm{Cube}_1(j,\vec{z},\vec{a})\rangle \tag{7.432}$$

$$+ \frac{1}{2}\langle \mathrm{Cube}_2(j,\vec{z},\vec{a})|H_2|\mathrm{Cube}_2(j,\vec{z},\vec{a})\rangle \tag{7.433}$$

$$= \begin{cases} 0 + \frac{1}{256} + \frac{1}{256} & j = 1 \\ \frac{1}{256} + \frac{1}{256} + \frac{1}{128} & j \in \{2,\ldots,M-1\} \\ \frac{1}{256} + 0 + \frac{1}{256} & j = M \end{cases} \tag{7.434}$$

$$= \begin{cases} \frac{1}{128} & j \in \{1, M\} \\ \frac{1}{64} & j \in \{2,\ldots,M-1\}. \end{cases} \tag{7.435}$$

In the second line we used equation (7.409). Looking at equation (7.408), we see that the only nonzero off-diagonal matrix elements of H_2 in this basis are of the form

$$\langle C(j-1,\vec{z},\vec{a})|H_2|C(j,\vec{z},\vec{a})\rangle \quad \text{or} \quad \langle C(j,\vec{z},\vec{a})|H_2|C(j-1,\vec{z},\vec{a})\rangle = \langle C(j-1,\vec{z},\vec{a})|H_2|C(j,\vec{z},\vec{a})\rangle^* \tag{7.436}$$

for $j \in \{2, \ldots, M\}$, $\vec{z}, \vec{a} \in \{0,1\}^n$. To compute these matrix elements we first use equation (7.410) to evaluate

$$\langle \mathrm{Cube}_w(j-1, \vec{z}, \vec{a})|H_2|\mathrm{Cube}_v(j, \vec{z}, \vec{a})\rangle \tag{7.437}$$

for $v, w \in \{0,1,2\}$ and $j \in \{2, \ldots, M\}$. For example, using the second case of equation (7.410), we get

$$\langle \mathrm{Cube}_1(j-1, \vec{z}, \vec{a})|H_2|\mathrm{Cube}_0(j, \vec{z}, \vec{a})\rangle = \frac{1}{2^{n-2}} \sum_{\vec{d} \in \mathcal{D}_0^j} \sum_{\vec{c} \in \mathcal{D}_1^{j-1}} (-1)^{\sum_{i \in [n]}(c_i + d_i)} \langle j-1, \vec{c}, \mathrm{In}(\vec{z}), \vec{a}|H_2|j, \vec{d}, \mathrm{In}(\vec{z}), \vec{a}\rangle \tag{7.438}$$

$$= \frac{1}{2^{n-2}} \sum_{\vec{d} \in \mathcal{D}_0^j : d_{s(j-1)} = 1} (-1) \cdot \frac{1}{64} = -\frac{1}{128}. \tag{7.439}$$

To go from the first to the second line we used the fact that, for each $\vec{d} \in \mathcal{D}_0^j$ with $d_{s(j-1)} = 1$, there is one $\vec{c} \in \mathcal{D}_1^{j-1}$ for which $\langle j-1, \vec{c}, \mathrm{In}(\vec{z}), \vec{a}|H_2|j, \vec{d}, \mathrm{In}(\vec{z}), \vec{a}\rangle = \frac{1}{64}$ (with all other such matrix elements equal to zero). This $\vec{c}$ satisfies $c_1 = c_{s(j-1)} = 1$ and $c_{s(j)} = 0$, with all other bits equal to those of $\vec{d}$, so

$$(-1)^{\sum_{i=1}^n (c_i + d_i)} = (-1)^{c_1 + c_{s(j)} + c_{s(j-1)} + d_1 + d_{s(j)} + d_{s(j-1)}} = -1 \tag{7.440}$$

for each nonzero term in the sum.

We perform a similar calculation using cases 1, 3, and 4 in equation (7.410) to obtain

$$\langle \mathrm{Cube}_w(j-1, \vec{z}, \vec{a})|H_2|\mathrm{Cube}_v(j, \vec{z}, \vec{a})\rangle = \begin{cases} -\frac{1}{128} & (w,v) = (1,0) \\ \frac{1}{128\sqrt{2}} & (w,v) \in \{(2,0),(1,2)\} \\ -\frac{1}{256} & (w,v) = (2,2) \\ 0 & \text{otherwise.} \end{cases} \tag{7.441}$$

Hence

$$\langle C(j-1, \vec{z}, \vec{a})|H_2|C(j, \vec{z}, \vec{a})\rangle \tag{7.442}$$

$$= \frac{1}{4}\langle \mathrm{Cube}_1(j-1, \vec{z}, \vec{a})|H_2|\mathrm{Cube}_0(j, \vec{z}, \vec{a})\rangle - \frac{1}{2\sqrt{2}}\langle \mathrm{Cube}_2(j-1, \vec{z}, \vec{a})|H_2|\mathrm{Cube}_0(j, \vec{z}, \vec{a})\rangle \tag{7.443}$$

$$+ \frac{1}{2}\langle \mathrm{Cube}_2(j-1, \vec{z}, \vec{a})|H_2|\mathrm{Cube}_2(j, \vec{z}, \vec{a})\rangle - \frac{1}{2\sqrt{2}}\langle \mathrm{Cube}_1(j-1, \vec{z}, \vec{a})|H_2|\mathrm{Cube}_2(j, \vec{z}, \vec{a})\rangle \tag{7.444}$$

$$= -\frac{1}{128}. \tag{7.445}$$

Combining this with equation (7.435), we see that $H_2|_{S_2}$ is block diagonal in the basis (7.431), with a block for each pair of n-bit strings $\vec{z}, \vec{a} \in \{0,1\}^n$. Each of the 2^{2n} blocks is equal to

the $M \times M$ matrix

$$\frac{1}{128}\begin{pmatrix} 1 & -1 & 0 & 0 & \cdots & 0 \\ -1 & 2 & -1 & 0 & \cdots & 0 \\ 0 & -1 & 2 & -1 & \ddots & \vdots \\ 0 & 0 & -1 & \ddots & \ddots & 0 \\ \vdots & \vdots & \ddots & \ddots & 2 & -1 \\ 0 & 0 & \cdots & 0 & -1 & 1 \end{pmatrix}. \tag{7.446}$$

This matrix is just $\frac{1}{128}$ times the Laplacian of a path of length M, whose spectrum is well known. In particular, it has a unique eigenvector with eigenvalue zero (the all-ones vector) and its eigenvalue gap is $2(1-\cos(\frac{\pi}{M})) \geq \frac{4}{M^2}$. Thus for each of the 2^{2n} blocks there is an eigenvector of $H_2|_{S_2}$ with eigenvalue 0, equal to the uniform superposition $|\mathcal{H}(\vec{z},\vec{a})\rangle$ over the M states in the block. Furthermore, the smallest nonzero eigenvalue within each block is at least $\frac{1}{32M^2}$. Hence

$$\gamma(H_2|_{S_2}) \geq \frac{1}{32M^2}. \tag{7.447}$$

To get the stated lower bound on $\gamma(H(G_3, G_X oc, n))$, we apply Lemma **??** with

$$H_A = H(G_2, G_X oc, n) \qquad H_B = H_2|_{\mathcal{I}(G_3, G_X oc, n)} \tag{7.448}$$

and

$$\gamma(H_A) \geq \frac{\mathcal{K}_0}{35000n} \qquad \gamma(H_B|_{S_2}) = \gamma(H_2|_{S_2}) \geq \frac{1}{32M^2} \qquad \|H_B\| \leq \|H_2\| \leq n\|h_2\| = 2n \tag{7.449}$$

from Lemma 30, equation (7.447), and the fact that $\|h_2\| = 2$ from (7.95). This gives

$$\begin{aligned} \gamma(H(G_3, G_X oc, n)) &\geq \frac{\mathcal{K}_0}{32M^2\mathcal{K}_0 + 35000n + 2n(35000n)(32M^2)} \qquad (7.450) \\ &\geq \frac{\mathcal{K}_0}{M^2n^2(32 + 35000 + 70000 \cdot 32)} \geq \frac{\mathcal{K}_0}{10^7 M^2 n^2}. \end{aligned}$$

□

Lemma 32. *The nullspace S_4 of $H(G_4, G_X oc, n)$ is spanned by the states*

$$|\mathcal{H}(\vec{z},\vec{a})\rangle \quad \textit{where} \quad \vec{z} = z_1 z_2 \ldots z_{n_{in}} \underbrace{00\ldots0}_{n-n_{in}} \tag{7.451}$$

for $\vec{a} \in \{0,1\}^n$ and $z_1, \ldots, z_{n_{in}} \in \{0,1\}$. Its smallest nonzero eigenvalue satisfies

$$\gamma(H(G_4, G_X oc, n)) \geq \frac{\mathcal{K}_0}{10^{10} M^3 n^3} \tag{7.452}$$

where $\mathcal{K}_0 \in (0,1]$ is the absolute constant from Lemma 27.

Proof. Using equation (7.411), we find

$$\langle C(k,\vec{x},\vec{b})|H_{\text{in},i}|C(j,\vec{z},\vec{a})\rangle = \delta_{k,j}\delta_{\vec{x},\vec{z}}\delta_{\vec{a},\vec{b}}\Bigg(\frac{1}{4}\langle \text{Cube}_0(j,\vec{z},\vec{a})|H_{\text{in},i}|\text{Cube}_0(j,\vec{z},\vec{a})\rangle \tag{7.453}$$

$$+\frac{1}{4}\langle \text{Cube}_1(j,\vec{z},\vec{a})|H_{\text{in},i}|\text{Cube}_1(j,\vec{z},\vec{a})\rangle \tag{7.454}$$

$$+\frac{1}{2}\langle \text{Cube}_2(j,\vec{z},\vec{a})|H_{\text{in},i}|\text{Cube}_2(j,\vec{z},\vec{a})\rangle\Bigg) \tag{7.455}$$

$$= \delta_{k,j}\delta_{\vec{x},\vec{z}}\delta_{\vec{a},\vec{b}}\left(\frac{1}{64}\delta_{z_i,1}\right)\begin{cases}\frac{1}{4}\cdot\frac{1}{2}+\frac{1}{4}\cdot\frac{1}{2}+\frac{1}{2}\cdot\frac{1}{2} & j<j_{\min,i}\\ \frac{1}{4}+0+0 & j=j_{\min,i}\\ 0+0+0 & j>j_{\min,i}\end{cases} \tag{7.456}$$

for each $i \in \{n_{\text{in}}+1,\ldots,n\}$. Hence

$$\langle \mathcal{H}(\vec{x},\vec{b})|\sum_{i=n_{\text{in}}+1}^{n} H_{\text{in},i}|\mathcal{H}(\vec{z},\vec{a})\rangle = \frac{1}{M}\delta_{\vec{x},\vec{z}}\delta_{\vec{a},\vec{b}}\sum_{i=n_{\text{in}}+1}^{n}\frac{1}{64}\left(\frac{j_{\min,i}-1}{2}+\frac{1}{4}\right)\delta_{z_i,1}. \tag{7.457}$$

Therefore

$$\sum_{i=n_{\text{in}}+1}^{n} H_{\text{in},i}\big|_{S_3} \tag{7.458}$$

is diagonal in the basis $\{|\mathcal{H}(\vec{z},\vec{a})\rangle\colon \vec{z},\vec{a}\in\{0,1\}^n\}$. The zero eigenvectors are given by equation (7.451), and the smallest nonzero eigenvalue is

$$\gamma\left(\sum_{i=n_{\text{in}}+1}^{n} H_{\text{in},i}\big|_{S_3}\right) \geq \frac{1}{256M}. \tag{7.459}$$

since $j_{\min,i}\geq 1$. To get the stated lower bound we now apply Lemma **??** with

$$H_A = H(G_3, G_X oc, n) \qquad H_B = \sum_{i=n_{\text{in}}+1}^{n} H_{\text{in},i}\big|_{\mathcal{I}(G_4,G_X oc,n)} \tag{7.460}$$

and

$$\gamma(H_A)\geq\frac{\mathcal{K}_0}{10^7M^2n^2} \qquad \gamma(H_B|_{S_3})\geq\frac{1}{256M} \qquad \|H_B\|\leq n\left\|\sum_{i=n_{\text{in}}+1}^{n} h_{\text{in},i}\right\| = n \tag{7.461}$$

where we used Lemma 31, equation (7.459), and the fact that $\left\|\sum_{i=n_{\text{in}}+1}^{n} h_{\text{in},i}\right\| = 1$ (from equation (7.94). This gives

$$\gamma\left(H(G_4,G_X oc,n)\right) \geq \frac{\mathcal{K}_0}{256M\mathcal{K}_0+10^7n^2M^2+n(256M)(10^7n^2M^2)} \tag{7.462}$$

$$\geq \frac{\mathcal{K}_0}{(M^3n^3)(256+10^7+256\cdot 10^7)} \geq \frac{\mathcal{K}_0}{10^{10}M^3n^3}. \qquad \square$$

7.5.4 Completeness and Soundness

Well fuck.

7.6 Discussion and open problems

While these results generalized the problem of the Bose-Hubbard model to arbitrary interactions between bosons, it leaves open the related question of fermions. I would expect that our proof would naturally extend to fermions as well, but the extensions where too extensive to finish in time for this thesis.

Making the eventual graph regular.

Remove the restriction to fixed particle number. Currently, this corresponds to

Chapter 8

Ground energy of spin systems

We reduce Frustration-Free Bose-Hubbard Hamiltonian to an eigenvalue problem for a class of 2-local Hamiltonians defined by graphs. The reduction is based on a well-known mapping between hard-core bosons and spin systems, which we now review.

We define the subspace $\mathcal{W}_N(G) \subset \mathcal{Z}_N(G)$ of N hard-core bosons on a graph G to consist of the states where each vertex of G is occupied by either 0 or 1 particle, i.e.,

$$\mathcal{W}_N(G) = \mathrm{span}\{\mathrm{Sym}(|i_1, i_2, \ldots, i_N\rangle) \colon i_1, \ldots, i_N \in V,\ i_j \neq i_k \text{ for distinct } j, k \in [N]\}.$$

A basis for $\mathcal{W}_N(G)$ is the subset of occupation-number states (**??**) labeled by bit strings $l_1 \ldots l_{|V|} \in \{0,1\}^{|V|}$ with Hamming weight $\sum_{j \in V} l_j = N$. The space $\mathcal{W}_N(G)$ can thus be identified with the weight-N subspace

$$\mathrm{Wt}_N(G) = \mathrm{span}\{|z_1, \ldots, z_{|V|}\rangle :\ z_i \in \{0,1\},\ \sum_{i=1}^{|V|} z_i = N\}$$

of a $|V|$-qubit Hilbert space. We consider the restriction of H_G^N to the space $\mathcal{W}_N(G)$, which can equivalently be written as a $|V|$-qubit Hamiltonian O_G restricted to the space $\mathrm{Wt}_N(G)$. In particular,

$$H_G^N\big|_{\mathcal{W}_N(G)} = O_G\big|_{\mathrm{Wt}_N(G)} \tag{8.1}$$

where

$$\begin{aligned} O_G &= \sum_{\substack{A(G)_{ij}=1 \\ i \neq j}} \big(|01\rangle\langle 10| + |10\rangle\langle 01|\big)_{ij} + \sum_{A(G)_{ii}=1} |1\rangle\langle 1|_i \\ &= \sum_{\substack{A(G)_{ij}=1 \\ i \neq j}} \frac{\sigma_x^i \sigma_x^j + \sigma_y^i \sigma_y^j}{2} + \sum_{A(G)_{ii}=1} \frac{1 - \sigma_z^i}{2}. \end{aligned}$$

Note that the Hamiltonian O_G conserves the total magnetization $M_z = \sum_{1=1}^{|V|} \frac{1-\sigma_z^i}{2}$ along the z axis.

We define $\theta_N(G)$ to be the smallest eigenvalue of (8.1), i.e., the ground energy of O_G in the sector with magnetization N. We show that approximating this quantity is QMA-complete.

Problem 5 (**XY Hamiltonian**). We are given a K-vertex graph G, an integer $N \leq K$, a real number c, and a precision parameter $\epsilon = \frac{1}{T}$. The positive integer T is provided in unary; the graph is specified by its adjacency matrix, which can be any $K \times K$ symmetric 0-1 matrix. We are promised that either $\theta_N(G) \leq c$ (yes instance) or else $\theta_N(G) \geq c + \epsilon$ (no instance) and we are asked to decide which is the case.

8.1 Relation between spins and particles

8.1.1 The transform

8.2 Hardness reduction from frustration-free BH model

Theorem 5. *XY Hamiltonian is QMA-complete.*

Proof. An instance of XY Hamiltonian can be verified by the standard QMA verification protocol for the Local Hamiltonian problem [**?**] with one slight modification: before running the protocol Arthur measures the magnetization of the witness and rejects unless it is equal to N. Thus the problem is contained in QMA.

To prove QMA-hardness, we show that the solution (yes or no) of an instance of Frustration-Free Bose-Hubbard Hamiltonian with input G, N, ϵ is equal to the solution of the instance of XY Hamiltonian with the same graph G and integer N, with precision parameter $\frac{\epsilon}{4}$ and $c = N\mu(G) + \frac{\epsilon}{4}$.

We separately consider yes instances and no instances of Frustration-Free Bose-Hubbard Hamiltonian and show that the corresponding instance of XY Hamiltonian has the same solution in both cases.

Case 1: no instances

First consider a no instance of Frustration-Free Bose-Hubbard Hamiltonian, for which $\lambda_N^1(G) \geq \epsilon + \epsilon^3$. We have

$$\lambda_N^1(G) = \min_{\substack{|\phi\rangle \in \mathcal{Z}_N(G) \\ \langle\phi|\phi\rangle = 1}} \langle\phi| H_G^N - N\mu(G) |\phi\rangle \tag{8.2}$$

$$\leq \min_{\substack{|\phi\rangle \in \mathcal{W}_N(G) \\ \langle\phi|\phi\rangle = 1}} \langle\phi| H_G^N - N\mu(G) |\phi\rangle \tag{8.3}$$

$$= \min_{\substack{|\phi\rangle \in \mathrm{Wt}_N(G) \\ \langle\phi|\phi\rangle = 1}} \langle\phi| O_G - N\mu(G) |\phi\rangle \tag{8.4}$$

$$= \theta_N(G) - N\mu(G) \tag{8.5}$$

where in the inequality we used the fact that $\mathcal{W}_N(G) \subset \mathcal{Z}_N(G)$. Hence

$$\theta_N(G) \geq N\mu(G) + \lambda_N^1(G) \geq N\mu(G) + \epsilon + \epsilon^3 \geq N\mu(G) + \frac{\epsilon}{2},$$

so the corresponding instance of XY Hamiltonian is a no instance.

Case 2: yes instances

Now consider a yes instance of Frustration-Free Bose-Hubbard Hamiltonian, so $0 \leq \lambda_N^1(G) \leq \epsilon^3$.

We consider the case $\lambda_N^1(G) = 0$ separately from the case where it is strictly positive. If $\lambda_N^1(G) = 0$ then any state $|\psi\rangle$ in the ground space of H_G^N satisfies

$$\langle\phi| \sum_{w=1}^{N} \left(A(G) - \mu(G)\right)^{(w)} + \sum_{k \in V} \widehat{n}_k(\widehat{n}_k - 1)|\phi\rangle = 0.$$

Since both terms are positive semidefinite, the state $|\phi\rangle$ has zero energy for each of them. In particular, it has zero energy for the second term, or equivalently, $|\phi\rangle \in \mathcal{W}_N(G)$. Therefore

$$\lambda_N^1(G) = \min_{\substack{|\phi\rangle \in \mathcal{W}_N(G) \\ \langle\phi|\phi\rangle = 1}} \langle\phi| H_G^N - N\mu(G)|\phi\rangle = \min_{\substack{|\phi\rangle \in \mathrm{Wt}_N(G) \\ \langle\phi|\phi\rangle = 1}} \langle\phi| O_G - N\mu(G)|\phi\rangle = \theta_N(G) - N\mu(G),$$

so $\theta_N(G) = N\mu(G)$, and the corresponding instance of XY Hamiltonian is a yes instance.

Finally, suppose $0 < \lambda_N^1(G) \leq \epsilon^3$. Then $\lambda_N^1(G)$ is also the smallest *nonzero* eigenvalue of $H(G, N)$, which we denote by $\gamma(H(G, N))$. (Here and throughout this paper we write $\gamma(M)$ for the smallest nonzero eigenvalue of a positive semidefinite matrix M.) Note that $\lambda_N^1(G) > 0$ also implies (by the inequalities (8.2)–(8.5)) that $\theta_N(G) - N\mu(G) > 0$, so

$$\theta_N(G) - N\mu(G) = \gamma\left(\left(O_G - N\mu(G)\right)\big|_{\mathrm{Wt}_N(G)} \right).$$

To upper bound $\theta_N(G)$ we use the Nullspace Projection Lemma (Lemma **??**). We apply this Lemma using the decomposition $H(G, N) = H_A + H_B$ where

$$H_A = \sum_{k \in V} \widehat{n}_k(\widehat{n}_k - 1)\big|_{\mathcal{Z}_N(G)} \qquad H_B = \sum_{w=1}^{N} \left(A(G) - \mu(G)\right)^{(w)} \big|_{\mathcal{Z}_N(G)}.$$

Note that H_A and H_B are both positive semidefinite, and that the nullspace S of H_A is equal the space $\mathcal{W}_N(G)$ of hard-core bosons. To apply the Lemma we compute bounds on $\gamma(H_A)$, $\|H_B\|$, and $\gamma(H_B|_S)$. We use the bounds $\gamma(H_A) = 2$ (since the operators $\{\widehat{n}_k \colon k \in V\}$ commute and have nonnegative integer eigenvalues),

$$\|H_B\| \leq N\|A(G) - \mu(G)\| \leq N(\|A(G)\| + \mu(G)) \leq 2N\|A(G)\| \leq 2KN \leq 2K^2$$

(where we used the fact that $\|A(G)\|$ is at most the maximum degree of G, which is at most the number of vertices K), and

$$\begin{aligned}
\gamma(H_B|_S) &= \gamma\left(\sum_{w=1}^{N} \left(A(G) - \mu(G)\right)^{(w)} \big|_{\mathcal{W}_N(G)} \right) \\
&= \gamma\left(\left(O_G - N\mu(G)\right)\big|_{\mathrm{Wt}_N(G)} \right) \\
&= \theta_N(G) - N\mu(G).
\end{aligned}$$

Now applying the Lemma, we get

$$\lambda_N^1(G) = \gamma(H(G,N)) \geq \frac{2(\theta_N(G) - N\mu(G))}{2 + (\theta_N(G) - N\mu(G)) + 2K^2}.$$

Rearranging this inequality gives

$$\theta_N(G) - N\mu(G) \leq \lambda_N^1(G)\frac{2(K^2+1)}{2-\lambda_N^1(G)} \leq 4K^2\lambda_N^1(G) \leq 4K^2\epsilon^3$$

where in going from the second to the third inequality we used the fact that $1 \leq K^2$ in the numerator and $\lambda_N^1(G) \leq \epsilon^3 < 1$ in the denominator. Now using the fact (from the definition of Frustration-Free Bose-Hubbard Hamiltonian) that $\epsilon \leq \frac{1}{4K}$, we get

$$\theta_N(G) \leq N\mu(G) + \frac{\epsilon}{4},$$

i.e., the corresponding instance of XY Hamiltonian is a yes instance. □

Chapter 9

Conclusions

Many-body systems have, in general, been found to be extremely difficult to understand.

9.1 Open Problems

While we have shown several interesting results, many interesting avenues remain open for investigation.

References

[1] Dorit Aharonov and Amnon Ta-Shma, *Adiabatic Quantum State Generation and Statistical Zero Knowledge*, Proceedings of the Thirty-fifth Annual ACM Symposium on Theory of Computing, STOC '03, pp. 20–29, ACM, 2003, arXiv:quant-ph/0301023.

[2] Andris Ambainis, *Quantum walk algorithm for element distinctness*, SIAM Journal on Computing **37** (2007), no. 1, 210–239, quant-ph/0311001, Preliminary version in FOCS 2004.

[3] Sanjeev Arora and Boaz Barak, *Computational Complexity: A Modern Approach*, Cambridge University Press, 2009.

[4] Dominic W. Berry, Graeme Ahokas, Richard Cleve, and Barry C. Sanders, *Efficient Quantum Algorithms for Simulating Sparse Hamiltonians*, "Communications in Mathematical Physics **270** (2007), no. 2, 359–371, arXiv:quant-ph/0508139.

[5] Dominic W. Berry and Andrew M. Childs, *Black-box Hamiltonian simulation and unitary implementation*, Quantum Information & Computation **12** (2012), no. 1-2, 29–62, arXiv:0910.4157.

[6] Dominic W Berry, Andrew M Childs, Richard Cleve, Robin Kothari, and Rolando D. Somma, *Exponential improvement in precision for simulating sparse Hamiltonians*, Proceedings of the 46th Annual ACM Symposium on Theory of Computing, pp. 283–292, ACM, 2014, arXiv:1312.1414.

[7] Dominic W. Berry, Andrew M. Childs, Richard Cleve, Robin Kothari, and Rolando D. Somma, *Simulating Hamiltonian dynamics with a truncated Taylor series*, Physical review letters **114** (2015), no. 9, 090502, arXiv:1412.4687.

[8] Dominic W. Berry, Andrew M. Childs, and Robin Kothari, *Hamiltonian simulation with nearly optimal dependence on all parameters*, Foundations of Computer Science (FOCS), 2015 IEEE 56th Annual Symposium on, pp. 792–809, IEEE, 2015, arXiv:1501.01715.

[9] Benjamin A. Blumer, Michael S. Underwood, and David L. Feder, *Single-qubit unitary gates by graph scattering*, Physical Review A **84** (2011), no. 6, 062302, arXiv:1111.5032.

[10] Andrew M. Childs, *Universal computation by quantum walk*, Physical Review Letters **102** (2009), no. 18, 180501, arXiv:0806.1972.

[11] Andrew M. Childs, *On the relationship between continuous- and discrete-time quantum walk*, Communications in Mathematical Physics **294** (2010), 581–603, arXiv:0810.0312.

[12] Andrew M. Childs, Richard Cleve, Enrico Deotto, Edward Farhi, Sam Gutmann, and Daniel A. Spielman, *Exponential algorithmic speedup by quantum walk*, Proceedings of the 35th ACM Symposium on Theory of Computing, pp. 59–68, 2003, quant-ph/0209131.

[13] Andrew M. Childs and David Gosset, *Levinson's theorem for graphs II*, Journal of Mathematical Physics **53** (2012), no. 10, 102207, arXiv:1203.6557.

[14] Andrew M. Childs, David Gosset, Daniel Nagaj, Mouktik Raha, and Zak Webb, *Momentum switches*, Quantum Information and Computation **15** (2015), 601–621, arXiv:1406.4510.

[15] Andrew M. Childs, David Gosset, and Zak Webb, *Universal computation by multiparticle quantum walk*, Science **339** (2013), no. 6121, 791–794, arXiv:1205.3782.

[16] ———, *The Bose-Hubbard model is QMA-complete*, Proceedings of the 41st International Colloquium on Automata, Languages, and Programming, pp. 308–319, 2014, arXiv:1311.3297.

[17] Andrew M. Childs and DJ Strouse, *Levinson's theorem for graphs*, Journal of Mathematical Physics **52** (2011), no. 8, 082102, arXiv:1103.5077.

[18] John D. Cook, *Upper and lower bounds for the normal distribution function*, 2009.

[19] Edward Farhi, Jeffrey Goldstone, and Sam Gutmann, *A quantum algorithm for the Hamiltonian NAND tree*, Theory of Computing **4** (2008), no. 1, 169–190, quant-ph/0702144.

[20] Richard Feynmann, *Simulating Physics with Computers*, International Journal of Theoretical Physics **21** (1982), 467–488.

[21] ———, *Quantum Mechanical Computers*, Optics News **11** (1985), 11–20.

[22] David J. Griffiths, *Introduction to Quantum Mechanics*, 2nd ed., Pearson, 2005.

[23] Seth Lloyd, *Universal Quantum Simulators*, Science **273** (1996), no. 5278, 1073–1078, http://science.sciencemag.org/content/273/5278/1073.full.pdf.

[24] Bojan Mohar, *Eigenvalues, diameter, and mean distance in graphs*, Graphs Combin. **7** (1991), 53–64.

[25] David Poulin, Angie Qarry, Rolando Somma, and Frank Verstraete, *Quantum simulation of time-dependent Hamiltonians and the convenient illusion of Hilbert space*, Physical review letters **106** (2011), no. 17, 170501, arXiv:1102.1360.

[26] Michael Saks and Avi Wigderson, *Probabilistic boolean decision trees and the complexity of evaluating game trees*, Foundations of Computer Science, 1986., 27th Annual Symposium on, pp. 29–38, IEEE, 1986.

[27] Jun John Sakurai, *Modern Quantum Mechanics*, Addison-Wesley, 1994.

[28] Miklos Santha, *On the monte carlo boolean decision tree complexity of read-once formulae*, Random Structures & Algorithms **6** (1995), no. 1, 75–87.

[29] Michael Sipser, *Introduction to the Theory of Computation*, 2 ed., Thomas Course Technology, 2006.

[30] Elias M. Stein and Rami Shakarchi, *Complex Analysis*, Princeton University Press, 2003.

[31] John Watrous, *Quantum computational complexity*, Encyclopedia of Complexity and System Science, Springer, 2009, arXiv:0804.3401.

[32] Nathan Wiebe, Dominic W. Berry, Peter Høyer, and Barry C Sanders, *Simulating quantum dynamics on a quantum computer*, Journal of Physics A: Mathematical and Theoretical **44** (2011), no. 44, 445308, arXiv:1011.3489.